Increasing Flexibility in the Design and Operation of Instrument Flight Procedures

by

Sandro Salgueiro Rodrigues Filho

B.S.E. Aerospace Engineering, University of Michigan, 2015
S.M. Aeronautics and Astronautics, Massachusetts Institute of Technology, 2017

Submitted to the Department of Aeronautics and Astronautics
in partial fulfillment of the requirements for the degree of

DOCTOR OF PHILOSOPHY IN AIR TRANSPORTATION SYSTEMS

at the

MASSACHUSETTS INSTITUTE OF TECHNOLOGY

February 2024

Authored by:	Sandro Salgueiro Rodrigues Filho Department of Aeronautics and Astronautics January 22, 2024
Certified by:	R. John Hansman T. Wilson Professor in Aeronautics Thesis Supervisor
Certified by:	Amedeo R. Odoni T. Wilson Professor Emeritus of Aeronautics and Astronautics Thesis Committee Member
Certified by:	James K. Kuchar Assistant Division Head, MIT Lincoln Laboratory Thesis Committee Member
Accepted by:	Jonathan P. How R. C. Maclaurin Professor of Aeronautics and Astronautics Chair, Graduate Program Committee

Increasing Flexibility in the Design and Operation of Instrument Flight Procedures

by

Sandro Salgueiro Rodrigues Filho

Submitted to the Department of Aeronautics and Astronautics
on January 22, 2024 in partial fulfillment of the requirements for the degree of

DOCTOR OF PHILOSOPHY IN AIR TRANSPORTATION SYSTEMS

ABSTRACT

Instrument Flight Procedures determine aircraft departure and arrival trajectories in terminal airspaces. While their main objective is to ensure safe aircraft navigation, flight procedures also have a significant effect on the capacity, efficiency, access, and noise characteristics of airspaces by defining their route structure. The design of procedures is limited by a variety of constraints that restrict achievable aircraft trajectories. Many constraints originate from safety considerations and can interact in complex ways to limit flight procedure flexibility and system performance.

It is hypothesized that opportunities to increase system flexibility may exist through a better understanding of constraints and opportunities to reevaluate them based on technology improvements. Following a review of constraints and their effect on flexibility, the required geometric separation between flight procedures is identified as a significant constraint in the design of flight procedures and is chosen as the focus of an in-depth study to identify constraint reevaluation opportunities.

The collision risk between procedures is identified as the main driver of their required separation. Through an analysis of modern aircraft navigation performance in normal operations, it is found that the collision risk between procedures is expected to be dominated by the risk due to non-normal events (i.e., deviations), which can be controlled through the use of collision mitigation capabilities. As a result, it is posited that a better understanding of the collision risk between flight procedures under the effect of mitigations represents a key mechanism for identifying how technology improvements may enable the reevaluation of separation. To that end, a model of the mitigated collision risk between flight procedures is developed and presented.

In example applications of the proposed mitigated collision risk model, several potential system improvement paths are identified and discussed that could result in lower separation between procedures and therefore greater flexibility. These include improvements to mitigation technologies, better aircraft navigation reliability, and greater knowledge of aircraft non-normal behaviors that could lead to less conservative assumptions in collision risk modeling. Examples discussed in this thesis include the evaluation of the achievable separation between real procedures at Boston Logan Airport (BOS), which could offer noise benefits, and the evaluation of the achievable separation between future Advanced Air Mobility (AAM) routes. The methods presented in this thesis could be used to support the evaluation of future changes to separation as well as the planning of future mitigation systems.

Thesis supervisor: R. John Hansman
Title: T. Wilson Professor in Aeronautics

Contents

Chapter 1

Introduction

1.1 Instrument Flight Procedures

Instrument flight procedures, or flight procedures for short, are pre-planned navigation routes designed to be flown by aircraft during departure and arrival operations in terminal airspace under Instrument Flight Rules (IFR). Flight procedures are documented as sequences of navigation instructions, which when executed by eligible aircraft result in specific flight trajectories (Figure 1-1). Procedures can specify both lateral and vertical profiles. The primary purpose of flight procedures is to provide safe aircraft navigation within terminal airspace. In addition to this safety objective, flight procedures also have a significant effect on the efficiency, capacity, and noise characteristics of an airspace, as they determine its route structure.

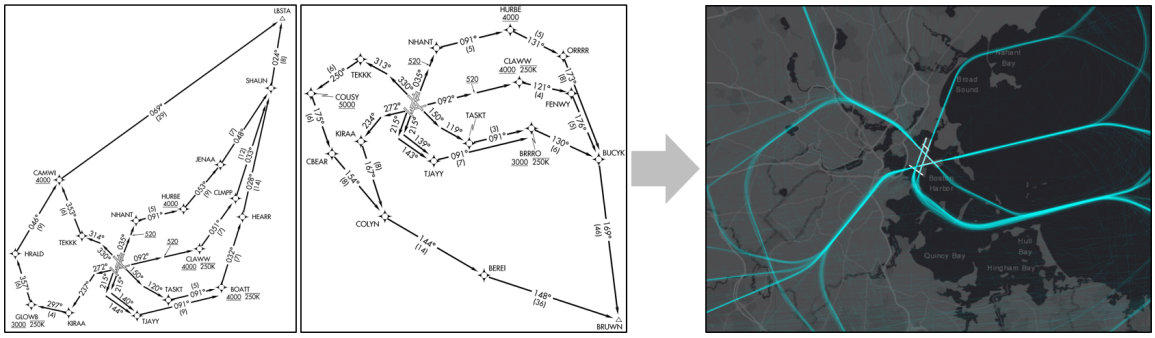

Figure 1-1: Left: Example departure procedures at Boston Logan Airport (BOS). Right: Resulting aircraft trajectories as observed from radar data.

1.2 Types of Flight Procedures

Flight procedures can be classified based on the phase of flight for which they are designed, as well as on the navigation equipment they require aircraft to have. In terms of phase of flight, flight procedures are classified as:

- **Departure procedures**: procedures that guide aircraft from a departure runway to enroute airspace, where the aircraft typically joins an airway.
- **Arrival procedures**: procedures that guide aircraft from enroute airspace to a point where an approach may be initiated (e.g., an Initial Approach Fix).
- **Approach procedures**: procedures that guide aircraft from an Initial Approach Fix to a landing runway.

In terms of the navigation equipment they require, flight procedures have undergone several evolutions over the last decades. Early instrument navigation in the 20th century primarily relied on Air Traffic Control (ATC) radar vectors and ground beacons such as the VHF Omnidirectional Range (VOR) and the Non-Directional Beacon (NDB). Because VORs and NDBs are physical beacons installed on the ground, procedures that relied on them had their geometry limited by the location of these beacons.

More recently, a new navigation standard known as *Performance-Based Navigation* (PBN) has replaced VORs and NDBs as the default method of aircraft instrument navigation [1]. Unlike VOR and NDB-based flight procedures that require aircraft to have specific VOR/NDB onboard equipment, PBN procedures instead specify a required level of navigation performance that eligible aircraft must meet. This minimum performance specification is largely agnostic to the equipment being used to meet it. The main parameter used to specify navigation performance is *accuracy*, which is defined as the 95th percentile value of an aircraft's total navigation error. PBN performance requirements are typically satisfied with a combination of GPS receivers and inertial navigation systems, which together allow an aircraft to navigate

independently from ground beacons such as VORs and NDBs. Through this independence of ground infrastructure, PBN flight procedures can offer significantly greater trajectory flexibility, as their geometries are not limited by the physical location of ground beacons (Figure 1-2). Today, PBN represents the default choice for modern flight procedure design due to the widespread availability of GPS navigation and its associated benefits.

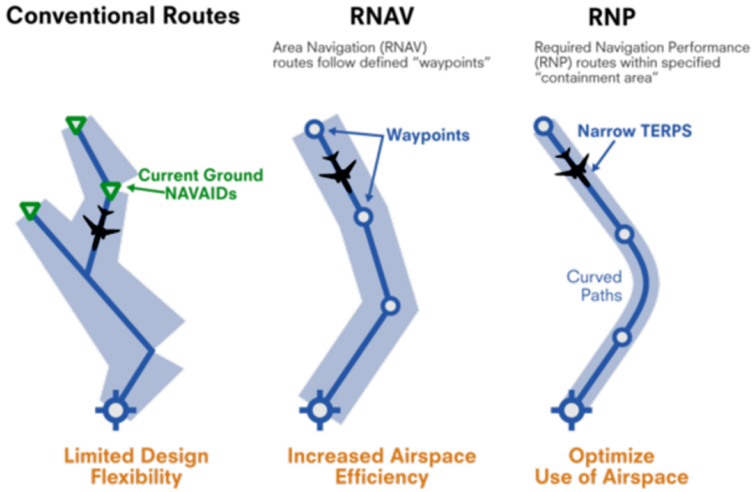

Figure 1-2: Notional comparison of ground-based navigation, RNAV, and RNP. Source: Federal Aviation Administration.

1.3 PBN Navigation Specifications

Every PBN flight procedure is designed with a specific combination of navigation performance requirements, which may include requirements on accuracy, flight deck alerting capabilities (e.g., ability to alert the crew of a lateral deviation), and path definition capabilities (e.g., ability to fly curved segments). These requirements are grouped into what is known as a *Navigation Specification*, or *NavSpec*. Once published, a procedure's NavSpec is indicated on charts distributed to flight crews, and only aircraft approved for that NavSpec are eligible to fly it.

PBN NavSpecs are divided into Area Navigation (RNAV) specifications and Required Navigation Performance (RNP) specifications. In addition to enforcing accuracy requirements, RNP specifications also require aircraft to be equipped with

specific flight deck alerting capabilities to alert the crew in case of navigation performance degradation. RNAV specifications, on the other hand, do not require the same type of flight deck alerting capabilities. NavSpecs are generally named using the scheme *RNAV/RNP XX*, where *XX* is the accuracy requirement of the NavSpec. For example, the *RNAV 1* NavSpec is an RNAV NavSpec that requires an accuracy of 1 nautical mile.

Different NavSpecs are traditionally reserved for specific phases of flight. Departure (SID) and arrival (STAR) procedures are commonly designed using the *RNAV 1* NavSpec, while RNAV approaches use the *RNP APCH* NavSpec and RNP approaches use the *RNP AR APCH* NavSpec [1]. A breakdown of the NavSpecs currently in use in the United States is shown in Figure 1-3.

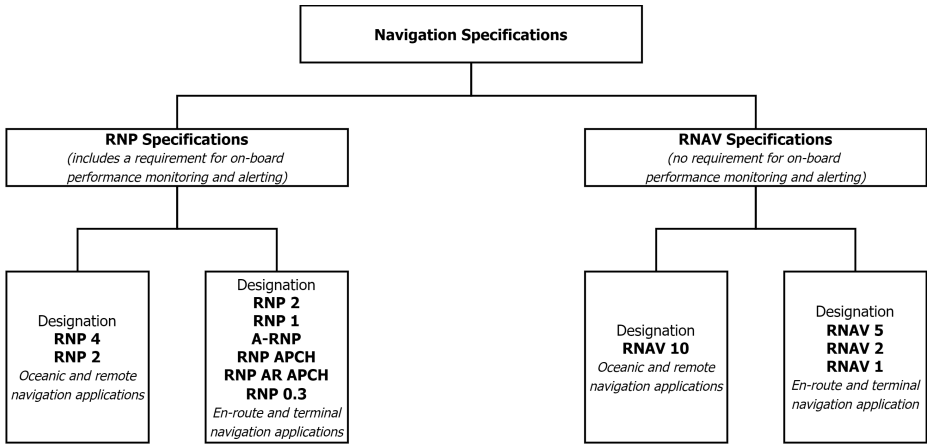

Figure 1-3: RNAV and RNP Navigation Specifications. Image source: Federal Aviation Administration [1].

1.4 Flight Procedure Flexibility and Constraints

Flight procedure flexibility is defined as the ability of a flight procedure to be designed with different geometries and to be operated in different conditions. During flight procedure design, higher flexibility translates into a larger geometric design space for the trajectory being planned. Although all procedures are designed to meet safety objectives, higher flexibility can enable trajectories that are better optimized for performance metrics such as capacity, efficiency, and noise. As a result, system

performance in terminal airspace is directly connected to flight procedure flexibility.

Flexibility is limited by *flight procedure constraints*, which are defined as factors limiting the feasible geometry and operation of flight procedures. Many constraints originate from safety considerations, and constraints can interact in complex ways to limit flight procedure flexibility. Examples of flight procedure constraints, which are discussed in further detail in the next chapter, include the requirement for separation from terrain and other flight procedures. By restricting achievable aircraft trajectories, constraints indirectly limit system performance.

1.5 Thesis Objectives and Outline

Given the benefits associated with higher flexibility, this work seeks to identify opportunities to increase flexibility through a better understanding of flight procedure constraints and the mechanisms by which technology improvements may allow for their reevaluation.

Following a review of constraints in the next chapter, the required geometric separation between published procedures is identified as a major constraint and chosen as the subject of an in-depth study for identifying constraint reevaluation opportunities. Due to several system improvements related to communication (e.g., Datalink), navigation (e.g., RNAV and RNP) and surveillance (e.g., ADS-B) that have occurred in the last few decades, this work seeks to better understand how these and other technology improvements may affect the required separation between published procedures, which could lead to opportunities to increase flexibility.

Chapter 2 of this thesis discusses key flight procedure constraints and proposes a classification scheme based on their sources and effects. Techniques for visualizing the effects of constraints are discussed, which can be used for both the identification and communication of constraints. From this review of constraints, the required geometric separation between flight procedures is identified as a major constraint limiting the feasible geometry of flight procedures in terminal airspace, and is chosen as the focus of an in-depth study to identify constraint reevaluation opportunities.

Chapter 3 reviews historical efforts to reevaluate the required separation between

flight procedures, from which limitations and opportunities for improvement are identified. The general concept of a Target Level of Safety (TLS) as a basis for judging the acceptability of a change is reviewed. From this literature review, it is posited that the consideration of collision mitigation capabilities represents a key mechanism for identifying how technology improvements may enable the reevaluation of separation, and it is argued that past safety assessments have not always taken credit for the availability of mitigations.

Chapter 4 presents a mitigated collision risk model for evaluating the collision risk between geometrically separate flight procedures under the effect of mitigations, which parses the risk into normal and non-normal components. As part of the evaluation of non-normal risk, a geometric model is proposed for evaluating the effects of mitigations on the collision risk.

Chapter 5 identifies and discusses key parameters in mitigation and flight procedure design that can be used to control the collision risk between procedures, based on the mitigated collision risk model presented in the prior chapter. Opportunities for improving mitigation performance through the development of future mitigation systems are identified and discussed.

Chapter 6 provides example applications of the mitigated collision risk model presented in Chapters 4 and 5, in which the methodology presented in previous chapters is used to evaluate the achievable separation between flight procedures under several potential system improvement paths. The examples considered included a generic case of two co-altitude jet aircraft procedures, a real case at Boston Logan Airport involving a departure and an approach procedure, and a hypothetical case of two Advanced Air Mobility (AAM) routes.

Finally, **Chapter 7** concludes the thesis by summarizing key findings and opportunities identified to increase flight procedure flexibility through the reevaluation of the required separation between published procedures.

Chapter 2

Constraints in Instrument Flight Procedure Design and Operation

The design and operation of flight procedures are constrained by numerous factors, many of which are related to safety considerations. These factors are termed *flight procedure constraints*. Constraints limit flexibility by restricting the available geometric design space of flight procedures, as well as their utilization. This chapter reviews key constraints affecting the design and operation of PBN flight procedures. Following this review, the visualization of constraints is presented as a method for identifying their effects on the geometric design space of flight procedures.

Flight procedure constraints are classified into two groups: **Geometric Constraints** are defined as constraints that limit both the feasible geometry and the placement of a flight procedure within the airspace. **Stakeholder Acceptance Constraints** are more complex constraints that originate from the subjective evaluation of a flight procedure concept by operational stakeholders (e.g., pilots, ATC), which can impose additional barriers on the implementation of a flight procedure.

The following sections provide a review of these two classes of flight procedure constraints, focusing on key constraints within each class and their impact on overall flight procedure flexibility. While other types of constraints may exist in certain cases, such as speed restrictions required at procedure waypoints to improve traffic predictability and reduce controller workload, the two classes discussed here are ar-

gued to represent the dominant constraints affecting the design and implementation of PBN flight procedures in the current air traffic system.

2.1 Geometric Constraints

Geometric constraints are constraints that impose limitations on the feasible geometry and placement of flight procedure within an airspace. Enforcement of geometric constraints attempts to ensure that procedures can be safely flown and that their interaction with other system elements such as aircraft and ATC systems is acceptable. Based on their source, geometric flight procedure constraints can be grouped under three categories:

- **Terrain Clearance Constraints:** constraints requiring a procedure to be separated from terrain and ground obstacles.
- **ATC Structure Constraints:** constraints requiring a procedure to be compatible with the local airspace structure and air traffic control rules.
- **Flyability Constraints:** constraints requiring procedure segments and turns to accommodate standard aircraft performance and navigation system capabilities, so that procedures can be repeatably and reliably flown by eligible aircraft.

The next few sections describe key constraints within these three categories.

2.1.1 Terrain Clearance Constraints

Terrain clearance constraints separate flight procedures from terrain and ground obstacles. Current design criteria specifying the required separation between flight procedures and terrain is documented in the United States Standard for Terminal Instrument Procedures, commonly known as TERPS [2]. Based on methods described in TERPS, flight procedures are separated from terrain and ground obstacles through the application of a protected volume of airspace built around the procedure, which must be free of terrain and obstacles. The lateral component of this protected airspace

is known as the Obstacle Evaluation Area (OEA), while its bottom surface is known as the Obstacle Clearing Surface (OCS), illustrated in Figure 2-1. In order to satisfy terrain clearance constraints, the OCS of a flight procedure must not be penetrated by terrain or ground obstacles. In addition, the actual vertical path of the procedure must be separated from the OCS by an altitude margin known as the Required Obstacle Clearance (ROC), which is the minimum vertical separation from terrain that a flight procedure guarantees.

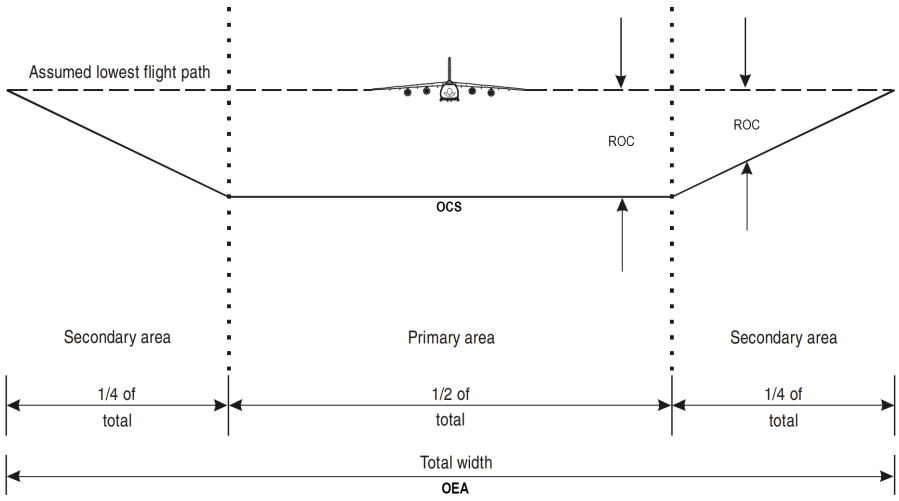

Figure 2-1: Vertical cross-section of an RNAV procedure's protected airspace, showing the OEA, OCS (bottom surface), and the ROC. Image source: International Civil Aviation Organization [3].

The width of the OEA is specified by the procedure's NavSpec, and is a function of the required navigation accuracy. For RNAV departure and arrival procedures, the OEA is divided into a *primary area* and a *secondary area*. The primary area has a width equal to four times the required accuracy (also known as the Cross-Track Tolerance, or XTT). The secondary area extends the width of the OEA by 1×XTT in each direction, as illustrated in Figure 2-2. RNAV departure and arrival procedures are typically designed with the RNAV 1 NavSpec, which requires a 1 NM navigation accuracy. These procedures have a primary area that is 4 NM wide, with the secondary area increasing the total width of the OEA to 6 NM. The primary and secondary areas each use a different Obstacle Clearing Surface (OCS) (see Figure 2-1). Within the primary area, the cross-section of the OCS is a flat line. In the

secondary area, the OCS's cross-section is a sloping line that provides maximum obstacle clearance where it meets the primary area and zero obstacle clearance at the outer edge of the secondary area.

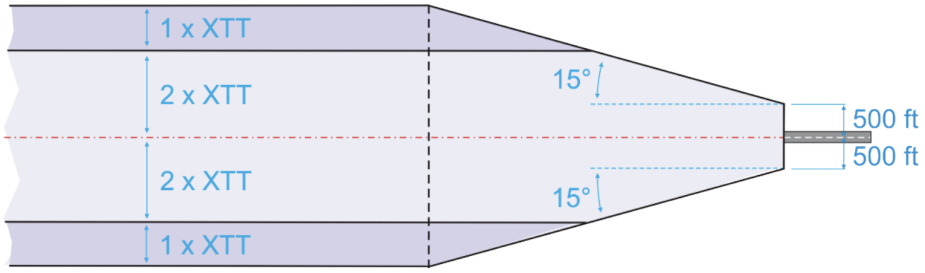

Figure 2-2: Illustration of the OEA used for a straight RNAV departure. Image source: Federal Aviation Administration [4].

For departure and approach procedures, the OCS is a sloping surface that climbs (departures) or descends (approaches) along the flight path. For departures, the standard slope of the OCS is 40:1, or 152 ft/NM (feet per nautical mile). This parameter can be increased based on the selection of a higher *minimum climb gradient* during procedure design, with the highest allowed minimum climb gradient of 500 ft/NM providing an OCS slope of 380 ft/NM. For approaches with vertical guidance, the OCS slope is a function of the approach's glidepath angle (Figure 2-3). For a standard 3-degree glidepath, the OCS has a slope of 179 ft/NM.

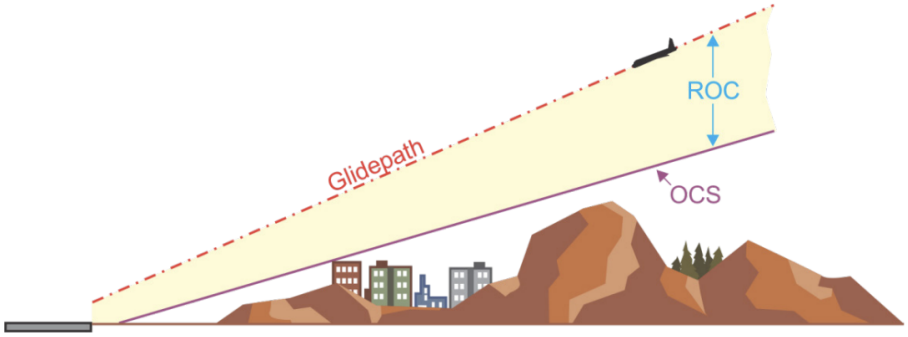

Figure 2-3: Illustration of a sloping OCS applied to an approach procedure. Image source: Federal Aviation Administration [2].

Compared to RNAV procedures, RNP procedures do not have a secondary area in their OEA. This is justified based on the higher navigation accuracy of RNP systems

and the availability of flight deck alerting functions that RNP specifications require. As a result, the width of an RNP OEA is simply four times the required navigation accuracy (Figure 2-4). For example, a departure procedure designed with the RNP 0.3 NavSpec has an OEA that is 1.2 NM wide.

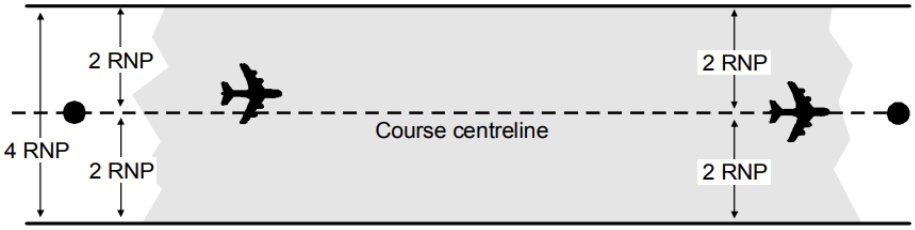

Figure 2-4: Illustration of the OEA of an RNP procedure. Image source: International Civil Aviation Organization [5].

During the design of a flight procedure, a complete candidate procedure is necessary before an Obstacle Clearance Surface (OCS) can be generated. Geometric formulas used to draw the OCS are documented in TERPS. Once defined, the OCS must be evaluated and verified to be clear of penetrations by terrain or ground obstacles, which satisfies terrain clearance constraints. If a procedure is changed in any way, a new OCS must be drawn and evaluated.

2.1.2 ATC Structure Constraints

Terminal areas around major airports are highly structured environments, designed to facilitate the routine provision of air traffic control services (i.e. aircraft separation, flow management) by human air traffic controllers. Elements of this structure impose several constraints on the geometry of flight procedures, as they must be designed to be compatible with the existing local structure and rules of the air traffic control system. Key geometric constraints related to ATC structure are discussed next.

Separation between Flight Procedures

Aircraft flying in controlled airspace must be separated from each other according to FAA air traffic control rules documented in Order 7110.65 [6]. Two sets of separation rules exist: radar separation rules, and non-radar separation rules.

Radar separation rules assume radar coverage and are based on distances between aircraft measured on a controller's radar screen. Non-radar rules rely on time-based and heading-based separation, and can be applied in situations where radar coverage is not guaranteed. Either type of separation can be used to satisfy aircraft separation requirements. Radar separation is typically in effect for the majority of cases within a terminal airspace, while non-radar rules are sometimes applied near airports due to the distance between departing and arriving aircraft initially not satisfying radar separation standards and due to the possibility of aircraft being momentarily below radar coverage at low altitudes.

Radar separation rules in general terminal operations typically require aircraft to be separated by at least 3 NM laterally or 1000 ft vertically in terminal airspace. When separated longitudinally on the same route or flight procedure (i.e., directly behind), aircraft must also be separated based on additional wake turbulence rules. Wake turbulence separation rules vary based on the weight class of the aircraft involved, and are documented in Order 7110.126 [7]. On final approach, aircraft may be separated by 2.5 NM longitudinally (instead of 3 NM) whenever the weight class of the leading aircraft is the same or lower than that of the trailing aircraft.

Aircraft separation in busy terminal airspaces is typically designed into the geometry of flight procedures and therefore manifests as a geometric flight procedure constraint. By being geometrically separated, flight procedures can be operated independently and aircraft separation is assured in normal operations with minimal ATC involvement. The most common separation criteria used to separate procedures is the standard radar separation of 3 NM laterally or 1000 ft vertically.

Because aircraft vertical profiles are not controlled to the same extent as their lateral profiles, the application of lateral separation is typically prioritized in flight procedure design. In PBN departure procedures, for example, a large dispersion of aircraft vertical paths is often observed, while lateral trajectories remain tightly concentrated about the procedure path. An example of this can be observed at Boston Logan Airport (BOS) in the separation between runway 22R departures and runway 27 arrivals (Figure 2-5). In this case, the departure procedure's vertical profile is unrestricted, and a minimum lateral separation between the two procedures is enforced to separate aircraft regardless of their vertical trajectories.

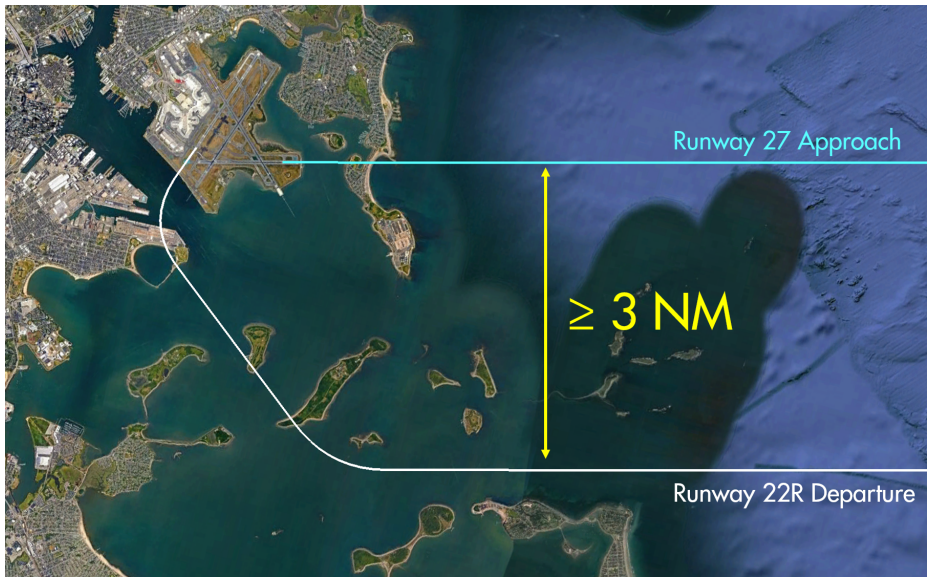

Figure 2-5: Example of lateral separation being prioritized in the design of flight procedures, due to aircraft vertical profiles not being controlled to the same extent as their lateral profiles.

When procedures must be separated near an airport (e.g., a departure and an approach procedure), non-radar rules are often used. This type of procedure separation is often applied in the form of a minimum heading divergence between procedures that must be satisfied until the distance between aircraft is sufficient to meet radar separation rules. At airports with parallel runways spaced by 2500 ft or more, PBN departure procedures must diverge by at least 10 degrees immediately after takeoff in order to be operated independently [6]. At airports with converging runways, procedures must diverge by at least 45 degrees. An example of the latter case can be

observed in the initial separation between the runway 22R departure procedure and the runway 27 approach procedure at BOS, shown in Figure 2-6.

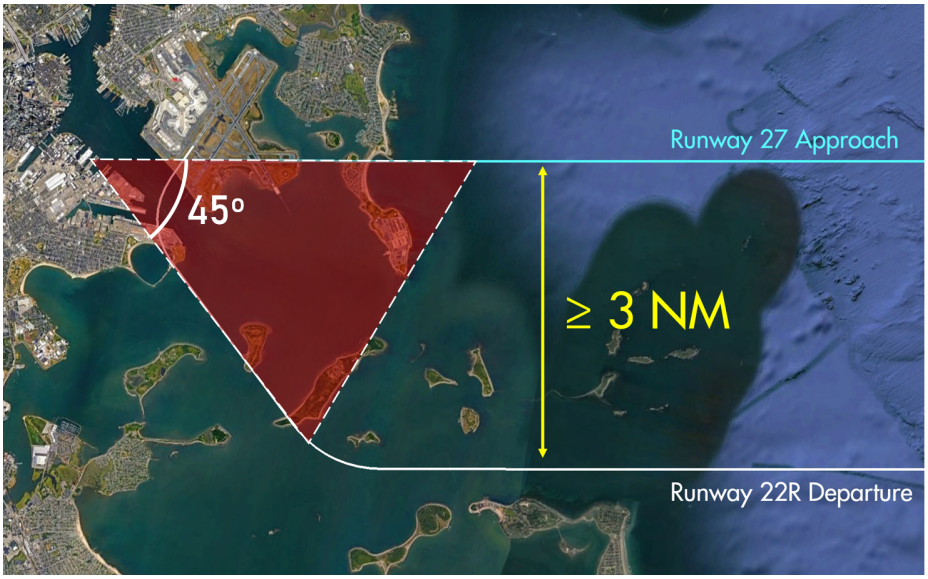

Figure 2-6: Example of non-radar separation based on heading divergence between a departure and an approach procedure. In this case, a minimum divergence angle of 45 degrees must be maintained until the procedures are separated by 3 NM.

Separation from ATC Sector Boundaries

In addition to being separated from each other, flight procedures are also required to be separated from elements of the airspace structure known as *sector boundaries*. Sector boundaries are the geographical limits of airspace sectors, which are volumes of the airspace managed by different air traffic controllers.

Sectors are typically reserved for specific operations (e.g., departure vs. approach sectors, westbound vs. southbound sectors, etc.). If a flight procedure does not meet the criteria for accessing a given sector, then it must be laterally separated by at least 1.5 NM from the boundary of that sector [6]. Examples of this constraint include departure procedures being separated from final approach sectors, and procedures departing in a specific direction (e.g., westbound departures) being separated from sectors that manage other-direction traffic (e.g., southbound departures). The 1.5 NM separation from a sector's boundary is enforced so that a 3 NM lateral separation is maintained between aircraft flying in neighboring sectors at all times. The

locations of sector boundaries are dependent on the runway configuration in use at the airport, with each runway configuration having its corresponding *sector map*. If a flight procedure is intended for use in multiple runway configurations, it must be separated from the relevant sector boundaries of all applicable configurations.

Sector maps are typically documented in an ATC facility's Standard Operating Procedures (SOP) manual and Letters of Agreement (LoA). For illustration, Figure 2-21 shows the sector structure around Boston Logan Airport for a particular runway configuration (landings on runway 27, departures from runways 22L/R).

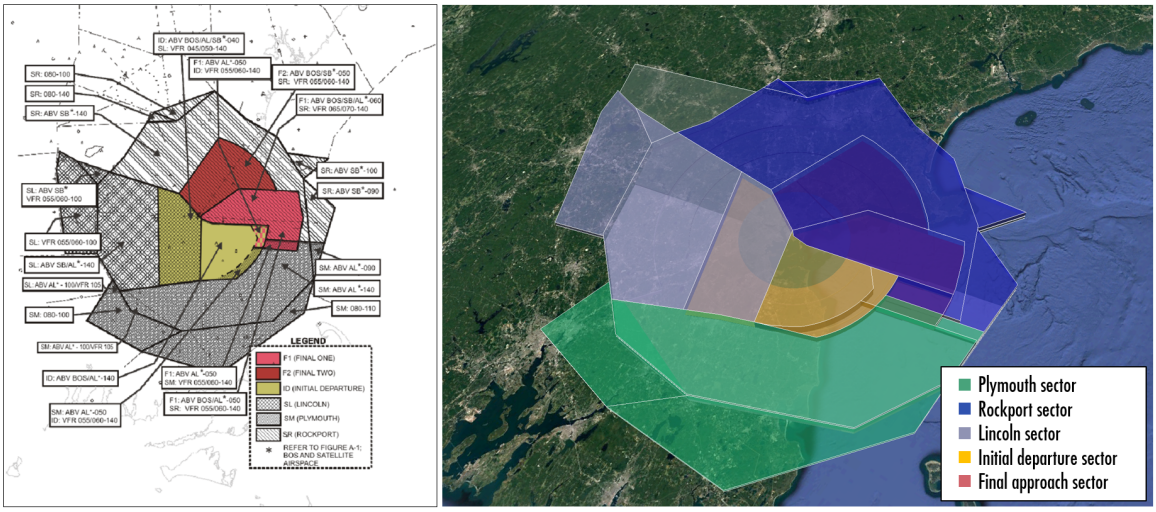

Figure 2-7: Left: Boston airspace sector structure in 27/22 configuration [8]. Right: A matching 3D model of this airspace structure.

An example of this constraint in effect can be observed in the HYLND6 departure from runway 33L at Boston Logan Airport, where the procedure is designed to be separated by more than 1.5 NM from an ATC sector boundary to the east (Figure 2-8).

Figure 2-8: Illustration of the HYLND6 departure procedure from runway 33L at Boston Logan Airport (in red), designed to be separated by more than 1.5 NM from the highlighted ATC sector boundary.

Compatibility with TCAS Logic and Minimizing Nuisance Alerts

The Traffic Alert and Collision Avoidance System (TCAS) is a required aircraft equipment for passenger-carrying operations in the United States. By interrogating aircraft transponders in its vicinity and providing traffic alerts in the flight deck, TCAS mitigates the risk of midair collisions between aircraft sharing the same airspace. When an imminent conflict is detected, TCAS produces an alert known as a *Resolution Alert* (RA). An RA instructs the flight crew to execute an immediate vertical maneuver (i.e., climb or descend) in order to avoid the conflicting traffic [9].

While TCAS RAs provide safety value, the generation of nuisance resolution alerts can, in some cases, have an adverse impact on the capacity and efficiency of the air traffic system. The FAA defines a nuisance alert as "*an alert generated by a system that is functioning as designed but which is inappropriate or unnecessary for the particular condition* [10]." Nuisance RAs have been documented at various airports across the National Airspace System (NAS) where simultaneous approaches are flown to closely-spaced parallel runways [11]. Although collision risk assessments have found

these simultaneous approaches to be safe, the generation of nuisance TCAS alerts can contribute to an overall loss of system performance by causing unnecessary missed approaches. This, in turn, negates some of the capacity and efficiency benefits offered by simultaneous approaches.

During the design of flight procedures serving parallel runways, an analysis of the TCAS RA logic may therefore be required to determine whether the proposed procedure geometry may introduce nuisance TCAS alerts. Based on TCAS logic, RA "protection volumes" may be predicted based on expected final approach intercept locations, groundspeeds, and altitudes [12]. A common technique employed to minimize the probability of nuisance alerts during simultaneous instrument approaches is to design the procedures with different glideslope intercept altitudes, thus preventing a scenario where aircraft are flying on converging courses at the same altitude. Designing one of the approaches to be laterally offset relative to the other may also increase the distance between aircraft early on the approach, thus contributing to a lower rate of nuisance TCAS alerts. This type of offset approach is currently in use at San Francisco Airport (SFO), where the RNAV approach to runway 28R is offset laterally by 3 degrees from the approach to runway 28L (Figure 2-9).

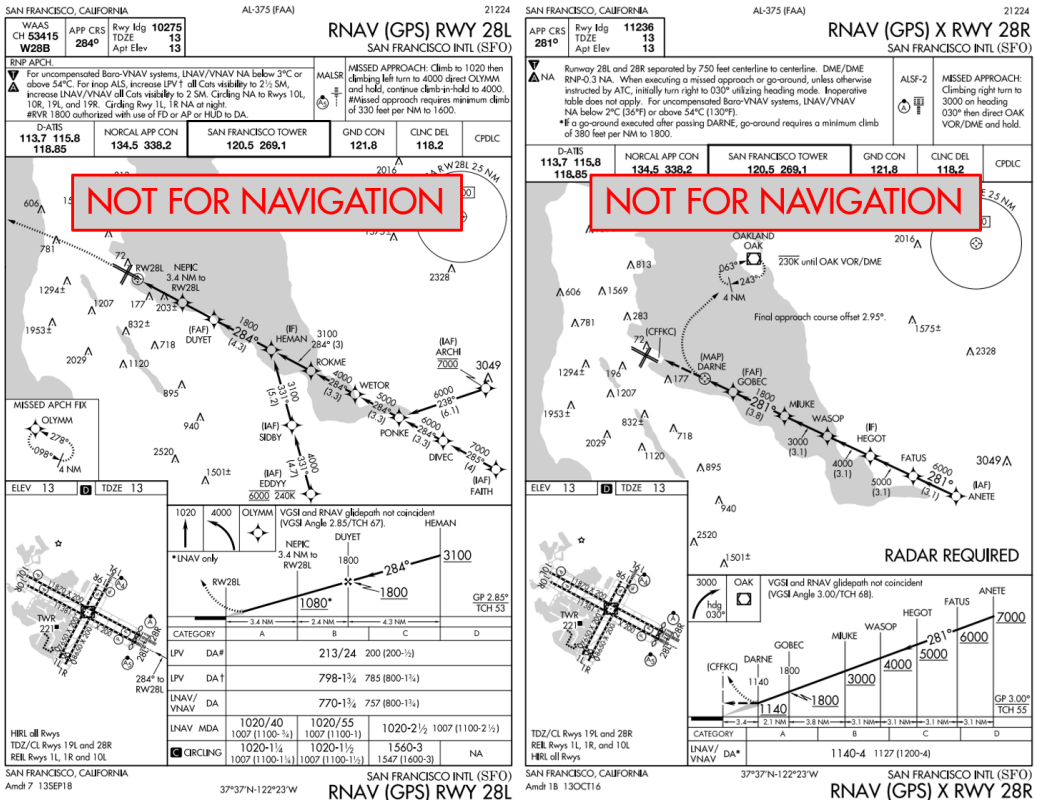

Figure 2-9: Left: RNAV approach to runway 28L at SFO. Right: RNAV approach to runway 28R at SFO. The 28L approach has a final approach course of 284, while the 28R approach uses 281 (offset by 3 degrees).

Other Airspace Constraints

Additional flight procedure constraints that are related to the local airspace structure may exist in some cases. Of note, ATC Letters of Agreement (LoA) may specify standard handoff locations for aircraft transiting between TRACON and Center airspace. These require the location of certain waypoints on departure and arrival flight procedures to remain fixed unless the LoA can be modified, thus imposing *point* constraints on these procedures. Another potential source of airspace constraints are Records of Decision (ROD). A ROD represents an agreement signed between two or more parties involved with airport operations, which may include the airport authority, ATC facilities, and neighboring communities. Among other restrictions, RODs are capable of imposing mandatory waypoint crossings, which can impose additional point constraints on procedures.

2.1.3 Flyability Constraints

Flyability constraints impose limitations on the geometry of flight procedures to ensure that aircraft maneuvering limitations are respected given typical aircraft dynamics, required navigation capabilities, and worst-case environmental conditions. Flyability constraints manifest in the internal shape of a flight procedure rather than in its placement within the airspace. Because navigation capabilities can affect how aircraft maneuver while tracking a flight procedure, flyability constraints can vary based on the NavSpec used to construct a procedure. Like terrain clearance constraints, flyability constraints are documented in TERPS [2]. Key flyability constraints applicable to PBN procedures are discussed next.

Minimum Leg Length

A minimum leg length constraint refers to the shortest distance allowed between two consecutive waypoints connected by straight segments (also known as TF legs), which is enforced to prevent overshoots during transitions between segments given aircraft maneuvering limitations. This minimum distance is determined based on assumptions of aircraft speed, bank angle during a turn, and worst-case tailwind [2], which are used to determine an expected aircraft turn radius. Given a sequence of procedure waypoints, the minimum length allowed for each segment is computed based on this calculated aircraft turn radius, the turn angle at the beginning of the segment, and the turn angle at the end of the segment. This calculation is illustrated in Figure 2-10. When curved segments (also known as RF legs) are used to connect waypoints in RNP procedures, a minimum turning radius is enforced directly, as opposed to a minimum segment length.

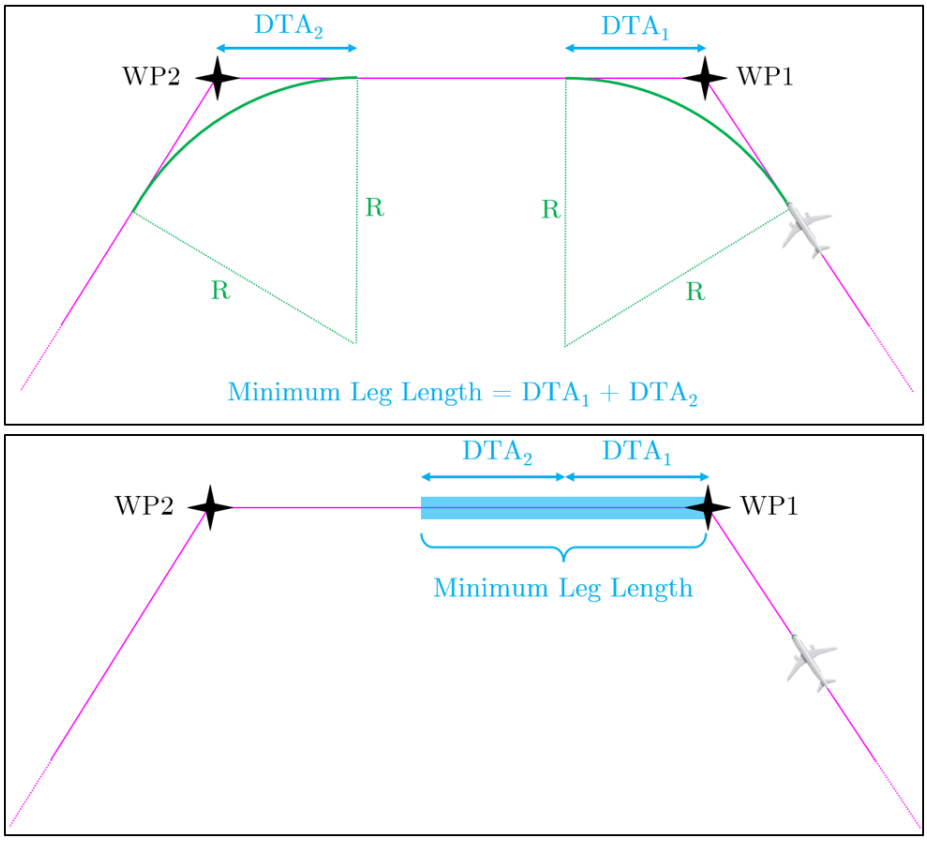

Figure 2-10: The minimum length of a segment is a function of the expected aircraft turning radius and turn angles. A *Distance-to-Turn-Anticipation* (DTA) value is computed for each turn, and the minimum leg length is the sum of the DTA at the beginning of the segment (DTA_1) and at the end of the segment (DTA_2).

Maximum Turn Angle

A maximum turn angle constraint refers to the maximum angle allowed between two straight procedure segments. In the United States, the FAA has set the maximum turn angle between straight segments on PBN procedures to 90 degrees below 19,500 ft and 70 degrees above 19,500 ft [4]. On approach procedures, a lower maximum turn angle is enforced at the Final Approach Fix (FAF). For an RNAV approach, the maximum turn angle at the FAF is 15 degrees when using LNAV/VNAV minimums (i.e., vertical guidance is available), and 30 degrees when using LNAV minimums (i.e., vertical guidance not available) [4]. These turn angle limits are based on certification standards for aircraft navigation systems [13] and on the observed tracking performance of current autopilot systems during turns [14].

The maximum turn angle constraint translates into a range of available outbound headings at each waypoint of a procedure (Figure 2-11). This constraint does not apply to curved RF segments in RNP procedures, since in those segments the change in aircraft heading occurs continuously over the course of the segment and the turn path is defined precisely. In fact, RNP approach procedures commonly use a 180-degree turn (RF) segment connecting the downwind to the final.

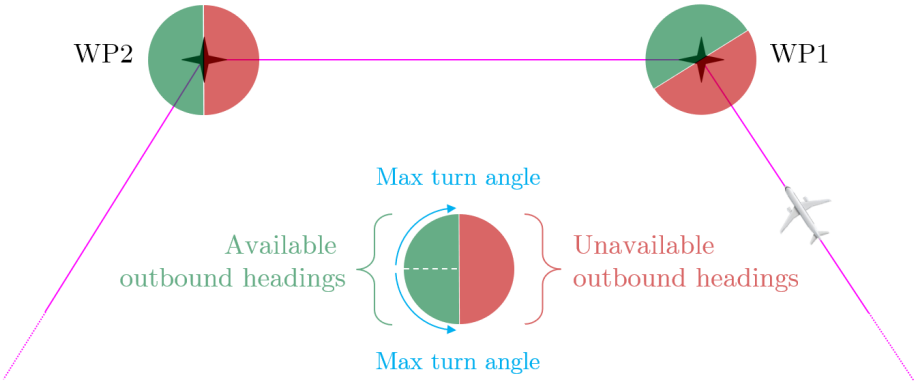

Figure 2-11: The maximum turn angle constraint limits the range of available outbound headings at each procedure waypoint.

Minimum Final Approach Length

On RNAV instrument approach procedures, the beginning of the final approach segment is marked by a Final Approach Fix (FAF). The minimum final approach length is the lowest distance allowed between the FAF and the runway threshold. TERPS states that *"the minimum length of the final approach segment must be sufficient to provide adequate distance for an aircraft to make the required descent"* [2]. This translates into a requirement that, at the FAF, an instrument approach must guarantee at least 500 ft of vertical separation from the tallest obstacle in the approach path. Once at the FAF, the aircraft must then be able to execute the rest of the descent using a standard glidepath angle (Figure 2-12). For an approach with no obstacles and a 3-degree glidepath, the FAF can be positioned 1.41 nautical miles from the runway threshold, which corresponds to the lowest possible final approach length [15].

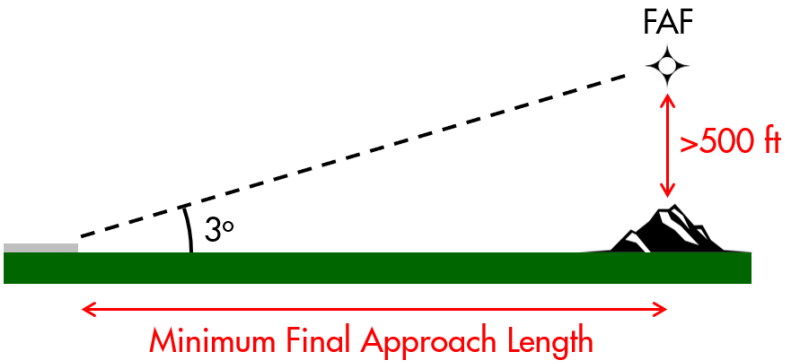

Figure 2-12: Illustration of the minimum final approach length as a function of obstacle height.

In addition to the minimum final approach length required by TERPS, operators typically have their own requirements for the lowest acceptable length of a final approach. In the United States, most airlines require pilots to be stabilized and aligned with the runway at an altitude of 1000 ft (3 NM from the threshold) [16]. This usually results in the minimum final approach length value used in practice being larger than the minimum required by regulations.

Climb and Descent Gradients

Departure, arrival, and approach procedures have limitations imposed on the climb and descent gradients that they are allowed to require from aircraft. For departure procedures, all aircraft are required to meet a minimum climb gradient of 200 ft/NM. Based on operational needs to clear terrain, this minimum required climb gradient may be increased up to a maximum of 500 ft/NM. While most commercial jet aircraft can easily meet a 200 ft/NM climb gradient, a 500 ft/NM climb gradient may not be achievable by large widebody aircraft. As a result, the local fleet mix must be studied during flight procedure design to determine whether a high climb gradient is compatible with the aircraft that are expected to use the procedure.

For arrivals, the highest required descent gradient that can be designed into a procedure is 330 ft/NM (approximately 3.11 degrees) above 10,000 ft and 318 ft/NM (approximately 3 degrees) below 10,000 ft. These values are based on typical jet aircraft lift-to-drag ratios and deceleration profiles [2].

For approaches, maximum descent gradients of 500 ft/NM in the initial approach segment and 318 ft/NM in the intermediate segment are allowed. In the final approach segment, a maximum glidepath angle is specified instead, and is dependent on the aircraft approach category, as shown in the table below [2]. Note that these values apply to PBN (RNAV and RNP) approaches, and are different for ILS approaches.

Aircraft Approach Category	Maximum Glidepath Angle
A (80 knots or less)	6.40
A (81-90 knots)	5.70
B	4.20
C	3.77
D	3.50
E	3.10

Table 2.1: Maximum glidepath angles allowed during final approach segment on RNAV and RNP approaches [2].

Minimum LNAV Engagement Altitude

The initial segment of a PBN departure procedure is geometrically constrained by the minimum altitude that it must allow an aircraft to reach before commanding a turn. This altitude is known as the minimum LNAV engagement altitude, which refers to the altitude at which aircraft navigation systems are assumed to be set to lateral navigation mode. Based on current fleet capabilities, the FAA has set this value to 500 ft above airport elevation [4]. In the case where the highest possible minimum climb gradient of 500 ft/NM is applied to the initial departure segment, this constraint translates into a requirement to have a 1 NM straight segment at the beginning of an RNAV or RNP departure. This distance is measured from the Departure End of the Runway (DER).

2.2 Stakeholder Acceptance Constraints

During the design and implementation of PBN procedures in the United States, procedure concepts are formally evaluated through a structured FAA process described in Order 7100.41 [17]. During this process, operational stakeholders (e.g., pilots, air traffic controllers) may identify and raise concerns based on their own expert-based evaluation of a procedure concept. This can result in additional barriers being imposed on the implementation of a flight procedure, which are more complex than the geometric constraints previously discussed.

While geometric constraints can be addressed by changing a flight procedure's geometry, addressing stakeholder acceptance constraints may require external solutions such as additional personnel training or deployment of new capabilities.

Stakeholder acceptance constraints can vary significantly in their severity, ranging from additional restrictions being imposed on a procedure's geometry to an outright rejection of a new procedure implementation. Factors considered by operational stakeholders when evaluating a flight procedure implementation include:

- **Training and proficiency**

  Pilots and controllers may resist the implementation of a flight procedure if they perceive their current training and proficiency as inadequate for the proposed operation.

- **Workload**

  Pilots and controllers may resist the implementation of a flight procedure if they perceive that the proposed procedure will lead to an unacceptable increase in their workload.

- **Complexity and potential for error**

  Pilots and controllers may resist the implementation of a flight procedure if they perceive it as operationally complex, which could increase the likelihood of human errors.

- **Trajectory predictability**

  Controllers may resist the implementation of flight procedures that reduce the predictability of aircraft trajectories, as they would demand increased monitoring and more frequent tactical interventions leading to an increase in workload.

- **Controllability during merging and spacing**

  Controllers may resist the implementation of fixed-path approach procedures that reduce options for tactical separation control and create merging and spacing challenges. For example, controllers may resist RNP AR approach procedures that limit ATC control to the control of aircraft speed only.

- **Mixed equipage**

  Controllers may resist the implementation of flight procedures that require new and specific aircraft equipment, and which may only be available to a subset of the fleet. This stems from ATC challenges in merging and spacing aircraft on different flight procedures close to the airport.

- **Compatibility with operator SOP**

  Operators may resist the implementation of procedures that violate their Standard Operating Procedures (SOP). For example, approach procedures with short final approaches may violate airline approach stabilization criteria, which commonly require aircraft to be stabilized on a final approach at 1000 ft, approximately 3 nautical miles from the runway [16].

- **Operator fuel burn**

  Operators may resist the implementation of flight procedures that would result in significant increases in path length and fuel burn.

- **Operator equipage cost**

  Operators may resist the implementation of flight procedures that would require aircraft retrofitting. Where new navigation systems are required, the expected

benefits from the utilization of the procedure must outweigh new equipment costs.

- **Memory limitations of Flight Management Systems (FMS)**

  Operators may resist the implementation of flight procedures that would use significant amounts of storage memory when loaded onto an aircraft's FMS navigation database, due to memory limitations in these systems.

Because geometric constraints are more readily quantifiable than stakeholder acceptance constraints, and because they are formally documented in FAA policy, the remainder of this thesis will focus on them as a potential area for improving flexibility. To that end, the remainder of this chapter discusses the visualization of geometric constraints as a method for identifying and communicating their effects on the available geometric design space of procedures.

2.3 Visualizing the Effects of Geometric Constraints

This section discusses techniques for visualizing geometric constraints, which can be used for identifying and communicating the effects of geometric constraints on a flight procedure's geometric design space. For visualization purposes, geometric constraints can be divided into two groups:

- **Volumetric geometric constraints**

  Volumetric geometric constraints are those that can be visualized as three-dimensional volumes of unavailable airspace, and include terrain clearance and ATC structure constraints. Volumetric constraints limit the placement of a procedure within the airspace.

- **Non-volumetric geometric constraints**

  Non-volumetric geometric constraints are those that cannot be visualized as volumes of unavailable airspace. Flyability constraints belong in this category,

since they are internal geometric constraints limiting the intrinsic shape of a flight procedure rather than its placement within the airspace.

The following sections describe visualization techniques for these two types of geometric constraints.

2.3.1 Visualizing Volumetric Geometric Constraints

Visualizing Terrain Clearance Constraints

Terrain and ground obstacles relevant to the design of flight procedures can be identified in the FAA's Digital Obstacle File (DOF) database. Once identified, relevant obstacles can be visualized three-dimensionally as illustrated in Figure 2-13.

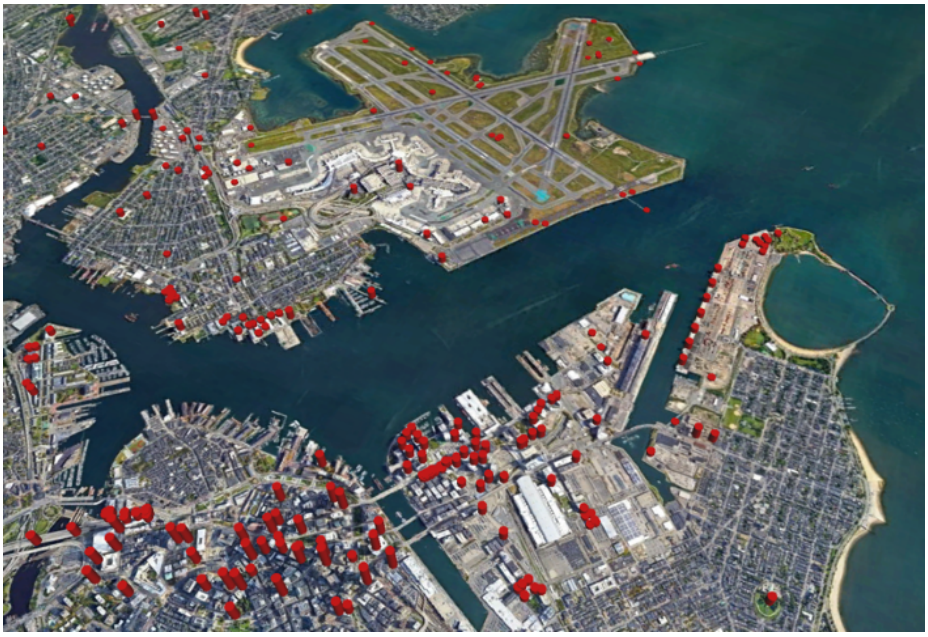

Figure 2-13: Red cylinders indicate ground obstacles as recorded in the FAA's DOF database for the Boston area.

Given a complete procedure candidate, its Obstacle Clearing Surface (OCS) can be drawn based on TERPS criteria and illustrated three-dimensionally. Taking an example departure procedure from runway 22R at Boston Logan Airport (BOS), Figure 2-14 illustrates both the procedure's OCS and ground obstacles in the same geometric space. In order to verify that the procedure meets terrain clearance constraints, its

OCS is checked for any penetrations. In the event that the OCS is penetrated by an obstacle, its geometry must be modified.

Figure 2-14: Illustration of the Obstacle Clearing Surface (OCS) in green for a departure procedure off runway 22R at BOS, drawn based on TERPS criteria. Obstacles are shown as red cylinders.

Obstacle clearance constraints can also be approximated and represented without a complete candidate procedure by inverting the concept of the OEA/OCS protected airspace and transforming it into a series of volumes of unavailable airspace placed around known obstacles. This concept is illustrated notionally in Figure 2-15 below.

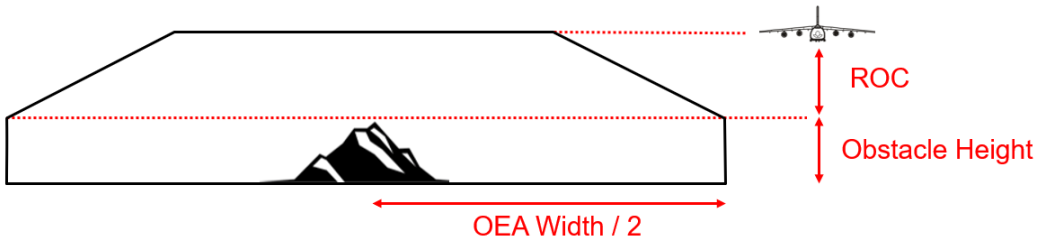

Figure 2-15: Illustration of unavailable airspace due to obstacle constraints. The value of the ROC and OEA width are determined from TERPS criteria.

Applying this technique to all relevant obstacles in the BOS runway 22R departure example, a conservative set of terrain constraints can be drawn as shown in Figure 2-16.

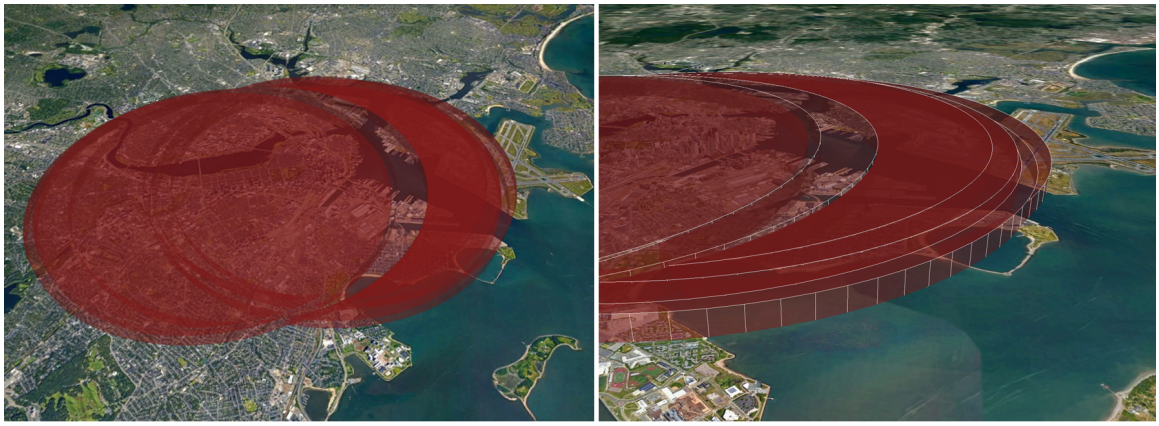

Figure 2-16: The red volumes represent areas of the airspace unavailable to the departure procedure due to obstacle clearance constraints based on the conservative inverse OEA/OCS method.

In the visualization shown in Figure 2-16, only relevant obstacles are displayed. In other words, obstacles that cannot physically penetrate an upward-sloping OCS (200 ft/min) from the runway are disregarded. Furthermore, it is noted that the unavailable airspace illustrated in this example encompasses part of the airport itself. In the actual application of TERPS, an Initial Climb Area (ICA) covers, at a minimum, the first mile of a departure procedure. The ICA is a unique part of a procedure's protected airspace with different obstacle clearance rules (Figure 2-17). Therefore, the inverse OEA/OCS method outlined here should only be used as a first-order illustration of general obstacle constraints in the airspace before a candidate procedure has been created. Once a candidate procedure is available, terrain clearance constraints must be verified using the standard OCS method from TERPS.

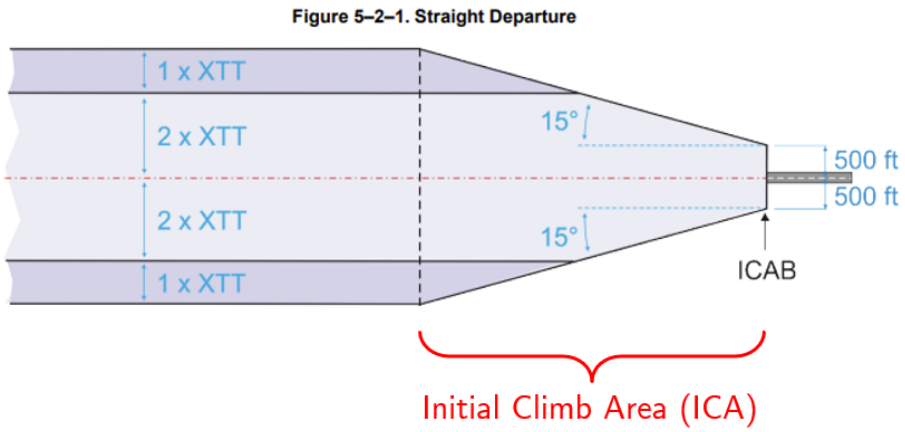

Figure 2-17: Example of Initial Climb Area (ICA) construction for straight-out RNAV departure procedure. Image source: FAA [4].

Finally, it is noted that the FAA's official flight procedure design software TARGETS is capable of automatically drawing a flight procedure's OCS. After drawing the procedure's OCS, TARGETS can automatically identify violations of terrain clearance constraints and highlight any obstacles penetrating the OCS (Figure 2-18).

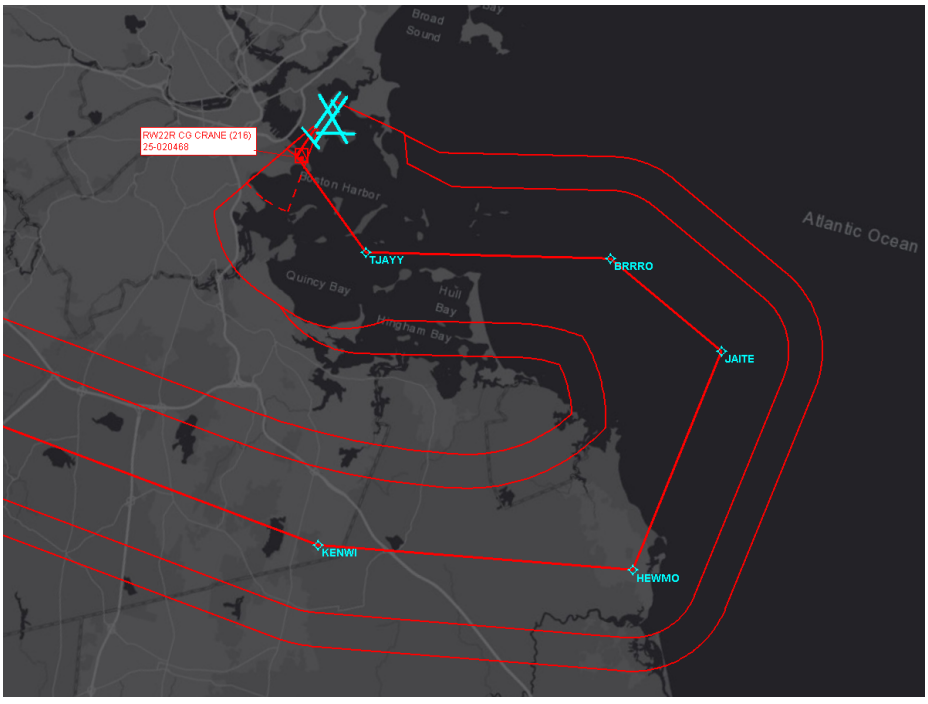

Figure 2-18: TARGETS evaluation of candidate flight procedure's OEA/OCS, shown as the red volume drawn around the flight procedure (2D view).

Visualizing ATC Structure Constraints

1. *Separation between Flight Procedures*

   Procedure separation constraints can be visualized as volumes of unavailable airspace around existing flight procedures, which are sized according to the separation required between flight procedures. In order to visualize these volumes, the set of active flight procedures in an airspace must first be identified. This set of procedures is a function of the active runway configuration at the airport. As an example, consider the procedure separation constraints affecting a departure procedure serving runway 22R at BOS. This departure procedure is expected to be operated while runways 22L and 27 are being used for arrivals. Based on this runway configuration, the set of active arrival and approach procedures serving the two landing runways is identified and shown in Figure 2-19.

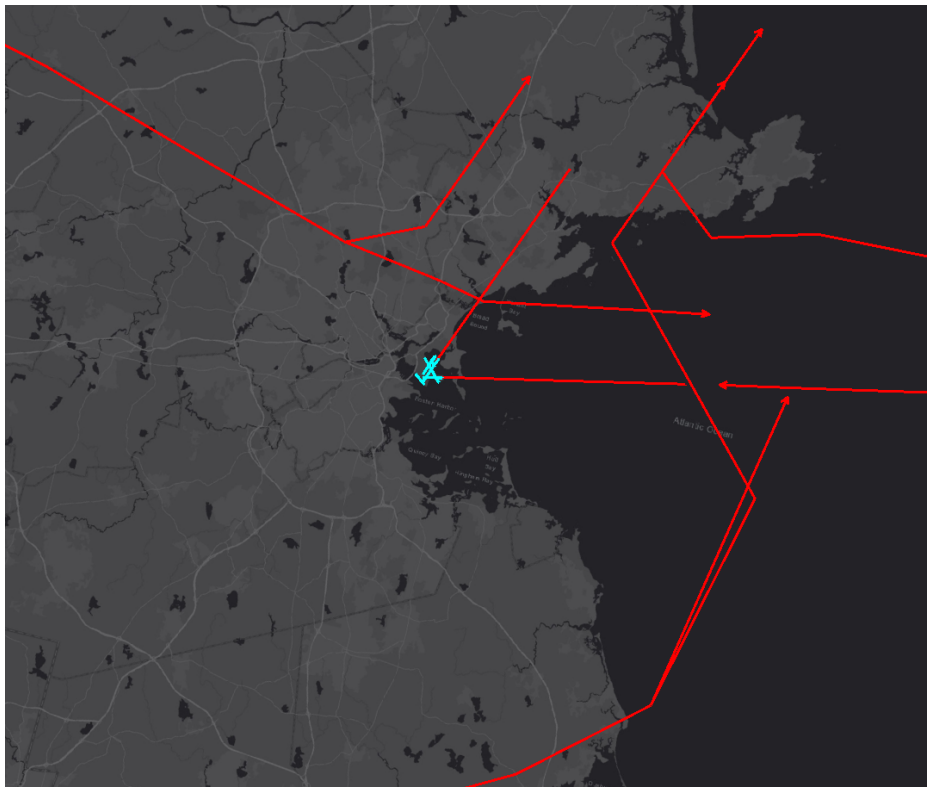

Figure 2-19: Active set of arrival and approach procedures at BOS when in a 27/22 runway configuration (TARGETS view).

Given this set of active arrival and approach procedures, volumes of constrained

airspace can be drawn around each procedure based on the minimum required separation of 3 NM (laterally) or 1000 ft (vertically). These volumetric constraints represent sectors of the airspace that are unavailable to a departure procedure because they are currently reserved for arrivals and approaches (Figure 2-20).

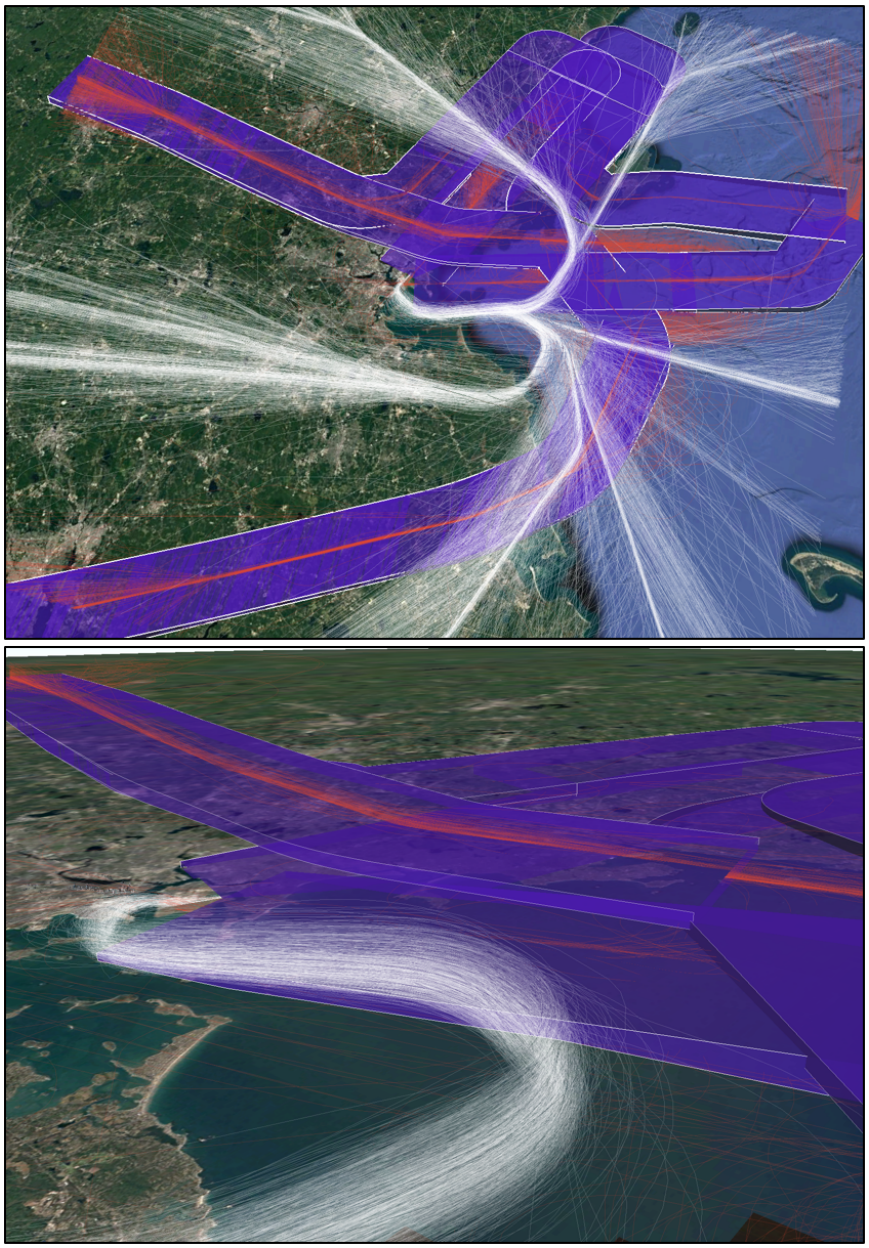

Figure 2-20: The airspace reserved for arrivals and approaches is illustrated in purple. The constrained airspace volume around each arrival and approach procedure enforces 3 NM of lateral separation and 1000 ft of vertical separation. The white tracks represent departure trajectories from runway 22R.

At major terminal areas such as Boston's, the required separation between flight procedures is observed to be a significant constraint limiting flexibility.

2. *Separation from ATC Sector Boundaries*

   Flight procedures must be laterally separated from the boundaries of unavailable airspace sectors by at least 1.5 NM, based on ATC regulations [6]. Considering again the example of a runway 22R departure procedure at BOS, the location of sector boundaries can be identified from the sector map applicable to the relevant runway configuration. For a 27/22 runway configuration (aircraft departing from runway 22R and landing on runway 27), the associated sector structure is shown in Figure 2-21.

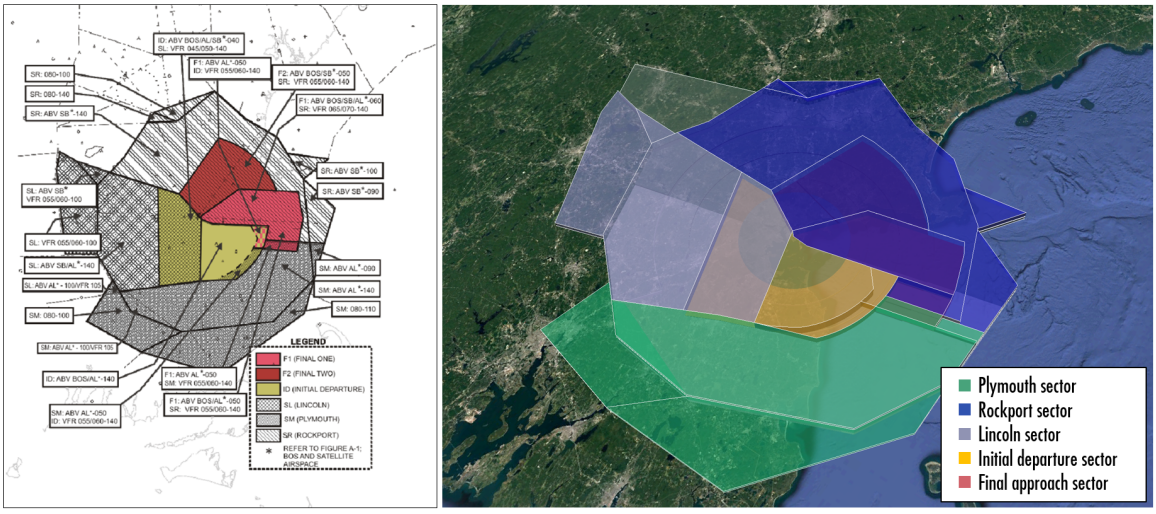

Figure 2-21: Left: Boston airspace sector structure for the 27/22 runway configuration [8]. Right: A matching 3D model of this airspace structure.

The local ATC facility's SOP manual describes how these different sectors are assigned to different operations. The red area in Figure 2-21 indicates airspace reserved for the *final approach controller*, which is unavailable to departure operations. This sector therefore imposes a volumetric constraint on departure procedures from runway 22R, with an additional 1.5 NM of lateral separation required from its boundaries (Figure 2-22).

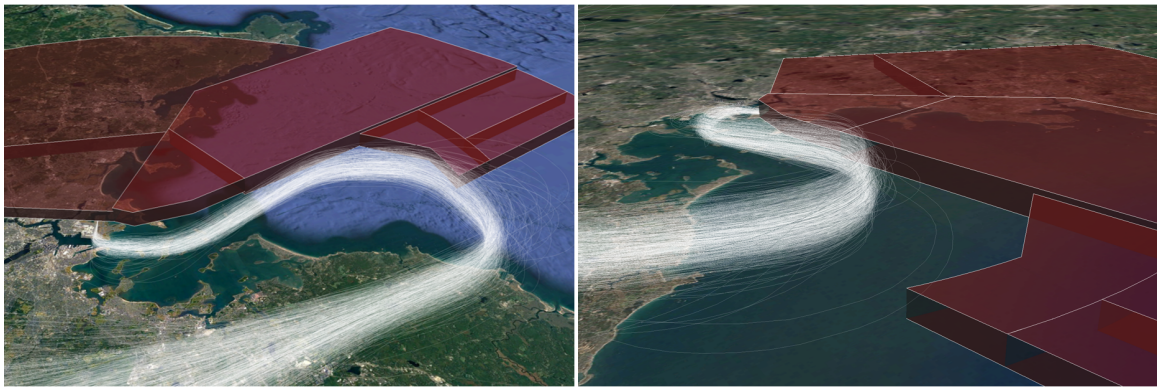

Figure 2-22: The red volume highlighted represents airspace unavailable to a departure procedure due to it being allocated to the *final approach controller* in the 27/22 runway configuration. The white tracks represent current aircraft trajectories on westbound departures off runway 22R.

An additional sector south of the airport (*Plymouth Sector* in green) is reserved for southbound departures and arrivals. For departure procedures from runway 22R that are departing the airspace to the west, this sector introduces yet another volumetric constraint. The volumetric constraint imposed by this sector on westbound departures is shown in Figure 2-23.

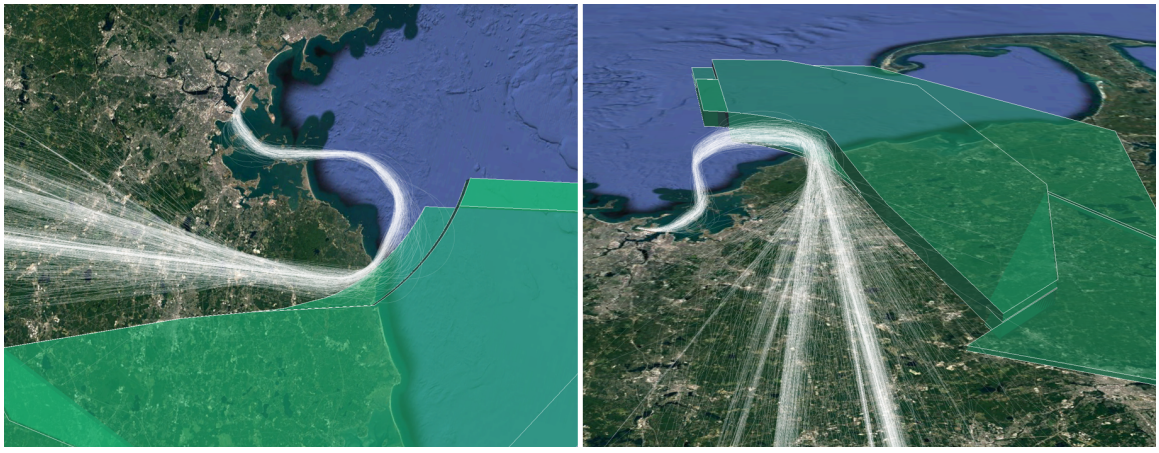

Figure 2-23: The green volume highlighted represent airspace unavailable to a westbound departure procedure due to it being allocated to southbound operations. The white tracks represent current aircraft trajectories on westbound departures off runway 22R.

It should be noted that a change in the airport's runway configuration will also change its sector structure and the associated sector boundaries. In the case of BOS, a second runway configuration that uses runway 22R for departures (and

runway 22L for arrivals) exists (Figure 2-24).

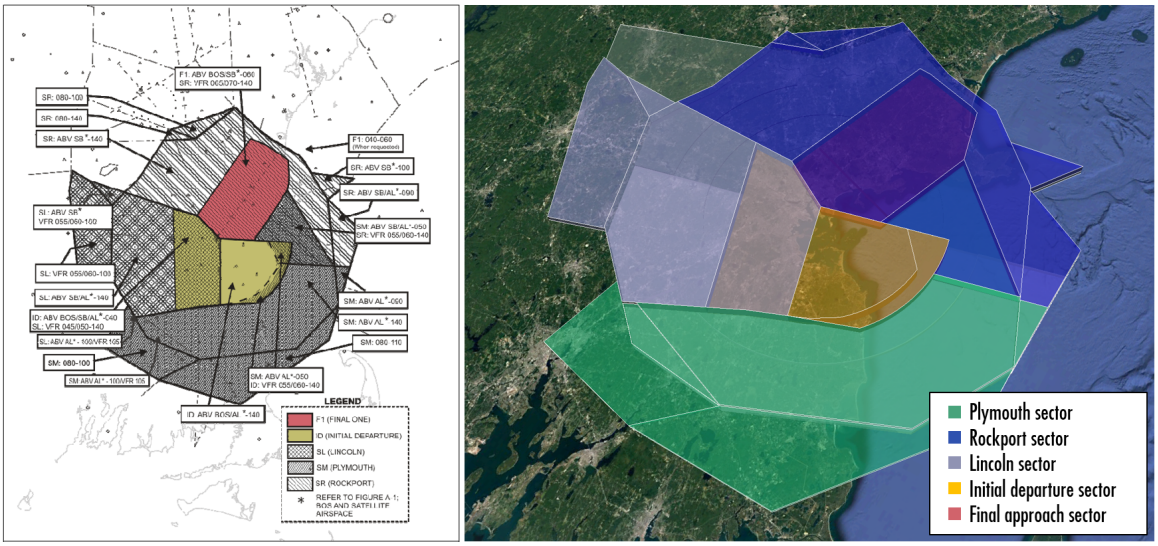

Figure 2-24: Left: Boston airspace sector structure for the 22/22 runway configuration [8]. Right: A matching 3D model of this airspace structure.

In this configuration, runway 27 is not used for arrivals, and as a result, the final approach sector restricts a smaller volume of the airspace (Figure 2-25).

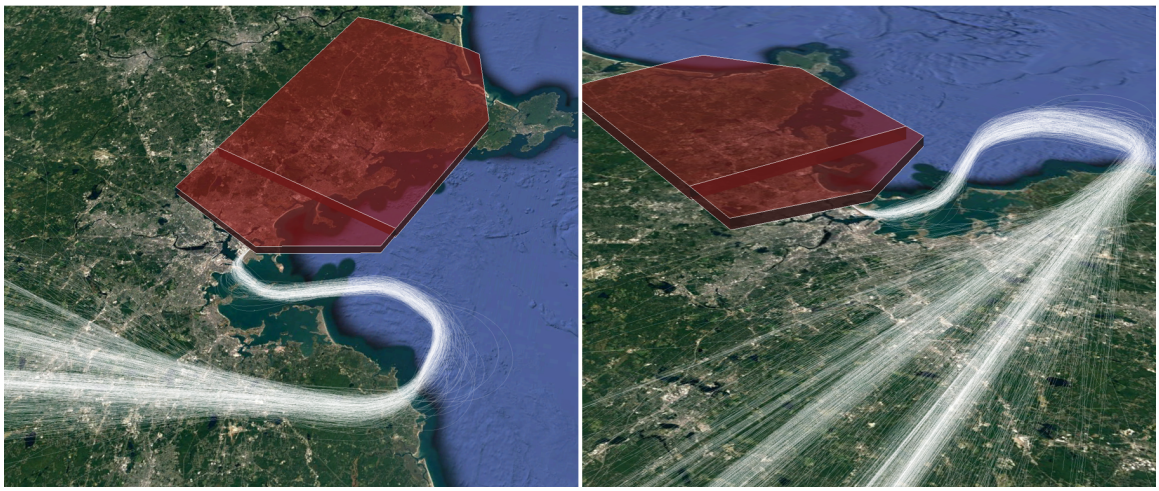

Figure 2-25: The red volume highlighted represents airspace unavailable to a departure procedure due to it being allocated to the *final approach controller* in the 22/22 runway configuration. The white tracks represent current aircraft trajectories on westbound departures off runway 22R.

If a flight procedure is intended for use in multiple runway configurations, it must be separated from the relevant sector boundaries of all applicable config-

urations.

3. *Combining Volumetric Airspace Constraints*

   Using the BOS runway 22R departure procedure example under the 27/22 runway configuration (landings on runway 27, departures from runway 22R), the volumetric airspace constraints identified thus far can be combined in a single graphic to illustrate the overall airspace volume that is unavailable to a westbound departure procedure due to ATC structure constraints (Figure 2-26).

Figure 2-26: The magenta volume highlighted represents the combined volumetric airspace constraints affecting a westbound departure procedure from runway 22R. They include airspace reserved for arrival and approach procedures, airspace reserved for the final approach controller, and airspace reserved for the south sector controller.

In this visualization, it can be observed that ATC structure constraints appear as significant constraints limiting the feasible geometric design space of a new flight procedure.

2.3.2 Visualizing Non-Volumetric Geometric Constraints

Visualizing Flyability Constraints

Flyability constraints manifest within the internal geometry of a flight procedure. As a result, they can only be illustrated once a complete candidate procedure is available. The two main flyability constraints affecting the geometry of PBN flight procedures are minimum leg length and turn angle constraints.

As discussed in a previous section, the minimum length allowed for a segment is computed based on the expected aircraft turning radius, the turn angle at the beginning of the segment, and the turn angle at the end of the segment. Once computed, the minimum leg length of a segment can be visualized as an overlay on the segment, as shown in Figure 2-10. Based on whether the actual length of a segment satisfies its minimum leg length constraint, the overlay can be colored to express this result accordingly (Figure 2-27).

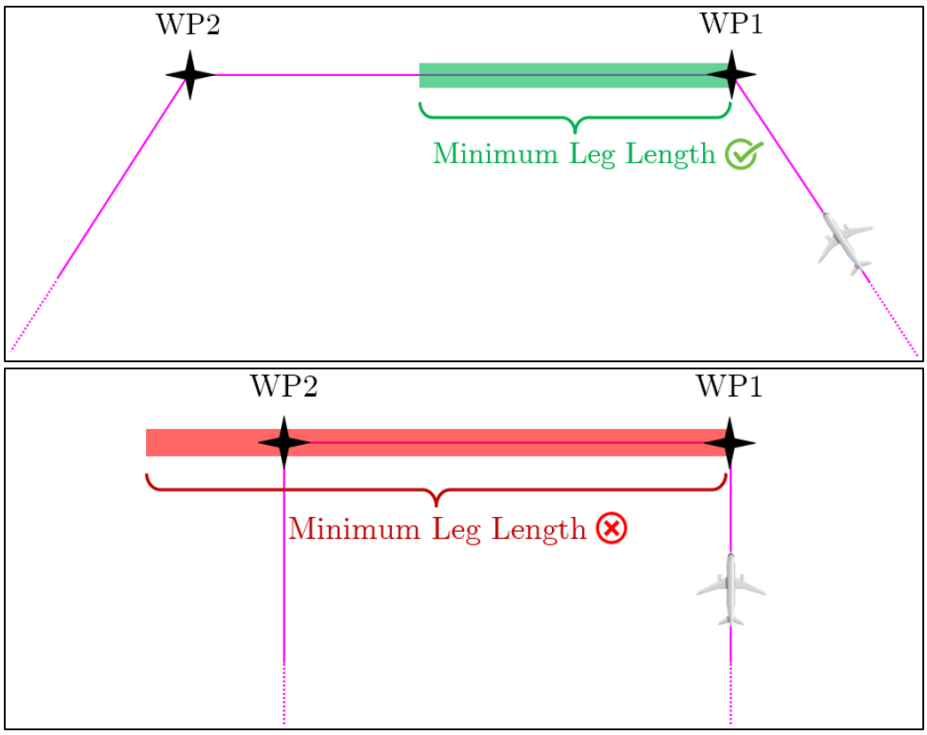

Figure 2-27: Top: Illustration of a segment that meets the minimum leg length constraint. Bottom: Illustration of a segment that violates the minimum leg length constraint.

Returning to the example of a current westbound departure procedure from runway 22R at BOS, the minimum leg length of each segment can be illustrated using the technique described above, as seen in Figure 2-28.

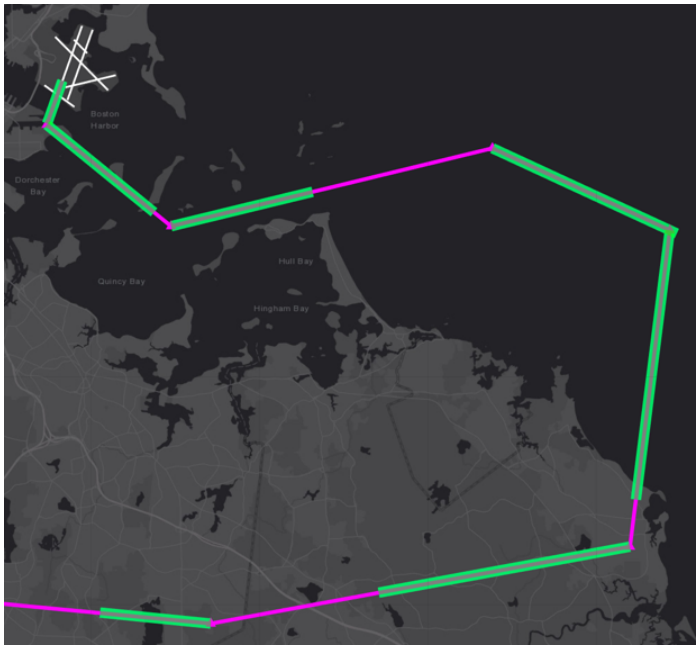

Figure 2-28: Minimum leg lengths are illustrated as shaded areas overlaid on each segment of this runway 22R departure at BOS. Since all minimum leg length constraints are satisfied in this case, they are all shaded in green.

To illustrate maximum turn angle constraints (e.g., maximum 90° turns at waypoints), an arc of available outbound headings can be overlaid on each waypoint of a procedure. Waypoints where the constraint is violated can then be highlighted, as shown in Figure 2-29.

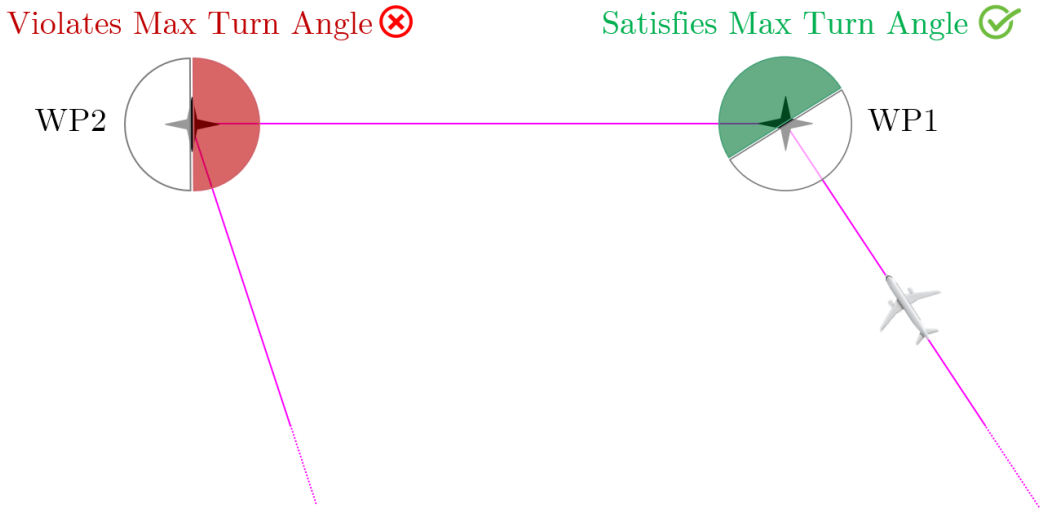

Figure 2-29: Illustration of the maximum turn angle constraint being satisfied at *WP1* but violated at *WP2*.

In the BOS example, the turn angle constraint can be illustrated as seen in Figure 2-30.

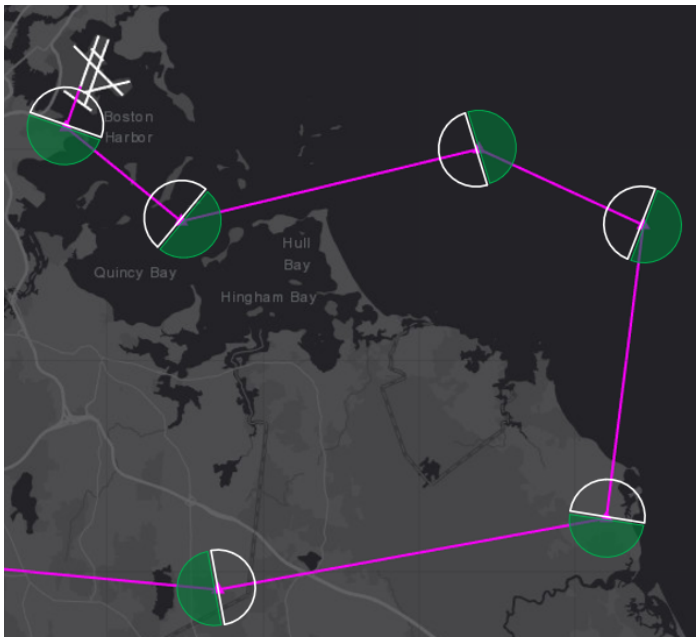

Figure 2-30: Illustration of available outbound headings at each waypoint of the current westbound departure procedure from runway 22R at BOS. Maximum turn angle constraints are satisfied at all waypoints, and are therefore colored green.

Finally, the visualizations of minimum leg length and turn angle constraints can be combined in a single graphic, shown in Figure 2-31.

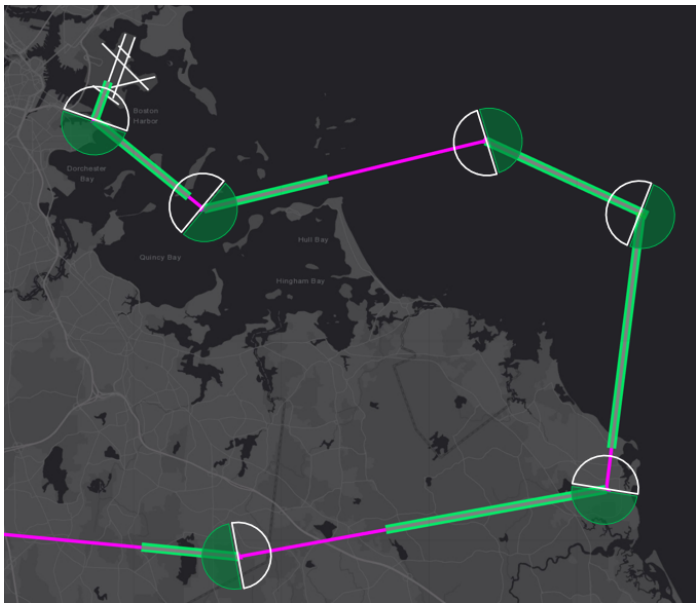

Figure 2-31: Combined illustration of minimum leg length and turn angle constraints for the current westbound departure procedure from runway 22R at BOS.

It is noted that the FAA's TARGETS software is capable of automatically calculating minimum leg lengths and maximum turn angles for a given flight procedure, though it offers no built-in visualization of these constraints.

2.3.3 Summary of Constraint Visualization

This section discussed techniques for visualizing geometric constraints, which were proposed as a method for identifying constraints and their effects on flight procedure flexibility. Volumetric constraints (terrain clearance and ATC structure) were found to limit the placement of a flight procedure within the airspace, while non-volumetric constraints (flyability) limit a procedure's internal shape. Volumetric constraints can be illustrated and visualized within the airspace without a candidate flight procedure being available. Conversely, non-volumetric constraints require a candidate procedure to be visualized.

In addition to its use as an analysis tool, the visualization of flight procedure constraints may be especially useful for communicating the effects of constraints to non-technical stakeholder groups, such as airport communities.

2.4 Potential Opportunity for Increasing Flexibility: Reevaluating Required Separation between Procedures

Among the constraints identified and discussed in this chapter, the required geometric separation between flight procedures appears as a major constraint limiting the geometric design space of procedures, and represents a constraint that scales unfavorably with the number of operations and procedures within an airspace.

It can be observed that several system improvements have occurred since the introduction of the current 3 NM lateral separation standard used to separate flight procedures, such as significant improvements in communication (e.g., Datalink), navigation (e.g., RNAV and RNP), and surveillance (e.g., ADS-B). As a result, it is hypothesized that opportunities may exist to reevaluate this constraint. To that end, the remainder of this work seeks to better understand how these and other technology improvements may affect the required separation between flight procedures, which may lead to opportunities to increase flexibility.

The next chapter presents a literature review of prior efforts to understand and evaluate the required separation between flight procedures.

Chapter 3

Literature Review

This chapter offers a literature review of topics relevant to the reevaluation of aircraft separation, including prior efforts to reevaluate the required separation between flight procedures, the general concept of a Target Level of Safety (TLS) as a change acceptability criterion, and prior efforts to develop collision risk models that serve as analysis tools for demonstrating the safety of proposed separation changes.

3.1 Historical Development of Separation Standards and Basis for Acceptable Separation

A potential challenge in the reevaluation of legacy constraints is that the rationale and assumptions behind them may not be obvious or documented. In the case of the required separation between flight procedures in terminal airspace, the standard separation criteria of 3 NM or 1000 ft was originally introduced in the 1950s and lacks a documented rationale. One FAA document from the early 1970s, for instance, asserts that *"no rationale exists for the broadband radar minima"* [18]. Past research found that the development of this standard was most likely a product of subjective stakeholder consensus, with the chosen criteria thought to implicitly consider factors such as radar accuracy, display target size, and human reaction time [19].

Current FAA safety policy in the United States, known as the Safety Manage-

ment System (SMS), identifies safety criteria that all proposed changes to air traffic operations must meet. Under this policy, all hazards associated with a change that have potentially catastrophic consequences must be demonstrated to meet a 10^{-9} target level of safety [20]. In the context of a change to the separation between flight procedures in terminal airspace, this means that a proposed change must not increase the rate of midair collisions above 1 in 1 billion operations (i.e., 10^{-9} collisions per operation). While the current target level of safety value of 10^{-9} is a relatively recent requirement, historical efforts to reevaluate separation have always involved demonstrating a certain level of safety as the primary basis for change acceptance.

Because direct observation of collision rates associated with a change is impossible before the change is implemented, demonstration of a given level of safety has historically been achieved through a type of mathematical analysis known as *collision risk modeling*. The following sections review the historical development of collision risk models, discuss the concept of a target level of safety, and review factors motivating historical efforts to change separation.

3.2 Collision Risk Modeling

A Collision Risk Model (CRM) is a mathematical model used to numerically estimate the risk of collision between aircraft in a given operation. The first documented collision risk model was developed in 1963 [21]. An improved version of this model known as the Reich Collision Risk Model [22, 23] became, in 1968, the first model to be accepted by regulators for the purpose of defining the minimum separation between aircraft routes [24]. The Reich CRM provides estimates of the risk of collision between aircraft tracking two routes or procedures as a function of the probability density functions of aircraft position along each route, which can be derived from historical aircraft trajectory data [25]. The Reich model was used in 1968 to determine the minimum lateral separation between air traffic routes in the North Atlantic airspace. In that instance, the study concluded that North Atlantic routes must be laterally separated by 120 nautical miles to be acceptably safe. To manage uncertainty in

risk estimates, the North Atlantic study identified the need for all assumptions made in the modeling to be conservative, an approach to risk estimation that is still used today. In other words, overestimating the risk of collision between aircraft is perceived as acceptable since this naturally produces a safer outcome in practice. Conversely, an underestimation of the risk is seen as unacceptable.

Before the introduction of the Reich model, it was believed that the minimum lateral separation between routes should be set based on the standard deviation of the distributions of lateral position error on each route. During application of the Reich model to the North Atlantic separation problem, however, it was identified that the distribution of lateral deviations had notably thicker tails than a standard Gaussian distribution. This led to the conclusion that the standard deviation metric was a poor estimate of the total risk, since tail events contributed a significant portion of the risk [24]. More than 14,000 radar measurements of lateral position errors on North Atlantic tracks were obtained at the time to determine more accurate distributions of aircraft lateral behavior. The statistical models created from this data were used to compare the estimated risk of lateral collision between oceanic tracks separated by 90 and 120 nautical miles. The risk estimate obtained for the 90-mile separation case was 6×10^{-8} collisions per flight hour, and for the 120-mile case it was 1×10^{-8}. Given that both results relied on identical modeling assumptions, the relative difference between the two risk estimates (a factor of 6) was used to subjectively justify maintaining the separation at 120 nautical miles at the time. It should be noted that the Reich model does not consider the effect of air traffic control surveillance on the risk, and assumes that potential collision events are always unmitigated.

The first application of collision risk modeling in terminal airspace occurred as part of efforts to reduce the minimum required lateral separation between simultaneous approaches to closely spaced parallel runways. At airports with parallel runways, the ability to land aircraft on both runways simultaneously in instrument conditions is known to offer increased throughput [26]. As a result, several studies have attempted to model the risk of collision between aircraft flying parallel Instrument Landing System (ILS) approaches in an effort to reduce the minimum lateral separation required

between them [27]. As this minimum separation is reduced, more airports with parallel runways are able to operate them simultaneously, therefore improving the overall capacity of the air traffic system. Similar to previous findings from oceanic studies, studies of the parallel approach scenario identified that the risk of collision between two ILS approaches is dominated by abnormal deviations from the localizer. During development of collision risk models for this scenario, MITRE proposed a *worst-case blunder model* as a method for modeling abnormal deviations and estimating their impact on the overall risk. Given the rarity of actual deviations and the difficulty of observing them in practice, the MITRE model assumed that worst-case deviations would involve aircraft flying at a fixed 30° lateral angle away from their assigned trajectories [28]. No specific technical basis seems to exist for the choice of a 30° deviation angle, though it is noted that this matches the standard angle at which aircraft intercept the localizer during an ILS approach. Use of 30° as a worst-case deviation angle has continued in other safety studies since, and it has remained a general consensus among FAA, airline industry, pilots and air traffic controllers that protection against this value is adequate [29]. Results of several collision risk modeling studies have led to gradual reductions in the minimum separation between independent parallel ILS approaches, down to 4300 ft in 1974, 3400 ft in 1991, and 3200 ft in 2021 [29, 6].

More recent collision risk modeling efforts in terminal airspace have been successful at reducing the minimum lateral separation between two RNP AR approaches to parallel runways, known as *Established-on-RNP* (EoR) operations, and at reducing the minimum divergence angle between two RNAV departures, known as *Equivalent Lateral Spacing Operations* (ELSO).

The EoR concept involves the use of simultaneous RNP AR approaches to parallel runways, with curved flight procedure segments (known as RF legs) defining the path from downwind to final. Due to the shorter GPS-defined path of RNP approaches, this concept offers fuel savings for participating aircraft. The collision risk model developed for analysis of the EoR concept assumes that the risk of collision between aircraft on two RNP approaches is dominated by abnormal deviations from the procedure, based on findings from prior ILS studies. To determine this component of the

risk, the model assumes that aircraft may experience a navigation failure at a random location along the procedure's curved RF segment, leading them to fly in a straight line towards the adjacent procedure [30]. The EoR study included an early attempt at modeling the effects of pilot and controller intervention on the risk [31]. Distributions of pilot and controller response times to a deviation were derived from small-scale human-in-the-loop (HITL) trials using simulators [30]. During the modeling of deviation trajectories, random samples were extracted from these distributions, and human responses were modeled as changes to the original deviation trajectory. The overall collision risk of the operation was calculated by generating and evaluating several of these modeled deviation trajectories. Having received regulatory approval in 2017, the EoR concept currently allows for the operation of simultaneous independent RNP AR approaches to parallel runways separated by 3600 ft or more.

The ELSO concept was originally pursued to allow the Hartsfield-Jackson Atlanta International Airport (ATL) to operate additional independent departures from parallel runways when aircraft are using RNAV departure procedures. Prior to ELSO being implemented in 2011, aircraft departing simultaneously from two of Atlanta's five parallel runways were required to diverge by at least 15° during the initial departure segment to meet separation rules. This required angle limited the number of runways that could be used for parallel departure operations. Based on projected throughput and efficiency benefits that a potential reduction of this minimum divergence angle could offer, a safety analysis was conducted by MITRE and the FAA to determine whether the tracking precision granted by RNAV could allow a reduction in the minimum divergence angle between simultaneous RNAV departure to 10° [32]. The collision risk model used in the ELSO study was a modified version of the Reich model discussed previously, and did not consider the possibility of blunders or deviations from the nominal flight tracks. This choice was made with the assumption that a reduction in the divergence angle would not significantly change the risk posed by deviations [33]. Instead, the study focused on developing statistical models to describe the nominal tracking performance of aircraft on RNAV departure procedures, which were created based on ASDE-X (i.e., surveillance) data collected

at the airport. This collision risk model was used to demonstrate that a reduction in the minimum divergence angle to 10° satisfied a 10^{-9} target level of safety, which led to the regulatory approval of ELSO. In Atlanta, the FAA has reported that the implementation of ELSO, along with a redesign of the RNAV departure procedures, enabled the airport to handle 12 additional departures per hour, therefore providing a significant throughput benefit [34].

Latest efforts in the United States to reevaluate separation standards in terminal airspace have been led by the FAA's Flight Technologies and Procedures Division (AFS-400), and have focused on further lowering the separation between approaches to parallel runways [35, 36, 37]. These recent FAA studies have relied on more sophisticated simulation tools such as the Airspace Simulation and Analysis Tool (ASATng) to estimate the risk of new proposed operations. ASATng uses statistical models of aircraft navigation performance, environmental conditions, surveillance performance, and human performance (i.e., pilot and ATC response times) to generate a large number of hypothetical aircraft trajectories and operational conditions [38]. By simulating the evolution of these aircraft trajectories in a continuous-time environment, the tool provides a Monte Carlo-based approach for estimating collision risk. While the data available to ASATng allows for reliable estimates of the risk in normal operations, aircraft deviation behaviors remain poorly understood, and modeling of abnormal behaviors remains based on hypothetical worst-case deviations.

3.3 Prior Efforts to Model Mitigations

Estimating the risk of collision due to abnormal deviations from flight procedures presents many challenges, including understanding how available collision mitigation capabilities, such as ATC tactical intervention, may affect the risk. The system's response to a deviation, which attempts to prevent it from resulting in a collision, is known as a *mitigation*. Prior collision risk studies involving parallel runway operations have attempted to quantify the effect of ATC-based mitigation on the risk by modeling the response processes of both controllers and pilots [39, 31]. In these studies, the

mitigation response was modeled as the combined response of controllers and pilots to produce a total time elapsed before a correcting maneuver is initiated by an aircraft. Controller and pilot response times have historically been derived from human-in-the-loop studies using simulators [40, 41]. While this approach can capture some of the effects of mitigations on the risk, it is argued to be limited in two aspects: 1) the mitigation performance is treated as a static property of the system and not as a potential system design variable, and 2) only traditional ATC intervention is considered, with other potential mitigations such as TCAS not being evaluated.

The development and implementation of the Precision Runway Monitor (PRM) for parallel ILS approaches in the 1990s represents a key instance of a mitigation system being designed as part of efforts to reduce the separation between procedures. The PRM project identified low controller response time during aircraft deviations from a localizer as a key requirement for enabling lower separation between ILS procedures [39]. To enable faster controller response, the resulting PRM system design included a high-update-rate surveillance radar, automated deviation alerting for controllers, and the addition of a dedicated air traffic controller whose sole responsibility was the monitoring of the airspace between two parallel runways [42]. During PRM operations, the mitigation system issues an alert whenever an aircraft is predicted to enter a predesignated *No Transgression Zone* (NTZ) within 10 seconds, with the distance between the localizer and the NTZ typically being 700 ft (Figure 3-1).

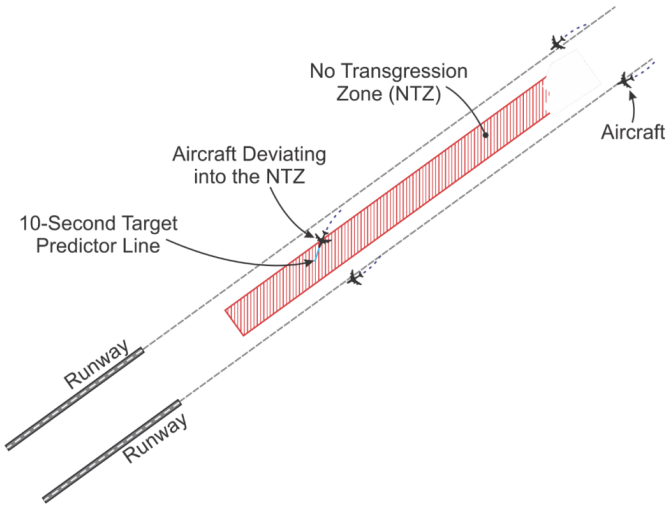

Figure 3-1: During PRM operations, an alert is generated if an aircraft is predicted to enter a No Transgression Zone within 10 seconds. Image source: Federal Aviation Administration [36].

Further development of the PRM concept took place in the late 1990s and early 2000s through the development of the Airborne Information for Lateral Spacing (AILS) system. AILS was envisioned as an airborne system that could replace or complement the monitoring controller in PRM approaches with an automated flight deck alerting system, potentially offering lower mitigation response times and even lower separation between approaching aircraft [43]. The AILS alerting system was designed for the airborne detection of deviations by "paired" aircraft through ADS-B position reports. Due to it requiring additional changes to flight deck avionics, flight crew training, and ATC procedures, the system did not achieve large-scale deployment.

During studies of the PRM and AILS systems, the effect of mitigations on the collision risk between parallel ILS approaches was modeled based on several efforts to quantify and understand pilot and controller response times. In addition, several studies were conducted to identify adequate mitigation maneuvers for the parallel approach case [44].

PRM and AILS remain the only mitigation systems known to have been developed with the specific purpose of enabling lower separation values between flight

procedures. Although PRM was successfully deployed, its application has remained limited to the specific scenario of parallel instrument approaches, and instances of similar mitigation systems being planned for general terminal operations are not known.

While the effects of TCAS on collision risk have historically not been credited during collision risk assessments, this appears to be a conservative policy decision given the perceived uncertainty around collision risk estimates [45, 46]. From a purely technical perspective, the availability of TCAS is expected to further reduce the collision risk in the event of a deviation. Safety assessments of TCAS have historically been performed in isolation from any specific operational scenario, and have focused on quantifying the probability of a successful conflict resolution using general event trees and conflict geometries [47]. Due to these capabilities not being credited towards operational safety, the results of these analyses have traditionally not been integrated into the evaluation of collision risk between flight procedures.

Given the potentially significant effect of mitigations on collision risk, and given that the consideration of mitigations in past studies has been limited to a few specific scenarios (e.g., parallel instrument approaches), it is hypothesized that the more systematic treatment of mitigations as a potential system design variable for planning general terminal operations could represent a key mechanism for identifying opportunities to enable closer separation between procedures in the future.

3.4 Target Level of Safety

Once the risk associated with an operation has been determined, the acceptability of that risk must be decided. The concept of a Target Level of Safety (TLS) has been adopted by aviation regulators worldwide to address this and set a maximum acceptable risk threshold for policymaking purposes. A target level of safety is quantified as the maximum acceptable number of fatal accidents that an operation may cause during a given exposure period. For terminal operations, this exposure period is typically one operation or transit of a flight procedure, while in enroute airspace

the exposure period considered is typically one flight hour [20].

Use of the TLS concept to analyze the acceptability of changes to air traffic operations was first documented in the 1960s during efforts to change the minimum lateral spacing between North Atlantic tracks. In that instance, the rate of accidents in the North Atlantic airspace was first measured for a 10-year period to determine the baseline risk. Based on this statistic, and by applying a desired improvement factor of 2 to the then-current risk, the TLS for oceanic operations was set at 2×10^{-8} collisions between aircraft on laterally separated tracks per flight hour [48]. Given the throughput observed in North Atlantic airspace at the time, it was estimated that this corresponded to one collision every 150 years.

In the decades that followed, the TLS used in risk analyses of aviation operations was typically set by the requirement that an operational change must not increase the risk for a particular phase of flight above that of existing operations. During the Precision Runway Monitor (PRM) program pursued in 1992 in an effort to reduce the minimum separation between parallel ILS approaches, for example, the TLS was set at 4×10^{-6} accidents per operation [19]. While higher than previous TLS values used for enroute cases, this matched the then-current accident rate during approaches in instrument conditions, which was regarded as a more hazardous phase of flight. This type of relative risk analysis approach can be beneficial when the proposed change is not expected to lead to a risk increase (e.g., increasing separation), and may offer shorter approval processes compared to the demonstration of an absolute TLS.

Current FAA safety policy in the United States, known as the Safety Management System (SMS), requires any proposed changes to air traffic operations to meet a 10^{-9} target level of safety when it poses hazards with catastrophic consequences (e.g., a midair collision). Introduction of the SMS policy has driven the application of a fixed 10^{-9} target level of safety to all proposed changes within the National Airspace System (NAS), which in many scenarios has resulted in a more strict TLS value being enforced in new risk analyses.

Latest aviation accident statistics published by the International Air Transport Association (IATA) and Boeing suggest that the worldwide rate of fatal aviation

accidents involving jet aircraft has averaged approximately 0.1 for every 1 million departures (i.e., 1×10^{-7} per operation) over the last 10 years [49, 50]. The same metric is approximately 0.04 for every 1 million departures (i.e., 4×10^{-8} per operation) for the North American region. This data is shown in Figure 3-2. It should therefore be noted that the actual rate of fatal accidents in North America currently exceeds a 10^{-9} TLS by a factor of approximately 40 based on IATA statistics [49]. In this regard, the 10^{-9} TLS can be regarded as an aspired level of risk during planning of the airspace system.

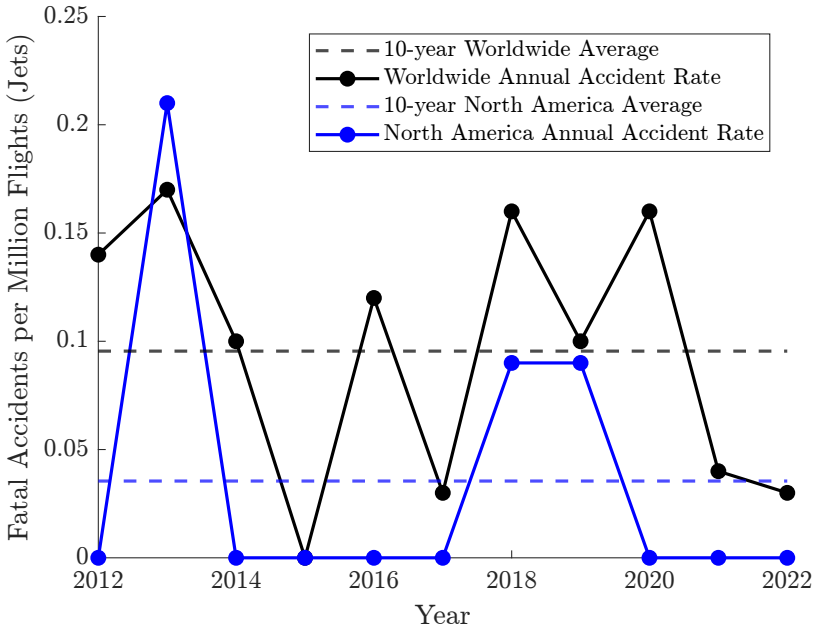

Figure 3-2: Worldwide (black) and North America (blue) rate of fatal aviation accidents involving jet aircraft between 2012 and 2022. Data source: International Air Transport Association (IATA) [49].

3.5 Societal Perception of Risk

The enforcement of a target level of safety can be regarded as an indirect expression of a societal risk threshold, and many researchers in the risk literature have attempted to relate the concept of a quantitative TLS to societal expectations [48, 51, 52, 53]. Societal perception of risk is considered a complex sociotechnical variable that can be affected by a variety of factors. Because this perception may affect the choice of

a TLS enforced on the system, Fischhoff describes a person's perception of risk as depending on "*how well the risk is understood, how equitably the risk is distributed across the population, how well individuals can control the risk they face, and whether the risk is assumed voluntarily or is imposed on people without their approval* [52]." Tversky posits that people's thresholds for risk are commonly derived from the perceived likelihood that a hazardous event could happen during their lifetime. In other words, "*there is a strong perceptual preference for risk elimination within the frame of reference of one's life expectancy* [54]." Based on this hypothesis, an acceptable risk threshold is one that puts the expected frequency of an event outside of an individual's lifetime. Keeney observed that people's perception of risk is also affected by the number of fatalities potentially involved in a single accident. This effect is known *catastrophe avoidance*, and describes the fact that "*most people feel that a small probability of a catastrophic loss of life is worse than a larger probability of a smaller loss of life* [55]," an effect that can be observed when comparing societal risk tolerance towards aviation and road accidents. Rowe additionally posits that society's threshold for risk is not static and in fact changes over time as the technology and institutions built around the system in question evolve [56]. According to this theory, society's tolerance for risk in air transportation is expected to decrease as the public becomes aware of improvements in technology and regulations. This, in turn, could lead to increasing target levels of safety over time.

The pros and cons of using a discrete target level of safety in policymaking have been a target of some debate. Barnett points out that the use of a discrete TLS assumes that societal tolerance for risk is a step function, and that it does not consider the tradeoff between economics and the risk of a proposed change. According to him, this can be illustrated by recognizing that a large change to the risk of an operation that remains below the TLS but which offers only marginal economic benefit would be acceptable under the TLS concept. Conversely, a small change to the risk that slightly violates the TLS but which offers significant economic benefits would not [57]. Machol asserts that *"the concept of a TLS is in fact well-established and, in many cases, unavoidable."* According to him, the use of a "hard-and-fast" standard

is a necessary element of risk policy that facilitates the communication of risk, and similar concepts can be observed in regulations applicable to water and air quality [53].

3.6 Changes in the Air Transportation System

The reevaluation of the required separation between flight procedures can be framed as a problem of change management in the air transportation system. Today's system is a complex evolved system with diverse stakeholders and mixed capabilities, to which safety is the highest value objective. While its impressive safety track record surpasses that of other transportation systems, this safety record has contributed, to a certain degree, towards resistance to change.

Past research into change processes in aviation suggests that successful system changes have been traditionally been linked to strong transition drivers [58]. The main drivers of transition are observed to be safety, security, capacity, efficiency, environmental, and access. Many historical large-scale changes within the air transportation system have been motivated by safety concerns. In many of these cases, a safety event such as an aircraft accident can be observed to have acted as a catalyst in initiating and building momentum for the change. Examples of these changes include the development and deployment of early enroute radar systems, the Traffic Collision Avoidance System (TCAS), and the Ground Proximity Warning System (GPWS). On the other hand, changes motivated by other factors such as capacity and efficiency often lack a catalytic event to stimulate change to the same degree [58]. For these cases, awareness of a problem or opportunity is typically built gradually among the relevant system stakeholders.

Once enough awareness of a problem or opportunity exists among stakeholders of the system, the change process generally progresses through stages of objective definition, action selection, and solution implementation. Detailed evaluations of change feasibility, such as the safety assessment of separation changes, occur in the solution implementation phase of the change process (Figure 3-3).

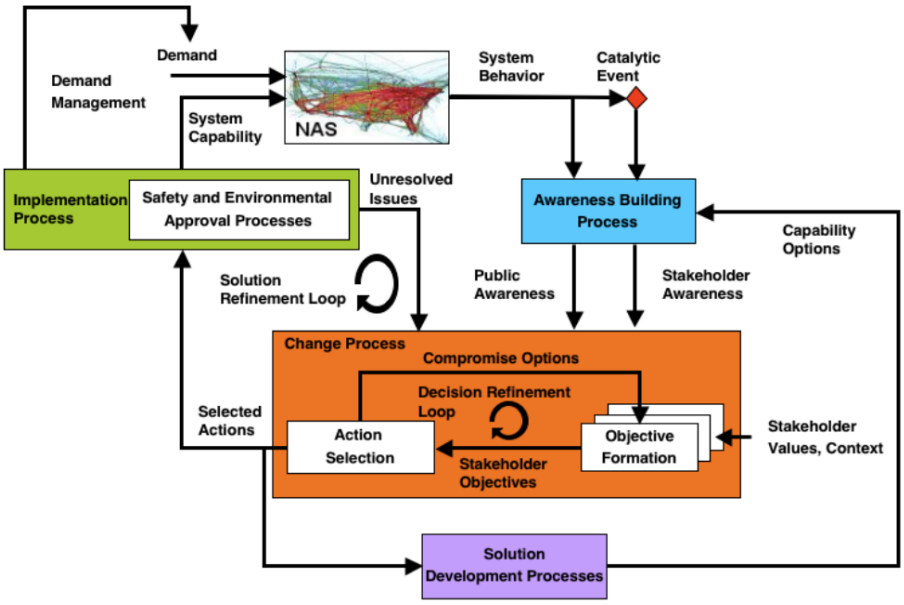

Figure 3-3: Transition model for the air transportation system [58].

Weibel identified that a key challenge in the implementation of large-scale changes is an increased scope of the safety analysis required, which in some cases may require the development of new analysis tools and methodologies [59].

In considering the likelihood of stakeholder support for a change, past research identifies that the distribution of costs and benefits associated with a change is a key determinant of change support. Changes with symmetric costs and benefits, meaning those whose associated costs and benefits are evenly distributed among stakeholder groups, are found to be more likely to garner stakeholder support [60]. When considering the benefits of potential changes to separation, the consideration of diverse stakeholder groups may therefore be beneficial for creating momentum for a change.

3.7 Benefit Analyses Supporting Constraint Reevaluation

Efforts to reevaluate separation changes must be motivated by the identification of potential benefits in system performance, due to the cost and resources needed to pursue regulatory changes. Historically, the majority of changes to air traffic oper-

ations have been motivated by potential capacity improvements. For example, in both the North Atlantic and the parallel ILS approach cases, a key factor motivating the pursuit of lower separation was the expectation that delays would increase significantly in the future as traffic was projected to grow. A lower separation value, it was posited, would allow for higher system capacity and therefore keep delays in check. The identification of such capacity "bottlenecks" has therefore served as a strong driver for change [19].

More recently under NextGen, a wider set of benefit metrics have been considered by stakeholders to motivate regulatory changes. When analyzing the potential benefits associated with reductions in separation, more recent studies have considered metrics such as track miles, climb continuity, departure delay, and daily maximum throughput [32, 61]. In addition, benefits of NextGen initiatives have been evaluated at several airports across the NAS to understand their effects at a system level. While this type of benefit analysis represents a step forward in considering a wider set of potential benefits, the majority of benefit metrics used remain operator-focused. In particular, community-focused metrics such as aircraft noise impacts have traditionally not been considered a driver of separation changes, despite significant industry efforts in other areas to reduce aviation noise, such as in the design and certification of increasingly quieter engines.

Jensen analyzed the potential aircraft noise exposure benefits from optimizing aircraft approach paths at 35 major airports in the United States. He found that by optimizing aircraft approach trajectories for minimum population noise exposure, up to 402 million fewer significant noise events would be experienced daily by communities at the 35 airports [15]. Since this result is based on an unconstrained analysis with no consideration of procedure separation constraints, it is likely that an increase in flight procedure flexibility through lower separation values between published procedures would make a larger number of these noise-optimal trajectories available.

In considering the potential benefits of a change, it is posited that both the scale and the breadth of the benefit analysis are important in the formulation of future change proposals. Scale-wise, a change may be more likely to be prioritized if benefits

can be scaled to multiple areas or parts of the National Airspace System (NAS). In terms of breadth, by expanding the pool of benefits evaluated to include the objectives of multiple stakeholders, more opportunities for improving system performance may be identified.

3.8 Limitations Identified and Proposed Contribution

In this literature review, the treatment of mitigations was identified as a limitation of past collision risk assessments of flight procedures operating in terminal airspace. In many of the cases in which mitigations were considered in previous collision risk assessments, mitigation performance was found to have been treated as a static property of the system and not as a potential system design variable. Other studies that have conducted more detailed assessments of mitigations were found to be limited to the scenario of parallel instrument approaches and have not considered general terminal operations.

Due to the potentially significant effect of mitigations on the collision risk between flight procedures, it is hypothesized that the more systematic treatment of mitigations as a potential system design variable in the planning of general terminal operations could represent a key mechanism for identifying opportunities to reevaluate the required separation between procedures. As such, the remainder of this work will be dedicated to the study of the collision risk between flight procedures in terminal airspace under the effect of mitigations, which could lead to the identification of more effective mitigations and potential opportunities to enable closer separation between procedures in the future.

Chapter 4

Evaluating Mitigated Collision Risk

In Chapter 3, the collision risk between flight procedures was identified as the main metric by which a change in separation is evaluated for its acceptability. In the United States, the FAA Air Traffic Organization's Safety Management System (SMS) requires the risk of aircraft collisions to meet a Target Level of Safety (TLS) of 10^{-9} per operation/per flight hour, which is defined as the highest acceptable frequency of catastrophic hazards [20]. As a result, any proposed change to separation must be demonstrated to meet this requirement. This is typically accomplished through collision risk modeling, a process that attempts to numerically estimate the risk associated with an operation.

During the review of past efforts to reevaluate the required separation between procedures based on collision risk modeling, it was found that, outside of the parallel instrument approach case, previous analyses often had a limited treatment of collision mitigation capabilities and how they affect the overall collision risk. Because the effect of mitigations on the real system risk may be significant, this chapter seeks to develop a better understanding of the collision risk between geometrically separated flight procedures under the effect of mitigations.

The following sections discuss how the risk between flight procedures can be parsed and evaluated, and identify key parameters in both flight procedure and mitigation design that may be used to control the collision risk between procedures.

4.1 Scope of Collision Risk Analysis

This study defines collision risk as the expected number of midair collisions experienced by a single flight or operation during transit of a flight procedure, which is expected to be a number much lower than 1.

The analysis discussed in this chapter considers the collision risk between two geometrically separated flight procedure segments bounded by waypoints (Figure 4-1). In addition, due to lateral separation being the more common and more conservative dimension of geometric separation applied between procedures, the analysis of collision risk between laterally separated procedures is chosen as the focus of this discussion.

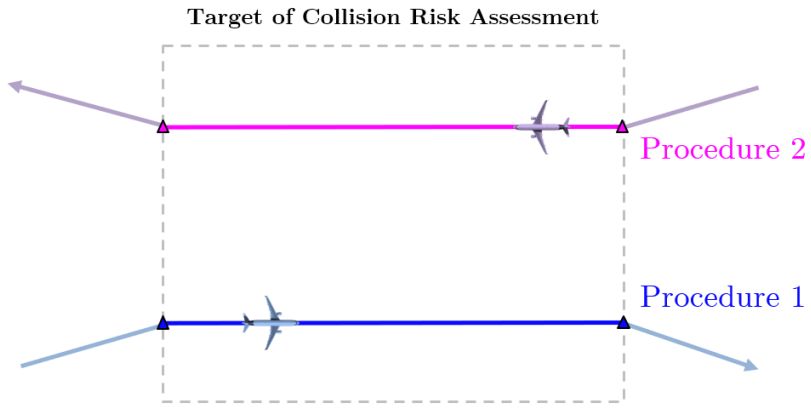

Figure 4-1: The collision risk analysis discussed in this chapter considers the collision risk between two geometrically separated flight procedure segments bounded by waypoints.

When illustrating risk calculations in this chapter, an example case of parallel, laterally separated flight procedures is used. This case is treated as a worst case (i.e., highest risk) for two laterally separated procedures, in which the minimum allowed separation between the procedures is held for the entire length of the two segments. In addition, as will be discussed later, the angles at which aircraft intercept two parallel segments may also cause additional variation in the risk of this assumed worst case.

Note that the case of crossing procedures in which aircraft are separated in time is outside the scope of this study, but may become relevant in future Trajectory-Based Operations (TBO).

4.2 Parsing Collision Risk

The collision risk between two geometrically separated flight procedures can be parsed into **Normal Risk** and **Non-Normal Risk**, which originate from distinct processes.

Normal Risk is defined as the risk experienced when all aircraft are tracking their assigned flight procedures, and any deviations from the procedures are a result of expected navigation errors (Figure 4-2). Normal risk is primarily controlled in the design of procedures by geometrically separating them.

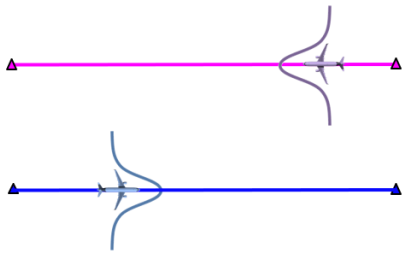

Figure 4-2: During normal operations, position errors are a result of expected navigation errors.

Non-Normal Risk is defined as the risk experienced when at least one aircraft is no longer tracking its assigned flight procedure due to a non-normal event, and deviations outside the nominal range of navigation errors are possible. Examples of non-normal events that may induce a deviation include navigation system failures, engine failures, and pilot errors. During an operation, a deviation may occur in either one of the two procedures, or in both procedures simultaneously (Figure 4-3). Non-normal risk is controlled both in the design of the procedures and in operations through the use of mitigations.

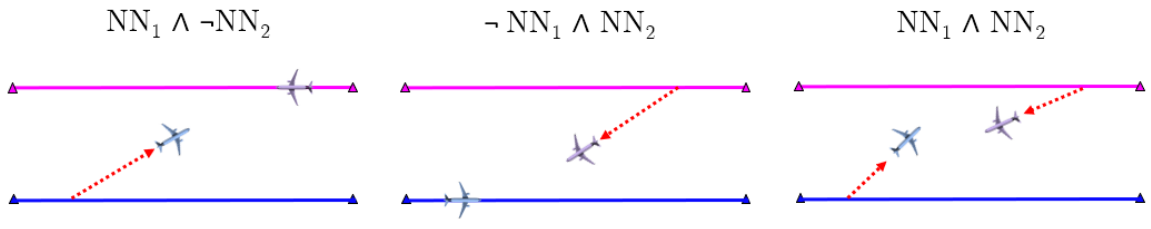

Figure 4-3: Possible non-normal scenarios include deviations from either procedure (NN_1, NN_2) as well as simultaneous deviations from both procedures.

The total collision risk between aircraft on two flight procedures is the sum of normal and non-normal risk components and can be expressed as follows, where *Normal* conditions are abbreviated as $\boldsymbol{N}$ and *Non-Normal* conditions are abbreviated as $\boldsymbol{NN}$:

$$\begin{aligned} Collision\ Risk = {} & P(N) \times P(Collision \mid N) \\ & + P(NN_1, \neg NN_2) \times P(Unmitigated\ Collision \mid NN_1, \neg NN_2) \times \\ & \quad [1 - P(Mitigation \mid NN_1, \neg NN_2)] \\ & + P(\neg NN_1, NN_2) \times P(Unmitigated\ Collision \mid \neg NN_1, NN_2) \times \\ & \quad [1 - P(Mitigation \mid \neg NN_1, NN_2)] \\ & + P(NN_1, NN_2) \times P(Unmitigated\ Collision \mid NN_1, NN_2) \times \\ & \quad [1 - P(Mitigation \mid NN_1, NN_2)] \end{aligned} \tag{4.1}$$

Where $P(N)$ is the probability of normal operations, $P(Collision \mid N)$ is the probability of collision during normal operations, $P(NN_1, \neg NN_2)$ is the probability of a non-normal event happening in *Procedure 1* but not in *Procedure 2*, *P(Unmitigated Collision* $\mid NN_1, \neg NN_2$) is the probability that an unmitigated deviation from *Procedure 1* will result in a collision, and $P(Mitigation \mid NN_1, \neg NN_2)$ is the probability that this deviation is successfully mitigated. The remaining terms follow the same notation.

While the occurrence of simultaneous deviations from both procedures may be plausible under certain environmental conditions that include GPS outages and spoofing, this study will focus on evaluating a class of problems in which such conditions are assumed to have an extremely remote probability of occurring. As such, deviations are treated as rare and independent events, leading to deviations from different procedures being treated as mutually exclusive events. With this simplification, the collision risk between aircraft on two flight procedures can be parsed according to the diagram shown in Figure 4-4.

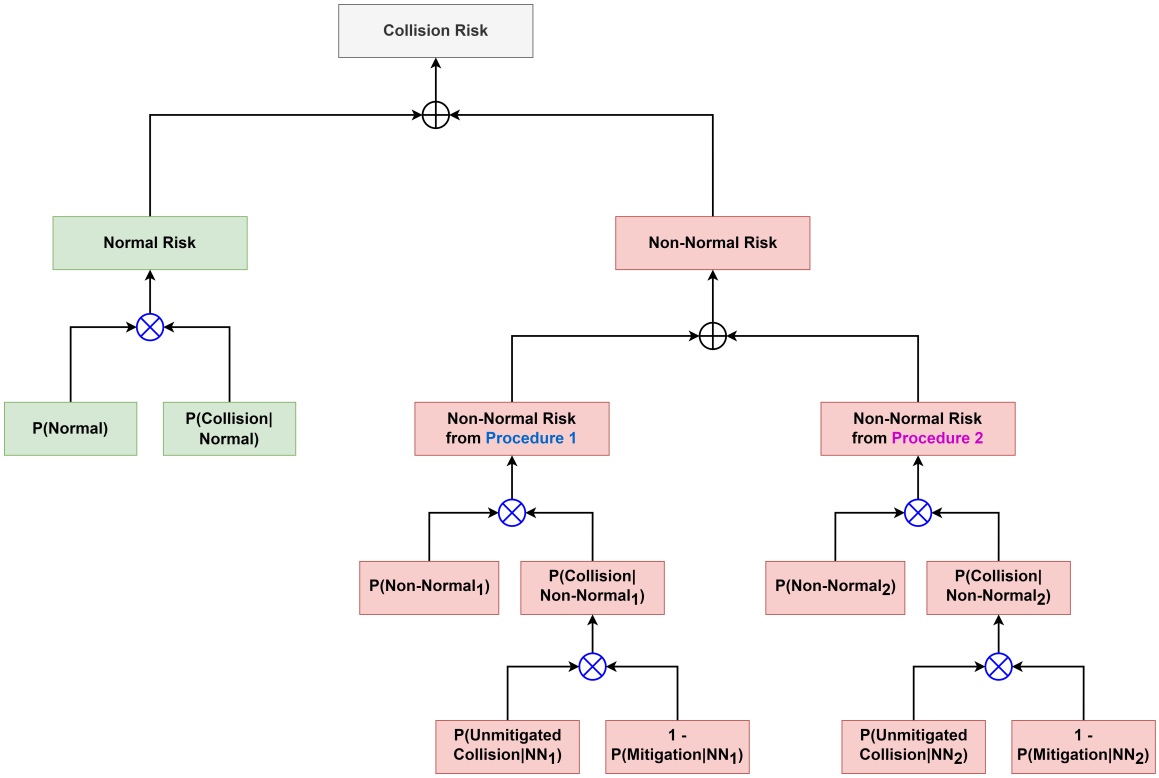

Figure 4-4: Parsing of the collision risk between geometrically separated flight procedures, which includes both normal and non-normal components.

The equation form of this diagram is provided below:

$$\begin{aligned} &Collision\ Risk = P(N) \times P(Collision \mid N) \\ &+ P(NN_1) \times P(Unmitigated\ Collision \mid NN_1) \times [1 - P(Mitigation \mid NN_1)] \\ &+ P(NN_2) \times P(Unmitigated\ Collision \mid NN_2) \times [1 - P(Mitigation \mid NN_2)] \end{aligned} \tag{4.2}$$

A detailed description of the individual terms of this equation is given below based on a *collisions per operation* risk metric, which considers the risk experienced by a single flight on one of the procedures. The notation used treats *Procedure 1* as the procedure being flown by the operation under evaluation, and *Procedure 2* as the opposing procedure. Note that the FAA's Safety Management System also defines *collisions per flight hour* as an acceptable risk metric. The latter considers the collision risk within a large airspace volume and has historically been used in

oceanic risk analyses [20]. (Appendix A describes how the calculation described here changes when a *collisions per flight hour* risk metric is used.)

- **Collision Risk**: The overall collision risk between two geometrically separated flight procedures, measured as the expected number of midair collisions per operation of a flight procedure. For an operation to be acceptable, this value must be lower than 10^{-9} collisions per operation [20].

- **P(N)**: The probability that all aircraft operate in normal conditions (i.e., that no non-normal events are experienced). This probability is calculated as $P(N) = 1 - P(NN_1) - P(NN_2)$.

- **P(Collision | N)**: The probability of collision between aircraft in normal operations, measured as the expected number of collisions per operation in normal conditions.

- **P($\mathbf{NN_1}$)**: The probability of a non-normal event occurring in *Procedure 1*. When the risk is evaluated as *collisions per operation*, $P(NN_1)$ represents the probability of an *ownship* deviation during the operation, where the ownship is the operation considered in the denominator of the risk metric. Historical analyses estimate this probability at 10^{-5} per operation [30].

- **P($\mathbf{NN_2}$)**: The probability of a non-normal event occurring in *Procedure 2*. When the risk is evaluated as *collisions per operation*, $P(NN_2)$ represents the probability of a deviation occurring in the opposing procedure during the ownship operation. This probability is a function of the individual probability of deviation per aircraft (e.g., 10^{-5} per operation) and the number of aircraft in the opposing procedure. If aircraft on both procedures have an equal chance of deviating, this term takes the form of $P(NN_2) = KP(NN_1)$, where K is the number of completed operations in *Procedure 2* during one operation of *Procedure 1*. More details on the calculation of the scaling parameter K are provided in Appendix B.

- **P(Unmitigated Collision | $\mathbf{NN_i}$)**: The probability of collision between aircraft due to an unmitigated deviation from *Procedure 'i'*. Measured as the fraction of unmitigated deviations that are expected to result in a collision. When the risk is evaluated as *collisions per operation*, only collisions involving the ownship operation are counted. For brevity, the conditional term has been omitted in the diagram above.

- **P(Mitigation | $\mathbf{NN_i}$)**: The probability of a deviation from *Procedure 'i'* that would otherwise result in a collision being successfully mitigated. In this formulation, it is assumed that the mitigation will not increase the collision risk. For brevity, the conditional term has been omitted in the diagram above.

In the sections that follow, the evaluation of normal and non-normal risks are discussed.

4.3 Evaluating Normal Risk

The *Reich Collision Risk Model (CRM)* is recognized by the FAA and ICAO as an acceptable method for estimating the normal collision risk between aircraft tracking different air traffic routes. This model was previously introduced in Chapter 3, and its application for evaluating the normal risk between flight procedures is covered in further detail here.

The Reich CRM computes the risk of collision between a pair of aircraft based on statistical distributions of aircraft position and rates of position change. Given that the air traffic system operates in normal conditions for the majority of the time, these distributions can be derived from widely available aircraft trajectory data.

The Reich model is set up based on the following scenario: two aircraft (A and B) are positioned in three-dimensional space (Figure 4-5). A Cartesian coordinate frame is placed at the center of gravity of aircraft A, with its x-axis aligned with that aircraft's velocity vector. A collision box with dimensions $\{2\lambda_x, 2\lambda_y, 2\lambda_z\}$ is placed around aircraft A. (The FAA has traditionally used a collision box with dimensions

$\{2\lambda_x = 530 \text{ ft}, 2\lambda_y = 530 \text{ ft}, 2\lambda_z = 160 \text{ ft}\}$, which are based on the dimensions of two Airbus A380 aircraft [35].) A collision event is recorded whenever aircraft B, treated as a point mass, penetrates the collision box around aircraft A.

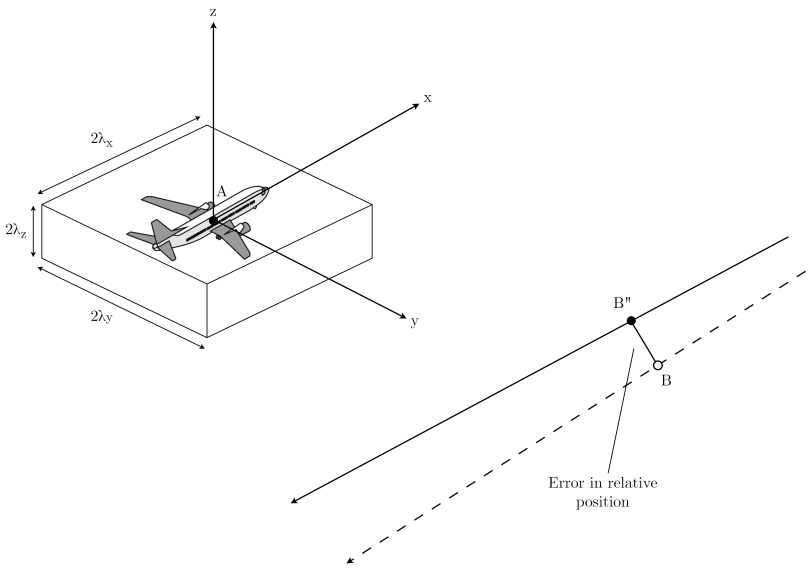

Figure 4-5: Scenario considered in the Reich Collision Risk Model (image adapted from [25]).

In the Reich model, longitudinal, lateral, and vertical collisions are differentiated based on which surface of the collision box is penetrated by aircraft B. A longitudinal collision, for instance, takes place whenever aircraft B penetrates the surfaces either in front of or behind aircraft A.

The expected number of longitudinal collisions can be computed as $n_x P_y P_z$, where n_x is the expected number of times that the x-position of aircraft B is within $[-\lambda_x, \lambda_x]$, and P_y and P_z are the probabilities that the y-position and z-position of aircraft B are within $[-\lambda_y, \lambda_y]$ and $[-\lambda_z, \lambda_z]$ during the longitudinal overlap, respectively.

By extension, the expected number of lateral and vertical collisions are computed by $n_y P_x P_z$ and $n_z P_x P_y$ respectively, and the total number of collisions is simply $n_x P_y P_z + n_y P_x P_z + n_z P_x P_y$. Further simplification of this formula leads to the final form of the Reich model, which describes the normal collision risk between two aircraft as a function of their probabilities of position overlap and the duration of the overlap condition [25]:

$$P(Collision \mid Normal) = (P_x P_y P_z)\left(\frac{1}{t_x} + \frac{1}{t_y} + \frac{1}{t_z}\right) \tag{4.3}$$

The individual terms of this equation are described below.

- $\mathbf{P_x}$: The probability that the positions of the two aircraft overlap in the x-dimension. Equivalent to the fraction of the operation spent in overlap in the x-dimension.

- $\mathbf{P_y}$: The probability that the positions of the two aircraft overlap in the y-dimension. Equivalent to the fraction of the operation spent in overlap in the y-dimension.

- $\mathbf{P_z}$: The probability that the positions of the two aircraft overlap in the z-dimension. Equivalent to the fraction of the operation spent in overlap in the z-dimension.

- $\mathbf{t_x}$: The average duration of an overlap condition between two aircraft in the x-dimension.

- $\mathbf{t_y}$: The average duration of an overlap condition between two aircraft in the y-dimension.

- $\mathbf{t_z}$: The average duration of an overlap condition between two aircraft in the z-dimension.

The overlap probabilities (P_x,P_y,P_z) can be computed from distributions of aircraft position error, which are functions of navigation performance. This calculation is discussed in the next section as part of an example application of the Reich model.

4.3.1 Example Application of Reich Model to Case of Parallel, Opposite-Direction Procedures

In order to illustrate the application of the Reich model to geometrically separated flight procedures, this section considers the evaluation of the normal risk between two parallel, laterally separated, opposite-direction flight procedures (Figure 4-6).

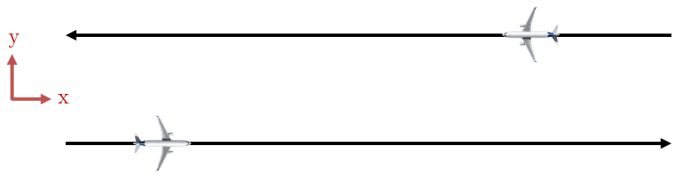

Figure 4-6: Example scenario used to illustrate the application of Reich model.

The normal collision risk between the two aircraft illustrated in Figure 4-6 can be computed based on the standard form of the Reich model:

$$P(Collision \mid Normal) = (P_x P_y P_z)\left(\frac{1}{t_x} + \frac{1}{t_y} + \frac{1}{t_z}\right) \tag{4.4}$$

Because the aircraft are flying in opposite directions, their relative speed along the x-axis is large, and the duration of their longitudinal overlap (t_x) can be considered much smaller than t_y and t_z. As a result, the term $\frac{1}{t_x}$ dominates in Equation 4.4. Based on this observation, the normal collision risk between this pair of aircraft can be simplified as follows:

$$P(Collision \mid Normal) \approx \frac{P_x P_y P_z}{t_x} = \frac{P_x}{t_x} P_y P_z = n_x P_y P_z \tag{4.5}$$

Where n_x is the number of longitudinal passes experienced (1 per aircraft pair), P_y is the probability of a lateral overlap during the pass, and P_z is the probability of a vertical overlap during the pass.

Probabilities of overlap can be computed based on statistical distributions of aircraft position in the y- and z-dimensions, which are related to their navigation per-

formance. Consider two identical distributions of lateral position along the two flight procedures. If U_1 is the random variable denoting the lateral position of the aircraft on procedure 1, and U_2 is the random variable denoting the lateral position of the aircraft on procedure 2, then $W = U_1 - U_2$ is the random variable representing the lateral separation between the two aircraft. It can be shown that the probability density function of W can be computed as the convolution of the probability density functions (PDF) of U_1 and $-U_2$ (see Appendix C for proof).

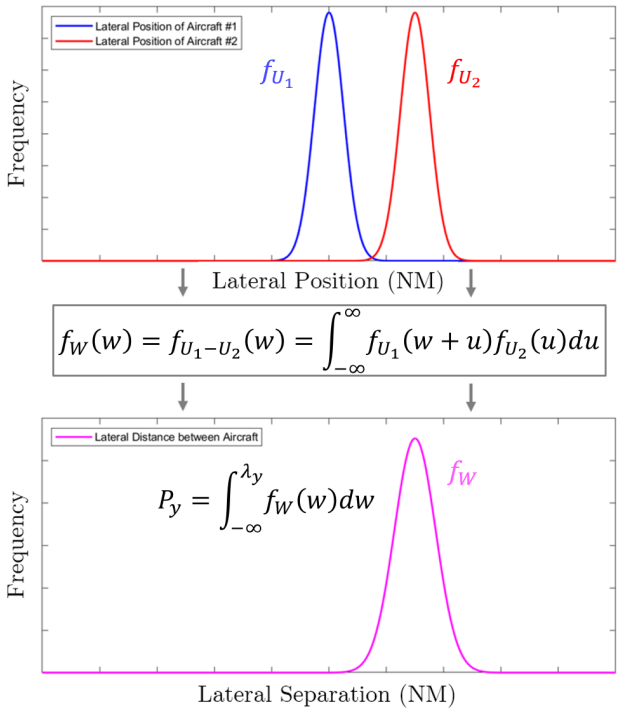

Figure 4-7: The probability of a lateral overlap can be computed as the probability that the random variable W is less than λ_y.

In Figure 4-7, the magenta curve is the PDF of W, and represents the distribution of the lateral separation between the aircraft pair. Integration of this curve over $[-\infty, \lambda_y]$ yields the probability that a lateral overlap (P_y) occurs during a longitudinal pass. The same method can be extended to the evaluation of P_z, the probability of a vertical overlap. The total collision probability during a pass is then computed as $P_y P_z$.

In this example, due to the short duration of the longitudinal pass between the aircraft pair (i.e., $t_x \ll t_y, t_z$), the probabilities of overlap can be evaluated as discrete

random events. The assumption of negligible exposure periods has often been used in past studies of normal collision risk in terminal airspace, due to the short duration of exposure periods between aircraft tracking different flight procedures. In the event that exposure periods are large, such as when evaluating enroute operations, the calculation of the normal collision risk must rely on the general form of the Reich model, which explicitly considers exposure durations (t_x, t_y, t_z).

4.3.2 Analysis of Actual Navigation Performance in RNAV Procedures

The probability of a lateral overlap (P_y) can be calculated from distributions of aircraft lateral position, as discussed in the previous section. In order to evaluate these distributions in actual operations, 30,000 flight tracks of aircraft departing Boston Logan Airport (BOS) on RNAV procedures were analyzed.

These flight tracks represent one year of departures from runway 22R at the airport (2017). The entire set of flight trajectories captured in data set is shown in Figure 4-8.

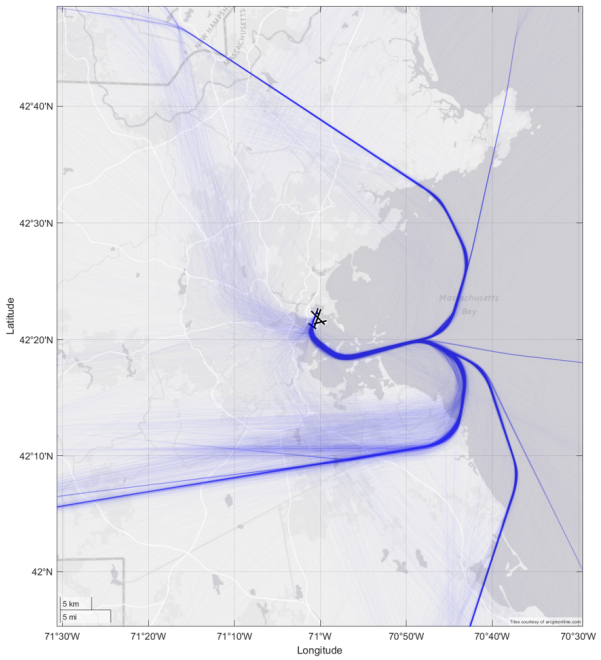

Figure 4-8: Flight tracks representing one year of departures from runway 22R at Boston Logan Airport (BOS).

In order to identify aircraft tracking an RNAV departure procedure, these flight tracks were filtered based on whether they visited every waypoint of a given RNAV procedure. An aircraft was defined as having visited a waypoint if it came within 1.5 NM of the waypoint. While the resulting filtered set may include non-RNAV aircraft that were vectored along a similar path as an RNAV procedure, the inclusion of these aircraft leads to a conservative estimate of navigation performance. Figure 4-9 shows the results of the application of this filter for the HYLND departure procedure.

Figure 4-9: Flight tracks of aircraft tracking the HYLND RNAV departure procedure from runway 22R at BOS. Magenta circles represent 1.5 NM distance rings around each procedure waypoint.

Aircraft lateral navigation performance was subsequently analyzed at various cross-sections along the filtered trajectories. No significant difference in tracking performance was identified between different locations, although a larger lateral scatter can be observed during turns. An example cross-section of the procedure is shown in Figure 4-10 below, along with its observed values of lateral position error.

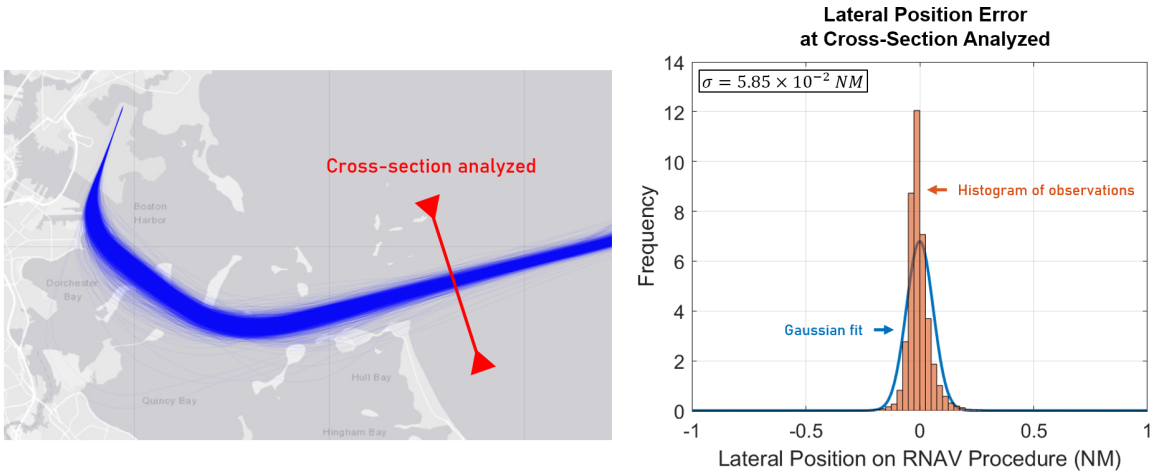

Figure 4-10: Left: Example cross-section of aircraft trajectories on RNAV departure procedure. Right: Distribution of lateral positions at the example cross-section.

Lateral navigation errors on RNAV procedures have typically been assumed to follow a Gaussian distribution [37]. The blue distribution curve in Figure 4-10 illustrates a Gaussian fit for the observed values of lateral position error. Based on this normal distribution, 95% of flights are estimated to remain within 0.12 NM of the flight procedure's nominal track. This navigation performance is significantly better than the minimum navigation performance required to fly RNAV departure and arrival procedures, which require aircraft to remain within 1.0 NM of the procedure's track with 95% probability.

Based on the Gaussian fit of lateral navigation errors above, the probability of lateral overlap (P_y) between two laterally separated procedures with this same navigation performance can be computed based on the method described in Figure 4-7. The calculation of P_y can be repeated for several values of lateral separation, which produces the plot in Figure 4-11 below.

The result in Figure 4-11 suggests that, based on the actual navigation performance observed on RNAV procedures and the assumption that navigation errors follow a Gaussian distribution, the normal collision risk between two aircraft is negligible (i.e., much lower than the 10^{-9} TLS) at lateral separation values greater than 0.5 NM.

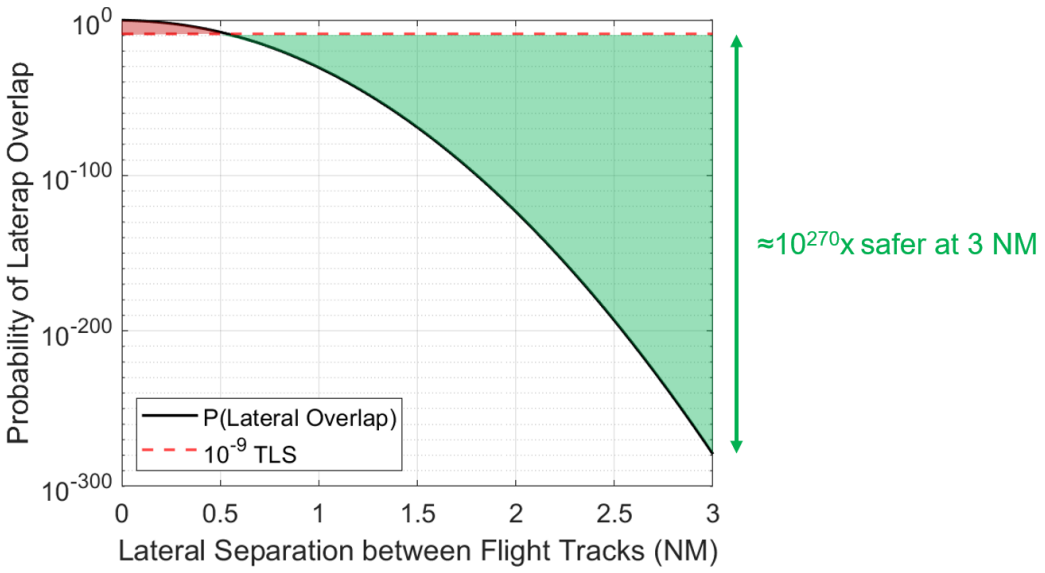

Figure 4-11: Plot of the probability of lateral overlap (P_y) as a function of lateral separation, based on the Gaussian distribution of lateral navigation performance shown in Figure 4-10.

This result is driven by significant improvements in navigation performance that have occurred over the last several decades (Figure 4-12), which allow aircraft to navigate significantly more precisely than in the past. As a result of these improvements, the risk of collision at current separation values is found to be constrained not by navigation performance, but by factors driving the non-normal component of the risk that will be discussed in the next section.

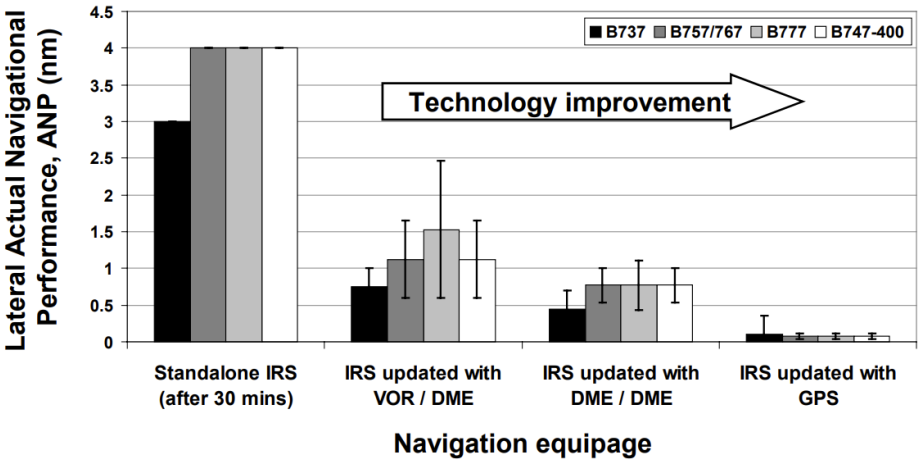

Figure 4-12: Evolution of Actual Navigation Performance (ANP). Image courtesy of Tom G. Reynolds [62].

4.4 Evaluating Non-Normal Risk

The non-normal risk between two geometrically separated flight procedures is the collision risk contributed by deviations originating from both procedures, considering the effect of mitigations.

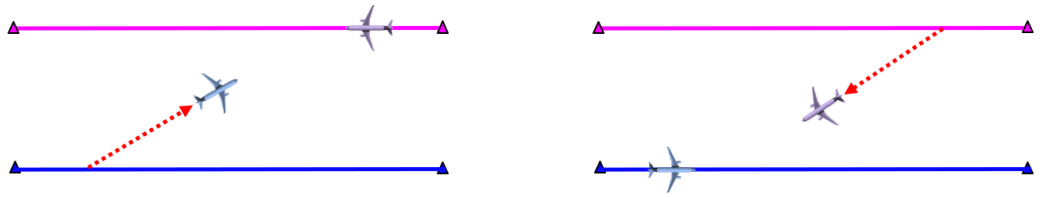

Figure 4-13: The overall non-normal risk between two procedures is the risk contributed by deviations from both procedures.

A deviation is defined as an event in which an aircraft has stopped tracking its assigned flight procedure due to a non-normal event and as a result may experience significant navigation errors. Examples of non-normal events that may induce a deviation include navigation system failures, engine failures, and pilot errors. The point at which a deviation begins may be ambiguous or difficult to define, and during operations deviations are detected based on a process known as *conformance monitoring*.

Conformance monitoring relies on a set of monitored aircraft states and a discrete conformance limit to determine whether an aircraft is deviating from its assigned flight procedure. Possible states used in conformance monitoring include aircraft position, velocity, acceleration, and autopilot modes. Figure 4-14 illustrates a two-dimensional aircraft state space, in which the black ellipse indicates an example conformance limit, and the trace represents the evolution of an aircraft's state trajectory over time. The time at which the aircraft's state trajectory crosses the conformance limit marks the earliest time at which it may be detected as a deviation.

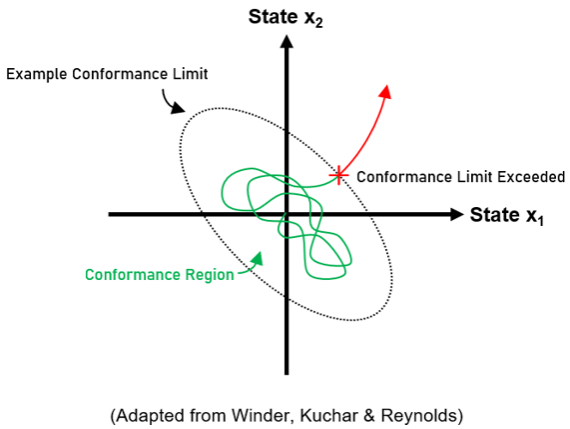

Figure 4-14: Example application of conformance monitoring using two aircraft states. Adapted from Winder, Kuchar, and Reynolds [62, 63].

The risk posed by deviations is a function of their trajectories, which may be affected by mitigations. In this study, mitigations are defined as operational procedures, devices, or techniques used to reduce the risk of collision between aircraft by inducing a change in aircraft trajectories. In the current system, available mitigations include tactical intervention by ATC, TCAS, flight deck alerting functions, and pilot response based on monitoring of basic aircraft instruments. To prevent a conflict in the event of a deviation, mitigations must produce an effective aircraft maneuver in a timely fashion, i.e., before a collision occurs. The mitigation process can be parsed into four distinct functions described below (Figure 4-15).

Figure 4-15: The mitigation process can be parsed into four distinct functions: detection, planning and decision-making, communication, and maneuver initiation.

- **Detection**: Function responsible for producing awareness of a deviation.
- **Decision-Making**: Function responsible for producing a mitigation plan or instruction (i.e., a maneuver to be executed by an aircraft) once a deviation has been detected.
- **Communication**: Function responsible for relaying the mitigation maneuver instruction to the aircraft/flight crew.

- **Maneuver Initiation**: Function responsible for initiating the mitigation maneuver (e.g., flight crew or autopilot).

The ability of a mitigation to provide a timely response is a function of its overall response time, which consists of the total time required for detection, decision-making, communication, and maneuver initiation.

Mitigations can be classified as **deviation mitigations** or **conflict mitigations** based on the event that they respond to. Deviation mitigation occurs in response to the initial detection of a deviation. This type of mitigation attempts to return the deviating aircraft to its nominal flight trajectory (Figure 4-16). Deviation mitigation relies only on knowledge of the states of the deviating aircraft.

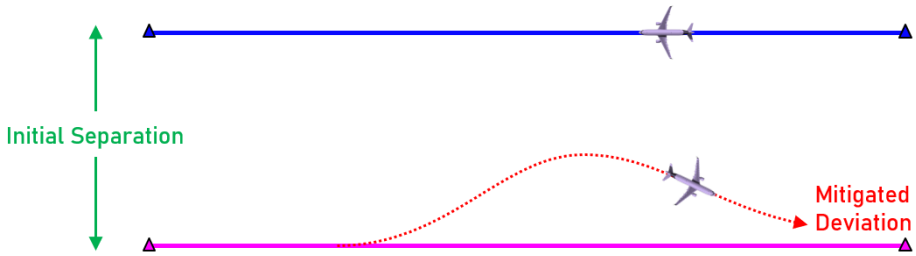

Figure 4-16: Deviation mitigation attempts to return a deviating aircraft to its nominal flight trajectory.

Conflict mitigation occurs in the event that a deviation is not corrected, and/or a conflict with another aircraft is imminent (Figure 4-17). This type of mitigation attempts to increase the separation between the two conflicting aircraft, and relies on knowledge of the states of both deviating and endangered aircraft

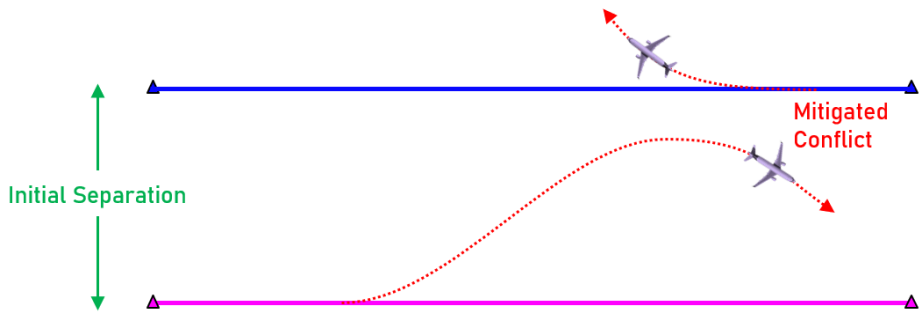

Figure 4-17: Conflict mitigation attempts to increase the separation between the deviating and the endangered aircraft.

In operations, multiple instances of each type of mitigation may be used simultaneously to increase the overall probability of a successful mitigation. For example, both ATC and TCAS are used as mitigations in the current system. To first order, the use of multiple mitigations adds redundancy to the mitigation process by enabling parallel mitigation opportunities.

Based on the previously introduced parsing of collision risk, the non-normal risk is mathematically expressed as:

$$\begin{aligned} &Non\text{-}Normal\ Risk = \\ &P(NN_1) \times P(Unmitigated\ Collision \mid NN_1) \times [1 - P(Mitigation \mid NN_1)] \\ &+P(NN_2) \times P(Unmitigated\ Collision \mid NN_2) \times [1 - P(Mitigation \mid NN_2)] \end{aligned} \tag{4.6}$$

Where $P(NN_i)$ is the probability of a deviation occurring from *Procedure 'i'*, $P(Unmitigated\ Collision \mid NN_i)$ is the probability of collision due to unmitigated deviations from *Procedure 'i'*, and $P(Mitigation \mid NN_i)$ is the probability of a deviation from *Procedure 'i'* that would otherwise result in a collision being successfully mitigated.

The sections that follow discuss the evaluation of the unmitigated risk and mitigation probability components described above.

4.4.1 Evaluating Probability of Collision due to Unmitigated Deviations

The risk posed by deviations is a function of their trajectories. Due to difficulties in observing and documenting historical deviation behaviors, the use of statistical models for estimating this component of the risk is typically not a reliable solution. Instead, the estimation of unmitigated non-normal risk can be achieved based on the modeling of individual aircraft deviation trajectories. In this case, the probability of collision due to unmitigated deviations from a flight procedure can be expressed as the cumulative probability across all deviation trajectories experienced.

Deviations may present diverse trajectories and may introduce both lateral and vertical navigation errors. The risk posed by a deviation trajectory is primarily a function of its cumulative displacement vector, the duration of the overlap condition it induces, and the time that the deviating aircraft takes to reach an endangered aircraft, as will be shown in later calculations. Due to actual deviation behaviors being poorly understood given their rare occurrence, deviation trajectories have historically been modeled as constant velocity vectors for the purpose of risk estimation (Figure 4-18). This simplification results in the assumption that unmitigated deviation trajectories may only cross an endangered procedure once and while flying in a constant direction. If this assumption holds, a linear deviation trajectory is able to reach every point on the endangered procedure in the lowest amount of time, thus producing a conservative estimate of the non-normal risk. Historically, a lateral deviation angle of 30 degrees has been accepted by safety stakeholders as a representative worst-case lateral deviation angle for assessing the risk between two laterally separated procedures [64].

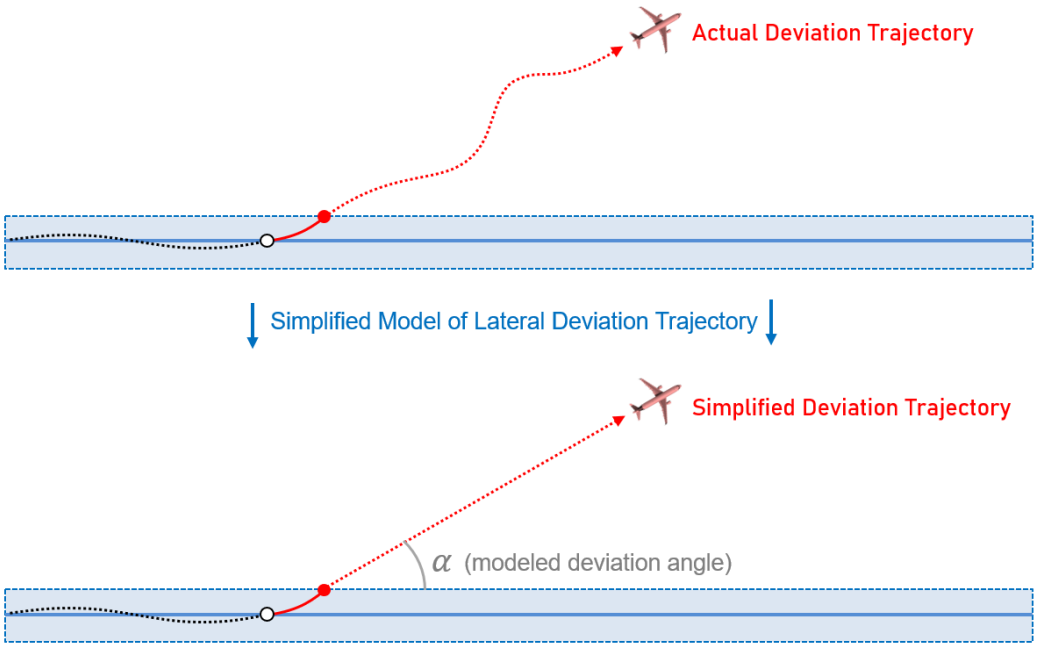

Figure 4-18: Lateral deviation trajectories have historically been simplified as constant velocity vectors with a 30-degree lateral deviation angle.

When a linear worst-case deviation is used for non-normal risk estimation, it is

necessary to consider the relative geometries of the procedures and the angles at which aircraft intercept the two proximate segments when determining the applicable worst-case scenario for analysis. When tracks are not parallel, but rather converging or diverging, the relative angle of a worst-case lateral deviation may change as illustrated in Figure 4-19.

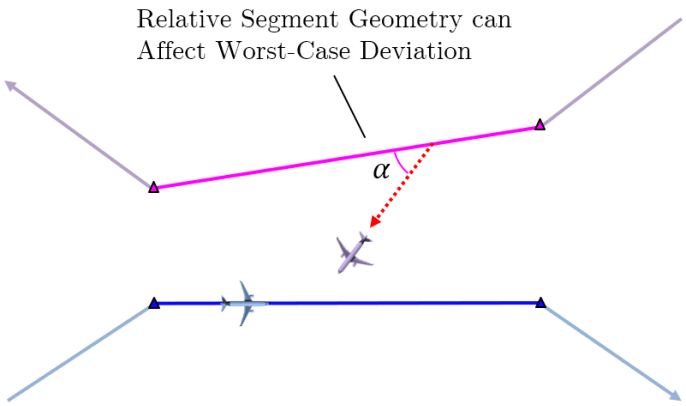

Figure 4-19: Converging/diverging segments may affect the worst-case deviation experienced.

In addition, the angles at which aircraft join two proximate flight procedure segments may also affect the non-normal risk due to possible waypoint overshoots (Figure 4-20), with larger intercept angles potentially introducing higher risk.

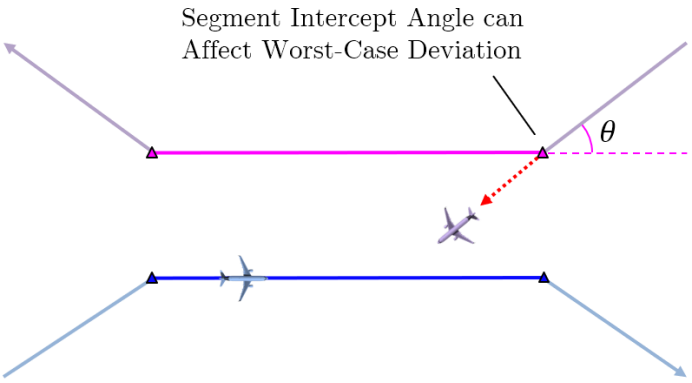

Figure 4-20: Waypoint overshoots may affect the worst-case deviation experienced.

In some cases, more complex deviation behaviors may exist that exhibit higher risk than a linear trajectory due to the assumption of a single trajectory crossing being inadequate. Examples of these higher-risk behaviors include aircraft intercepting the

wrong procedure, or making repeated turns on top of an endangered procedure. While the general methodology presented in this chapter can be applied to more complex deviation behaviors, linear trajectories will be used for illustration purposes due to more complex deviation behaviors being presently poorly understood. If more data on deviation behaviors becomes available in the future, Equation 4.6 could be further parsed into the non-normal risk contributed by different deviation types based on their individual probabilities of occurrence.

The collision condition due to a deviation can be stated as an event in which an intruder aircraft, treated as a point mass, penetrates the *collision box* around an endangered aircraft. This scenario is illustrated in Figure 4-21 below.

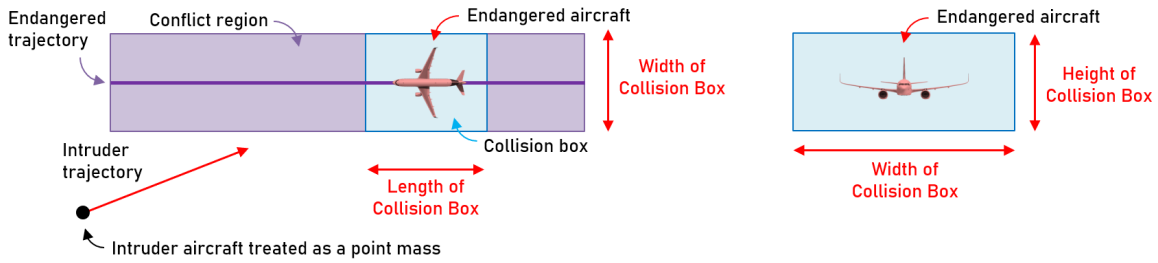

Figure 4-21: A collision due to a deviation occurs whenever a deviating aircraft penetrates the collision box around an endangered aircraft, which is shaped based on the combined geometry of both aircraft.

This collision condition can be parsed into two separate events that must take place simultaneously for a collision to occur:

- **Trajectory Overlap**: The condition where an intruder aircraft penetrates the *conflict region* of an endangered trajectory, illustrated in Figure 4-21. The conflict region is a spatial extension of the endangered aircraft's collision box about its trajectory. The probability of a trajectory overlap, $P(Trajectory\ Overlap \mid NN)$, represents the spatial component of the collision probability.

- **Exposure**: The condition where an endangered aircraft is present at the location of trajectory overlap at the same time as the intruder aircraft. The probability of exposure, $P(Exposure \mid Trajectory\ Overlap, NN)$, represents the temporal component of the collision probability.

Based on these definitions, the probability of collision due to an unmitigated deviation from *Procedure 'i'*, $P(Unmitigated\ Collision \mid NN_i)$, can be expanded as follows (Figure 4-22):

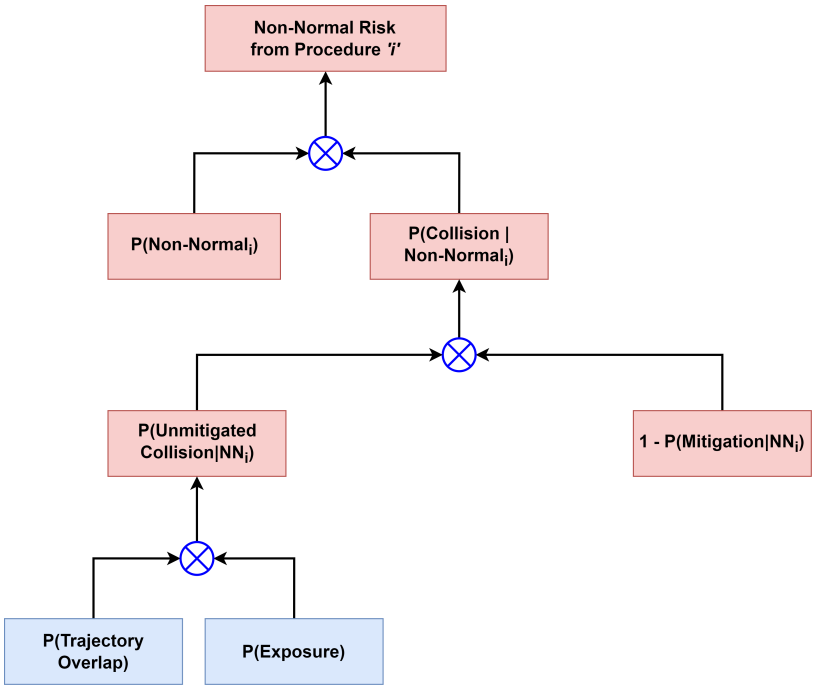

Figure 4-22: Expanded parsing of the unmitigated collision risk component. New terms are highlighted in blue.

In equation form, the non-normal risk from *Procedure 'i'* becomes:

$$
\begin{aligned}
&Non\text{-}Normal\ Risk\ from\ Procedure\ i = \\
&P(NN_i) \\
&\times P(Trajectory\ Overlap \mid NN_i) \times P(Exposure \mid Trajectory\ Overlap, NN_i) \\
&\times [1 - P(Mitigation \mid NN_i)]
\end{aligned}
\tag{4.7}
$$

The following sections describe the evaluation of the two newly introduced terms.

Probability of Trajectory Overlap

The probability of trajectory overlap due to deviations is a function of the relative geometries of the procedures considered, the locations where deviations occur, and the deviation trajectories experienced. The notion of a trajectory overlap condition is illustrated in Figure 4-23 below. Given a set of unmitigated deviation trajectories, the probability of trajectory overlap represents the fraction of deviation trajectories that penetrate an endangered procedure's three-dimensional conflict region.

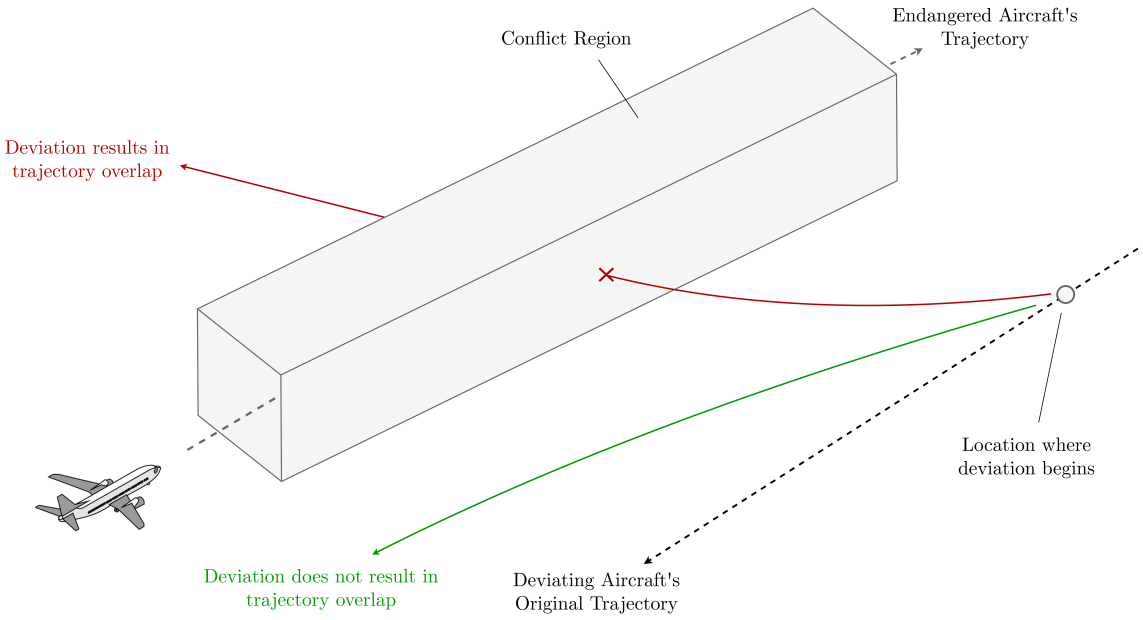

Figure 4-23: A trajectory overlap occurs when the deviation penetrates the conflict region around an endangered aircraft's trajectory. This condition is purely geometric.

The worst-case probability of trajectory overlap for two parallel, laterally separated flight procedures occurs when the procedures have infinitely long parallel segments with no vertical separation. Assuming linear-trajectory lateral deviations with no change in vertical position, the probability of trajectory overlap in this scenario is simply a function of whether deviations occur towards or away from the endangered procedure (Figure 4-24). Further assuming a symmetric distribution of deviation angles (α), the probability of trajectory overlap in this case is simply 0.5.

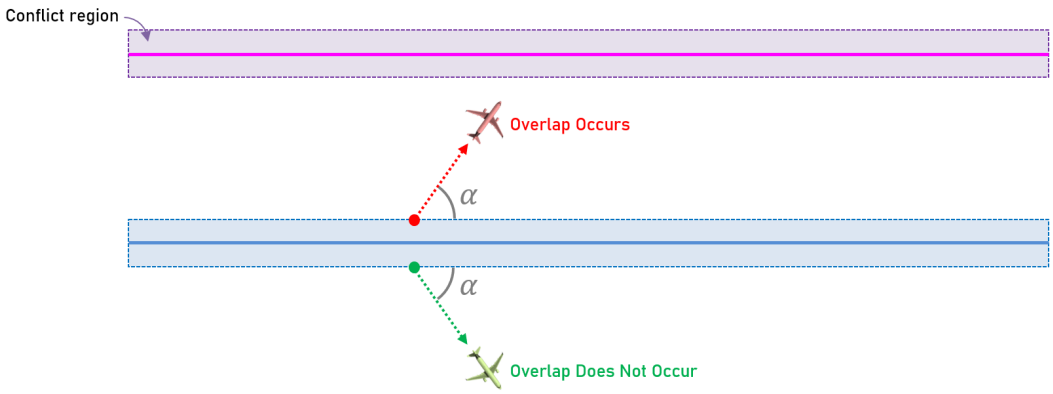

Figure 4-24: The probability of trajectory overlap due to a lateral deviation in the case of parallel, laterally separated flight procedures with no vertical separation is simply a function of the deviation angle, which is assumed constant.

The addition of vertical separation between the procedures can significantly reduce this value by introducing an additional dimension to the overlap condition. For more complex flight procedure geometries, the probability of trajectory overlap is best computed through geometric simulations of deviation trajectories based on a Monte Carlo approach. This probability component can be difficult to estimate accurately given the challenges associated with representing realistic deviation trajectories.

Probability of Exposure

The probability of exposure is the probability that an intruder aircraft will encounter another aircraft while crossing or occupying that aircraft's conflict region. Assuming that both flight procedures are operated independently, this probability is analogous to the probability of a pedestrian being struck by a vehicle while crossing a street at random. The probability of exposure given independent operations is derived in Appendix D and is a function of the time spent in trajectory overlap by the intruder aircraft, the relative traffic throughput on the endangered procedure experienced by the intruder aircraft, and the fraction of the endangered procedure's length that is occupied by aircraft (Equation 4.8).

$$P(Exposure \mid Trajectory\ Overlap, NN) =$$
$$(Time\ Spent\ in\ Trajectory\ Overlap) \times (Relative\ Throughput\ During\ Overlap)$$
$$+ (Occupancy\ Ratio\ of\ Endangered\ Procedure) \tag{4.8}$$

Equation 4.8 can be applied to any deviation trajectory and does not assume a linear deviation. Higher-exposure deviation behaviors, such as those that exhibit many turns or that intercept the wrong procedure, can have their associated probabilities of exposure calculated by accounting for the duration of the trajectory overlap conditions that they induce. In a high-exposure behavior, such as a wrong procedure intercept, the probability of exposure can reach a value of 1 if sufficient time is spent in trajectory overlap by the intruder aircraft.

For the case of laterally separated flight procedures, the highest probability of exposure occurs when the two procedures operate in opposite directions, which maximizes the closing speed between aircraft and the relative throughput experienced by an intruder aircraft during the crossing of the conflict region. By assuming a simplified linear deviation trajectory, Figure 4-25 below illustrates this worst-case scenario and introduces parameters used to calculate its probability of exposure.

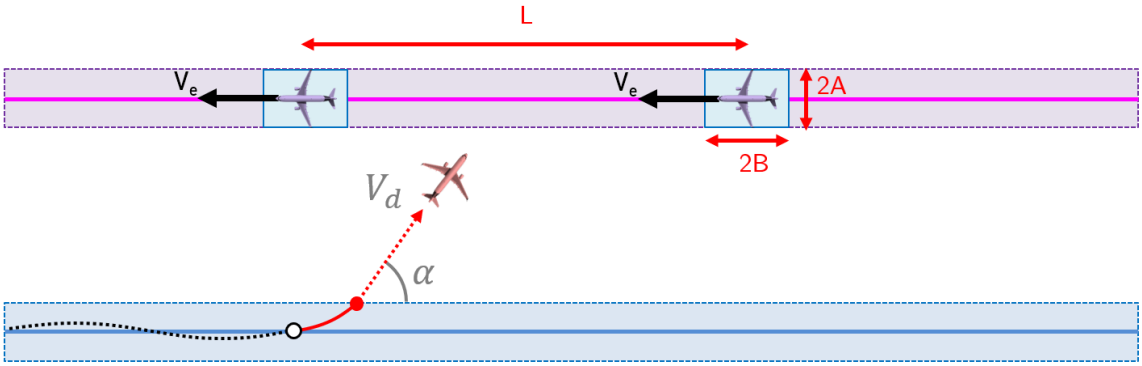

Figure 4-25: The probability of exposure is the probability that an intruder aircraft will encounter an endangered aircraft during its crossing of the conflict region.

The parameters labeled in Figure 4-25 are as follows:

- **A**: Half-width of collision box/conflict region around endangered aircraft.

- **B**: Half-length of collision box around endangered aircraft.

- $\mathbf{V_d}$: Groundspeed of the deviating aircraft.

- $\mathbf{V_e}$: Groundspeed of aircraft on the endangered procedure.

- α: Angle at which the intruder aircraft crosses the conflict region, assumed constant.

- **L**: In-trail separation between aircraft on the endangered procedure.

Based on these definitions, the probability of exposure associated with a linear-trajectory deviation assuming independent operations and opposite-direction traffic is computed as below. A derivation of this equation is provided in Appendix D.

$$P(Exposure \mid Trajectory\ Overlap, NN) = \min\left(\left(\frac{2A}{V_d sin\alpha}\right) \times \left(\frac{V_e + V_d cos\alpha}{L}\right) + \left(\frac{2B}{L}\right), 1\right) \tag{4.9}$$

Applying typical values for the dimensions of the collision box ($A = B = 265$ ft) and in-trail separation between aircraft on the endangered procedure ($L = 3$ NM), the probability of exposure for this scenario can be computed as a function of the deviation angle α (Figure 4-26).

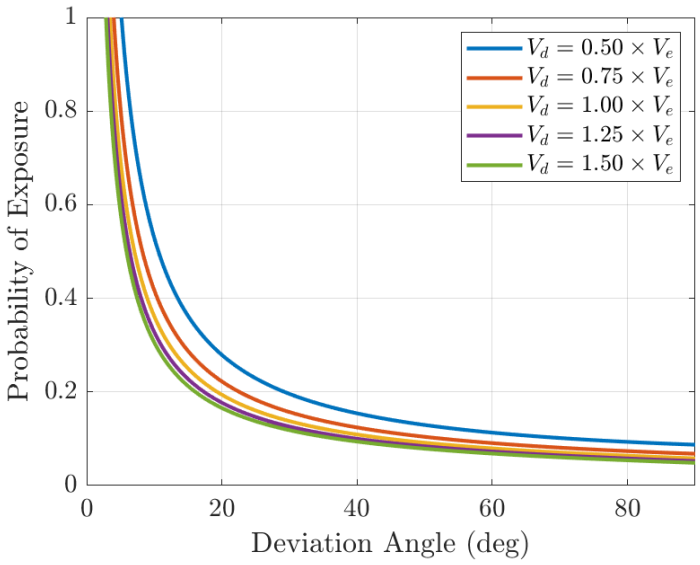

Figure 4-26: Probability of exposure for a linear deviation trajectory as a function of the deviation angle and the ratio between deviating and endangered aircraft groundspeeds. Procedures are assumed to be in opposite directions.

Based on these results, the probability of exposure for a 30° deviation angle can be observed to be approximately 0.2. At small deviation angles ($\alpha < 5°$), the overlap condition may last long enough for multiple aircraft on the endangered procedure to pass the intruder aircraft's position. In such a scenario, the probability of exposure should be limited to a maximum value of 1 since a collision with the first passing aircraft is assumed to be guaranteed.

The result of Equation 4.9 gives the probability of exposure from the perspective of the deviating aircraft. When evaluating the probability of exposure from the perspective of a single aircraft on the endangered procedure, this probability must be scaled down according to the number of aircraft sharing the endangered procedure, which can be assumed to share the risk uniformly. More information on this scaling step is discussed in Appendix B and will be revisited in examples explored in Chapter 6.

The probability of exposure can be controlled through the use of dependent operations, where the operation of one procedure becomes conditioned on the operation of another. An example of dependent operations in the current air traffic system includes the application of diagonal separation between instrument approaches to parallel run-

ways. In that scenario, the probability of exposure to a deviation is reduced by not having aircraft flying side-by-side, and can be calculated based on a probability density function describing the along-track position of an endangered aircraft relative to a deviating aircraft.

Summary of Probability of Collision due to Unmitigated Deviations

The probability of collision due to an unmitigated deviation from *Procedure 'i'* was evaluated as the product of $P(Trajectory\ Overlap \mid NN_i)$ and $P(Exposure \mid Trajectory\ Overlap, NN_i)$.

The probability of trajectory overlap due to a deviation, $P(Trajectory\ Overlap \mid NN_i)$, was defined as the spatial component of the collision probability, and calculated as the fraction of deviations that cross the path of an endangered procedure. This probability was found to be controllable through changes to the relative geometries of procedures, such as by adding vertical separation between them.

The probability of exposure, $P(Exposure \mid Trajectory\ Overlap, NN_i)$, was defined as the temporal component of the collision probability, and calculated as the probability that two aircraft occupy the same point in space during a trajectory overlap condition. This probability was found to be controllable through dependent operations, in which aircraft operations in one procedure are made dependent on the use of another procedure (e.g., metering), as well as by increasing the in-trail separation between aircraft.

For laterally separated flight procedures, the case of parallel, opposite-direction procedures with no vertical separation was identified as a geometry with high unmitigated non-normal risk. For this geometry, $P(Trajectory\ Overlap \mid NN_1)$ was estimated at 5×10^{-1} based on a linear-trajectory deviation assumption and a symmetric distribution of deviation angles. Similarly, $P(Exposure \mid Trajectory\ Overlap, NN_1)$ was estimated at 2×10^{-1} for a 30° deviation.

The probability of collision due to unmitigated deviations from *Procedure 1* in this scenario, $P(Unmitigated\ Collision \mid NN_1)$, is the product of these terms and equal to $(5 \times 10^{-1}) \times (2 \times 10^{-1}) = 10^{-1}$. This result indicates that 1 out of every 10

unmitigated deviations from *Procedure 1* are expected to result in a collision with an aircraft in *Procedure 2* under the assumptions considered.

When accounting for the frequency at which deviations occur, $P(NN)_1 \approx 10^{-5}$, the non-normal risk from *Procedure 1* before mitigations in this scenario is $(10^{-5}) \times (10^{-1}) = 10^{-6}$, which exceeds a 10^{-9} target level of safety even before adding the non-normal risk from *Procedure 2*. Such an operation would therefore only be considered acceptable if the effects of mitigations are such that the mitigated collision risk meets the target level of safety. The evaluation of mitigation effects on the risk is discussed in the next section.

4.4.2 Evaluating Probability of Mitigation

The effect of mitigations on the collision risk is represented by $P(Mitigation \mid NN)$, the probability of a deviation from a flight procedure that would otherwise result in a collision being successfully mitigated. The equation used to describe the non-normal risk from one flight procedure is repeated below:

$$\begin{aligned} &Non\text{-}Normal\ Risk\ from\ Procedure\ i = \\ &P(NN_i) \\ &\times P(Trajectory\ Overlap \mid NN_i) \times P(Exposure \mid Trajectory\ Overlap, NN_i) \\ &\times [1 - P(Mitigation \mid NN_i)] \end{aligned} \tag{4.10}$$

Where $P(Mitigation \mid NN_i)$ represents the probability of a deviation from *Procedure 'i'* being successfully mitigated.

A mitigation is defined as successful when it results in a maneuver that prevents a trajectory overlap condition. An example of a successful mitigation is illustrated in Figure 4-27, where a deviating aircraft executes a lateral mitigation maneuver and avoids penetrating the endangered aircraft's conflict region.

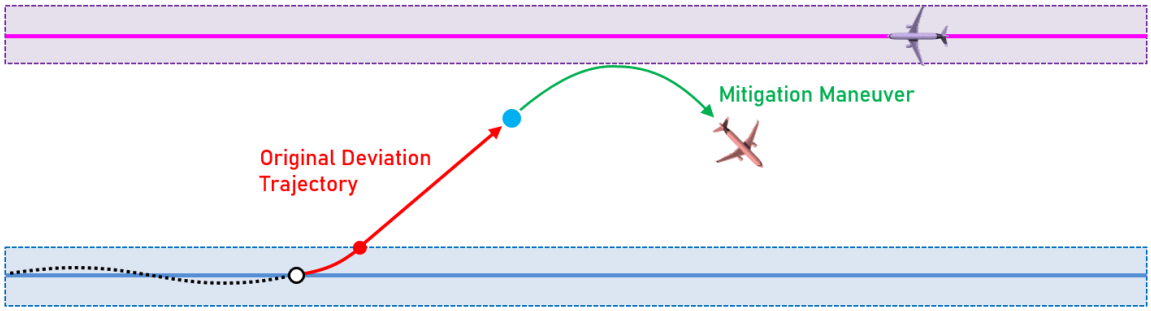

Figure 4-27: Example illustration of a successful mitigation using a lateral maneuver.

A successful mitigation is posited to require three conditions:

- **Mitigation must be available.** All mitigation functions, such as communication and surveillance capabilities, must be operational and operating as intended at the time of request.

- **Mitigation response must be timely.** The response must occur with sufficient time left for an effective maneuver to be executed.

- **Mitigation response must be correct.** The maneuver instruction issued to the aircraft as well as its execution must be adequate.

Based on the probabilities of these conditions being satisfied, the probability of a successful mitigation can be expanded as follows (Figure 4-28):

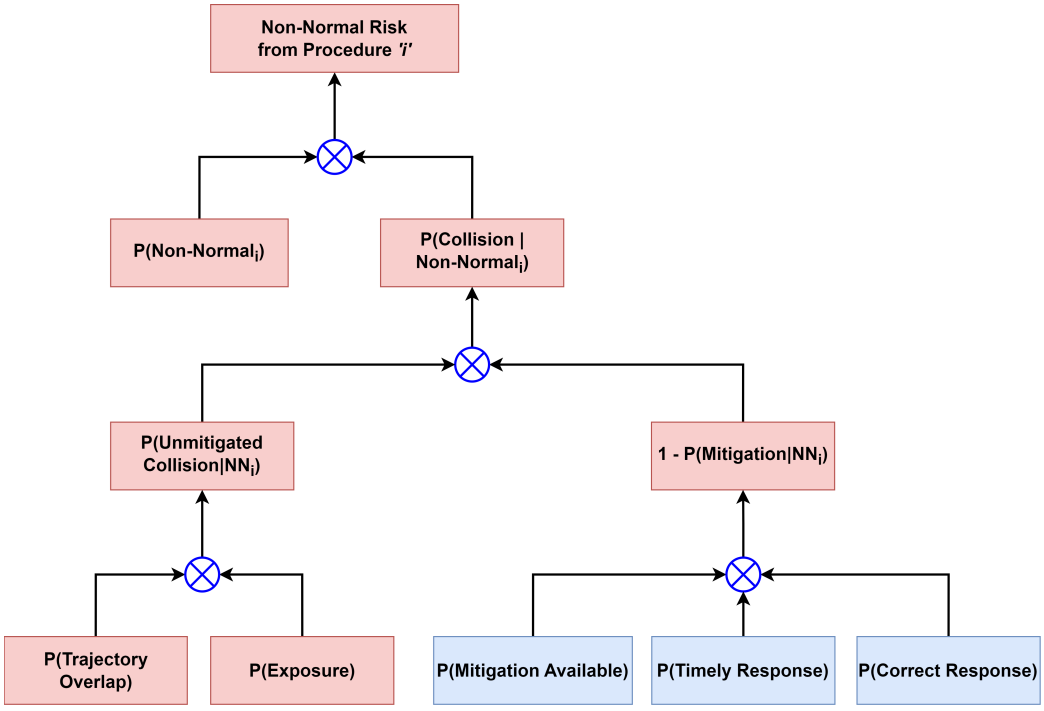

Figure 4-28: Expanded parsing of the mitigated collision risk component. New terms are highlighted in blue.

In equation form, the non-normal risk from *Procedure 'i'* becomes:

$$\begin{aligned} &Non\text{-}Normal\ Risk\ from\ Procedure\ i = \\ &P(NN_i) \\ &\times P(Trajectory\ Overlap \mid NN_i) \times P(Exposure \mid Trajectory\ Overlap, NN_i) \\ &\times [1 - (P(Mitigation\ Available) \times P(Timely\ Response) \times P(Correct\ Response))] \end{aligned} \tag{4.11}$$

While the evaluation of mitigation availability and response correctness is posited to require testing of the mitigation system, the probability of a timely response can be quantified based on the geometry of the mitigation scenario and the mitigation's response time performance.

The section that follows introduces a geometric model for evaluating the probability of a timely mitigation response. An example case of parallel, laterally separated procedures is used to illustrate the model, though the general method remains appli-

cable to other geometries. In addition, a single mitigation capability is considered in this discussion for simplicity.

Geometric Model for Evaluating Probability of Timely Mitigation Response

Given two parallel, laterally separated flight procedures with no vertical separation and assuming a linear-trajectory lateral deviation, the following geometric model of a mitigation scenario is proposed for evaluating the probability of a timely mitigation response (Figure 4-29). *(Note: the methodology that follows can similarly be applied to more complex geometries and deviation trajectories if desired.)* As done in the evaluation of the unmitigated non-normal risk, the deviating aircraft is treated as a point mass while a collision box is placed around the endangered aircraft to represent the collision condition.

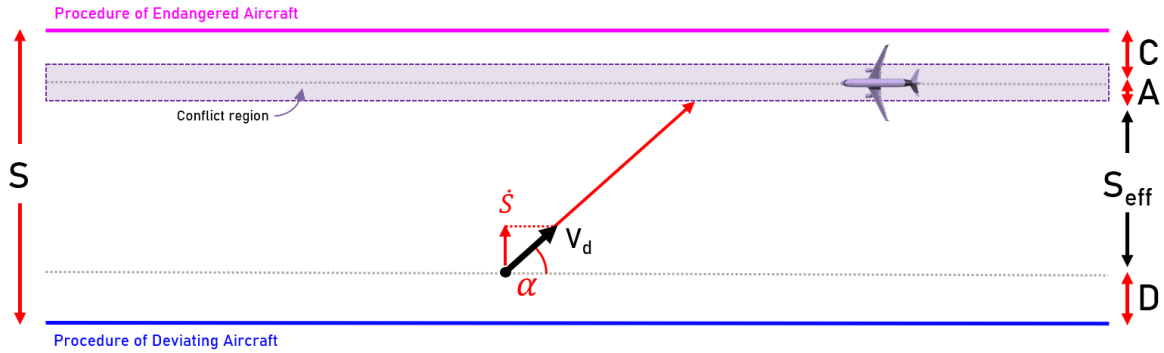

Figure 4-29: Geometric model of mitigation encounter.

The parameters labeled in Figure 4-29 are as follows:

- **S**: Lateral separation between the two flight procedure segments.
- **D**: Cross-track distance of deviating aircraft at the time it exceeds the procedure's conformance limit. This represents the earliest moment when an aircraft may be detected as a deviation, and marks the beginning of the mitigation process.
- **C**: Cross-track distance of endangered aircraft at the time of conflict.

- **A**: Half-width of collision box around endangered aircraft.
- $\mathbf{S_{eff}}$: Effective lateral separation between aircraft pair, defined as $S_{eff} = S - D - C - A$.
- $\mathbf{V_d}$: Groundspeed of deviating aircraft, assumed constant during the deviation.
- α: Lateral angle of the deviation before mitigation, assumed constant.

The time at which the deviating aircraft exceeds its procedure's conformance limit is treated as $\mathbf{t = 0}$ in the mitigation timeline (Figure 4-30).

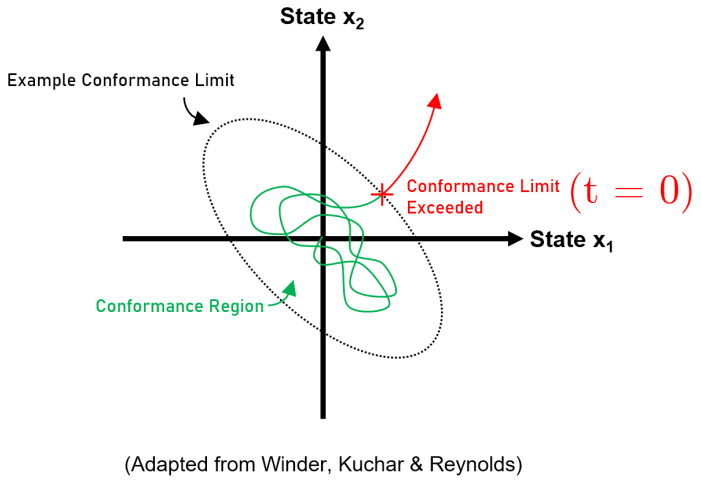

(Adapted from Winder, Kuchar & Reynolds)

Figure 4-30: The time at which an aircraft exceeds its procedure's conformance limit in a continuous state space marks the beginning of the mitigation process.

The **Time of Conflict** is defined as the time when the deviating aircraft enters (or is predicted to enter) the endangered aircraft's conflict region. The **Time-to-Collision** is defined as the time elapsed between $t = 0$ and the time of conflict, as shown in the timeline in Figure 4-31.

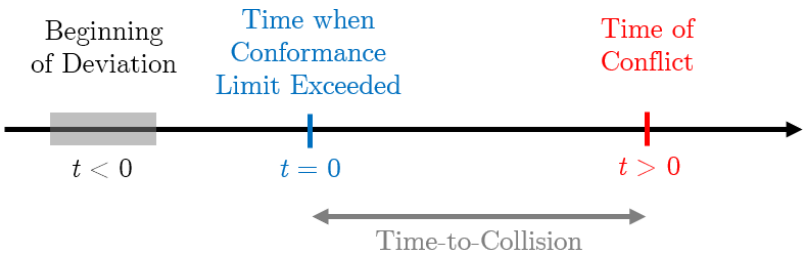

Figure 4-31: Schematic of mitigation timeline.

The time-to-collision imposes a physical limit on the available time window for mitigation. For the scenario above, the time-to-collision is computed as:

$$Time\text{-}to\text{-}Collision = \frac{S - D - C - A}{V_d \cdot sin\alpha} = \frac{S_{eff}}{V_d \cdot sin\alpha} \tag{4.12}$$

Given aircraft maneuvering dynamics, an additional time margin must also be considered to allow sufficient time for the successful execution of a mitigation maneuver. This margin is termed the **Maneuver Time Margin**. By defining the mitigation's **Time of Response** as the time when the mitigation maneuver is **initiated**, it follows that a timely mitigation response must satisfy the following condition:

$$Time\ of\ Response \leq Time\text{-}to\text{-}Collision - Maneuver\ Time\ Margin \tag{4.13}$$

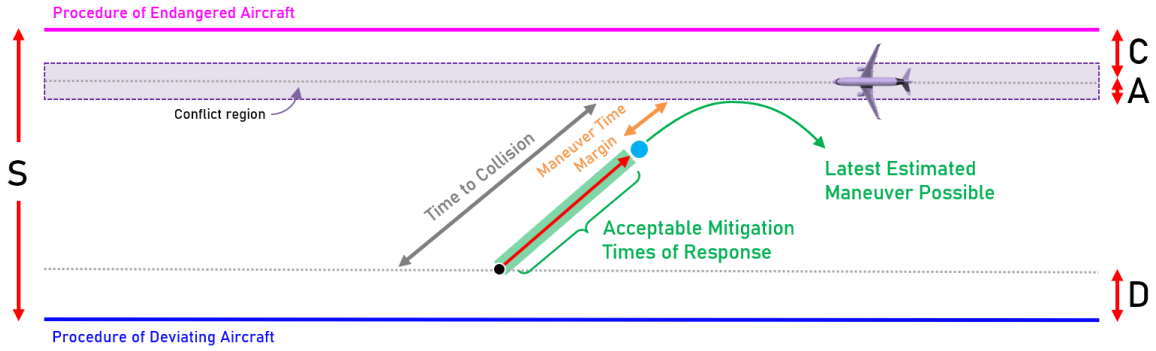

Figure 4-32: The mitigation response is considered timely when it occurs within the time interval $[0, Time\text{-}to\text{-}Collision - Maneuver\ Time\ Margin]$.

The maneuver time margin can be estimated based on a standard minimum maneuver specified for the mitigation. For instance, TCAS assumes a standard vertical maneuver with a minimum vertical acceleration of 0.25 g and a minimum target vertical speed of 1500 ft/min [9]. The value of the maneuver time margin is a function of aircraft dynamics during the mitigation maneuver used. For a lateral maneuver, this margin is associated with the time needed to reverse the rate of lateral closure

$\dot{S}$. For a vertical maneuver, it is associated with the time needed to climb/descend above/below the other trajectory. Because aircraft lateral dynamics are typically slower than vertical dynamics, lateral maneuvers are expected to require a larger maneuver time margin. In this discussion, a lateral maneuver will be assumed, which is expected to produce more conservative results. A comparison of the maneuver time margins associated with lateral and vertical maneuvers is provided in Appendix E.

The maneuver time margin can be parsed into two components: an *acceleration* component, and a *steady* component. During the acceleration phase of the maneuver, the aircraft is changing its attitude towards the target mitigation maneuver. For a lateral maneuver, this is characterized by a target roll rate ($\dot{\phi}$). During the steady phase, the aircraft holds a constant attitude corresponding to the target mitigation maneuver. For a lateral maneuver, this is characterized by a target bank angle (ϕ_{target}). The total maneuver time margin is the sum of the time margins required for both phases of the maneuver.

$$\begin{aligned} &Maneuver\ Time\ Margin = \\ &(Maneuver\ Time\ Margin)_{Acceleration} + (Maneuver\ Time\ Margin)_{Steady} \end{aligned} \tag{4.14}$$

By making the conservative assumption that the aircraft's trajectory does not change during the acceleration phase of the maneuver, the maneuver time margin for this phase is computed as:

$$(Maneuver\ Time\ Margin)_{Acceleration} = \frac{\phi_{target}}{\dot{\phi}} \tag{4.15}$$

The time margin for the steady phase of the maneuver can be derived geometrically based on the resulting maneuver turn radius (Figure 4-33):

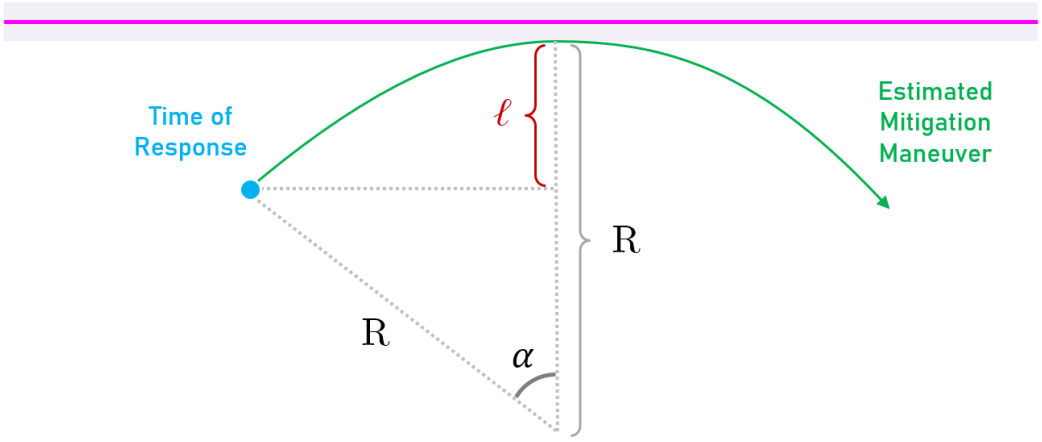

Figure 4-33: Geometry of a lateral mitigation maneuver with constant turn radius.

$$\ell = R(1 - cos\alpha) \Rightarrow$$

$$(Maneuver\ Time\ Margin)_{Steady} = \frac{R(1 - cos\alpha)}{V_d \cdot sin\alpha} \tag{4.16}$$

Where R is the turn radius resulting from the target bank angle ϕ_{target}. Expanding R as a function of ϕ_{target} yields:

$$R = \frac{V_d^2}{g \cdot tan\left(\phi_{target}\right)} \Rightarrow$$

$$\begin{aligned}(Maneuver\ Time\ Margin)_{Steady} =& \frac{V_d(1 - cos\alpha)}{g \cdot tan\left(\phi_{target}\right) \cdot sin\alpha} \\ =& \frac{V_d \cdot tan(\alpha/2)}{g \cdot tan(\phi_{target})}\end{aligned} \tag{4.17}$$

Where g is the gravitational acceleration. The total maneuver time margin thus becomes:

$$Maneuver\ Time\ Margin = \frac{V_d \cdot tan(\alpha/2)}{g \cdot tan(\phi_{target})} + \frac{\phi_{target}}{\dot{\phi}} \tag{4.18}$$

By substituting these results in Equation 4.14, the timely mitigation condition for the scenario described can be expressed as:

$$\begin{aligned} Time\ of\ Response &\leq Time\text{-}to\text{-}Collision - Maneuver\ Time\ Margin \\ &\leq \frac{S-D-C-A}{V_d \cdot sin\alpha} - \frac{V_d \cdot tan(\alpha/2)}{g \cdot tan(\phi_{target})} - \frac{\phi_{target}}{\dot{\phi}} \end{aligned} \tag{4.19}$$

It then follows that the probability of a timely mitigation response based on an estimated lateral maneuver is:

$$\boxed{\begin{aligned} &P(Timely\ Response) = \\ &P\left(Time\ of\ Response \leq \frac{S-D-C-A}{V_d \cdot sin\alpha} - \frac{V_d \cdot tan(\alpha/2)}{g \cdot tan(\phi_{target})} - \frac{\phi_{target}}{\dot{\phi}}\right) \end{aligned}} \tag{4.20}$$

Where shorthand notation is convenient, this equation may be written as:

$$P(Timely\ Response) = P\left(Time\ of\ Response \leq \frac{S_{eff}}{V_d \cdot sin\alpha} - \tau_{maneuver}\right) \tag{4.21}$$

In their most general form, both sides of Equation 4.20 can be considered stochastic. On the left side of the inequality, the *Time of Response* is the response time achieved by the mitigation, which can vary based on variations of the mitigation process including variations in human response time performance. On the right side, the parameters D, C, V_d, α and $\dot{\phi}$ may vary based on variations among the deviation trajectories experienced. As a result, both sides of this inequality can be visualized as probability density functions (Figure 4-34), and the probability of a timely response is the probability that the two distributions do not overlap.

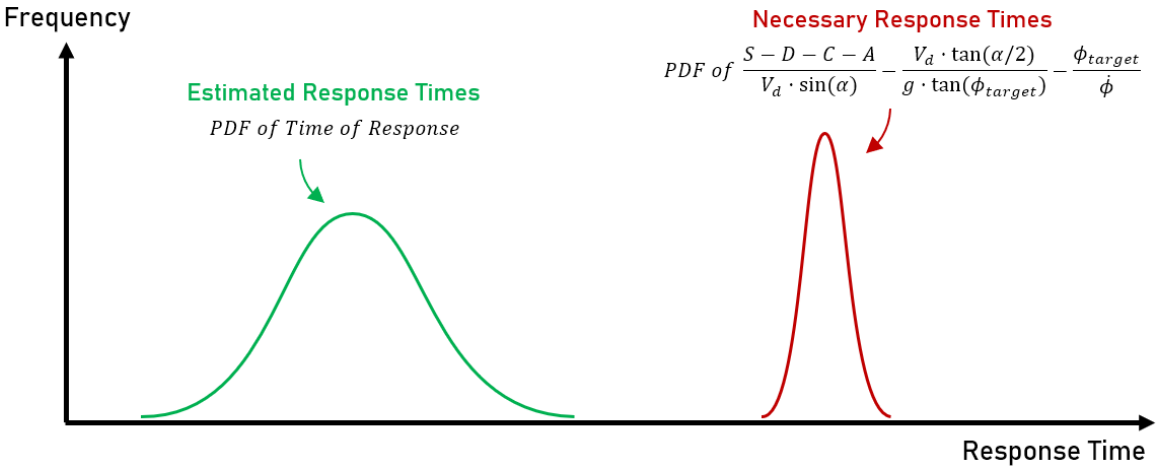

Figure 4-34: Example illustration of distributions of mitigation response times (*Time of Response*, in green) and deviation necessary response times (*Time-to-Collision − Maneuver Time Margin*, in red).

Mathematically, this probability can be calculated based on the convolution of the two distributions (assuming independence):

$$P(Timely\ Response) = \int_{-\infty}^{0} \int_{-\infty}^{\infty} f_{t_{response}}(t+\tau) f_{t_{necessary}}(\tau) d\tau dt \tag{4.22}$$

Identification of the mitigation response time distribution is posited to require testing of the mitigation system, while identification of the necessary response time distribution requires data on aircraft deviation behaviors. Given challenges in obtaining and analyzing historical deviation data, the necessary response time distribution may be simplified based on a representative worst-case deviation. By assigning representative worst-case values to the parameters D, C, V_d and α, the necessary response time distribution can be simplified as a conservative impulse function (Figure 4-35).

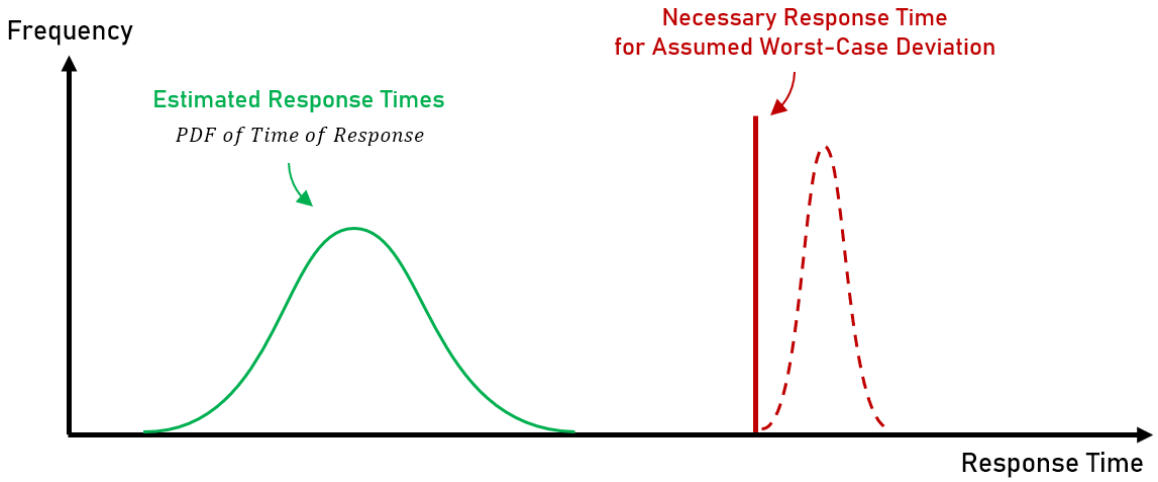

Figure 4-35: Simplification of the necessary response time distribution based on a worst-case deviation leads to its representation as an impulse function.

When this simplification is applied, mitigation of the representative worst-case deviation is assumed to guarantee the mitigation of all other deviations. The probability of a timely response in this case can be computed as the area of the mitigation response time distribution that lies to the left of the assumed worst-case deviation's necessary response time:

$$P(Timely\ Response) = \int_0^{\left(\frac{S-D-C-A}{V_d \cdot sin\alpha} - \frac{V_d \cdot tan(\alpha/2)}{g \cdot tan(\phi_{target})} - \frac{\phi_{target}}{\dot{\phi}}\right)_{Worst\ \ Case}} f_{t_{response}}(t)dt \tag{4.23}$$

Note on Possibility of Risk Increase due to Late Mitigation

The collision risk formulation presented thus far has assumed that mitigations will not increase the collision risk between flight procedures due to mitigations being sufficiently well-designed. However, in some cases, it may be possible for a late mitigation (i.e., one that does not satisfy the necessary response time) to cause an increase in risk. An example of this is the case of a late lateral maneuver being executed that causes the maneuvering aircraft to turn inside the endangered aircraft's conflict region, thus increasing the probability of exposure (Figure 4-36).

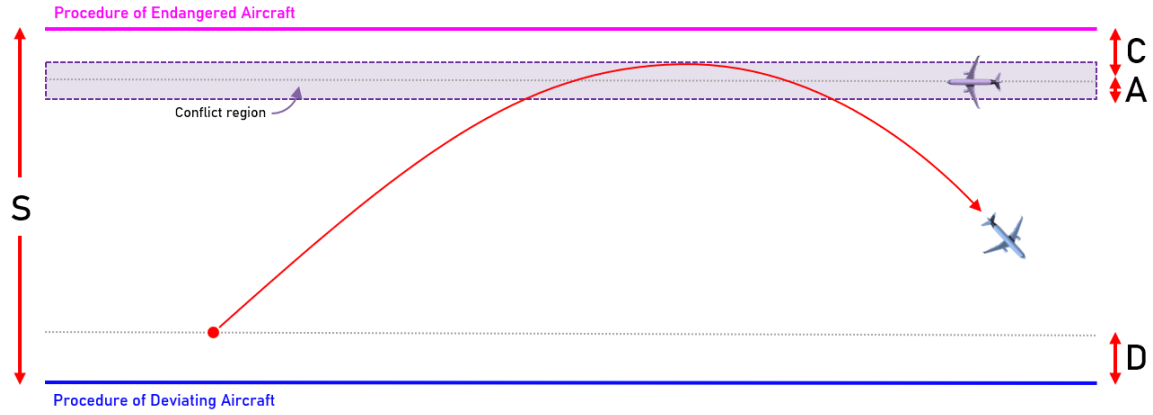

Figure 4-36: A late lateral maneuver may increase the probability of exposure by increasing the duration of an overlap condition.

The probability of such an event occurring with a well-designed mitigation is expected to be small due to the distributions of actual and necessary response times being well separated to achieve a required probability of mitigation. Nevertheless, where applicable, a potential increase in the probability of exposure due to a late response can be calculated based on the duration of the overlap condition induced by the late maneuver. The plot in Figure 4-37 illustrates how the duration of an overlap condition changes as a function of the mitigation response in the scenario above.

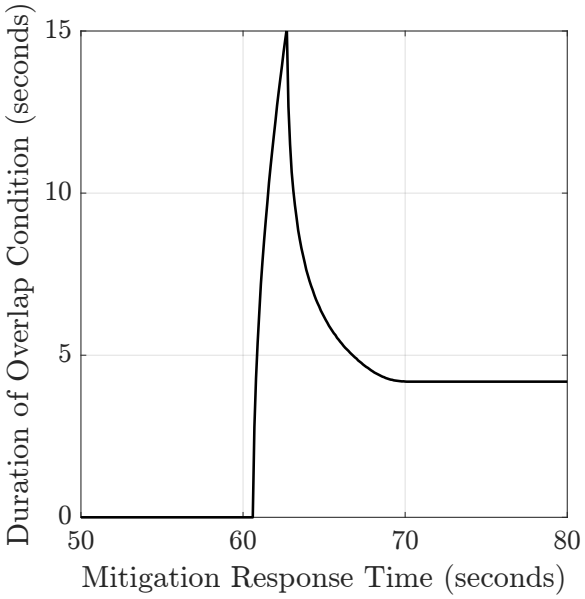

Figure 4-37: Duration of a trajectory overlap condition as a function of the mitigation response time. When the response is late, a higher probability of exposure occurs when the response occurs within a specific 5-second interval. Example parameters used: $S = 3$ NM, $V_d = 300$ kt, $\alpha = 30°$, $A = 265$ ft, $D = 0$ NM, $C = 0$ NM, $\phi_{target} = 30°$, $\dot{\phi} = 10°/sec.$

As shown in the plot in Figure 4-37, a higher probability of exposure is experienced when the mitigation response occurs within a specific time interval (between 61 and 69 seconds in this case). The overall risk contributed by the deviation under the effect of the mitigation can be calculated by integrating the probability of exposure, computed using Equation 4.8, over all possible values of the mitigation's response time (Equation 4.24).

$$\begin{aligned} &Non\text{-}Normal\ Risk\ from\ Procedure\ i = \\ &P(NN_i) \\ &\times P(Trajectory\ Overlap \mid NN_i) \\ &\times \int_0^\infty P(Exposure \mid t_{response} = t, Trajectory\ Overlap, NN_i) f_{t_{response}}(t) dt \end{aligned} \tag{4.24}$$

Summary of Evaluation of Probability of Mitigation

This section discussed the evaluation of the probability of mitigation, which was parsed into the probabilities of the mitigation being available, the mitigation's response being timely, and the mitigation's response being correct. The probabilities of availability and response correctness were posited to require testing of the mitigation system to be determined, while the probability of a timely mitigation response was found to be quantifiable based on the scenario geometry and the mitigation response performance.

A geometric model was proposed for evaluating the probability of a timely response, which was discussed in the context of the example case of two parallel, laterally separated flight procedures. For simplicity, this discussion considered maneuvering by a single aircraft (i.e., deviation mitigation). However, the model can likewise be applied to the case of maneuvering by the endangered aircraft (i.e., conflict mitigation) with minor modifications. For example, in the symmetric case in which aircraft on two parallel, opposite-direction flight procedures have the same groundspeed, the time window for successful mitigation is the same for both aircraft (assuming the same mitigation maneuver). This is illustrated in Figure 4-38 below.

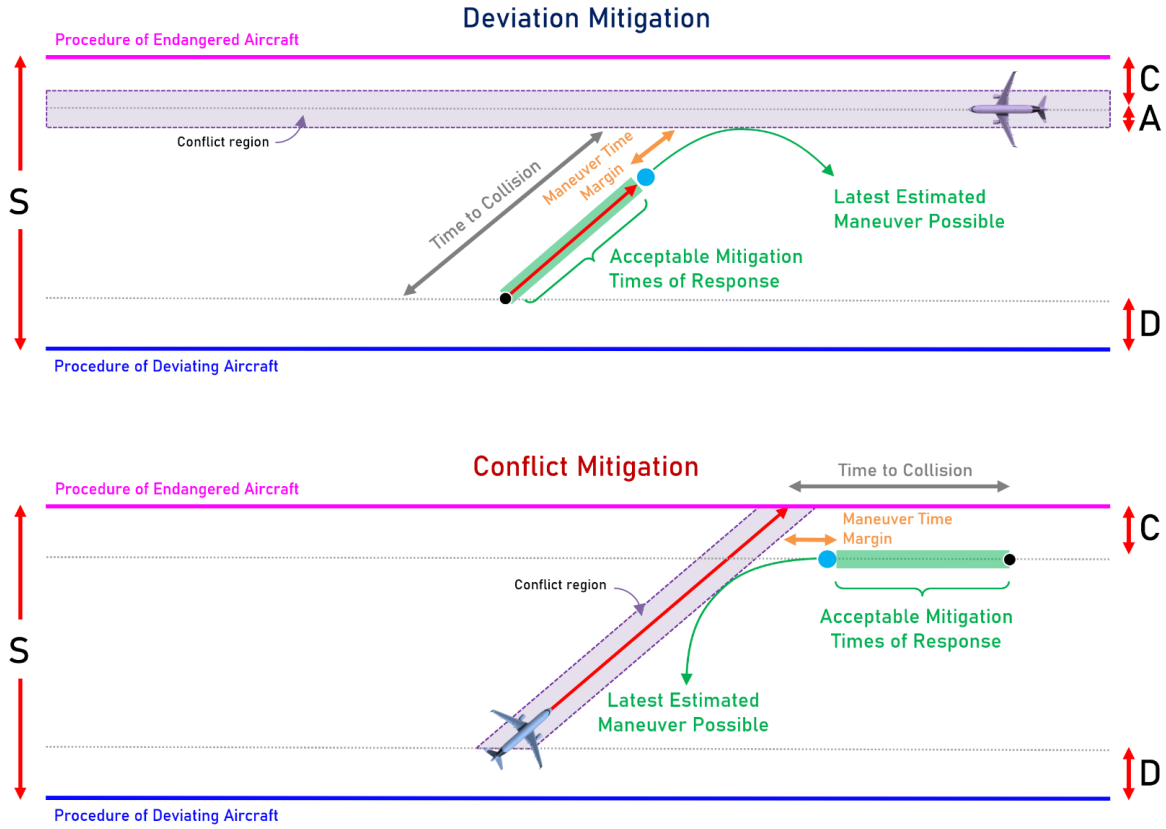

Figure 4-38: In the symmetric case in which aircraft have the same groundspeed and use the same mitigation maneuver, the mitigation response time requirement is the same for both aircraft.

By considering the availability of both mitigations simultaneously, the overall probability of mitigation increases. Further discussion on the effects of multiple available mitigations is provided in Appendix F.

The next chapter discusses key factors and levers available in mitigation and flight procedure design that can be used to control the probability of mitigation, which are identified from the geometric mitigation model covered in this chapter.

Chapter 5

Discussion of Factors Affecting Probability of Mitigation

The previous chapter identified parameters affecting the probability of a deviation being successfully mitigated. The equation derived for the probability of a timely mitigation response in the case of two parallel, laterally separated flight procedures was:

$$P(Timely\ Response) = \\ P\left(Time\ of\ Response \leq \frac{S - D - C - A}{V_d sin\alpha} - \frac{V_d \cdot tan(\alpha/2)}{g \cdot tan(\phi_{target})} - \frac{\phi_{target}}{\dot{\phi}}\right) \tag{5.1}$$

It follows that, to increase the probability of a timely response, the $Time\ of\ Response$ must be lowered and/or the necessary response time term must be increased. Visually, this is equivalent to increasing the distance between the two distributions in Figure 5-1.

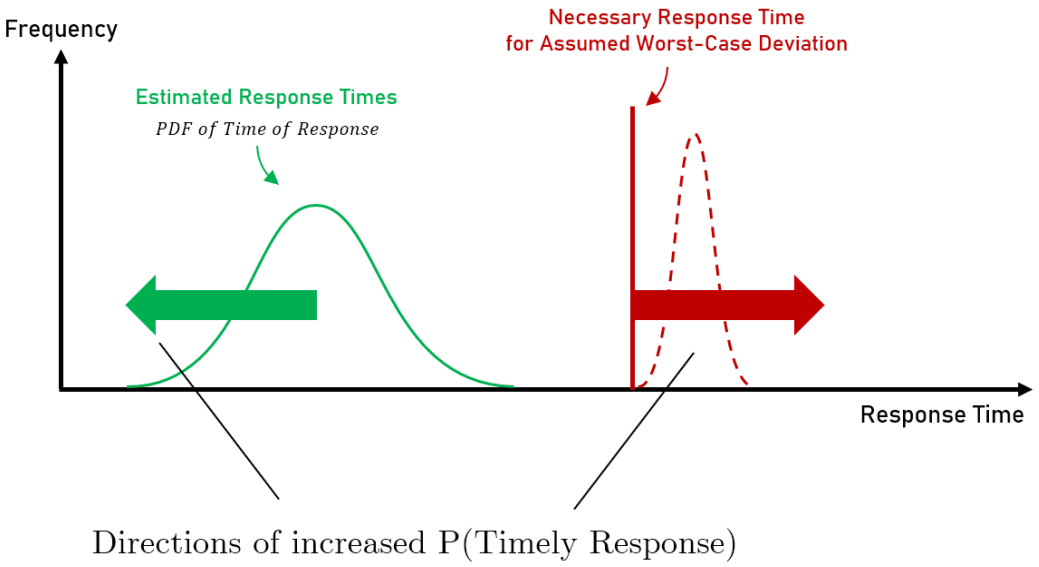

Figure 5-1: The probability of a timely mitigation response is increased when the distributions of mitigation response times and necessary response times are moved farther apart.

On the left side of the inequality, the response time achieved by the mitigation is the sum of the individual times required for detection, decision-making, communication, and maneuver initiation during the mitigation process (Figure 5-2). Reduction of any of these parameters leads to a reduction in the overall mitigation response time and an increase in the probability of mitigation.

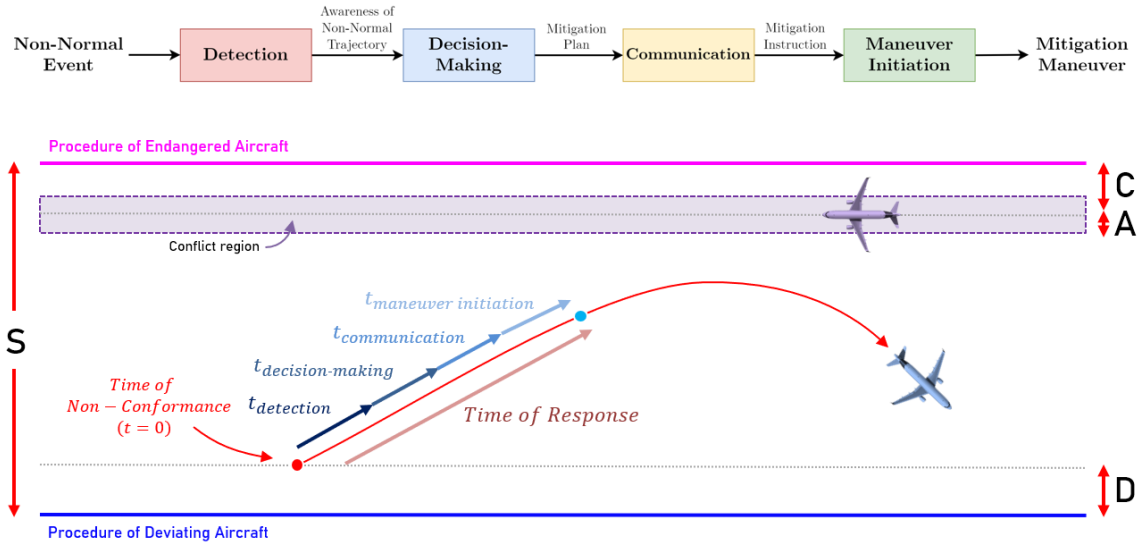

Figure 5-2: The mitigation response time is the sum of detection time, decision-making time, communication time, and maneuver initiation time.

On the right side of the inequality, the probability of mitigation can be increased by increasing the separation (S) between the procedures, decreasing the cross-track distance of the deviating aircraft at the conformance limit (D), decreasing the cross-track position of the endangered aircraft at the time of conflict (C), decreasing the groundspeed of the deviating aircraft (V_d), decreasing the deviation angle (α), and using faster maneuver dynamics (e.g., higher roll rate $\dot{\phi}$, higher target bank angle ϕ_{target}).

A summary of all factors identified for controlling the probability of a timely mitigation response in the case of laterally separated flight procedures is illustrated in Figure 5-3.

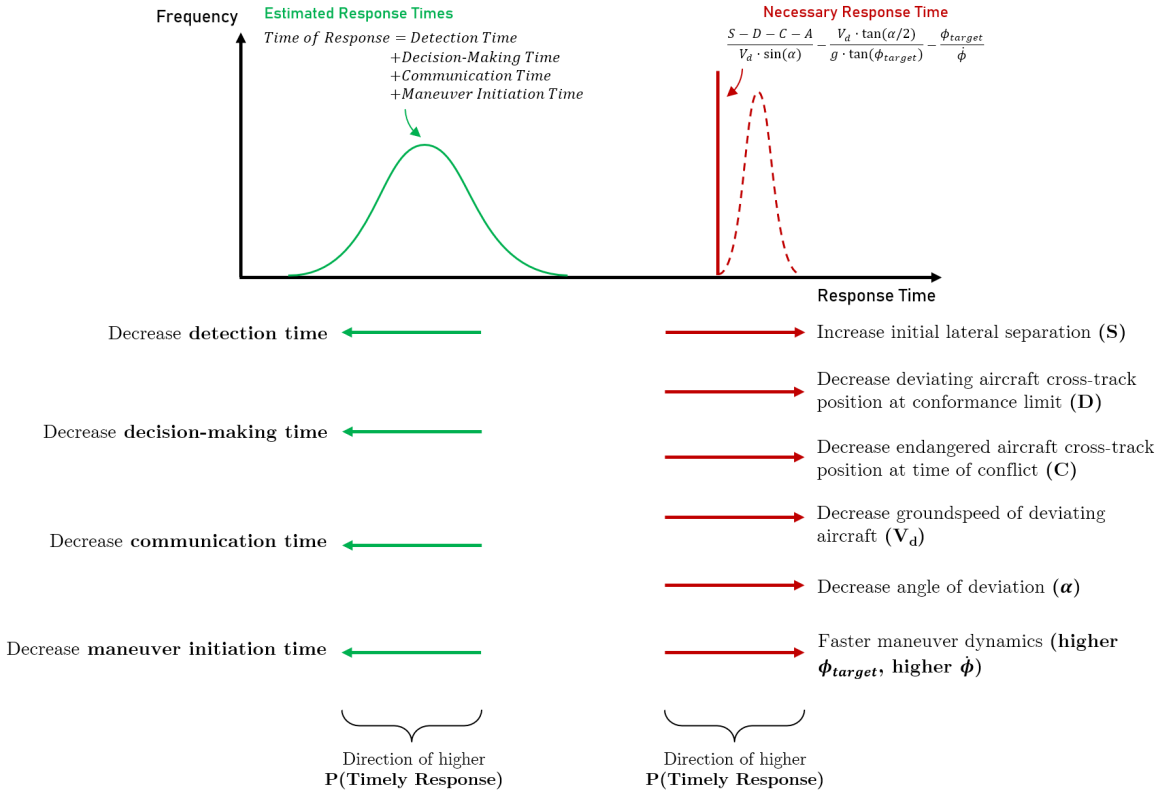

Figure 5-3: Levers available to increase the probability of a timely response in the case of parallel, laterally separated flight procedures.

The following sections discuss the levers available for controlling the probability of mitigation in further detail, including their sensitivities and potential opportunities for improving mitigations. Where applicable, the response time performance of the current system will be estimated based on available data for ATC-based mitigation.

5.1 Levers Related to Mitigation Design

Parameters related to mitigation design that affect the probability of a timely mitigation response are discussed next, with estimates of the current system's performance being discussed based on historical data.

5.1.1 Cross-Track Distance at Conformance Limit (D)

The cross-track distance of a deviating aircraft at the time it exceeds its procedure's conformance limit (D) is a function of the conformance logic used to monitor for deviations and the discrete conformance limit applied.

If the conformance logic relies only on the aircraft's cross-track position (i.e., single-state monitoring) to identify a deviation, then the variable D is deterministic and equal to the distance value selected as the conformance threshold. If the conformance logic uses additional aircraft states to identify a deviation, such as heading, then the value of D will be different for different deviation trajectories, since the conformance limit may be exceeded in more than one state dimension. The inclusion of additional states can decrease the average value of D experienced across many deviations, but it does not change its worst-case value, as illustrated in Figure 5-4. *(Note: the conformance region is assumed to be convex.)*

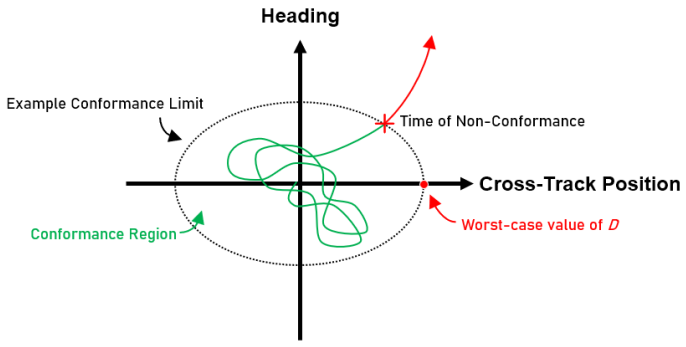

Figure 5-4: Example: when multiple aircraft states are used in conformance monitoring (e.g., cross-track position and heading), the cross-track position of aircraft at the conformance limit (D) is variable.

Given a conformance monitoring logic, a trade-off exists between the average achieved value of D and the rate of false detections. This trade-off is represented by

the performance curve shown in Figure 5-5.

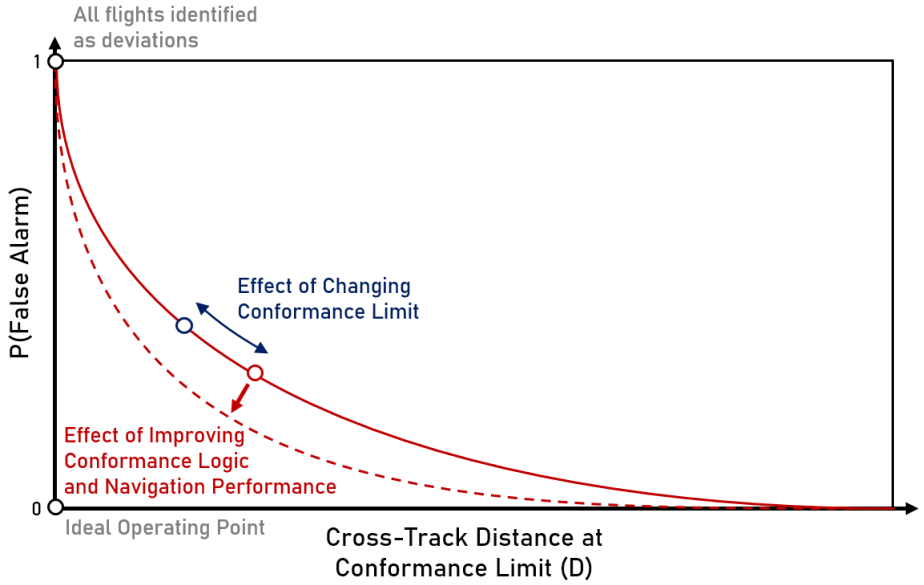

Figure 5-5: The cross-track distance of a deviating aircraft at the conformance limit (D) is related to the rate of false detections, $P(False\ Alarm)$. Adapted from Reynolds [62].

The performance curve of the conformance monitoring function can be improved through two mechanisms: 1) the development of better conformance algorithms, and 2) the improvement of aircraft navigation performance during normal operations.

In the first case, the use of more sophisticated algorithms that rely on a larger set of monitored aircraft states may allow the identification of deviation behaviors before they manifest as cross-track deviations. In the latter case, higher aircraft navigation precision allows the conformance region to be made smaller by concentrating aircraft closer to the intended trajectory. In both scenarios, a lower D can be achieved at the same rate of false detections.

An improved performance curve can offer a lower rate of false alarms at the same value of D or a lower value of D at the same rate of false alarms. While regulatory criteria do not specify a limit rate for false deviation detections, a false alarm could increase risk by causing a maneuver by a non-deviating aircraft. This hazard could be mitigated by the use of multiple conformance alert levels, in which the first alert simply results in a request for an aircraft to verify its current trajectory.

The highest possible benefit from improvements to the conformance monitoring

function can be evaluated by setting the variable D in Equation 5.1 to zero. This corresponds to the theoretical scenario in which all aircraft are identified as deviations.

As an example, the plot in Figure 5-6 illustrates how the required mitigation response time changes as a function of the cross-track distance at the conformance limit (D). Typical parameters for jet aircraft operations in terminal airspace are assumed for illustration purposes. Note that the values on the vertical axis correspond to the position of the red impulse function in Figure 5-3.

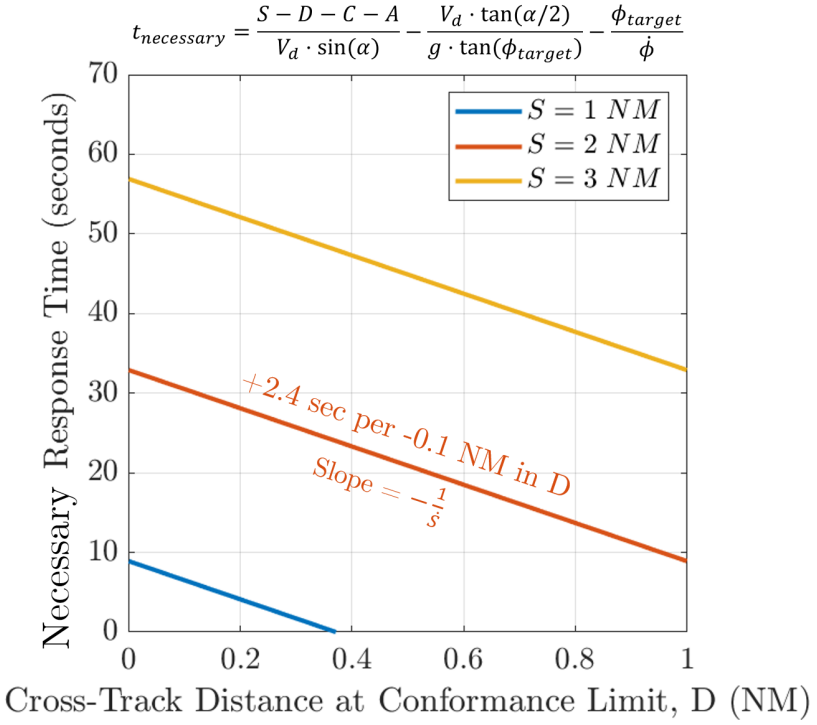

Figure 5-6: Example plot of required mitigation response time as a function of the cross-track distance of a deviating aircraft at the conformance limit. The case of $D = 0$ represents the highest performance gain possible from improvements to the conformance function. Example parameters assumed: $V_d = 300$ kt, $C = 0.2$ NM, $A = 265$ ft, $\alpha = 30°$, $\phi_{target} = 30°$, $\dot{\phi} = 10°/sec$.

In the current system, the Precision Runway Monitor (PRM) system represents the benchmark for conformance monitoring in terminal airspace. The aircraft states monitored by PRM are position, heading, and groundspeed, and its conformance logic can alert controllers of a deviation on an ILS approach within a maximum cross-track distance of 700 ft (≈ 0.1 NM) from the localizer [64]. For general terminal operations, the FAA's terminal automation system, known as STARS, does not offer an

automated conformance monitoring function. Instead, conformance monitoring in this environment is conducted through the visual scan of radar scopes by air traffic controllers, leading to imprecise or variable conformance limits. It is therefore posited that the development and implementation of automated conformance monitoring tools for PBN departure and arrival procedures could have a positive effect on the system's mitigation performance during general terminal airspace operations.

5.1.2 Detection Time

The mitigation detection time is defined as the time elapsed between an aircraft crossing the conformance limit of its procedure and the mitigation planner becoming aware of the deviation.

While actual aircraft states exist in a continuous state space, aircraft state trajectories are monitored in a discrete state space due to surveillance updates occurring at discrete intervals (Figure 5-7). As a result, a non-conformance condition is unlikely to become detectable at the exact time when the conformance limit is exceeded by an aircraft, but rather some moment later when the first non-conforming state update is received by the surveillance system. This delay is termed the *surveillance delay*. Receipt of the first non-conforming state update marks the first moment when a deviation becomes detectable by the mitigation planner. Any additional time required for the planner to become aware of the non-conforming condition is termed the *perception delay*. The detection time is thus the sum of surveillance and perception delays (Figure 5-8).

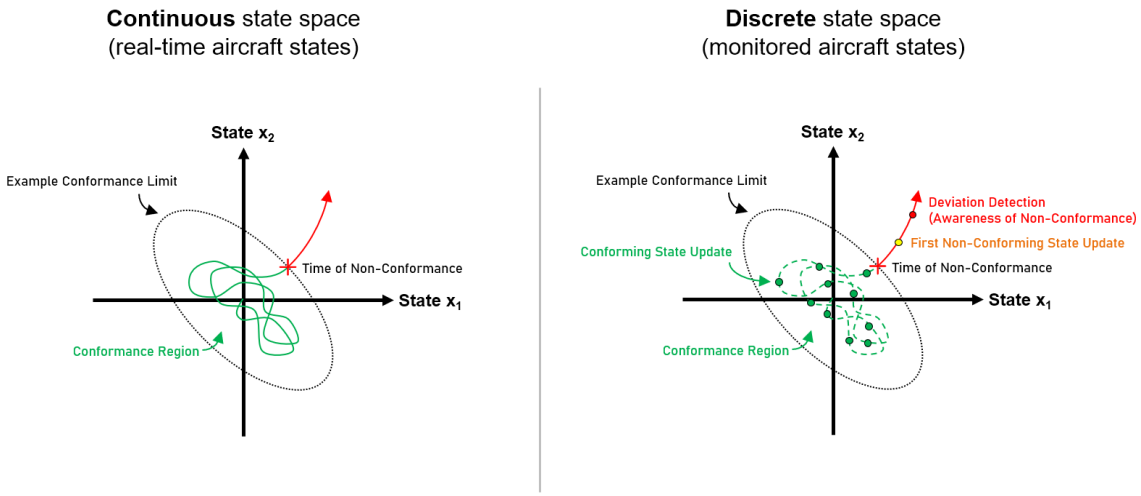

Figure 5-7: Left: continuous state space in which the aircraft operation takes place. Right: discrete state space monitored by the surveillance system.

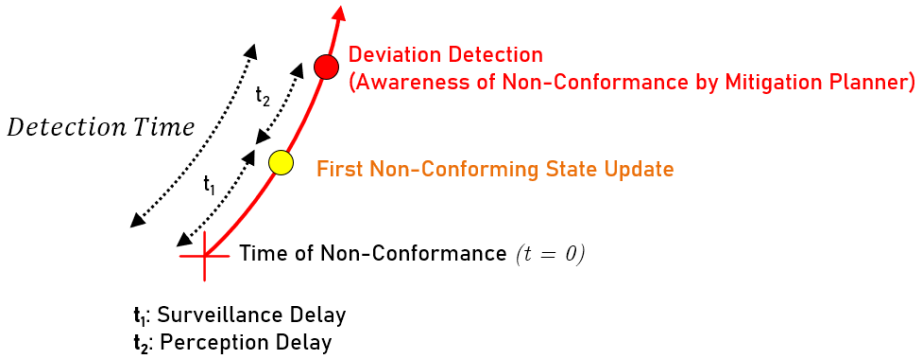

Figure 5-8: The detection time is defined as the sum of surveillance and perception delays.

Reduction of the surveillance delay is achieved by the use of higher-update-rate surveillance. In a worst-case detection scenario, the last conforming state update is received at the moment when the aircraft state position lies on the conformance limit boundary. As a result, detection of the non-conformance condition requires at least one complete surveillance update period beyond the conformance limit.

Available surveillance systems in terminal airspace today include the Approach Surveillance Radar (ASR), with an update rate of 4.8 seconds, and ADS-B, with an update rate of 1.0 seconds. Based on how many surveillance updates are used to confirm a non-conforming condition, the surveillance delay associated with each surveillance system in this scenario is shown in Figure 5-9. Note that total surveillance

delays may be slightly higher than these values due to data processing times.

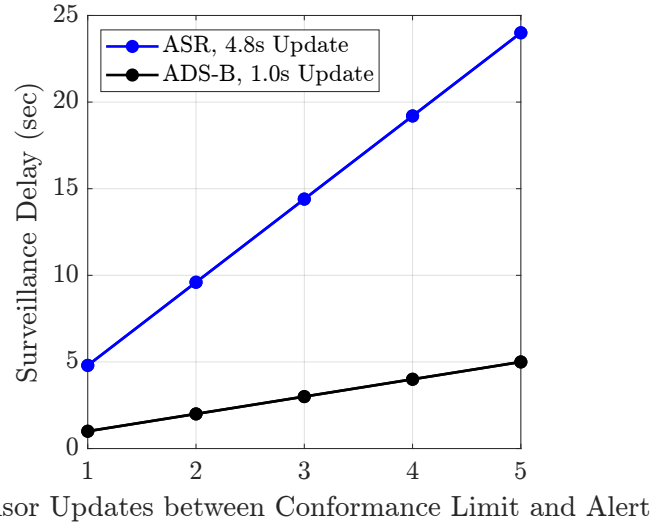

Figure 5-9: Plot of the surveillance delay associated with ASR and ADS-B for a worst-case detection scenario.

As can be observed in the plot in Figure 5-9, the use of high-update-rate surveillance systems such as ADS-B can offer significant reductions in detection time, with the lowest surveillance delay offered by ADS-B being 1 second compared to 4.8 seconds by ASR.

While the high update rate of ADS-B is attractive as a mechanism for reducing surveillance delay, the availability of ADS-B during deviation events must be carefully considered. Because ADS-B surveillance relies on self-reported aircraft states, it may be at higher risk of being unavailable during a non-normal event due to the position information broadcast by a deviating aircraft being potentially unreliable. In such a scenario, a surveillance sensor independent of the aircraft's own position solution, such as radar, must be used.

Reduction of the perception delay can be achieved with the use of visual and aural alerts when the mitigation planner remains a human agent (e.g., an air traffic controller). The current ATC automation system used by terminal facilities in the United States, STARS, does not provide automated alerting for aircraft deviating from departure and arrival procedures in terminal airspace. As a result, the perception delay in general terminal operations is likely to be higher than in scenarios for which an

alerting system is available, such as in parallel instrument approaches. In a potential future system in which the mitigation planner is an automated mitigation system, the perception delay can likely be made negligible by removing the requirement for perception by a human agent. In such a scenario, the detection time may be reduced to the value of the surveillance delay alone (e.g., 1 second for ADS-B).

In the current system, a precise conformance limit is not specified for general terminal operations. As a result, historical data measuring detection time in this operational environment was not found. As a representative estimate of this parameter, and assuming detection based on radar and human perception, a Gaussian distribution with a mean of 10 seconds and a standard deviation of 2.5 seconds will be used to represent the detection time in later example calculations (Figure 5-10).

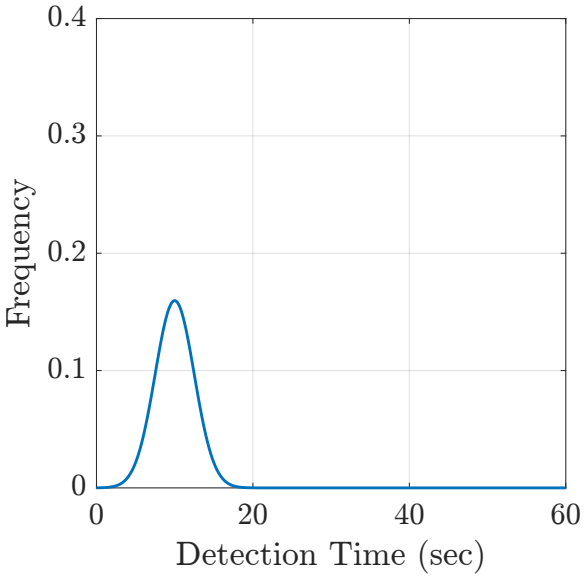

Figure 5-10: Representative estimate of detection time, which is assumed as a Gaussian process with a mean of 10 seconds and a standard deviation of 2.5 seconds based on radar performance and the requirement for human perception.

5.1.3 Decision-Making Time

The mitigation decision-making time is defined as the time needed for a mitigation plan or instruction to be devised once the mitigation planner has become aware of a deviation. In the case of deviation mitigation, this function has traditionally been served by air traffic controllers, while in the case of conflict mitigation it is also served by automation (e.g., calculation of escape maneuver by TCAS).

The decision-making time is typically a relatively short component of the overall mitigation response time. In one study evaluating the decision-making time of air traffic controllers in PRM operations, the mean decision-making time was found to be 2.3 seconds, with a standard deviation of 1.5 seconds (Figure 5-11).

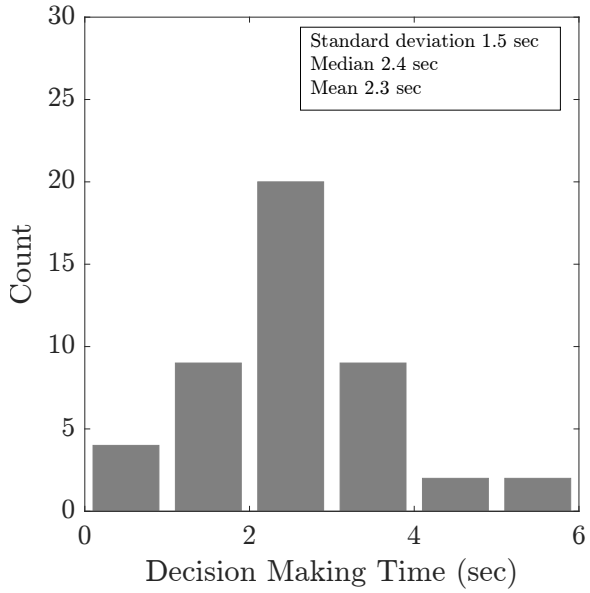

Figure 5-11: Observed decision-making time of air traffic controllers during PRM operations, measured as the time between a PRM system alert and the start of a controller transmission. Adapted from Shank et al [39].

If a Gaussian distribution is assumed for these results, the following distribution can be derived, which will be used in later example calculations as a representative estimate of the decision-making time (Figure 5-12).

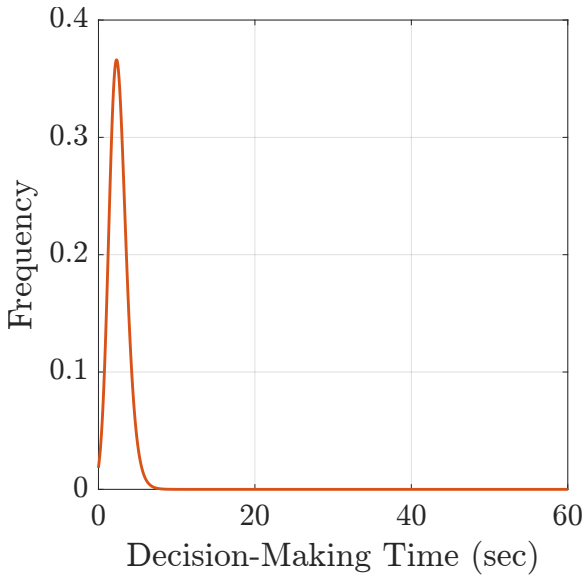

Figure 5-12: Representative estimate of decision-making time, based on a Gaussian fit of the data in [39].

Note that the data collected by prior studies have not considered the effects of traffic volume on controller decision-making time. As the number of aircraft in an airspace increases, the calculation of an appropriate mitigation plan or maneuver may become increasingly complex and therefore require more time. As a result, it is posited that automation of the mitigation planning function may offer improved response time performance in high-density environments, such as in future concepts of operations that integrate Advanced Air Mobility (AAM) traffic into terminal airspaces.

5.1.4 Communication Time

The communication time is the time needed to communicate a mitigation instruction to a target aircraft, which is also known as the *transaction time* [65]. The communication time is a function of the communication channel used in the mitigation process. In the current system, mitigation instructions from air traffic control are delivered to aircraft via voice instructions delivered by VHF radio.

In one study evaluating the time required for the transmission of ATC maneuvering instructions by voice, significant variations in transaction time were identified, which were related to factors such as frequency congestion, the ability of a flight crew to readily understand an instruction, the need for readbacks, and the potential need for

a repeat instruction (Table 5.1).

	Communication Time
Minimum	4 sec
Median	9 sec
Mean	10.85 sec
90th Percentile	17 sec
95th Percentile	23 sec
99th Percentile	40 sec
Maximum	40 sec

Table 5.1: Observed times required for the successful transmission of voice-based ATC maneuvering instructions, based on 80 transmissions. Adapted from Cardosi [66].

The values in Table 5.1 represent significant fractions of a typical ATC-based mitigation timeline. In a future mitigation system, it is posited that the use of Datalink communications could offer a significant improvement in communication time in scenarios where Datalink latency is low. By combining Datalink communications with an automated mitigation planner, the process of generating and transmitting a mitigation maneuver instruction is likely to be significantly faster than what is currently achievable with voice-based communications. In addition to its effect on the probability of a timely mitigation response, the use of Datalink communications may also improve the probability of a correct mitigation response, as it eliminates the possibility of an instruction being misheard by a flight crew.

By applying a Gaussian fit to the mean and standard deviation reported in [66], the following distribution can be obtained, which will be used in later example calculations as a representative estimate of the communication time (Figure 5-13).

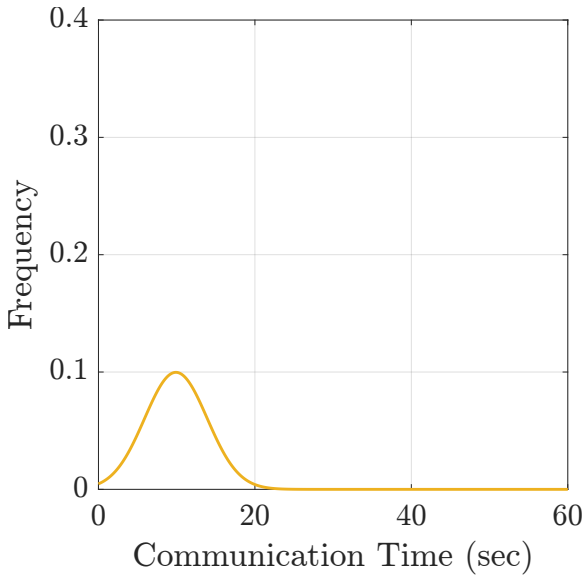

Figure 5-13: Representative estimate of communication time, based on a Gaussian fit of the data in [66].

5.1.5 Maneuver Initiation Time

The maneuver initiation time is the time elapsed between a mitigation instruction being delivered to a target aircraft and the maneuver being initiated. For a lateral mitigation maneuver, this corresponds to the time between an aircraft receiving a mitigation instruction and it beginning a roll maneuver.

In the current system, response to mitigation instructions is typically performed by a flight crew either through manual control of the aircraft or through adjustment of autopilot target parameters. In the case of mitigation by TCAS, certain aircraft are also equipped to fly TCAS maneuver instructions automatically using an autopilot system [67].

When response to a mitigation instruction is handled by pilots, the maneuver initiation time is driven by flight crew response time. The evaluation of pilot response time has been the subject of several studies, which show considerable variability in the response times achieved. Figure 5-14 below shows pilot response times recorded during testing of the PRM system [68].

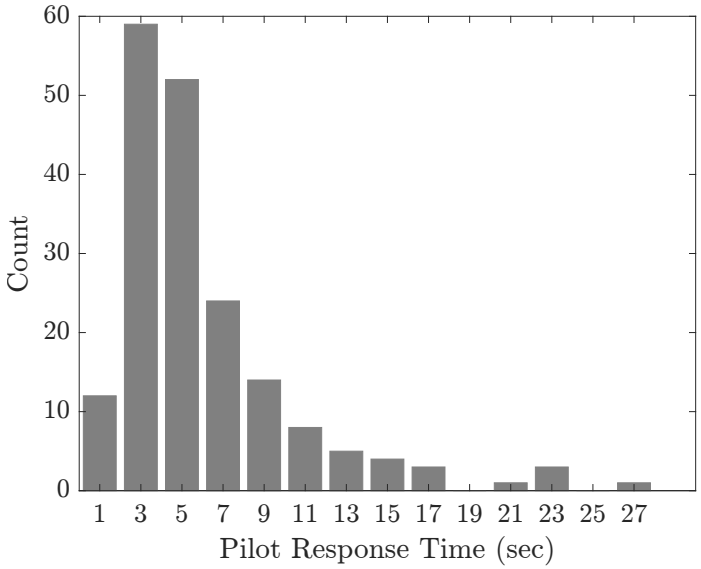

Figure 5-14: Observed pilot response time during PRM operations, measured as the time needed to initiate a roll maneuver after the end of a controller transmission, based on flight simulator trials. Adapted from PRM Program Office [68].

The values observed in Figure 5-14 represent significant fractions of a typical ATC-based mitigation timeline. Based on this data, it is posited that the automation of aircraft response in future mitigation systems may offer significant gains in response time performance. Such a capability could be combined with Datalink communications to produce mitigation instructions that are delivered directly to an aircraft's flight management system and subsequently executed by an autopilot.

A Johnson fit of the pilot response data above is provided in [69], and will be used in later example calculations as a representative estimate of the maneuver initiation time (Figure 5-15).

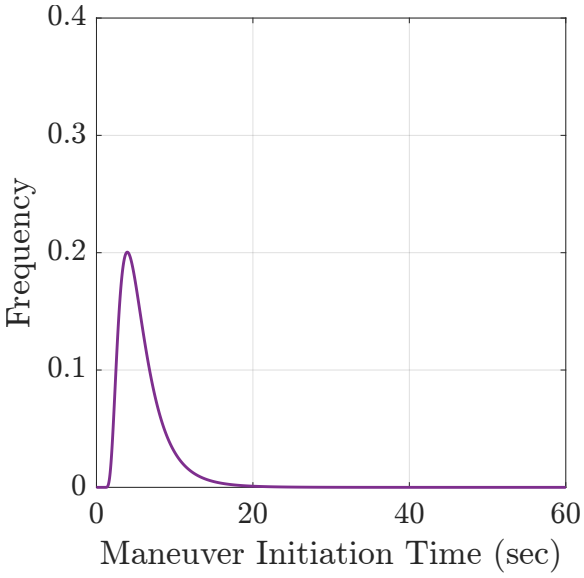

Figure 5-15: Representative estimate of communication time, based on a Gaussian fit of the data in [66].

5.1.6 Summary of Levers Available in Mitigation Design

Analysis of the different functions making up the mitigation process has led to the identification of several opportunities for improving mitigation performance. In the case of deviation mitigation, the current system is observed to rely primarily on air traffic controllers to detect, plan, and communicate mitigation instructions to aircraft via voice. Once received by aircraft, maneuver instructions are manually executed by flight crews. Due to its reliance on human performance, this process exhibits noticeable variance in its response time performance.

Figure 5-16 summarizes the response time components estimated for the current system based on mitigation by ATC, which were discussed in this section. By assuming that the four components are statistically independent, these distributions can be combined into a single response time distribution through a convolution (Time of Response = Detection Time + Decision-Making Time + Communication Time + Maneuver Initiation Time), with the result shown in Figure 5-17. This distribution, which is believed to be a representative estimate of the response time distribution of the current system, has an average response time of 28 seconds and a standard deviation of 6 seconds.

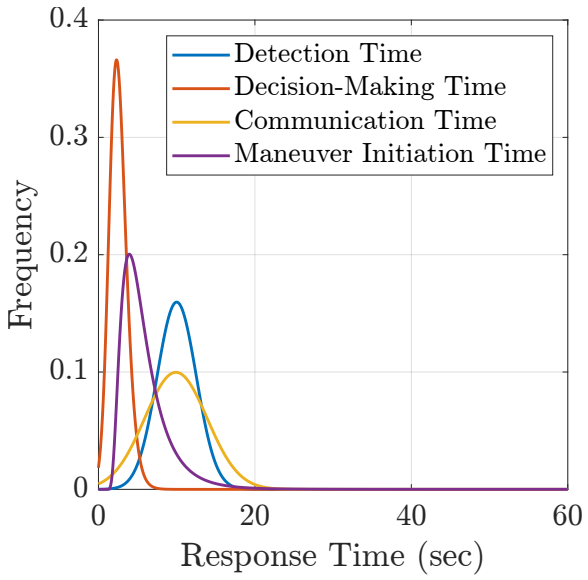

Figure 5-16: Representative estimates of detection, decision-making, communication, and maneuver initiation time for the current system based on mitigation by ATC.

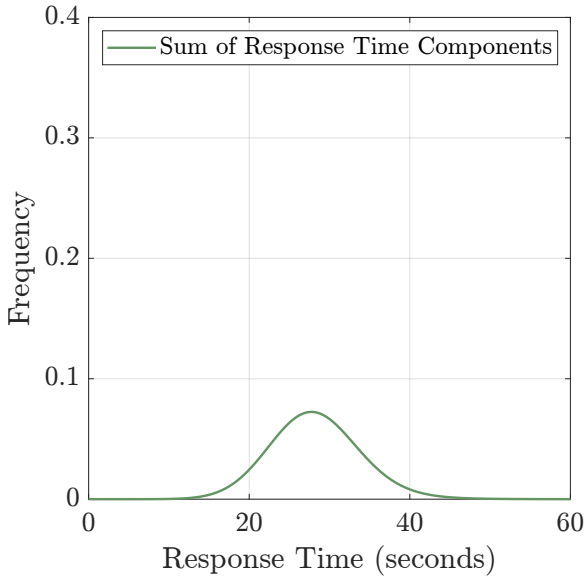

Figure 5-17: Representative estimate of the overall response time for the current system based on mitigation by ATC, calculated as the sum (convolution) of response time components in Figure 5-16.

Regarding conformance monitoring, the current system is observed to rely primarily on the visual scanning of radar scopes by air traffic controllers for this task in general terminal operations. As a result of this practice, actual conformance limits applied in practice may be imprecise and variable, which may result in relatively large

cross-track deviations before the mitigation process is initiated.

Based on these observations, it is posited that the development of a future mitigation system with automated conformance monitoring and detection, automated calculation of mitigation maneuvers, Datalink communications, and automated aircraft response could provide significant improvements in mitigation performance. A comparison of this potential future system against existing ATC-based mitigation is summarized in Table 5.2. While conformance monitoring, detection, and decision-making are performed on the ground in the case of ATC-based mitigation, these functions could potentially be implemented as airborne systems, e.g., aircraft on flight procedures could monitor each other's conformance.

Function	Current System	Potential Future System
Conformance Monitoring	Visual scan of aircraft position by controllers.	Automated conformance monitoring based on multiple aircraft states.
Detection	Radar-based surveillance (4.8-second updates).	High-update-rate surveillance (e.g., ADS-B).
Decision-Making	Planning by air traffic controllers.	Automated planning and maneuver calculation.
Communication	Mitigation instructions issued via voice (VHF).	Mitigation instructions issued via Datalink messages.
Maneuver Initiation	Maneuver executed manually by pilots.	Datalink instruction executed by autopilot.

Table 5.2: Comparison of mitigation functions currently used for deviation mitigation in the current system and those of a potential future mitigation system.

The combination of improved CNS technologies (e.g., ADS-B, Datalink) and greater automation use are posited to offer a lower average mitigation response time as well as more consistent performance with lower response time variance. Combined, these effects can contribute to a higher probability of mitigation by increasing the separation between *actual* mitigation response times and *necessary* response times (Figure 5-18).

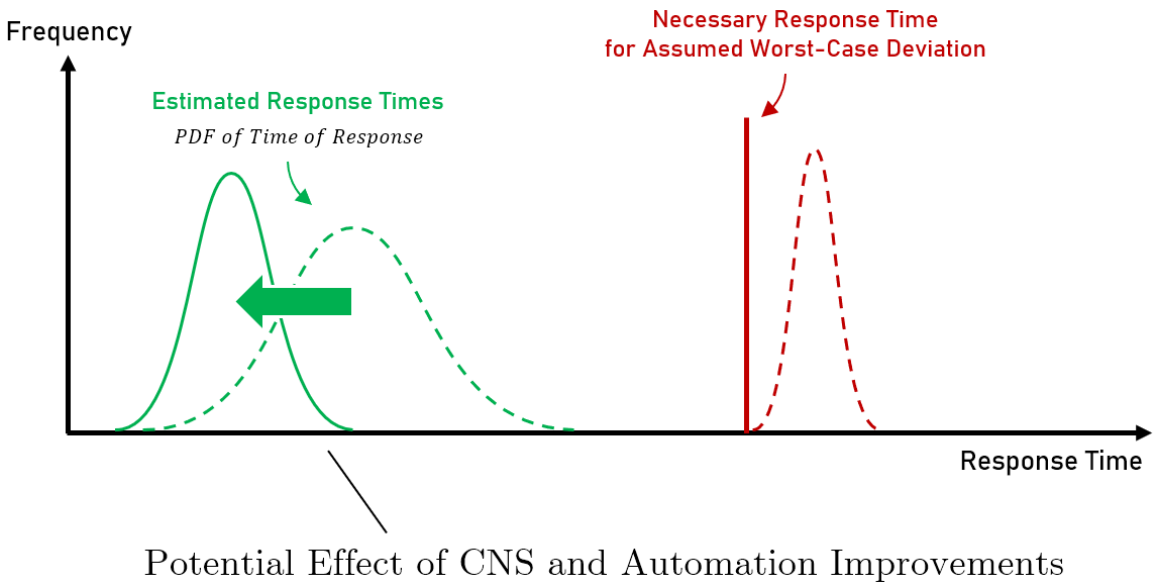

Figure 5-18: CNS and automation improvements can increase the probability of mitigation by reducing the average response time and response time variance.

The reduction of response time variance, which affects the tails of the response time distribution, is identified as an important mechanism for improving mitigation performance. This is because, as shown in Table 5.3, meaningful risk reductions through mitigation require relatively high probabilities of mitigation, which in turn require large percentiles of the response time distribution to meet necessary response times. Reductions in response time variance may be achievable through greater use of automation and lower reliance on human performance during the mitigation process.

Target Level of Safety	Unmitigated Risk	Required $P(Mitigation)$
10^{-9}	10^{-5}	>99.99%
	10^{-6}	>99.9%
	10^{-7}	>99%
	10^{-8}	>90%

Table 5.3: Required probability of successful mitigation as a function of the unmitigated non-normal risk, i.e., $P(NN) \times P(Unmitigated\ Collision \mid NN)$. Normal risk is assumed to be negligible.

5.2 Levers Related to Aircraft Operations and Flight Procedure Design

In addition to changes to the mitigation function, the probability of a timely mitigation response can be controlled through changes to aircraft operations and flight procedure design. Parameters related to these areas are discussed next.

5.2.1 Lateral Separation Between Procedures (S)

The separation between procedures, represented by the parameter S, affects the required mitigation response time (i.e., the red distribution in Figure 5-3) by changing the distance that a deviation must travel until collision, and is the main lever available in procedure design for regulating the time-to-collision of a deviation.

The plot in Figure 5-19 illustrates how the required mitigation response time changes as a function of S based on the application of Equation 5.1. Typical parameters for jet aircraft operations in terminal airspace are assumed for illustration purposes.

The effect of lateral separation (S) on the available time for mitigation is observed to scale according to the inverse of the rate of separation loss ($\dot{S}$) during a deviation. As a result, an increase in separation will produce a larger change in mitigation probability when $\dot{S}$ is smaller, such as when aircraft have lower groundspeeds. The effect of groundspeed on achievable separation values is discussed further in a subsequent section.

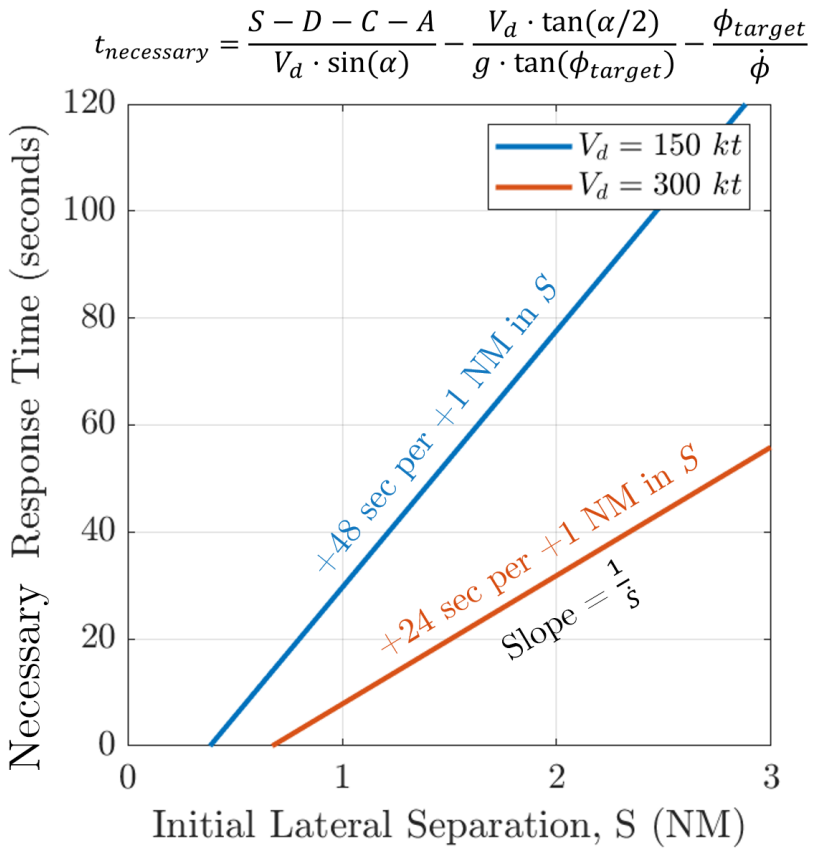

Figure 5-19: Example plot of required mitigation response time as a function of the lateral separation between procedures (S). Example parameters assumed: $D = 0.1$ NM, $C = 0.2$ NM, $A = 265$ ft, $\alpha = 30°$, $\phi_{target} = 30°$, $\dot{\phi} = 10°/sec$.

5.2.2 Endangered Aircraft Cross-Track Position (C)

The cross-track position of the endangered aircraft at the time of conflict, represented by the parameter C, affects the required mitigation response time (i.e., the red distribution in Figure 5-3) by changing the distance that a deviation must travel until collision. This parameter is linked to the precision with which aircraft on the endangered flight procedure maintain their nominal trajectory. An improvement in navigation performance in normal operations can therefore improve the probability of a timely response by reducing the possible values of C.

A representative worst-case value of C can be derived from the required navigation performance on the endangered procedure. Assuming RNAV performance, a value of 0.2 NM may be treated as a representative worst-case value of C based on prior

analysis conducted in Chapter 4.

Changes to the parameter C have a mathematically identical effect as changes to D (cross-track distance at conformance limit), which were previously discussed. The plot in Figure 5-20 illustrates how the required mitigation response time changes as a function of C based on the application of Equation 5.1. Typical parameters for jet aircraft operations in terminal airspace are assumed for illustration purposes.

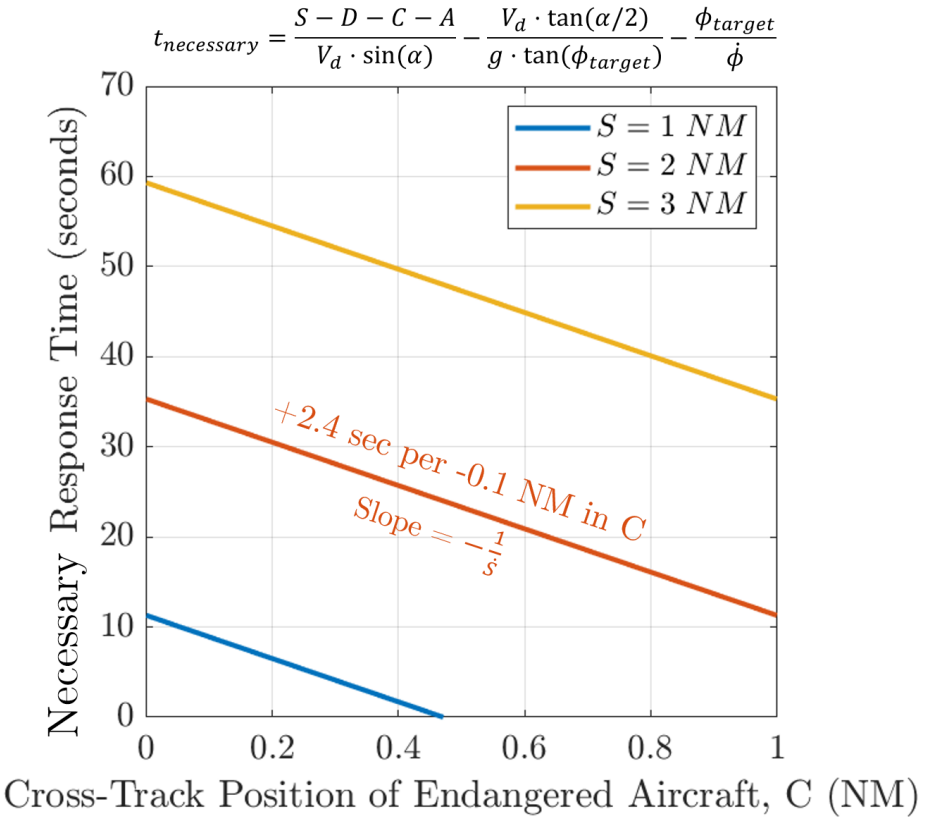

Figure 5-20: Example plot of required mitigation response time as a function of the cross-track position of the endangered aircraft (C). The case of $C = 0$ represents the highest performance gain possible from improvements to navigation performance. Example parameters assumed: $V_d = 300$ kt, $D = 0.1$ NM, $A = 265$ ft, $\alpha = 30°$, $\phi_{target} = 30°$, $\dot{\phi} = 10°/sec$.

The highest possible benefit from improvements to navigation performance on the endangered procedure can be evaluated by setting C to zero. This corresponds to the theoretical scenario in which aircraft on the endangered procedure have perfect navigation.

5.2.3 Groundspeed of Deviating Aircraft (V_d)

The groundspeed of a deviating aircraft (V_d) affects the time available for mitigation by changing the rate of separation loss during a deviation ($\dot{S} = V_d \times sin\alpha$). The groundspeed at which aircraft fly procedures in terminal airspace is a function of both operational considerations and speed restrictions that can be designed into flight procedures.

Effects of changes to V_d are illustrated in Figure 5-21, which shows how the required mitigation response time changes as a function of V_d. Typical parameters for jet aircraft operations in terminal airspace are assumed for illustration purposes.

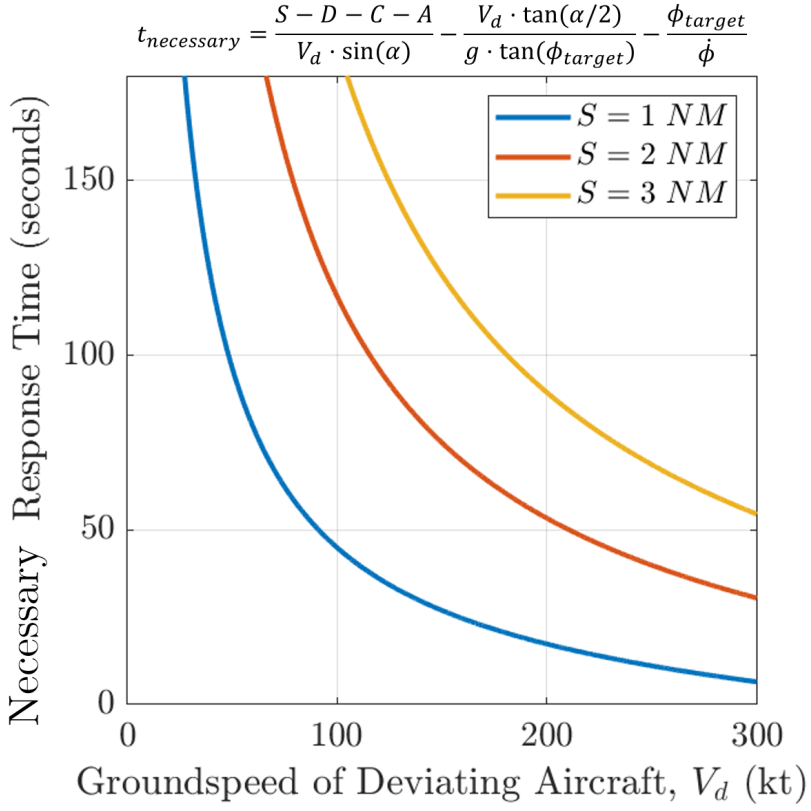

Figure 5-21: Example plot of required mitigation response time as a function of the groundspeed of the deviating aircraft (V_d). Example parameters assumed: $D = 0.1$ NM, $C = 0.2$ NM, $A = 265$ ft, $\alpha = 30°$, $\phi_{target} = 30°$, $\dot{\phi} = 10°/sec$.

The groundspeed (V_d) can be observed to have a significant effect on the time available for mitigation, with the necessary response time growing exponentially as the groundspeed is lowered. This result suggests that the separation between flight

procedures with lower groundspeeds (e.g., parallel approaches) can be lower than that between procedures with higher groundspeeds (e.g., high-altitude jet operations), assuming equal mitigation performance. In addition, the use of speed restrictions on flight procedures may be an effective mechanism for controlling aircraft groundspeed and enabling the use of lower separation values. Table 5.4 illustrates the relative gain in the available time for mitigation due to a reduction in groundspeed.

	Nec. Response Time at $S = 1$ NM	Nec. Response Time at $S = 2$ NM	Nec. Response Time at $S = 3$ NM
$V_d = 200\ kt$	17 seconds (+143%)	53 seconds (+71%)	89 seconds (+62%)
$V_d = 250\ kt$	11 seconds (+57%)	40 seconds (+29%)	69 seconds (+25%)
$V_d = 300\ kt$ (Reference)	7 seconds	31 seconds	55 seconds

Table 5.4: Values of required mitigation response time as a function of V_d and lateral separation (S). A reduction in the groundspeed from 300 kt to 250 kt causes the time available for mitigation to increase by 25% to 57%, depending on the initial separation between the procedures.

5.2.4 Angle of Deviation (α)

The parameter α corresponds to the lateral deviation angle assumed in the simplified deviation trajectory model used in Equation 5.1, which is used to represent the magnitude of a lateral deviation.

Similarly to groundspeed, the deviation angle (α) affects the time available for mitigation by changing the rate of separation loss ($\dot{S} = V_d \times sin\alpha$). In addition, for a lateral mitigation maneuver, it affects the maneuvering time required to reverse the closure rate, since $\dot{S}$ is reversed only when α changes signs.

Effects of changes to α are illustrated in Figure 5-22, which shows how the required mitigation response time changes as a function of α. Typical parameters for jet aircraft operations in terminal airspace are assumed for illustration purposes.

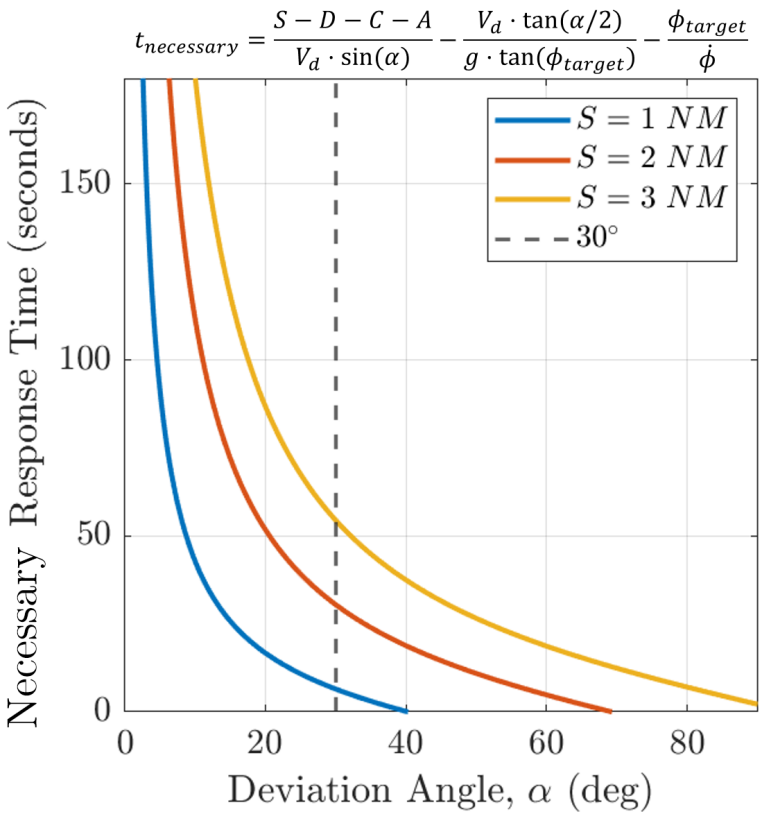

Figure 5-22: Example plot of required mitigation response time as a function of the deviation angle (α). The commonly assumed worst-case deviation angle of 30° has been highlighted. Example parameters assumed: V_d = 300 kt, D = 0.1 NM, C = 0.2 NM, A = 265 ft, $\phi_{target} = 30°$, $\dot{\phi} = 10°/sec$.

Among the parameters related to aircraft operations and flight procedure design, the deviation angle is observed to have the most significant effect on the required mitigation response time. When starting from the historically assumed deviation angle of 30°, relatively small changes in α can lead to significant changes in the required mitigation response time, as shown in Table 5.5.

	Nec. Response Time at $S = 1$ NM	Nec. Response Time at $S = 2$ NM	Nec. Response Time at $S = 3$ NM
$\alpha = 10°$	46 seconds (+514%)	115 seconds (+261%)	184 seconds (+227%)
$\alpha = 20°$	20 seconds (+143%)	55 seconds (+68%)	90 seconds (+58%)
$\alpha = 30°$ (Reference)	10 seconds	34 seconds	58 seconds

Table 5.5: Values of required mitigation response time as a function of α and lateral separation (S). A reduction in the deviation angle from 30° to 20° causes the time available for mitigation to increase by 58% to 143%, depending on the initial separation between the procedures.

The deviation angle (α) is a simplification of actual deviation trajectories, which were previously argued to not be well understood. While a value of 30° has historically been used to represent a worst-case deviation based on subjective consensus among safety stakeholders, a better understanding of actual deviation magnitudes may have a significant effect on collision risk estimates due to the sensitivity identified above. If worst-case deviations can be shown to occur at smaller magnitudes than previously thought, this may result in higher estimates of mitigation probabilities and increased opportunities to reevaluate the required separation between procedures.

From a mitigation design perspective, it is posited that the deviation angle may also be affected by the ability of a mitigation system to detect deviations before they develop into large-magnitude deviations. The use of aircraft velocity and acceleration states (e.g., heading, bank angle) as part of conformance monitoring, for instance, may enable the detection of lateral deviations before significant deviation angles develop, potentially reducing the magnitude of worst-case deviations.

5.2.5 Maneuver Dynamics ($\phi_{\mathbf{target}}, \dot{\phi}$)

The effect of maneuver dynamics on the available time for mitigation is represented by the maneuver time margin component of Equation 5.1. For a lateral mitigation

maneuver, the relevant maneuver parameters affecting the probability of mitigation were identified to be the roll rate ($\dot{\phi}$) and the target bank angle (ϕ_{target}), which result in a turn radius (R).

Effects of changes to the target bank angle (ϕ_{target}) are illustrated in Figure 5-23. The plot on the left shows how the required mitigation response time changes as a function of ϕ_{target}, while the plot on the right shows how the value of the maneuver time margin alone changes as a function of ϕ_{target}. Typical parameters for jet aircraft operations in terminal airspace are assumed for illustration purposes.

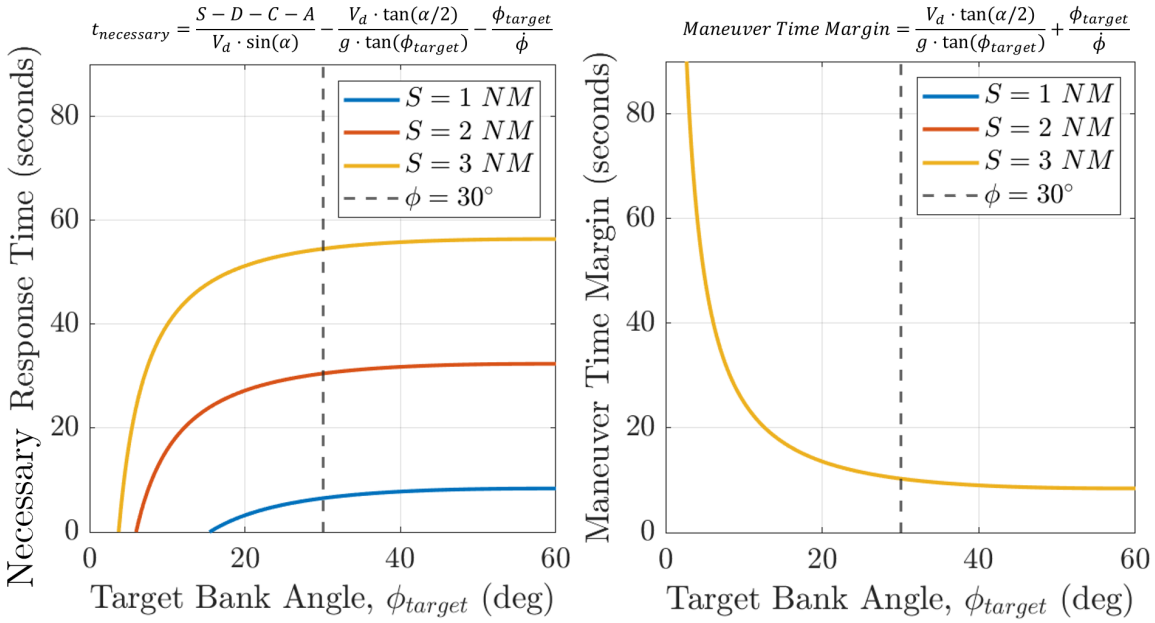

Figure 5-23: Left: Required mitigation response time as a function of ϕ_{target}. Right: Maneuver time margin as a function of ϕ_{target}. Example parameters assumed: $V_d = 300$ kt, $D = 0.1$ NM, $C = 0.2$ NM, $A = 265$ ft, $\alpha = 30°$, $\dot{\phi} = 10°/sec$.

The required mitigation response time is observed to be relatively insensitive to bank angles above 30°. At the groundspeed (V_d) of 300 kt applied in the example above, the maneuver time margin ranges between 8 and 10 seconds for target bank angles above 30°. While this example has only considered lateral maneuvers, the use of vertical maneuvers may offer a lower maneuver time margin due to faster dynamics.

Effects of changes to the roll rate ($\dot{\phi}$) are illustrated in Figure 5-24. The plot on the left shows how the required mitigation response time changes as a function of $\dot{\phi}$, while the plot on the right shows how the value of the maneuver time margin alone

changes as a function of $\dot{\phi}$. Typical parameters for jet aircraft operations in terminal airspace are assumed for illustration purposes.

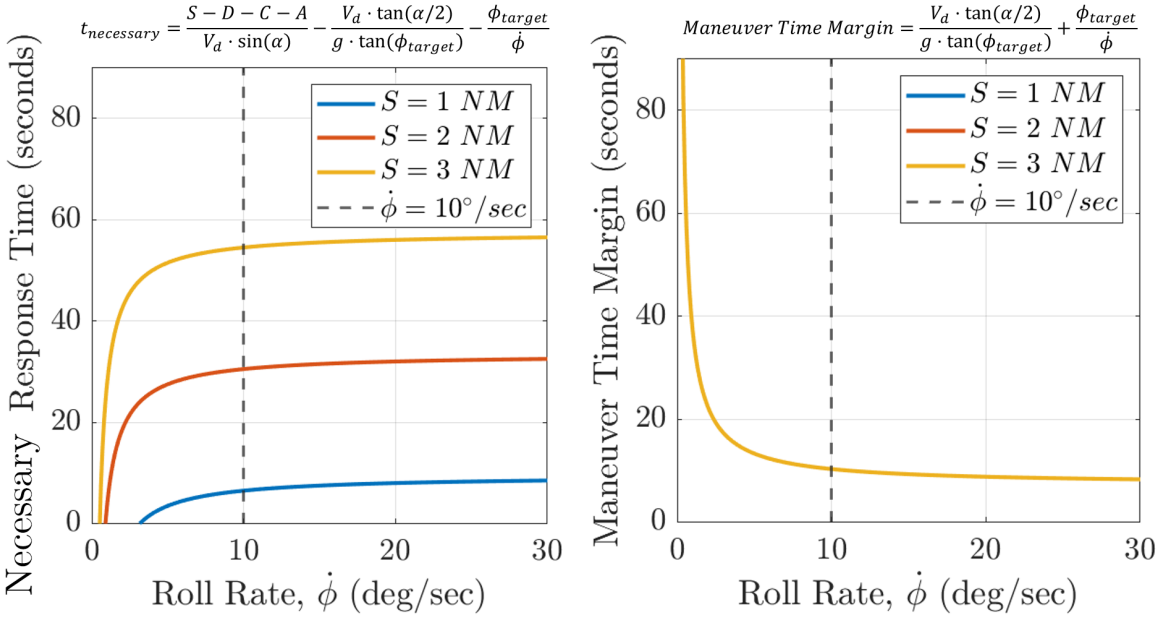

Figure 5-24: Left: Required mitigation response time as a function of $\dot{\phi}$. Right: Maneuver time margin as a function of $\dot{\phi}$. Example parameters assumed: $V_d = 300$ kt, $D = 0.1$ NM, $C = 0.2$ NM, $A = 265$ ft, $\alpha = 30°$, $\phi_{target} = 30°$.

Similarly to the effect of the target bank angle, roll rates above 10 degrees per second are observed to not have a significant effect on the required mitigation response time or the maneuver time margin.

These results suggest that a target bank angle of 30° coupled with a roll rate of 10° are reasonable specifications for a lateral mitigation maneuver, and that no significant benefits are expected from more aggressive lateral maneuvers at the groundspeed considered.

5.2.6 Summary of Levers Available in Aircraft Operations and Flight Procedure Design

This section analyzed and discussed several factors related to aircraft operations and flight procedure design that drive the required mitigation response time and that may be available as levers for controlling the probability of mitigation. The most sensitive parameters were found to be the angle of deviations (α) and the groundspeed

of deviating aircraft (V_d), which together determine the rate of separation loss ($\dot{S}$) during a deviation event. Potential opportunities to control these two parameters were identified in the design of mitigation systems that monitor aircraft velocity and acceleration states to detect deviations before they develop into large-magnitude deviations, and in the use of speed restrictions on flight procedures to limit aircraft groundspeed values when applicable.

Following the discussion of parameters driving the probability of a timely mitigation response in this chapter, the next chapter presents example applications of the mitigated collision risk model introduced thus far, and explores how the model can be used to explore how different system improvements may lead to future reductions in separation in different scenarios.

Chapter 6

Example Applications of Mitigated Collision Risk Model

This chapter discusses three example applications of the mitigated collision risk model covered in Chapters 4 and 5. The objective of these examples is to illustrate how the methods described can be used to evaluate achievable separation values between flight procedures based on mitigation performance and explore how different system improvements may allow for a reduction in separation and therefore an increase in flexibility. The three example scenarios considered are:

1. The evaluation of the mitigated collision risk for a generic case of two symmetric, parallel, opposite-direction, co-altitude flight procedures operated by jet aircraft, which are initially separated by 3 NM. This represents a worst-case scenario that is believed to be acceptable under current separation standards.
2. The evaluation of achievable separation values between an RNAV departure and an ILS approach serving converging runways, based on a real case at Boston Logan Airport (BOS) that could offer noise reduction benefits.
3. The evaluation of achievable separation values between two laterally separated Advanced Air Mobility (AAM) routes, which represents a hypothetical future scenario.

The following sections of this chapter present an overview of each example scenario and discuss the analysis performed for each case.

6.1 Generic Case of Laterally Separated Jet Aircraft Procedures

The example considered in this section evaluates the mitigated collision risk between two symmetric, parallel, opposite-direction, co-altitude flight procedures that are initially separated by 3 NM. This represents a worst-case scenario that is believed to be acceptable under current separation standards. The following assumptions will be made in the risk evaluation:

- The probability of non-normal events, $P(NN)$, is assumed to be 10^{-5} per aircraft operation based on historical estimates [30].
- Aircraft are assumed to be flying at a groundspeed of 350 kt, which represents a high value for terminal operations when accounting for tailwind and altitude effects.
- Aircraft are separated in-trail by 3 NM.
- Aircraft have RNAV tracking performance in normal operations.
- Non-normal events lead to lateral deviations with an angle of 30°.
- Mitigation of deviations is performed by ATC.

This example scenario is illustrated in Figure 6-4.

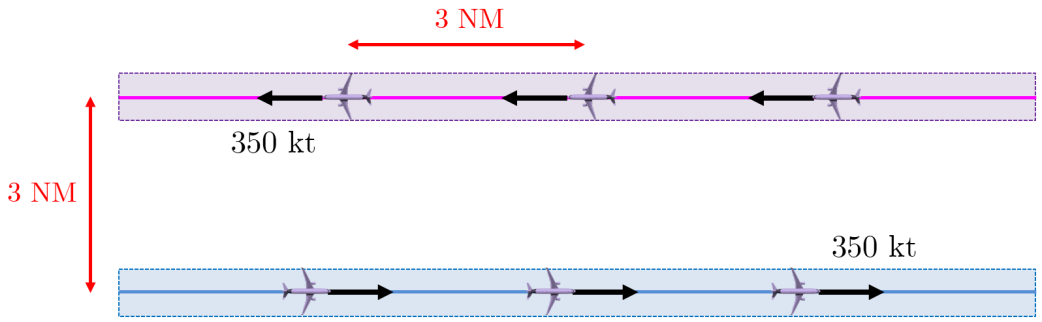

Figure 6-1: Example scenario of two symmetric, opposite-direction, parallel, laterally separated jet procedures. The two segments are initially separated by 3 NM.

In the calculation of non-normal risk, deviations are modeled as linear trajectories due to data on more complex deviation behaviors not being available. If this data becomes available in the future, the methodology presented here can be reapplied to evaluate the risk associated with these behaviors. Furthermore, the angle at which aircraft intercept the two proximate segments is assumed to be lower than 30°, and potential waypoint overshoots are assumed to not result in deviations with angles larger than this value.

6.1.1 Collision Risk Discussion

The collision risk between aircraft on the two procedures follows the collision risk parsing previously discussed in Chapter 4 (Figure 6-2).

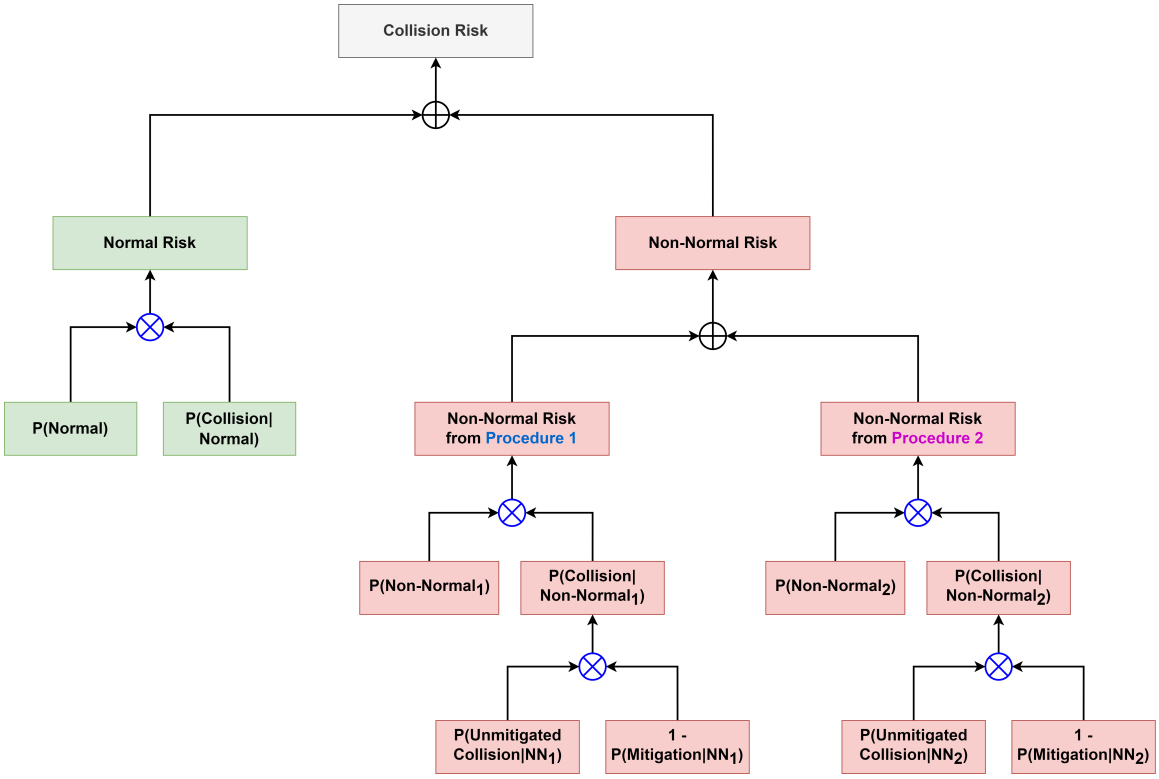

Figure 6-2: Parsing of the collision risk between geometrically separated flight procedures, which includes both normal and non-normal components.

The total collision risk, which must satisfy a 10^{-9} target level of safety, is expressed mathematically as:

$$
\begin{aligned}
&Collision\ Risk = P(N) \times P(Collision \mid N) \\
&+ P(NN_1) \times P(Unmitigated\ Collision \mid NN_1) \times [1 - P(Mitigation \mid NN_1)] \\
&+ P(NN_2) \times P(Unmitigated\ Collision \mid NN_2) \times [1 - P(Mitigation \mid NN_2)] \\
&< 10^{-9}
\end{aligned}
\tag{6.1}
$$

In Chapter 4, it was previously identified that the normal collision risk between aircraft navigating laterally separated flight procedures with RNAV/RNP performance can be considered negligible at separation distances greater than 0.5 NM. As such, this example will assume that the risk between the two procedures considered is dominated by non-normal risk, and that the normal risk is negligible (Equation 6.2).

$$
\begin{aligned}
&Collision\ Risk = \cancel{P(N) \times P(Collision \mid N)} \\
&+ P(NN_1) \times P(Unmitigated\ Collision \mid NN_1) \times [1 - P(Mitigation \mid NN_1)] \\
&+ P(NN_2) \times P(Unmitigated\ Collision \mid NN_2) \times [1 - P(Mitigation \mid NN_2)] \\
&< 10^{-9}
\end{aligned}
\tag{6.2}
$$

Because the two procedures considered in this example are symmetric, it follows that $P(NN_1) \times P(Unmitigated\ Collision \mid NN_1) \times [1 - P(Mitigation \mid NN_1)] = P(NN_2) \times P(Unmitigated\ Collision \mid NN_2) \times [1 - P(Mitigation \mid NN_2)]$. The collision risk equation can then be written as:

$$
\begin{aligned}
&Collision\ Risk = \\
&2 \times P(NN) \times P(Unmitigated\ Collision \mid NN) \times [1 - P(Mitigation \mid NN)] \\
&< 10^{-9}
\end{aligned}
\tag{6.3}
$$

The rate of non-normal events, $P(NN)$, will be assumed to be 10^{-5} per operation, based on historically estimated figures for RNAV flight procedures [30].

$$\begin{aligned} &Collision\ Risk = \\ &2 \times \cancel{P(NN)}^{10^{-5}} \times P(Unmitigated\ Collision \mid NN) \times [1 - P(Mitigation \mid NN)] \\ &< 10^{-9} \end{aligned} \tag{6.4}$$

The probability of collision due to an unmitigated deviation, $P(Unmitigated\,Collision \mid NN)$, is calculated as the product of the probability of trajectory overlap, $P(Trajectory\ Overlap \mid NN)$, and the probability of exposure, $P(Exposure \mid Trajectory\,Overlap, NN)$. These terms are calculated next using the methods described in Chapter 4.

Probability of Trajectory Overlap

By making the conservative assumption that aircraft navigating the two procedures are always at the same altitude and that the two segments are infinitely long, the probability of trajectory overlap due to a deviation, $P(Trajectory\ Overlap \mid NN)$, is estimated at **0.5**. This is illustrated in Figure 6-3 below, which shows that any deviation that occurs towards the opposing procedure will result in a trajectory overlap condition.

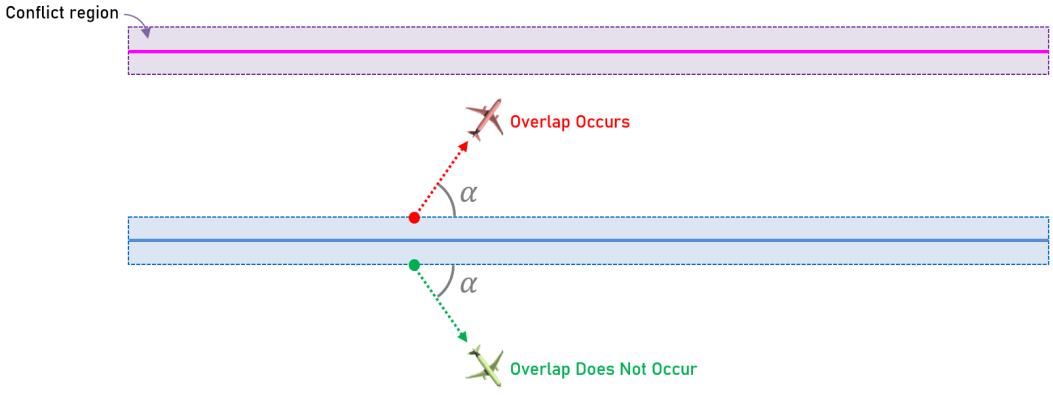

Figure 6-3: The probability of trajectory overlap due to a lateral deviation in the case of parallel, laterally separated procedures no vertical separation is simply a function of whether the deviation occurs towards or away from the endangered procedure.

Probability of Exposure

The probability of exposure, $P(Exposure \mid Trajectory\ Overlap, NN)$, is estimated according to Equation 6.5, which was first introduced in Chapter 4 and is repeated here for convenience.

$$P(Exposure \mid Trajectory\ Overlap, NN) = \left(\frac{2A}{V_d sin\alpha}\right) \times \left(\frac{V_e + V_d cos\alpha}{L}\right) + \left(\frac{2B}{L}\right) \tag{6.5}$$

This equation gives the probability that an exposure condition will occur given that a trajectory overlap occurs, and assumes that the two procedures are operated independently. For this example, aircraft on the two procedures are assumed to be flying in opposite directions at identical groundspeeds ($V_d = V_e = 350$ kt) and to be separated in-trail by 3 NM ($L = 3$ NM) on the same procedure. Deviations are assumed to occur at a 30° angle ($\alpha = 30°$). A standard collision box half-width of 265 ft is also assumed ($A = B = 265$ ft). A summary of the example parameters used is shown in Figure 6-4.

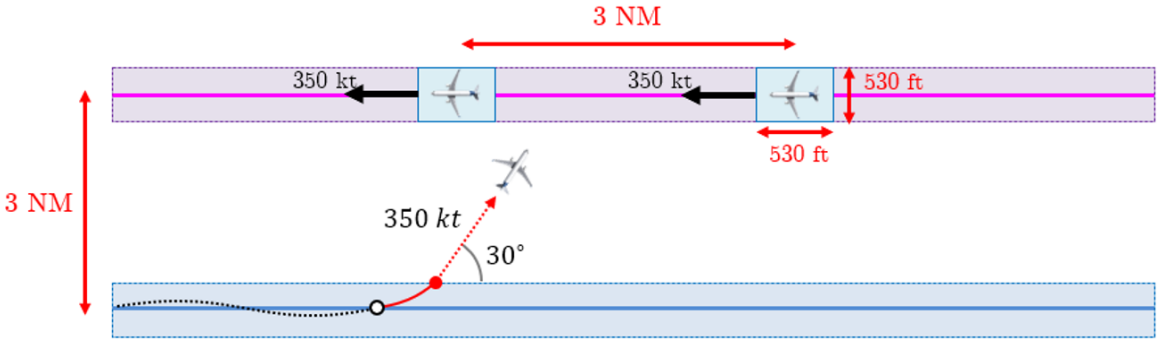

Figure 6-4: Example scenario of two symmetric, parallel, laterally separated jet procedures. The two segments are initially separated by 3 NM.

Application of these parameters to Equation 6.5 results in a probability of exposure of **0.14**.

Probability of Collision due to Unmitigated Deviation

The probability that an unmitigated deviation will result in a collision, $P(Unmitigated\ Collision \mid NN)$, is the product of the calculated probabilities of trajectory overlap and exposure: $(0.5) \times (0.14) = \mathbf{7 \times 10^{-2}}$. This result indicates that 7 out of every 100 unmitigated deviations are expected to result in a collision under the assumptions considered.

$$
\begin{aligned}
&Collision\ Risk = \\
&2 \times 10^{-5} \times P(Unmitigated\ Collision \mid NN) \times [1 - P(Mitigation \mid NN)] \\
&< 10^{-9}
\end{aligned}
\qquad \xrightarrow{\quad 7 \times 10^{-2} \quad} \qquad (6.6)
$$

Following these results, the next section evaluates the effect of the mitigation on the risk based on a representative estimate of the current system's response time distribution.

6.1.2 Mitigation Discussion

The probability of mitigation has previously been defined as the product of three individual probability terms: the probability that the mitigation is available at the time of request, the probability of a timely mitigation response, and the probability that the response is correct. This example will focus on evaluating the **probability of a timely response**, which can be quantified based on the mitigation response performance and the geometry of the mitigation scenario. Evaluation of the two other mitigation probability components is posited to require testing of a mitigation system. In this example, these additional probabilities will be assumed to be much higher than the probability of a timely response and will not be considered explicitly.

The probability of mitigation for the scenario described can be evaluated using the mitigation model introduced in Chapter 4 and repeated here, which assumes a lateral mitigation maneuver:

$$P(Mitigation \mid NN) =$$
$$P\left(Time\ of\ Response \leq \frac{S - D - C - A}{V_d \cdot sin\alpha} - \frac{V_d \cdot tan(\alpha/2)}{g \cdot tan(\phi_{target})} - \frac{\phi_{target}}{\dot{\phi}}\right) \tag{6.7}$$

The following parameters are assumed for a representative worst-case deviation:

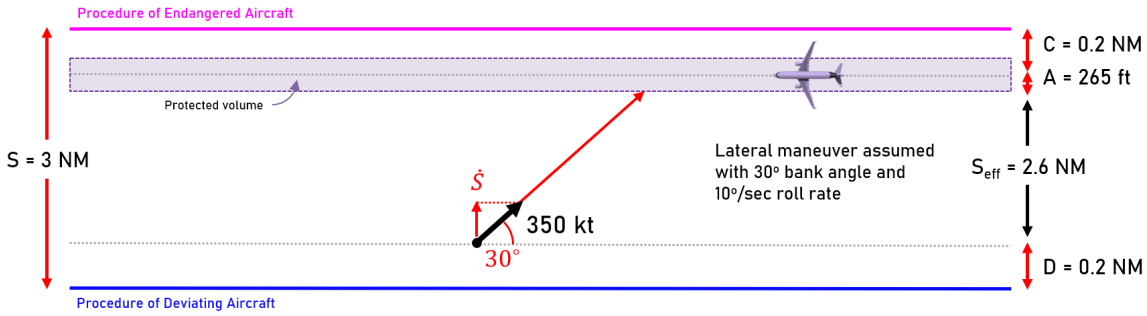

Figure 6-5: Overview of parameters used to describe a representative worst-case deviation in the generic example scenario. Distances and vehicle sizes not to scale.

- **S**: The lateral separation between the two procedures, initially set to **3 NM**.
- **D**: The cross-track distance of the deviating aircraft at the conformance limit. Assumed to be **0.2 NM** based on RNAV tracking performance during normal operations.
- **C**: The cross-track position of the endangered aircraft. Assumed to be **0.2 NM** based on RNAV tracking performance during normal operations.
- **A**: Half-width of collision box around endangered aircraft. Assumed to be **265 ft** based on standard collision box size used by FAA.
- $\mathbf{V_d}$: Groundspeed of deviating aircraft. Assumed to be **350 kt**.
- α: Lateral deviation angle. Assumed to be **30°** based on historically accepted value for a representative worst-case deviation.
- $\boldsymbol{\phi_{target}}$: The target bank angle during a lateral mitigation maneuver. Assumed to be **30°** based on typical aircraft bank angles.

- $\dot{\phi}$: The target roll rate during a lateral mitigation maneuver. Assumed to be **10°/sec** based on typical aircraft roll rates.

By applying the parameters above to Equation 6.7, the necessary response time to mitigate the assumed worst-case deviation is found to be **41 seconds**.

$$t_{necessary} = \frac{S - D - C - A}{V_d \cdot sin\alpha} - \frac{V_d \cdot tan(\alpha/2)}{g \cdot tan(\phi_{target})} - \frac{\phi_{target}}{\dot{\phi}} = 41 \ seconds \tag{6.8}$$

Based on this necessary response time, the probability of a timely mitigation response can be conservatively estimated as the probability that the mitigation response time is lower than the value of 41 seconds, as discussed in Chapter 4. Given the representative estimate for the response time distribution of the current system derived in Chapter 5, the probability of mitigation is estimated as follows:

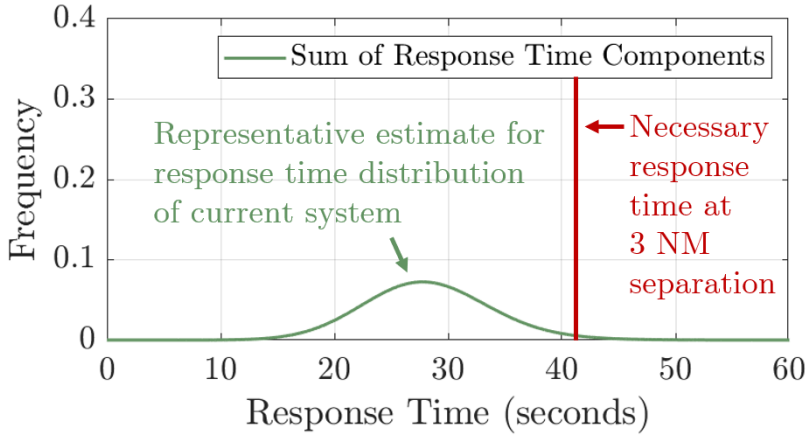

Figure 6-6: The probability of mitigation is estimated as the area of the response time distribution that lies to the left of the necessary response time to mitigate an assumed worst-case deviation.

$$P(Mitigation \mid NN) = \int_0^{41} f_{t_{response}}(t)dt = 0.981 \tag{6.9}$$

With this estimated probability of mitigation, the mitigated collision risk at a separation value of 3 NM is calculated as:

$$\begin{aligned} Collision\ Risk &= 2 \times 10^{-5} \times 7 \times 10^{-2} \times [1 - P(Mitigation \mid NN)] \\ &= 2.7 \times 10^{-8} \end{aligned} \qquad (6.10)$$

0.981

As can be observed, the resulting collision risk does not meet a target level of safety of 10^{-9}. As a result, it can be stated that, under the set of conservative assumptions used, the target level of safety cannot be demonstrated for the scenario analyzed.

6.1.3 Parametric Evaluation of Mitigated Risk

To determine the lowest separation possible to meet a target level of safety of 10^{-9}, a parametric evaluation of the collision risk can be performed as a function of the separation between the procedures. By varying the separation parameter S, the mitigation's necessary response time changes, which subsequently causes the probability of mitigation to change. The collision risk can then be recalculated at several values of separation to produce a plot of the risk as a function of separation. This process is illustrated in Figure 6-7 below. Note that under the conservative set of assumptions made, the unmitigated risk does not change with changes made to the separation.

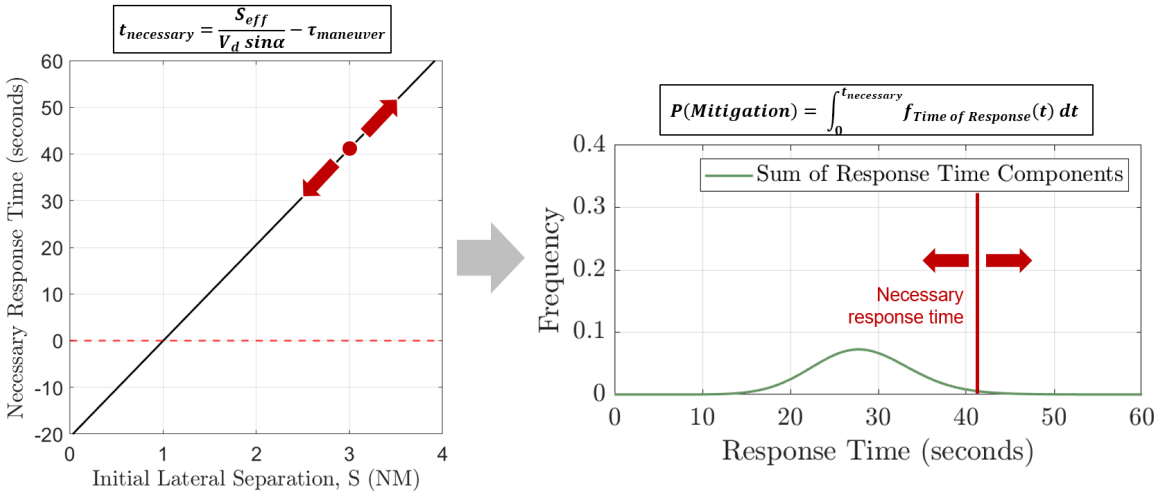

Figure 6-7: Varying the separation between the procedures causes the necessary response time to change, which then causes the probability of mitigation to change.

The resulting parametric plot of the collision risk as a function of separation is

shown in Figure 6-8 below.

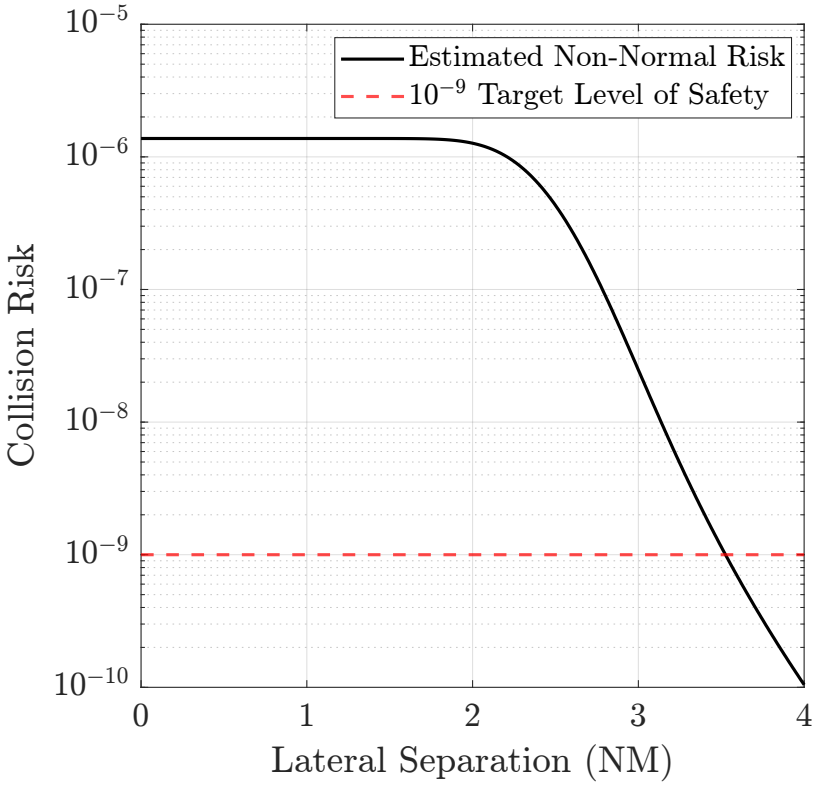

Figure 6-8: Plot of the collision risk as a function of lateral separation for the generic scenario of symmetric, parallel, opposite-direction, co-altitude flight procedures.

As observed in this plot, under the set of assumptions considered, the minimum lateral separation needed to satisfy a 10^{-9} target level of safety is **3.5 NM**. In reasoning the implications of this result, it should be considered that the real system may satisfy the target level of safety at a lower separation value if any of the following parameters are better in real operations than what has been assumed in this example:

- The response time distribution of the mitigation.
- The probability of non-normal events occurring.
- The average in-trail separation between aircraft.
- The deviation angles experienced.
- The groundspeed of deviating aircraft.

To evaluate the effects that these assumptions have on the estimated risk, the collision risk calculation can be repeated with modified parameters. The result of this exercise is shown in Figure 6-9 below, which shows four additional curves corresponding to changes made to the probability of non-normal events, in-trail separation, deviation angle, and aircraft groundspeed.

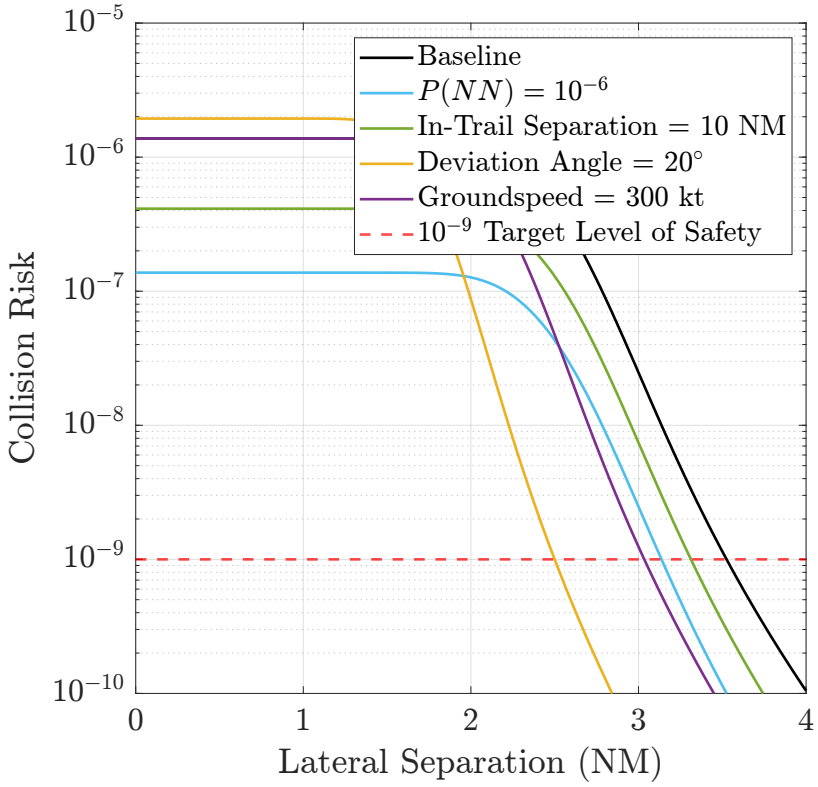

Figure 6-9: Plot of the collision risk as a function of lateral separation for the generic scenario of symmetric, parallel, opposite-direction, co-altitude flight procedures.

In Figure 6-9, the black curve represents the baseline risk previously computed using the initial set of assumptions. The blue curve illustrates how this risk changes when the probability of non-normal events is reduced from 10^{-5} to 10^{-6}. The green curve illustrates the risk change when the in-trail separation between aircraft is increased from 3 NM to 10 NM. The yellow curve represents the risk change when the assumed worst-case deviation angle is decreased from 30° to 20°. Finally, the purple curve shows the risk change when the assumed groundspeed associated with a worst-case deviation is reduced from 350 kt to 300 kt.

Among these parameters, reductions in the assumed worst-case deviation angle

and aircraft groundspeed are observed to have the largest effect on the required separation. In particular, a reduction of the deviation angle from 30° to 20° causes the required separation to be reduced from 3.5 NM to **2.5 NM**.

In reasoning the implications of this result, it can be hypothesized that the real system is likely to experience a range of deviation behaviors. In such a scenario, worst-case deviations such as a 30° deviation may occur much less frequently than less severe deviations. Under this hypothesis and based on the result of Figure 6-9, the 10^{-9} target level of safety may potentially be met at a separation of 3 NM. Based on this observation, it is posited that a better understanding of actual aircraft non-normal behaviors could provide significant value if current assumptions are found to be conservative, which could lead to a greater ability to demonstrate a target level of safety in safety assessments.

6.2 Example Case of Separation Between RNAV Departure and ILS Approach at Boston Logan Airport (BOS)

Boston Logan Airport (BOS) is a major Class B airport with a complex runway layout. In one of its most common runway configurations, the airport operates departures on runways 22L and 22R, and arrivals on runway 27. Near the airport, the two flight procedures serving these operations follow opposite-direction parallel tracks, with departures following an easterly heading and arrivals following a westerly one (Figure 6-10). Because both procedures can be operated simultaneously and independently, they are required to be geometrically separated. Furthermore, due to the vertical profiles of aircraft on the departure procedure being unrestricted, the use of lateral separation is prioritized, with the two procedures being laterally separated by more than 3 NM.

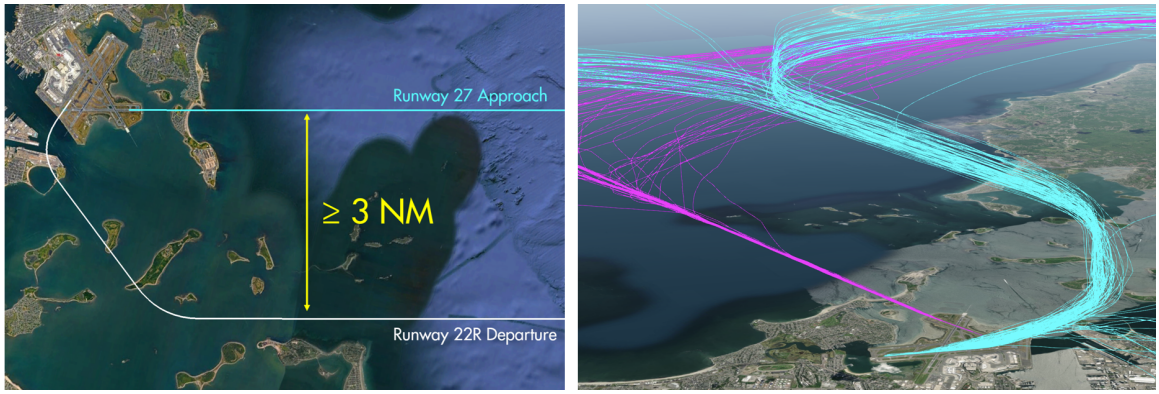

Figure 6-10: Left: Lateral procedure tracks for the RNAV departure from runway 22R (white) and ILS approach to runway 27 (cyan). Right: Example radar tracks of aircraft tracking both procedures. The higher dispersion in vertical profiles on the RNAV departure can be observed.

The proximity of the departure procedure to communities located southeast of the airport on the peninsula of Hull (Figure 6-11) has been a source of frequent noise complaints, with the airport engaging in multiple efforts to study the potential relocation of this procedure further to the north in the interest of noise abatement [70].

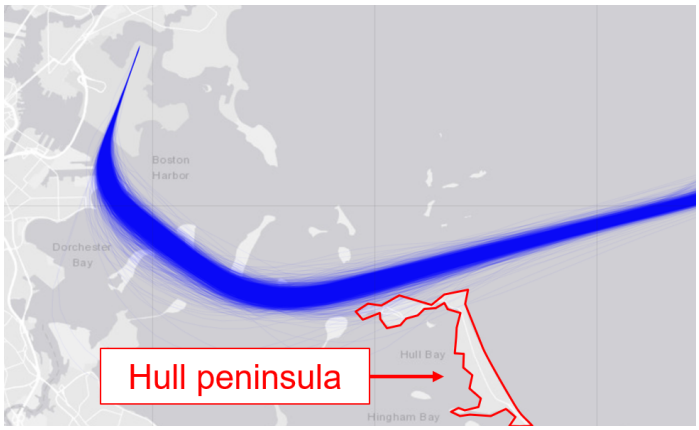

Figure 6-11: Example radar tracks of aircraft on the 22R departure procedure, highlighting their proximity to the peninsula of Hull.

Due to the requirement for the lateral separation between the two procedures to be greater than 3 NM, previous work identified that only a minor relocation of the departure procedure to the north would be possible without a change in regulations, as the lateral separation between the procedures had previously been set to 3.5 NM [70].

In order to investigate potential opportunities to reevaluate the required lateral separation between these two procedures, which could offer noise benefits, the mitigated collision risk model discussed in Chapters 4 and 5 is applied to evaluate achievable separation values between the two parallel procedure segments highlighted in Figure 6-12. In addition, various system improvements are evaluated to determine their potential effect on the required separation between the two procedures.

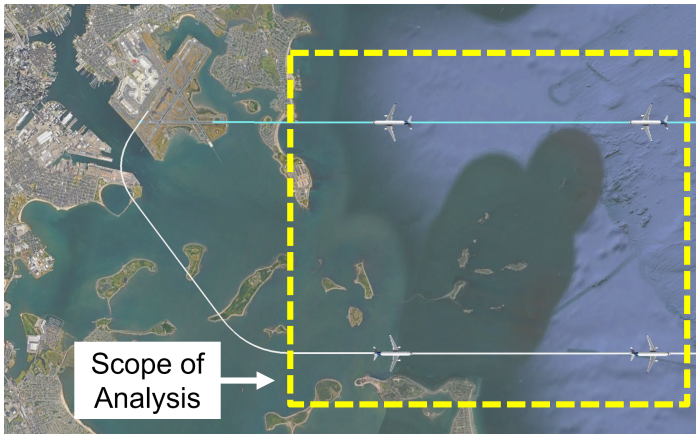

Figure 6-12: The analysis in the section considers the risk between the two parallel segments of the RNAV departure and ILS approach.

In the calculation of non-normal risk, deviations are modeled as linear trajectories due to data on more complex deviation behaviors not being available. If this data becomes available in the future, the methodology presented here can be reapplied to evaluate the risk associated with these behaviors.

6.2.1 Evaluation of Unmitigated Risk

The collision risk between aircraft on the departure and approach procedures depicted in Figure 6-12 follows the same collision risk parsing previously discussed (Figure 6-13).

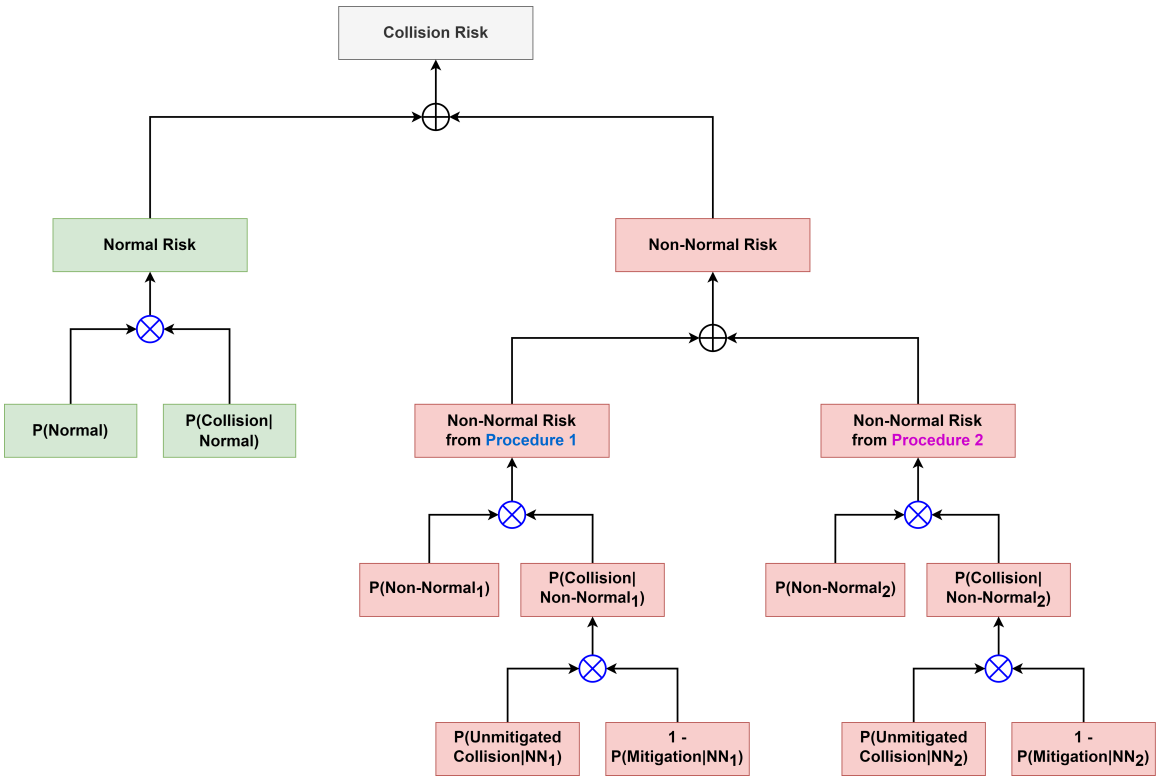

Figure 6-13: Parsing of the collision risk between geometrically separated flight procedures, which includes both normal and non-normal components.

The total collision risk, which must satisfy a 10^{-9} target level of safety, is expressed mathematically as:

$$
\begin{aligned}
&Collision\ Risk = P(N) \times P(Collision \mid N) \\
&+ P(NN_1) \times P(Unmitigated\ Collision \mid NN_1) \times [1 - P(Mitigation \mid NN_1)] \\
&+ P(NN_2) \times P(Unmitigated\ Collision \mid NN_2) \times [1 - P(Mitigation \mid NN_2)] \\
&< 10^{-9}
\end{aligned}
\tag{6.11}
$$

In this scenario, the departure and approach procedures considered are not symmetric, and aircraft on each procedure have different vertical profiles as well as different groundspeeds. Due to throughput differences between the two procedures, and since they must necessarily share the same number of total collisions, the ratio of *collisions per operation* experienced in each procedure is not necessarily the same. If aircraft are assumed to be separated in-trail by 3 NM in both procedures, then the procedure with lower groundspeeds is expected to experience more *collisions per operation*. Groundspeed values observed in each procedure using ASDE-X surveillance data are shown in Figure 6-14 below.

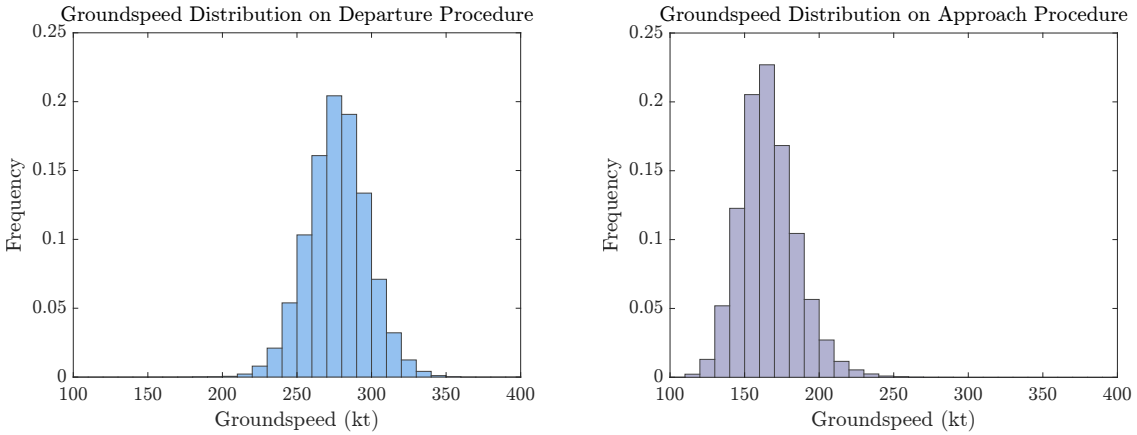

(a) Distribution of groundspeed values observed on departure procedure.

(b) Distribution of groundspeed values observed on approach procedure.

Figure 6-14: Distributions of groundspeed values observed in surveillance data.

As can be observed from this data, aircraft in the approach procedure can be expected to be flying at lower groundspeeds than aircraft in the departure procedure.

In the collision risk analysis that follows, the collision risk will therefore be calculated from the perspective of an approaching aircraft, which is expected to experience a higher number of collisions per operation. Based on this, Equation 6.11 can be restated as follows:

$$\begin{aligned} &Collision\ Risk = P(N) \times P(Collision \mid N) \\ &+ P(NN_{App}) \times P(Unmitigated\ Collision \mid NN_{App}) \times [1 - P(Mitigation \mid NN_{App})] \\ &+ P(NN_{Dep}) \times P(Unmitigated\ Collision \mid NN_{Dep}) \times [1 - P(Mitigation \mid NN_{Dep})] \\ &< 10^{-9} \end{aligned} \tag{6.12}$$

Unlike the previous example, in which aircraft were conservatively assumed to be flying at equal altitudes at all times, aircraft in the departure and approach procedures at BOS are known to be vertically separated. Aircraft on the approach to runway 27 follow a standard 3-degree glidepath to the runway, while aircraft on the departure procedure are observed to follow a vertical profile based on the individual climb performance of each aircraft. Differences in aircraft lateral and vertical position in the two procedures can be observed by analyzing cross-sections of each procedure. Example cross-sections are shown in Figure 6-15 below.

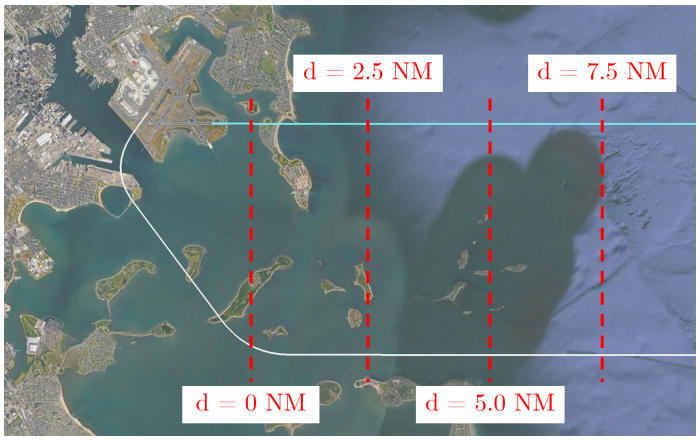

Figure 6-15: Example cross-sections of both procedures at BOS, spaced 2.5 NM apart from each other.

Surveillance data for 8,937 departure tracks and 21,965 approach tracks were analyzed at these cross-sections, with the resulting lateral and vertical position of aircraft on both procedures shown in Figure 6-16 below.

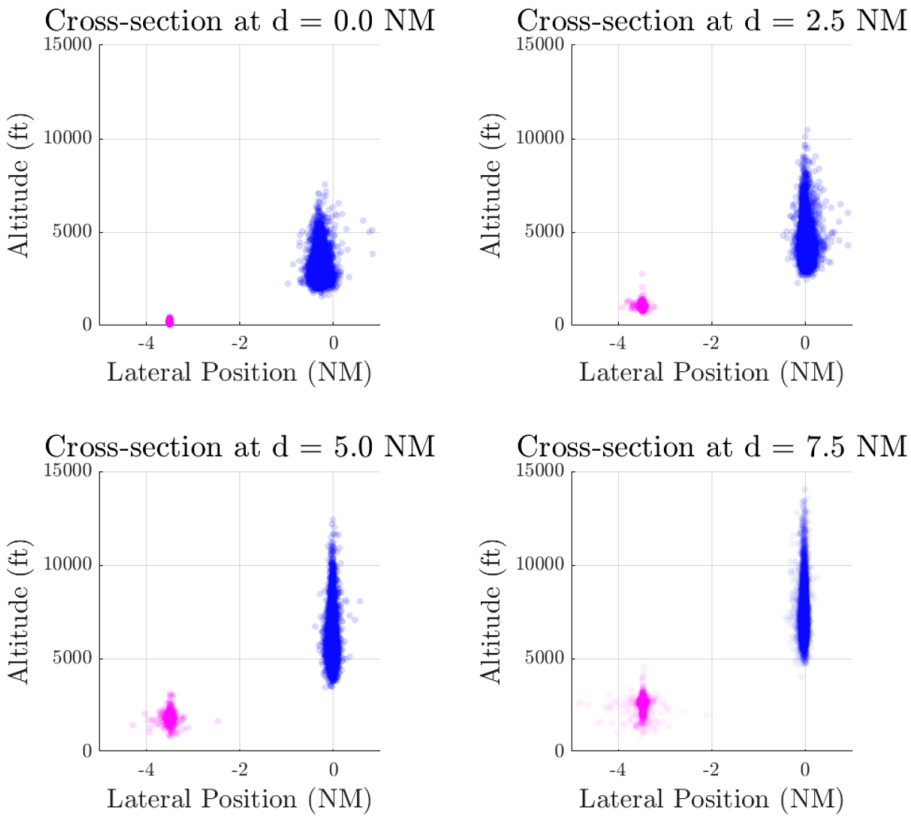

Figure 6-16: Scatter plots of aircraft position at the four cross-sections shown in Figure 6-15. Blue points represent aircraft on the departure procedure, and magenta points represent aircraft on the approach procedure.

Significant vertical scatter can be observed in the departure procedure (blue) due to aircraft flying their preferred climb profiles, while vertical trajectories on the approach (magenta) are concentrated around the glideslope. This position data is used to evaluate the risk of collision in normal operations, discussed next.

Normal Risk

Evaluation of the collision risk during normal operations is achieved by fitting statistical distributions to the aircraft position data shown in Figure 6-16 and applying them in the Reich CRM discussed in Chapter 4. By assuming that aircraft lateral and vertical positions follow Gaussian processes, normal distributions can be fit to both lateral and vertical position data. From these, distributions of lateral and vertical separation between aircraft in the two procedures can be computed through convolutions, discussed in Appendix C. The resulting lateral and vertical separation

distributions are shown in Figure 6-17 and 6-18, respectively.

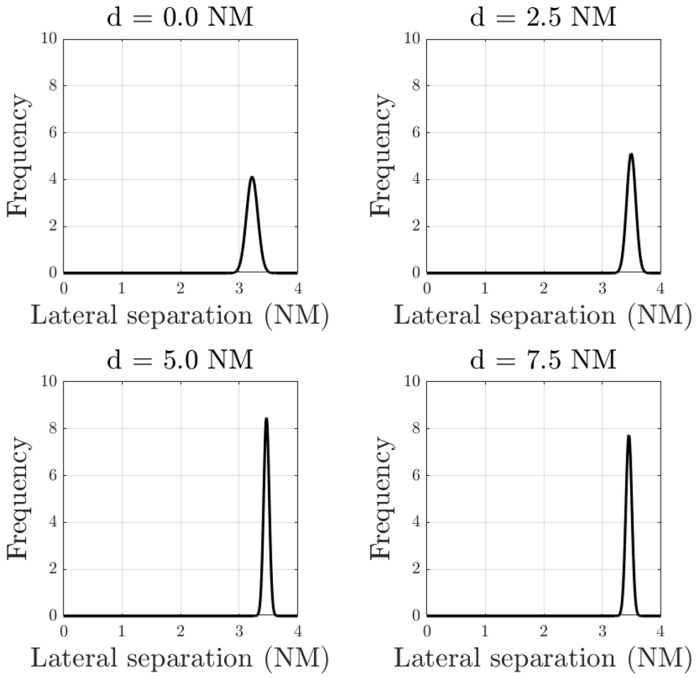

Figure 6-17: Distributions of lateral separation between a pair of aircraft in the two flight procedures for the four cross-sections analyzed.

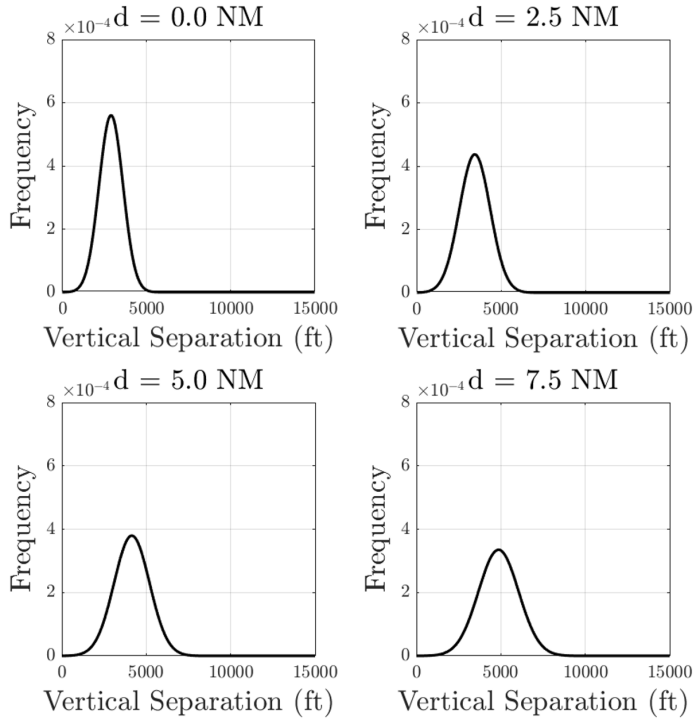

Figure 6-18: Distributions of vertical separation between a pair of aircraft in the two flight procedures for the four cross-sections analyzed.

The probabilities of lateral and vertical overlap can be computed by integrating these distributions over separation values lower than the collision box size assumed. A standard collision box is used here based on historically accepted assumptions [36]. By assuming that the lateral separation between two aircraft is independent of their vertical separation, the two overlap probabilities can be multiplied to yield the probability of collision between a pair of aircraft during normal operations.

$$\begin{aligned} P(Lateral\ Overlap) &= \int_{-\infty}^{265\ ft} f_{Lateral\ Separation}(y)\ dy \\ P(Vertical\ Overlap) &= \int_{-\infty}^{80\ ft} f_{Vertical\ Separation}(z)\ dz \\ P(Collision \mid Normal) &= P(Lateral\ Overlap) \times P(Vertical\ Overlap) \end{aligned} \tag{6.13}$$

d	$P(Lateral\ Overlap)$	$P(Vertical\ Overlap)$	$P(Collision \mid Normal)$
$d = 0.0$ NM	$< 10^{-50}$	3.17×10^{-5}	$< 10^{-50}$
$d = 2.5$ NM	$< 10^{-50}$	1.08×10^{-4}	$< 10^{-50}$
$d = 5.0$ NM	$< 10^{-50}$	4.91×10^{-5}	$< 10^{-50}$
$d = 7.5$ NM	$< 10^{-50}$	2.64×10^{-5}	$< 10^{-50}$

Table 6.1: List of parameters used in the evaluation of the non-normal risk due to deviations from the approach procedure.

The probability of collision in normal operations is found to be negligible based on the assumption that aircraft position errors follow a Gaussian process. As a result, the collision risk in this scenario is expected to be dominated by the non-normal risk component and the normal risk will be treated as negligible.

$$\begin{aligned} Collision\ Risk = &\cancel{P(N) \times P(Collision \mid N)} \\ &+ P(NN_{App}) \times P(Unmitigated\ Collision \mid NN_{App}) \times [1 - P(Mitigation \mid NN_{App})] \\ &+ P(NN_{Dep}) \times P(Unmitigated\ Collision \mid NN_{Dep}) \times [1 - P(Mitigation \mid NN_{Dep})] \\ &< 10^{-9} \end{aligned} \tag{6.14}$$

Non-Normal Risk due to Deviations from Approach

Because the departure and approach procedures considered in this example are not symmetric, the non-normal risk introduced by deviations from each procedure must be computed individually.

The non-normal risk contributed by deviations from the approach is highlighted in the overall risk equation below:

$$\begin{aligned} &Collision\ Risk = \\ &P(NN_{App}) \times P(Unmitigated\ Collision \mid NN_{App}) \times [1 - P(Mitigation \mid NN_{App})] \\ &+ P(NN_{Dep}) \times P(Unmitigated\ Collision \mid NN_{Dep}) \times [1 - P(Mitigation \mid NN_{Dep})] \\ &< 10^{-9} \end{aligned} \tag{6.15}$$

As before, the rate of non-normal events will be assumed to be $\mathbf{10^{-5}}$ per operation, based on historically estimated figures [30].

Parameter	Value
$P(NN_{App})$	10^{-5}

Table 6.2: List of parameters used in the evaluation of the non-normal risk due to deviations from the approach procedure.

The probability of collision due to an unmitigated deviation, $P(Unmitigated\,Collision \mid NN)$, is calculated as the product of the probability of trajectory overlap, $P(Trajectory\ Overlap \mid NN)$, and the probability of exposure, $P(Exposure \mid Trajectory\,Overlap, NN)$.

$$\begin{aligned} P(Unmitigated\ Collision \mid NN_{App}) =& P(Trajectory\ Overlap \mid NN_{App}) \\ &\times P(Exposure \mid Trajectory\ Overlap, NN_{App}) \end{aligned} \tag{6.16}$$

Estimation of the probability of trajectory overlap, $P(Trajectory\,Overlap \mid NN)$,

is more complex in this case due to the vertical separation between the two procedures as well as the variable vertical profiles on the departure procedure. To estimate this parameter, deviation trajectories must be modeled geometrically and individually evaluated for an overlap condition with the opposing flight procedure. In this example, deviations are modeled based on historically accepted assumptions and simplifications [35, 36, 37], listed below. The angle at which aircraft intercept the final approach to runway 27 is assumed to be lower than 30°, and potential overshoots are assumed to not result in deviations with angles larger than this value.

- Lateral deviations occur at a 30° angle.
- Deviating aircraft maintain a constant groundspeed.
- During a deviation, aircraft have an equal chance of either maintaining their original vertical path or leveling off.
- Deviations occur with uniform probability along the flight procedure segments considered.
- Aircraft groundspeed and altitude at the beginning of a deviation are the same as those observed in normal operations.

By simulating deviation trajectories based on these assumptions in a Monte Carlo environment, the frequency with which unmitigated deviations from the approach result in a trajectory overlap condition can be estimated. For this analysis, 20,000 deviation trajectories were simulated and 179 found to result in a trajectory overlap condition. Samples of simulated deviation trajectories that result in trajectory overlap are shown in Figure 6-19 below.

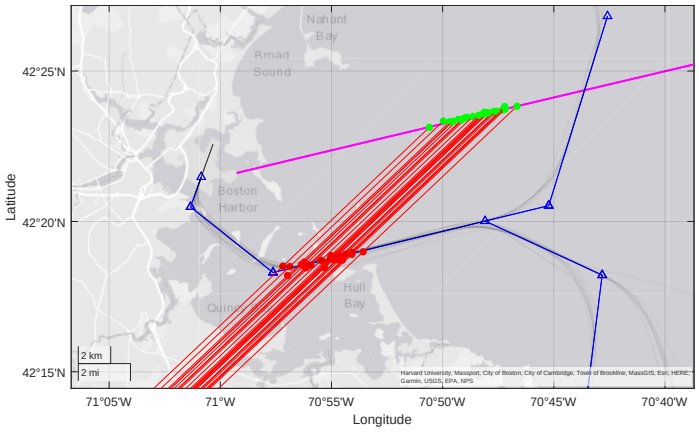

Figure 6-19: Simulated deviations from approach procedure that result in trajectory overlap.

From the set of simulated deviation trajectories, a trajectory overlap condition is evaluated geometrically by comparing each deviation trajectory to an endangered trajectory sampled at random from the surveillance data available for the endangered procedure. If the deviation trajectory comes within 265 ft (laterally) or 80 ft (vertically) of the endangered trajectory, a trajectory overlap is recorded. These values are based on the dimensions of a standard collision box used in historical studies [36]. This evaluation yields a probability of trajectory overlap of $\mathbf{8.8 \times 10^{-3}}$, which corresponds to the fraction of all simulated deviations that resulted in trajectory overlap. More detailed results of this Monte Carlo simulation are available in Appendix G.

Parameter	Value
$P(NN_{App})$	10^{-5}
$P(Trajectory\ Overlap \mid NN_{App})$	8.8×10^{-3}

Table 6.3: List of parameters used in the evaluation of the non-normal risk due to deviations from the approach procedure.

The probability of exposure, $P(Exposure \mid Trajectory\ Overlap, NN)$, is estimated according to Equation 6.22, which was first introduced in Chapter 4 and is repeated here.

$$P(Exposure \mid Trajectory\ Overlap, NN) = \left(\frac{2A}{V_d sin\alpha}\right) \times \left(\frac{V_e + V_d cos\alpha}{L}\right) + \left(\frac{2B}{L}\right) \tag{6.17}$$

Based on groundspeed data shown in Figure 6-14, worst-case groundspeed values of 100 kt for aircraft on the approach procedure ($V_d = 100$ kt) and 350 kt for aircraft on the departure procedure ($V_e = 350$ kt) are selected for this calculation. These are conservative values that yield a conservative probability of exposure. The in-trail separation between aircraft in the endangered procedure is assumed to be 3 NM ($L = 3$ NM), and deviations are assumed to occur at 30° angles ($\alpha = 30°$). A standard collision box is used with length and width of 530 ft ($A = B = 265$ ft). A visual summary of these parameters is shown in Figure 6-20.

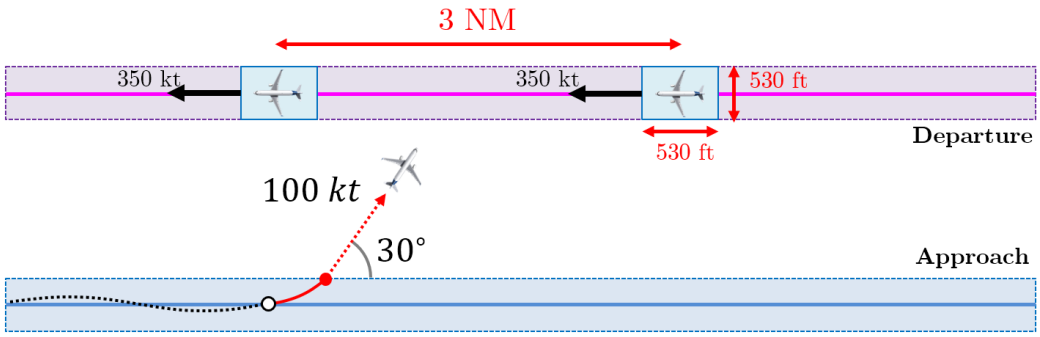

Figure 6-20: Summary of parameters used in the calculation of the probability of exposure to an approach deviation.

Application of these parameters to Equation 6.22 yields a probability of exposure of $\mathbf{2.8 \times 10^{-1}}$.

Parameter	Value
$P(NN_{App})$	10^{-5}
$P(Trajectory\ Overlap \mid NN_{App})$	8.8×10^{-3}
$P(Exposure \mid Trajectory\ Overlap, NN_{App})$	2.8×10^{-1}

Table 6.4: List of parameters used in the evaluation of the non-normal risk due to deviations from the approach procedure.

With these results, the probability of collision due to an unmitigated deviation from the approach is be calculated as $(8.8 \times 10^{-3}) \times (2.8 \times 10^{-1}) = \mathbf{2.5 \times 10^{-3}}$.

Parameter	Value
$P(NN_{App})$	10^{-5}
$P(Trajectory\ Overlap \mid NN_{App})$	8.8×10^{-3}
$P(Exposure \mid Trajectory\ Overlap, NN_{App})$	2.8×10^{-1}
$P(Unmitigated\ Collision \mid NN_{App})$	2.5×10^{-3}

Table 6.5: List of parameters used in the evaluation of the non-normal risk due to deviations from the approach procedure.

This result indicates that 25 out of every 10,000 unmitigated deviations from the approach procedure are expected to result in a collision.

Substituting the values in Table 6.5 into the original risk equation yields:

$$\begin{aligned} &Collision\ Risk = \\ &2.5 \times 10^{-8} \times [1 - P(Mitigation \mid NN_{App})] \\ &+ P(NN_{Dep}) \times P(Unmitigated\ Collision \mid NN_{Dep}) \times [1 - P(Mitigation \mid NN_{Dep})] \\ &< 10^{-9} \end{aligned} \tag{6.18}$$

The next section repeats this process for unmitigated deviations from the departure procedure.

Non-Normal Risk due to Deviations from Departure

The non-normal risk contributed by deviations from the departure is highlighted in the overall risk equation below:

$$
\begin{aligned}
&Collision\ Risk = \\
&2.5 \times 10^{-8} \times [1 - P(Mitigation \mid NN_{App})] \\
&+ P(NN_{Dep}) \times P(Unmitigated\ Collision \mid NN_{Dep} \times [1 - P(Mitigation \mid NN_{Dep})] \\
&< 10^{-9}
\end{aligned}
\tag{6.19}
$$

As before, the rate of non-normal events is 10^{-5} per aircraft. However, a single operation in the approach procedure, which is the target operation of the *collisions per operation* risk metric used in this example, can pass several aircraft in the departure procedure during its operation and therefore be exposed to multiple deviation chances. This requires $P(NN_{Dep})$ to be scaled to account for this effect (i.e., $P(NN_{Dep}) = K \times 10^{-5}$). The scaling parameter K, derived in Appendix B, is calculated as:

$$
K = \frac{(Length\ of\ Segment)}{(In\text{-}Trail\ Spacing)} \times \frac{(Groundspeed)_{Dep}}{(Groundspeed)_{App}} \tag{6.20}
$$

With the length of the parallel segments being 10 NM and the in-trail spacing assumed to be 3 NM, worst-case groundspeed values of $(Groundspeed)_{Dep} = 350$ kt and $(Groundspeed)_{App} = 100$ kt yield a conservative scaling factor of $K = 12$. This means that, in the worst case, 12 operations occur in the departure procedure during the time needed to complete one approach operation, yielding a departure deviation probability of 12×10^{-5} per approach operation.

Parameter	Value
$P(NN_{Dep})$	1.2×10^{-4}

Table 6.6: List of parameters used in the evaluation of the non-normal risk due to deviations from the departure procedure.

As before, the probability of collision due to an unmitigated deviation, $P(Unmitigated\ Collision \mid NN)$, is the product of the probability of trajectory overlap, $P(Trajectory$

$Overlap \mid NN)$, and the probability of exposure, $P(Exposure \mid Trajectory\, Overlap, NN)$.

$$P(Unmitigated\ Collision \mid NN_{Dep}) = P(Trajectory\ Overlap \mid NN_{Dep}) \times P(Exposure \mid Trajectory\ Overlap, NN_{Dep}) \tag{6.21}$$

To estimate the probability of trajectory overlap, $P(Trajectory\ Overlap \mid NN)$, an evaluation of simulated deviation trajectories from the departure procedure is conducted using the same assumptions used previously for simulating deviation trajectories from the approach procedure. Potential waypoint overshoots can be ignored in this case due to departing aircraft initially diverging from the final approach course and not contributing towards the risk. For this analysis, 19,902 deviation trajectories were simulated and 45 found to result in a trajectory overlap condition. Samples of simulated deviation trajectories that result in trajectory overlap are shown in Figure 6-21 below.

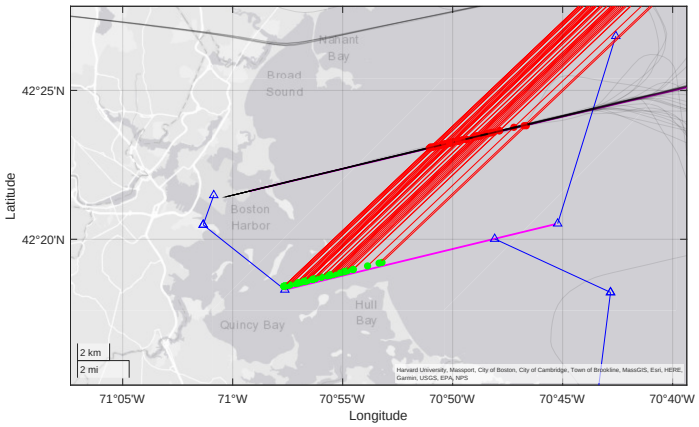

Figure 6-21: Simulated deviations from departure procedure that result in trajectory overlap.

Evaluation of these trajectories yields a probability of trajectory overlap of $\mathbf{2.3 \times 10^{-3}}$. Of note, this result is approximately four times lower than the same figure for deviations from the approach. This is because climbing deviations never pose a threat to aircraft on the approach, with the only deviations from the departure that result in an overlap being those that level off. More detailed results of this Monte Carlo

simulation are available in Appendix G.

Parameter	Value
$P(NN_{Dep})$	1.2×10^{-4}
$P(Trajectory\ Overlap \mid NN_{Dep})$	2.3×10^{-3}

Table 6.7: List of parameters used in the evaluation of the non-normal risk due to deviations from the departure procedure.

The probability of exposure, $P(Exposure \mid Trajectory\ Overlap, NN)$, is estimated according to Equation 6.22, which was first introduced in Chapter 4 and is repeated here.

$$P(Exposure \mid Trajectory\ Overlap, NN) = \left(\frac{2A}{V_d sin\alpha}\right) \times \left(\frac{V_e + V_d cos\alpha}{L}\right) + \left(\frac{2B}{L}\right) \tag{6.22}$$

Based on groundspeed data shown in Figure 6-14, worst-case groundspeed values of 100 kt for aircraft on the approach procedure ($V_d = 200$ kt) and 250 kt for aircraft on the departure procedure ($V_e = 250$ kt) are selected for this calculation. These are conservative values that yield a conservative probability of exposure. The in-trail separation between aircraft in the endangered procedure is assumed to be 3 NM ($L = 3$ NM), and deviations are assumed to occur at 30° angles ($\alpha = 30°$). A standard collision box is used with length and width of 530 ft ($A = B = 265$ ft). A visual summary of these parameters is shown in Figure 6-22.

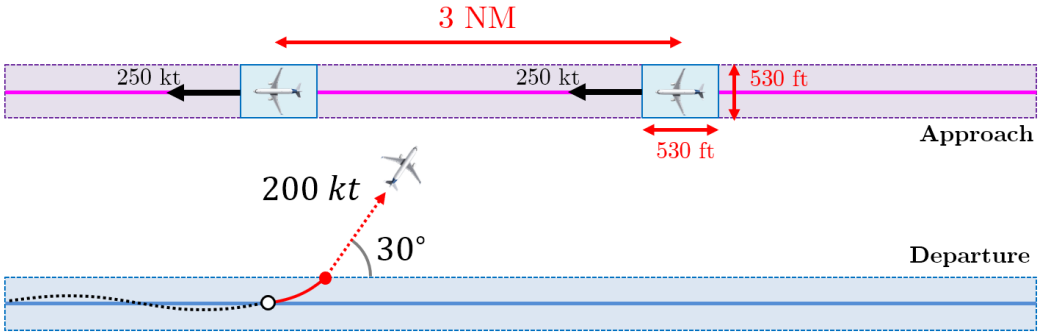

Figure 6-22: Summary of parameters used in the calculation of the probability of exposure to a departure deviation.

Application of these parameters to Equation 6.22 yields a probability of exposure of 1.5×10^{-1}, which is the probability of exposure from the perspective of the deviating aircraft. However, because the risk metric considered is the number of collisions experienced by a single operation in the approach procedure, this result must be scaled by the number of aircraft sharing the approach procedure at any given time (i.e., $P(Exposure \mid Trajectory\ Overlap, NN_{Dep}) = \frac{1}{M} 1.5 \times 10^{-1}$). The scaling parameter M, derived in Appendix B, is:

$$M = \frac{(Length\ of\ Segment)}{(In\text{-}Trail\ Spacing)} \tag{6.23}$$

Using a segment length of 10 NM and an in-trail spacing of 3 NM, this results in the probability of exposure to a deviation from the departure procedure from the perspective of a single aircraft on the approach procedure being $\mathbf{4.6 \times 10^{-2}}$.

Parameter	Value
$P(NN_{Dep})$	1.2×10^{-4}
$P(Trajectory\ Overlap \mid NN_{Dep})$	2.3×10^{-3}
$P(Exposure \mid Trajectory\ Overlap, NN_{Dep})$	4.6×10^{-2}

Table 6.8: List of parameters used in the evaluation of the non-normal risk due to deviations from the departure procedure.

With these results, the probability of collision due to an unmitigated deviation from the approach can be calculated as $(2.3 \times 10^{-3}) \times (4.6 \times 10^{-2}) = \mathbf{1.1 \times 10^{-4}}$.

Parameter	Value
$P(NN_{Dep})$	1.2×10^{-4}
$P(Trajectory\ Overlap \mid NN_{Dep})$	2.3×10^{-3}
$P(Exposure \mid Trajectory\ Overlap, NN_{Dep})$	4.6×10^{-2}
$P(Unmitigated\ Collision \mid NN_{Dep})$	1.1×10^{-4}

Table 6.9: List of parameters used in the evaluation of the non-normal risk due to deviations from the departure procedure.

Substituting the values in Table 6.9 into the original risk equation yields:

$$
\begin{aligned}
&\textit{Collision Risk} = \\
&2.5 \times 10^{-8} \times [1 - P(\textit{Mitigation} \mid NN_{App})] \\
&+ 1.2 \times 10^{-8} \times [1 - P(\textit{Mitigation} \mid NN_{Dep})] \\
&< 10^{-9}
\end{aligned}
\tag{6.24}
$$

At this stage, the total collision risk is a function of the probabilities of mitigation for deviations from both procedures, $P(Mitigation \mid NN_{App})$ and $P(Mitigation \mid NN_{Dep})$. Given differences in aircraft groundspeed in the two procedures, the available time for mitigation and therefore the probability of a timely mitigation response are expected to be lower for the procedure with faster aircraft (i.e., the departure). As a result, this calculation can be simplified with the conservative assumption that $P(Mitigation \mid NN_{App}) = P(Mitigation \mid NN_{Dep}) = P(Mitigation \mid NN)$, where this probability is determined solely by the probability of mitigating faster deviations from the departure procedure. The collision risk equation then simplifies to:

$$
\begin{aligned}
&\textit{Collision Risk} = \\
&3.7 \times 10^{-8} \times [1 - P(\textit{Mitigation} \mid NN)] \\
&< 10^{-9}
\end{aligned}
\tag{6.25}
$$

Following these results, the next section continues with the evaluation of the effect of the mitigation on the risk and evaluates the achievable separation values between the procedures under a variety of potential system improvements. Note that the unmitigated risk estimated in this section is not expected to increase as the lateral separation is reduced. In fact, the probability of collision due to unmitigated deviations in this scenario can be shown to decrease as the procedures are brought closer together. This fact is discussed further in Appendix H.

6.2.2 Parametric Evaluation of Mitigated Risk

The probability of mitigation has previously been defined as the product of three individual probability terms: the probability that the mitigation is available at the time of request, the probability of a timely mitigation response, and the probability that the response is correct. This example will focus on evaluating the **probability of a timely response**, which can be quantified based on the mitigation response performance and the geometry of the mitigation scenario. Evaluation of the two other mitigation probability components is posited to require testing of a mitigation system. In this example, these additional probabilities will be assumed to be much higher than the probability of a timely response and will not be considered explicitly.

The probability of mitigation for the scenario described can be evaluated using the mitigation model introduced in Chapter 4 and repeated here, which assumes a lateral mitigation maneuver:

$$P(Mitigation \mid NN) = \\ P\left(Time\ of\ Response \leq \frac{S - D - C - A}{V_d \cdot sin\alpha} - \frac{V_d \cdot tan(\alpha/2)}{g \cdot tan(\phi_{target})} - \frac{\phi_{target}}{\dot{\phi}}\right) \tag{6.26}$$

The following parameters are assumed for a representative worst-case deviation, which in this case represents a deviation from the departure procedure:

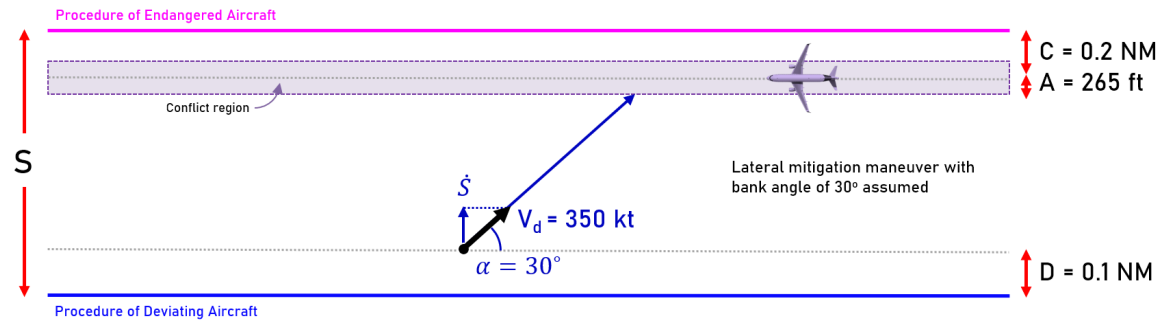

Figure 6-23: Overview of parameters used to describe a representative worst-case deviation in the BOS scenario. Distances and vehicle sizes not to scale.

- **S**: The lateral separation between the two procedures, initially set to **3 NM**.

- **D**: The cross-track distance of the deviating aircraft at the conformance limit. Assumed to be **0.2 NM** based on RNAV tracking performance during normal operations.

- **C**: The cross-track position of the endangered aircraft. Assumed to be **0.2 NM** based on RNAV tracking performance during normal operations.

- **A**: Half-width of collision box around endangered aircraft. Assumed to be **265 ft** based on standard collision box size used by FAA.

- $\mathbf{V_d}$: Groundspeed of deviating aircraft. Assumed to be **350 kt**.

- α: Lateral deviation angle. Assumed to be **30**° based on historically accepted value for a representative worst-case deviation.

- $\phi_{\mathbf{target}}$: The target bank angle during a lateral mitigation maneuver. Assumed to be **30**° based on typical aircraft bank angles.

- $\dot{\phi}$: The target roll rate during a lateral mitigation maneuver. Assumed to be **10°/sec** based on typical aircraft roll rates.

By applying the parameters above to Equation 6.26, the necessary response time to mitigate the assumed worst-case deviation is found to be **41 seconds**, which is the same value found in the previous example due to the assumed worst-case deviation being the same.

$$t_{necessary} = \frac{S - D - C - A}{V_d \cdot sin\alpha} - \frac{V_d \cdot tan(\alpha/2)}{g \cdot tan(\phi_{target})} - \frac{\phi_{target}}{\dot{\phi}} = 41 \ seconds \tag{6.27}$$

Based on this necessary response time, the probability of mitigation can be calculated given the representative estimate for the response time distribution of the current system derived in Chapter 5:

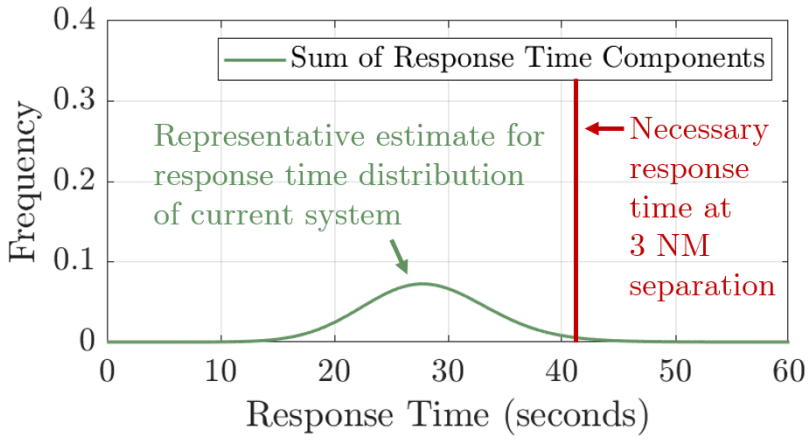

Figure 6-24: The probability of mitigation is estimated as the area of the response time distribution that lies to the left of the necessary response time to mitigate an assumed worst-case deviation.

$$P(Mitigation \mid NN) = \int_0^{41} f_{t_{response}}(t)dt = 0.981 \tag{6.28}$$

With this estimated probability of mitigation, the mitigated collision risk at a separation value of 3 NM is calculated as:

$$\begin{aligned} Collision\ Risk &= 3.7 \times 10^{-8} \times [1 - \cancelto{0.981}{P(Mitigation \mid NN)}] \\ &= 7 \times 10^{-10} \end{aligned} \tag{6.29}$$

As can be observed, the resulting collision risk satisfies a target level of safety of 10^{-9} at a separation of 3 NM under the assumptions considered. Compared to the previous example considered, this change is due to the introduction of vertical separation, which was not considered in the previous case.

Next, by letting the separation S vary, a new necessary response time for the mitigation can be computed as a function of separation based on the assumed worst-case deviation. The result of this analysis is shown in Figure 6-25.

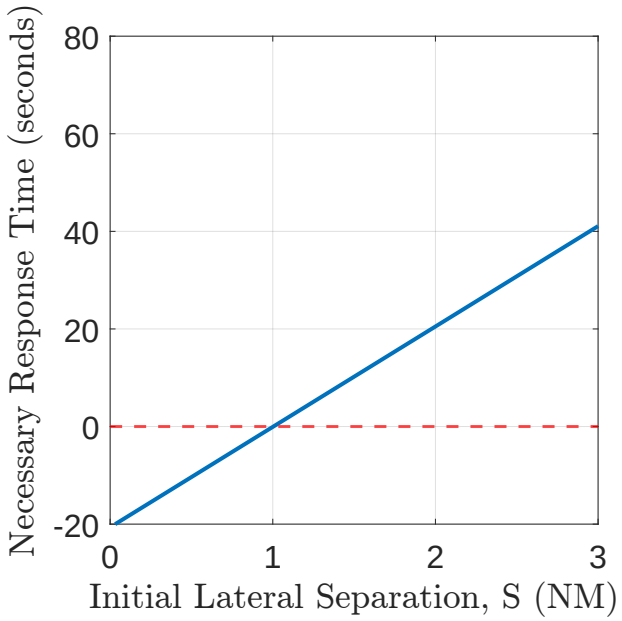

Figure 6-25: Plot of the necessary mitigation response time (i.e., available time for mitigation) as a function of the lateral separation between the two procedures considered, based on the assumed worst-case deviation.

As in the previous example, the collision risk can be recalculated at a range of separation values to produce a parametric plot of the risk as a function of separation. The result of this parametric analysis is shown in Figure 6-26.

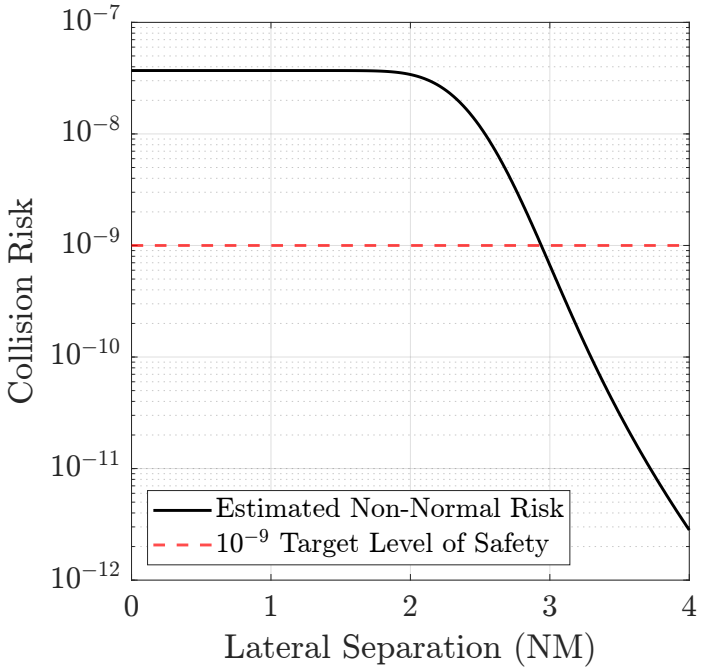

Figure 6-26: Plot of the collision risk as a function of lateral separation between the two procedures considered at BOS.

As observed in this result, the minimum separation needed to satisfy a target level of safety of 10^{-9} is **2.9 NM** based on the initial set of assumptions used.

Next, different system improvements are explored to investigate their potential effect on the required separation between the two procedures considered. The following improvements are evaluated and discussed next:

- Automated Detection and Alerting
- Higher Navigation Reliability
- Lower Aircraft Groundspeed
- Lower Deviation Angle

Effect of Automated Detection and Alerting

The implementation of an automated detection and alerting system has the potential to reduce detection time by alerting air traffic controllers of non-conformance conditions. To evaluate the potential effect of such a capability, a new hypothetical distribution of the detection time is used to represent the expected performance of an automated detection system. This distribution is modeled as a Gaussian with a 2-second mean and a 1-second standard deviation based on the expected use of high-update-rate surveillance (e.g., ADS-B) and automated alerting.

The resulting time distributions associated with each mitigation function as well as the resulting estimate for the total response time are shown in Figures 6-27 and 6-28 below.

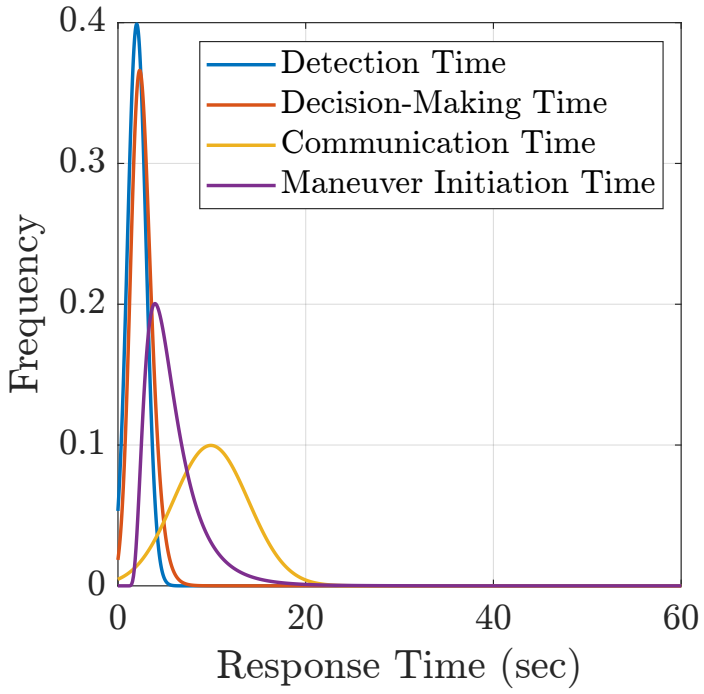

Figure 6-27: Estimates of individual response time components, with the new detection time distribution in blue.

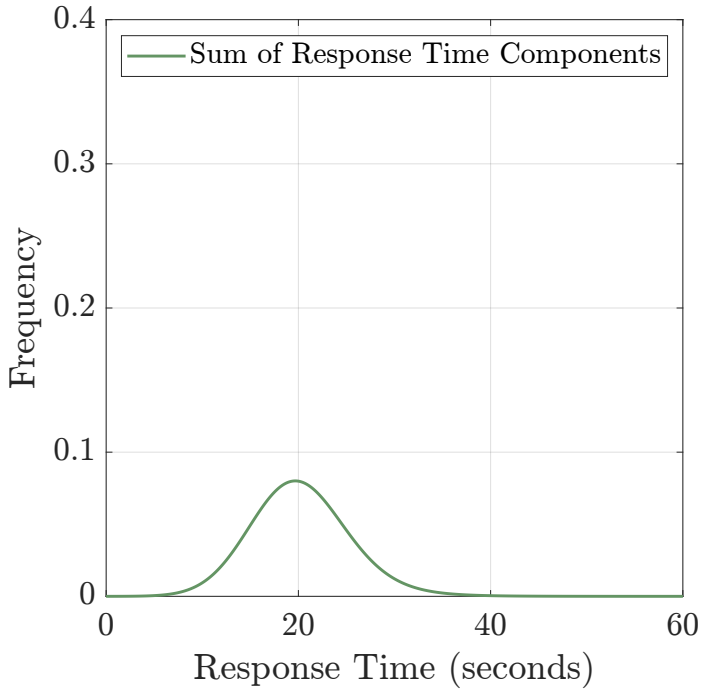

Figure 6-28: New estimate of response time distribution when accounting for the new assumed detection time distribution.

Using this new hypothetical response time distribution, the collision risk as a

function of the separation can be recalculated, with the result of this step shown in Figure 6-29.

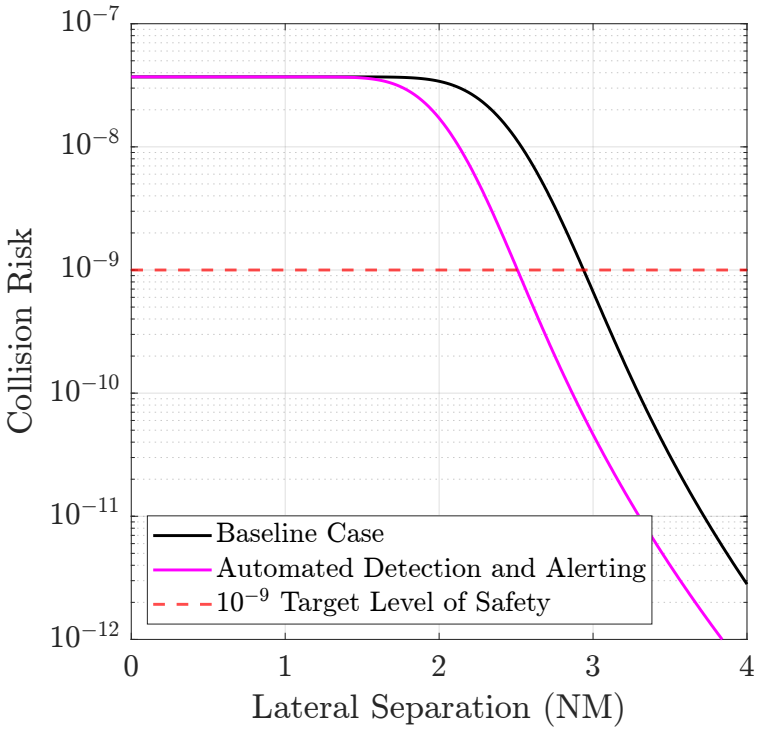

Figure 6-29: Effect of implementing an assumed automated detection and alerting system as part of the mitigation.

As can be observed in this result, implementation of the assumed automated detection and alerting system causes the minimum separation to reduce from 2.9 NM to **2.5 NM**, under the assumptions considered.

Next, additional improvements are considered while retaining this assumed automated detection and alerting system.

Effect of Higher Navigation Reliability

By improving aircraft navigation reliability, the frequency of non-normal events, quantified by $P(NN)$, can be reduced. This may be achieved by requiring the use of autopilot systems, implementing higher-integrity navigation systems, and disallowing manual programming of Flight Management Systems (FMS), for instance.

While retaining the previously considered automated detection and alerting sys-

tem, the value of $P(NN)$ is reduced from 10^{-5} to 10^{-6} to evaluate the effect of this improvement on the required separation. The result of this analysis is shown in Figure 6-30.

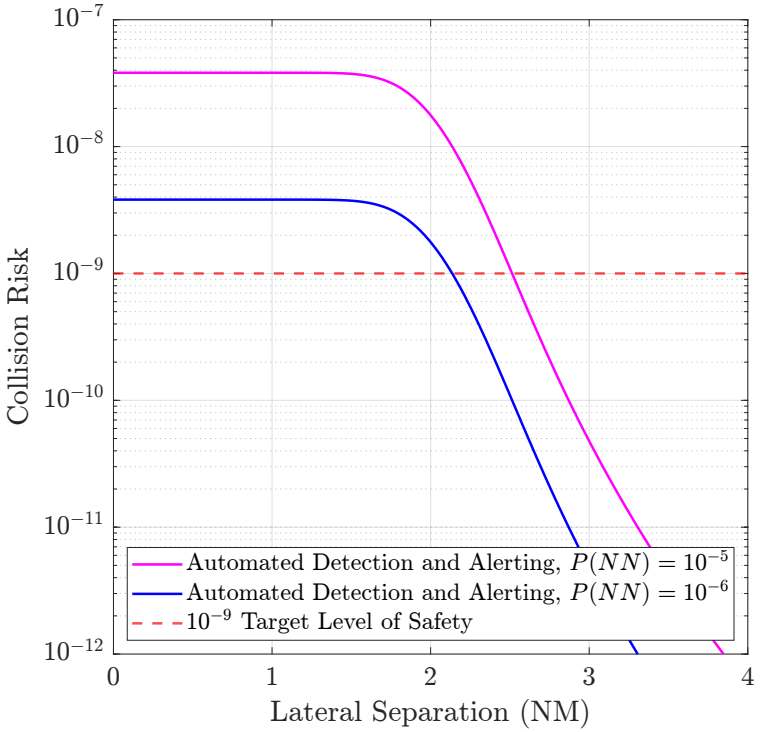

Figure 6-30: Effect of higher navigation reliability, which is posited to reduce the probability of non-normal events.

Based on this result, the reduction of the probability of non-normal events to 10^{-6} offers a further reduction in the required separation between the procedures to **2.1 NM** under the assumptions considered.

Effect of Lower Aircraft Groundspeed

By reducing the groundspeed of deviating aircraft, the time available for mitigation is increased by decreasing the rate of separation loss during a deviation. While aircraft on the departure procedure at BOS are observed to reach a groundspeed of 350 kt in the worst case, a reduction of this value may be achievable by introducing speed restrictions to the departure procedure.

To evaluate the potential effect of this change, the collision risk is recalculated with a new worst-case groundspeed of 300 kt while retaining the previously considered

automated detection and alerting system. The results of this analysis are shown in Figure 6-31.

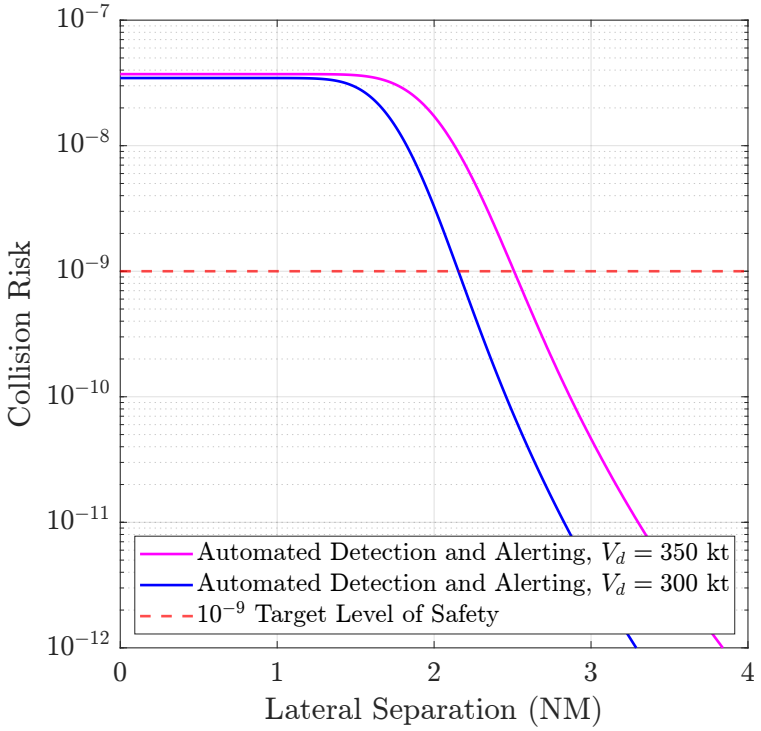

Figure 6-31: Effect of a lower assumed worst-case deviation groundspeed, which increases the time available for mitigation.

Reduction of the assumed worst-case groundspeed to 300 kt can be observed to reduce the required separation to **2.2 NM** under the assumptions considered.

Effect of Lower Deviation Angle

A lower deviation angle increases the time available for mitigation by decreasing the rate of separation loss during a deviation. While a 30° lateral deviation angle has historically been accepted as a standard worst-case deviation angle, future analysis of actual aircraft deviation behaviors may potentially lead to smaller deviation angles being identified as acceptable for the purposes of collision risk assessments.

Here, the reduction of the assumed worst-case deviation angle from 30° to 20° is evaluated for its effect on the required separation between the two flight procedures at BOS. The results of this analysis are shown in Figure 6-32.

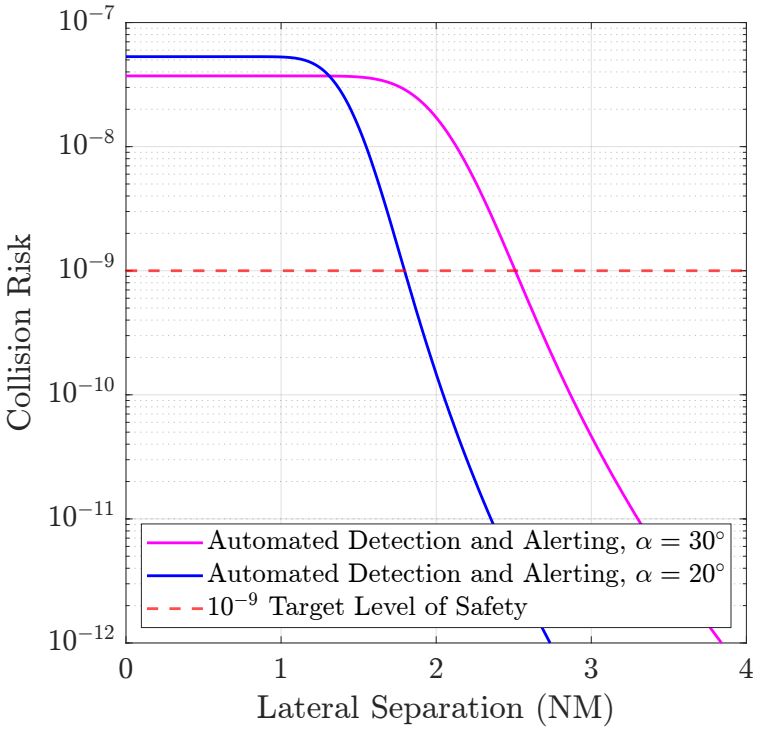

Figure 6-32: Effect of a lower assumed worst-case deviation angle, which increases the time available for mitigation.

The reduction of the deviation angle coupled with the use of an automated detection and alerting system is shown to reduce the required separation between the procedures to **1.9 NM** under the assumptions considered.

6.2.3 Summary of BOS Example

This section evaluated the mitigated collision risk between an RNAV departure and an ILS approach serving converging runways at Boston Logan Airport (BOS), which was found to be driven by non-normal risk. Through the application of the mitigated collision risk model introduced in Chapters 4 and 5, the analysis in this section explored how various system improvements may allow for future reductions in separation between the two procedures considered. Risk estimations were conducted based on representative estimates of mitigation response time distributions and an assumed worst-case deviation.

Based on mitigation by ATC, the minimum separation between the two procedures

was initially found to be 2.9 NM under the initial set of assumptions considered. The introduction of an automated detection and alerting system as part of the mitigation process was posited to provide a meaningful reduction in the mitigation response time, and recalculation of the risk based on a new assumed detection system resulted in a new minimum separation of 2.5 NM. Improvements in detection time were presumed based on the use of high-update-rate surveillance (e.g., ADS-B) and automated alerts to notify air traffic controllers of a deviation.

While retaining this assumed automated detection system, additional system changes were evaluated. Improvements to aircraft navigation reliability were evaluated by reducing the probability of non-normal events from 10^{-5} to 10^{-6}, which provided a reduction in the minimum separation from 2.5 NM to 2.1 NM. Changes to maximum aircraft groundspeed and deviation angle were also evaluated. A reduction in the worst-case groundspeed from 350 kt to 300 kt was shown to reduce the required separation from 2.5 NM to 2.2 NM, while a reduction in the assumed worst-case deviation angle from 30° to 20° was shown to reduce the required separation from 2.5 NM to 1.9 NM under the assumptions considered.

Based on these exploratory findings, it is hypothesized that the development of automated detection capabilities for general terminal operations could allow for meaningful reductions in the required separation between procedures. In addition, greater knowledge of actual aircraft non-normal behaviors could lead to less conservative assumptions in collision risk modeling in the future, with reductions in the assumed deviation angle shown to offer significant reductions in required separation.

Finally, the analysis in this example considered a single mitigation in the form of deviation mitigation by ATC. In current operations, TCAS is available as an additional mitigation, which can enable successful mitigations in scenarios in which ATC response time is insufficient. While the effect of TCAS has historically not been credited in the evaluation of acceptable separation values as a policy choice, the potential future inclusion of conflict mitigation as part of collision risk assessments could provide an additional path by which a target level of safety can be demonstrated. This in turn could offer additional opportunities for increasing flexibility.

6.3 Example Case of Laterally Separated Advanced Air Mobility (AAM) Routes

Advanced Air Mobility (AAM) represents a future concept of operations in which light aircraft, often with short or vertical take-off and landing capabilities, are used to transport a small number of passengers within an urban or regional area. A key question surrounding the future integration of AAM operations into the existing airspace system is whether these new aircraft will have sufficient access to airspace in order to make their proposed operations feasible and scalable. The degree of airspace access that will be available to AAM is believed to be partially driven by the required separation between AAM routes, which will determine the number of routes that can be operated simultaneously within a given volume of airspace. As such, the ability to reduce required separation values below those used for jet operations today is regarded by AAM stakeholders as a key enabler of future high-density AAM operations [71, 72].

The example considered in this section evaluates the achievable separation between two hypothetical symmetric, parallel, opposite-direction, co-altitude AAM routes as a function of mitigation performance, and considers how various system improvements may affect their required separation. The following assumptions are made in the risk evaluation of this hypothetical case:

- The probability of non-normal events, $P(NN)$, is assumed to be 10^{-5} per aircraft operation based on historical estimates [30].
- Aircraft are assumed to be flying at a groundspeed of 150 kt, which is lower than the speed previously assumed for jet aircraft.
- Aircraft are separated in-trail by 1 NM, which is lower than what is currently accepted for jet operations.
- Aircraft have RNP 0.1 tracking performance in normal operations.
- Non-normal events lead to lateral deviations with an angle of 30°.

This example scenario is depicted in Figure 6-33.

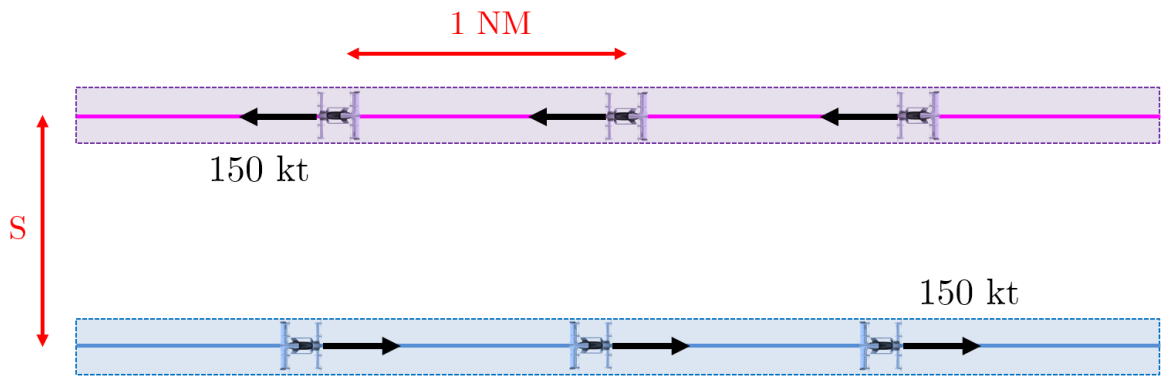

Figure 6-33: Example scenario of two parallel, laterally separated AAM route segments bounded by waypoints. The two segments are laterally separated by a distance of S.

In the calculation of non-normal risk, deviations are modeled as linear trajectories due to data on more complex deviation behaviors not being available. If this data becomes available in the future, the methodology presented here can be reapplied to evaluate the risk associated with these behaviors. Furthermore, the angle at which aircraft intercept the two proximate segments is assumed to be lower than 30°, and potential waypoint overshoots are assumed to not result in deviations with angles larger than this value.

6.3.1 Evaluation of Unmitigated Risk

The collision risk between aircraft on the two AAM routes depicted in Figure 6-33 follows the collision risk parsing previously discussed in Chapter 4 (Figure 6-34).

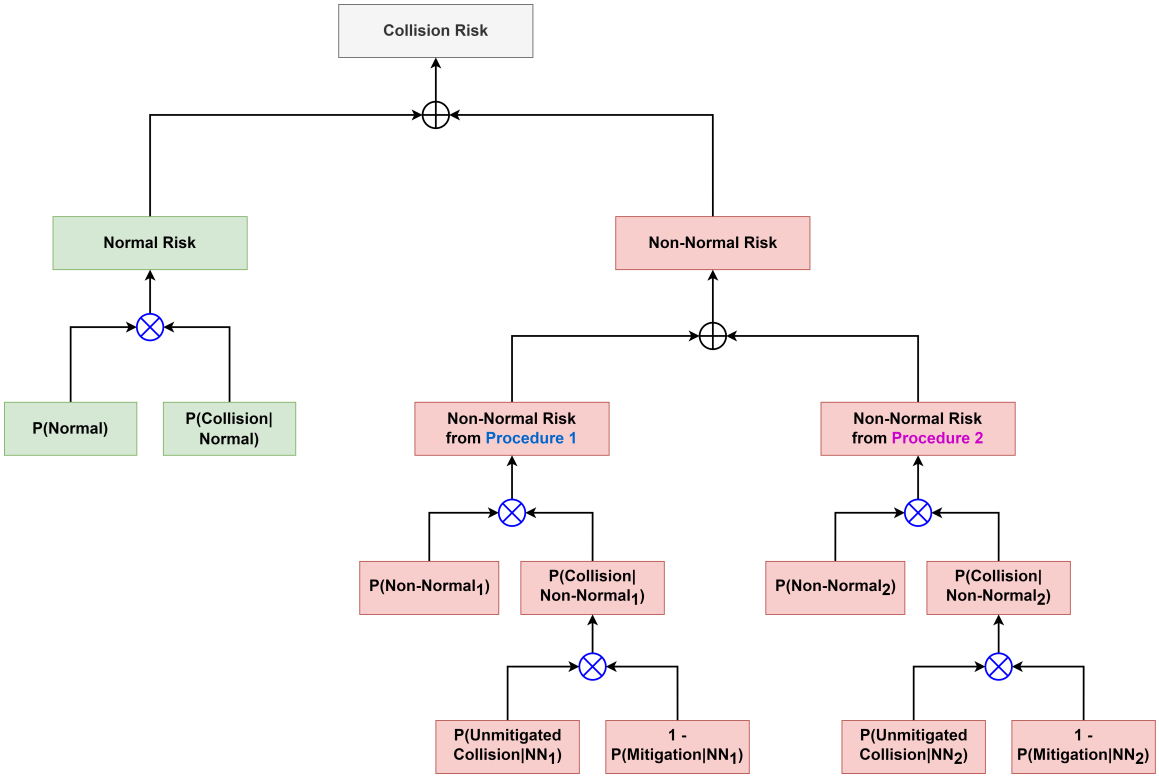

Figure 6-34: Parsing of the collision risk between geometrically separated flight procedures, which includes both normal and non-normal components.

The total collision risk, which must satisfy a 10^{-9} target level of safety, is expressed mathematically as:

$$\begin{aligned} &Collision\ Risk = P(N) \times P(Collision \mid N) \\ &+ P(NN_1) \times P(Unmitigated\ Collision \mid NN_1) \times [1 - P(Mitigation \mid NN_1)] \\ &+ P(NN_2) \times P(Unmitigated\ Collision \mid NN_2) \times [1 - P(Mitigation \mid NN_2)] \\ &< 10^{-9} \end{aligned} \tag{6.30}$$

In Chapter 4, it was previously identified that the normal collision risk between aircraft navigating laterally separated flight procedures with RNAV/RNP performance can be considered negligible at separation distances greater than 0.5 NM. As such, this example will assume that the risk between the two AAM routes considered is dom-

inated by non-normal risk, and that the normal risk is negligible (Equation 6.31). However, if separation distances lower than 0.5 NM are desired, the normal risk must be reevaluated based on the expected navigation performance of the AAM fleet.

$$\begin{aligned} &Collision\ Risk = \cancel{P(N) \times P(Collision \mid N)} \\ &+ P(NN_1) \times P(Unmitigated\ Collision \mid NN_1) \times [1 - P(Mitigation \mid NN_1)] \\ &+ P(NN_2) \times P(Unmitigated\ Collision \mid NN_2) \times [1 - P(Mitigation \mid NN_2)] \\ &< 10^{-9} \end{aligned} \tag{6.31}$$

Because the two AAM routes considered in this example are symmetric, it follows that $P(NN_1) \times P(Unmitigated\ Collision \mid NN_1) \times [1 - P(Mitigation \mid NN_1)] = P(NN_2) \times P(Unmitigated\ Collision \mid NN_2) \times [1 - P(Mitigation \mid NN_2)]$. The collision risk equation can then be written as:

$$\begin{aligned} &Collision\ Risk = \\ &2 \times P(NN) \times P(Unmitigated\ Collision \mid NN) \times [1 - P(Mitigation \mid NN)] \\ &< 10^{-9} \end{aligned} \tag{6.32}$$

The rate of non-normal events, $P(NN)$, will be assumed to be 10^{-5} per operation, based on historically estimated figures for RNAV flight procedures [30].

$$\begin{aligned} &Collision\ Risk = \\ &2 \times \cancel{P(NN)}^{10^{-5}} \times P(Unmitigated\ Collision \mid NN) \times [1 - P(Mitigation \mid NN)] \\ &< 10^{-9} \end{aligned} \tag{6.33}$$

The probability of collision due to unmitigated deviations, $P(Unmitigated\,Collision \mid NN)$, is calculated as the product of two terms, the probability of trajectory overlap, $P(Trajectory\ Overlap \mid NN)$, and the probability of exposure, $P(Exposure \mid Trajectory\ Overlap, NN)$. These terms are calculated using the methods described in Chapter 4.

Probability of Trajectory Overlap

By making the conservative assumption that aircraft navigating the two AAM routes have no vertical separation and that the two segments are infinitely long, the probability of trajectory overlap due to a deviation, $P(Trajectory\ Overlap \mid NN)$, is estimated at **0.5**. This is illustrated in Figure 6-35 below, which shows that any deviation that occurs towards the opposing procedure will result in a trajectory overlap condition.

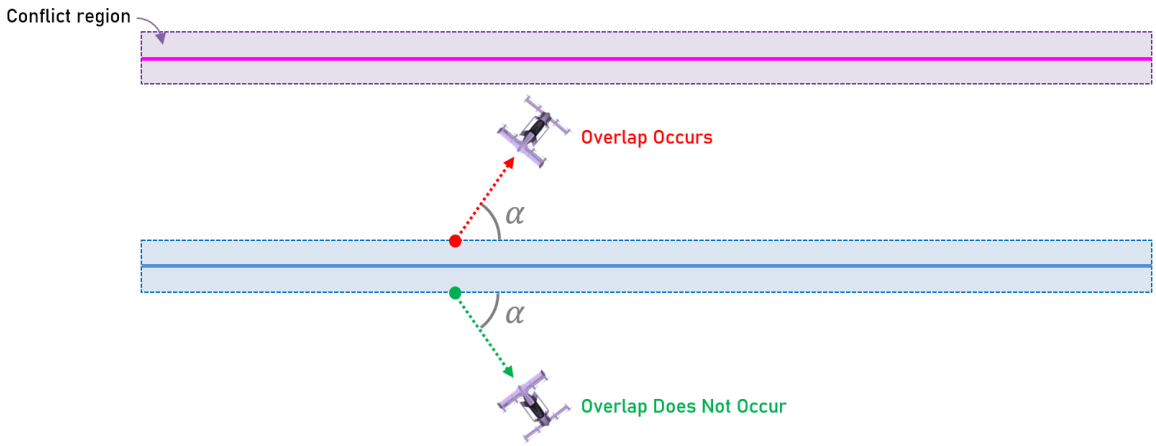

Figure 6-35: The probability of trajectory overlap due to a lateral deviation in the case of parallel, laterally separated AAM routes with no vertical separation is simply a function of the deviation angle, which is assumed constant.

Probability of Exposure

The probability of exposure, $P(Exposure \mid Trajectory\ Overlap, NN)$, is estimated according to Equation 6.34, which was first introduced in Chapter 4 and is repeated here for convenience.

$$P(Exposure \mid Trajectory\ Overlap, NN) = \left(\frac{2A}{V_d sin\alpha}\right) \times \left(\frac{V_e + V_d cos\alpha}{L}\right) + \left(\frac{2B}{L}\right) \tag{6.34}$$

This equation gives the probability that an exposure condition will occur given that a trajectory overlap occurs, and assumes that the two routes are operated independently. For this example, AAM aircraft on the two routes are assumed to be flying in opposite directions at identical groundspeeds (150 kt) and to be separated in-trail by 1 NM on the same route (note that this value is lower than the minimum in-trail separation values used today). Deviations are assumed to occur at a 30° angle. A standard collision box half-width of 265 ft is also assumed (conservative). A summary of the example parameters used is shown in Figure 6-36.

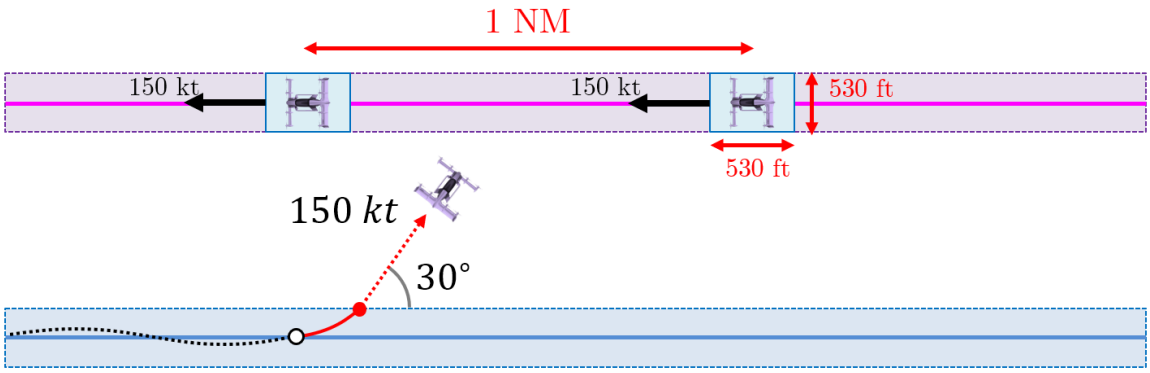

Figure 6-36: Summary of parameters used in the calculation of the probability of exposure to a deviation.

Application of these parameters to Equation 6.34 yields a probability of exposure of **0.4**.

Probability of Collision due to Unmitigated Deviation

The probability that an unmitigated deviation will result in a collision, $P(Unmitigated\ Collision \mid NN)$, is the product of the calculated probabilities of trajectory overlap and exposure: $(0.5) \times (0.4) = \mathbf{2 \times 10^{-1}}$. This result indicates that 2 out of every 10 unmitigated deviations are expected to result in a collision under the assumptions

considered.

$$
\begin{aligned}
&Collision\ Risk = \\
&2 \times 10^{-5} \times P(Unmitigated\ Collision \mid NN) \times [1 - P(Mitigation \mid NN)] \\
&< 10^{-9}
\end{aligned}
\qquad \xrightarrow{\quad 2 \times 10^{-1} \quad} \qquad (6.35)
$$

Following these results, the next section continues with the evaluation of the effect of the mitigation on the risk and evaluates the achievable separation values between the two AAM routes considered under a variety of potential system improvements.

6.3.2 Parametric Evaluation of Mitigated Risk

The probability of mitigation for the scenario described can be evaluated using the mitigation model introduced in Chapter 4 and repeated here, which assumes a lateral mitigation maneuver:

$$
\begin{aligned}
&P(Mitigation \mid NN) = \\
&P\left(Time\ of\ Response \leq \frac{S - D - C - A}{V_d \cdot sin\alpha} - \frac{V_d \cdot tan(\alpha/2)}{g \cdot tan(\phi_{target})} - \frac{\phi_{target}}{\dot{\phi}}\right)
\end{aligned}
\qquad (6.36)
$$

The following parameters are assumed for a representative worst-case deviation:

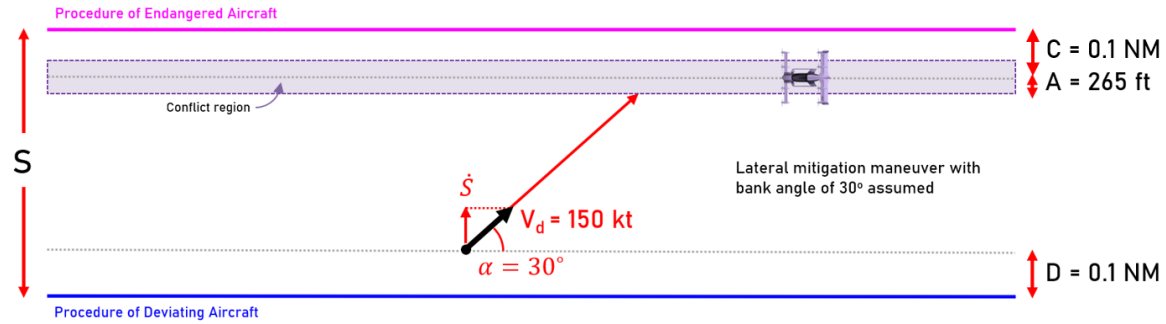

Figure 6-37: Overview of parameters used to describe a representative worst-case deviation in the AAM scenario. Distances and vehicle sizes not to scale.

- **D**: The cross-track distance of the deviating aircraft at the conformance limit. Assumed to be **0.1 NM** based on RNP 0.1 tracking performance during normal operations.

- **C**: The cross-track position of the endangered aircraft. Assumed to be **0.1 NM** based on RNP 0.1 tracking performance during normal operations.

- **A**: Half-width of collision box around endangered aircraft. Assumed to be **265 ft** based on standard collision box size used by FAA.

- $\mathbf{V_d}$: Groundspeed of deviating aircraft. Assumed to be **150 kt** based on typical speed value expected from AAM vehicles.

- α: Lateral deviation angle. Assumed to be $\mathbf{30}^\circ$ based on historically accepted value for a representative worst-case deviation.

- $\phi_{\mathbf{target}}$: The target bank angle during a lateral mitigation maneuver. Assumed to be $\mathbf{30}^\circ$ based on typical aircraft bank angles.

- $\dot{\phi}$: The target roll rate during a lateral mitigation maneuver. Assumed to be $\mathbf{10}^\circ/\mathbf{sec}$ based on typical aircraft roll rates.

By applying the parameters above to Equation 6.36 while keeping the lateral separation **S** a free variable, the necessary mitigation response time can be determined as a function of S (Figure 6-38).

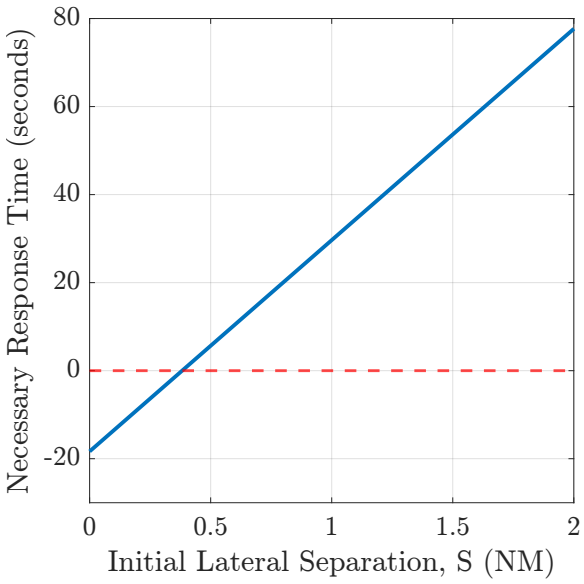

Figure 6-38: Plot of the necessary mitigation response time (i.e., available time for mitigation) as a function of the lateral separation between two AAM routes given the assumptions listed above.

This result specifies the response time that a mitigation must meet to mitigate the assumed worst-case deviation. As in previous examples, the separation between the two AAM routes can be varied to produce a parametric plot of the collision risk as a function of separation. By initially assuming mitigation by ATC as in previous examples, the following result is obtained (Figure 6-39).

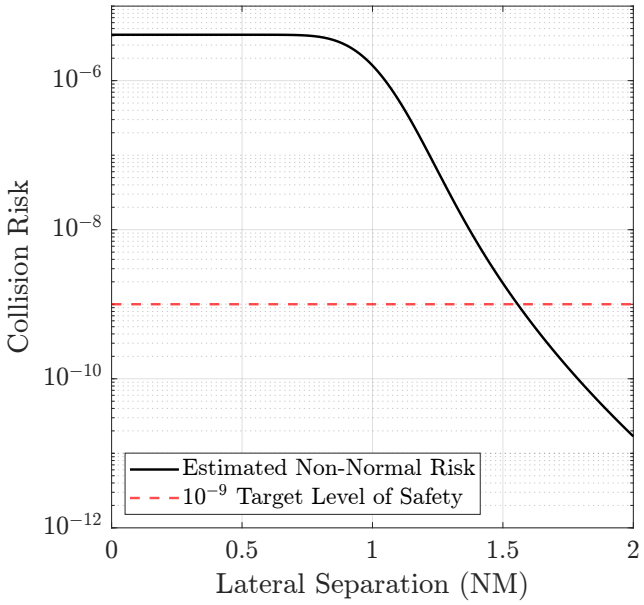

Figure 6-39: Plot of the collision risk as a function of lateral separation for the scenario of symmetric, parallel, opposite-direction, co-altitude AAM routes.

As observed in this result, the minimum separation needed to satisfy a target level of safety of 10^{-9} is **1.6 NM** based on the initial set of assumptions used. This result is lower than the value previously calculated for jet aircraft due to the lower speed of AAM vehicles.

Next, different system improvements are explored to investigate their potential effect on the required separation between AAM routes. The following improvements are evaluated and discussed next:

- Automated Detection and Alerting
- Fully Automated Mitigation
- Higher Navigation Reliability
- Advanced Conformance Monitoring and Navigation Performance

Effect of Automated Detection and Alerting

The implementation of an automated detection and alerting system has the potential to reduce detection time by alerting air traffic controllers of non-conformance conditions. To evaluate the potential effect of such a capability, a new hypothetical distribution of the detection time is used to represent the expected performance of an automated detection system. This distribution is modeled as a Gaussian with a 2-second mean and a 1-second standard deviation based on the expected use of high-update-rate surveillance (e.g., ADS-B) and automated alerting.

The resulting time distributions associated with each mitigation function as well as the resulting estimate for the total response time are shown in Figures 6-40 and 6-41 below.

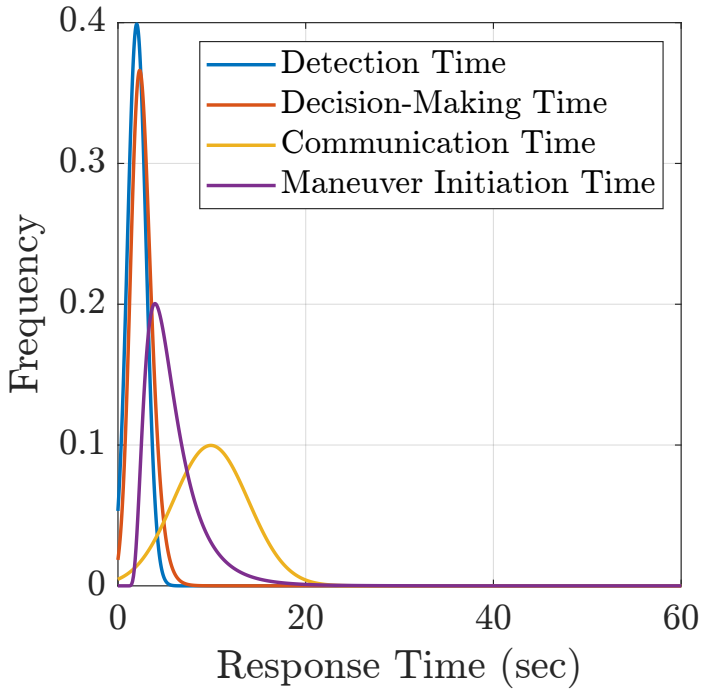

Figure 6-40: Estimates of individual response time components, with the new detection time distribution in blue.

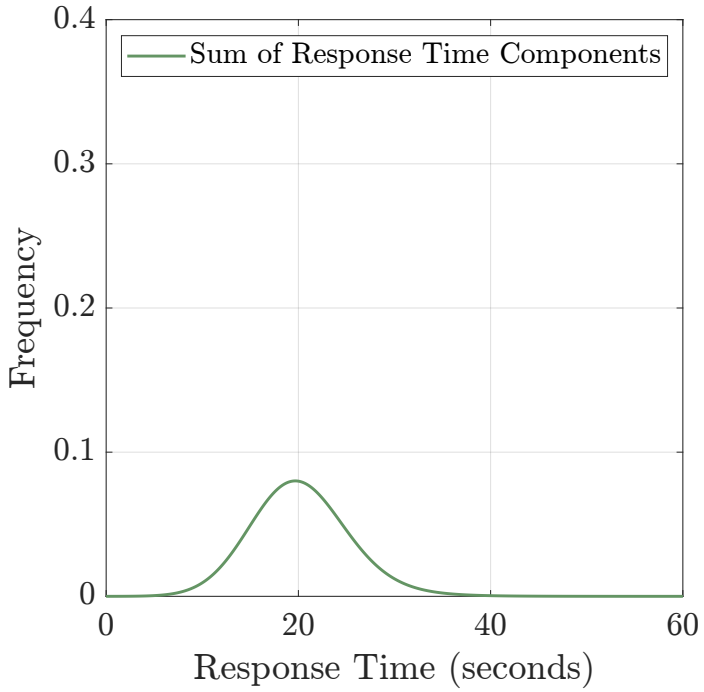

Figure 6-41: New estimate of response time distribution when accounting for the new assumed detection time distribution.

Using this new hypothetical response time distribution, the collision risk as a

function of the separation can be recalculated, with the result of this step shown in Figure 6-42.

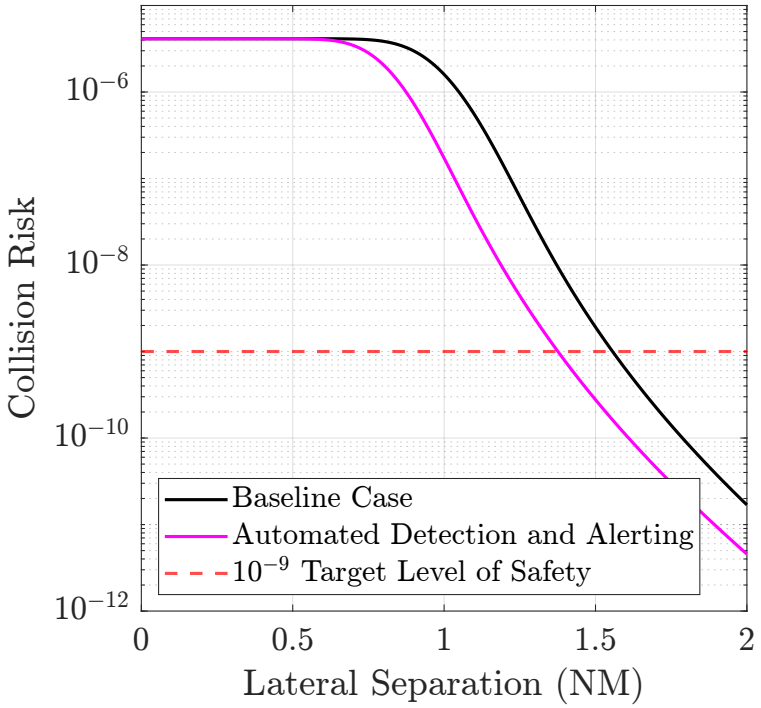

Figure 6-42: Effect of implementing an assumed automated detection and alerting system as part of the mitigation.

As can be observed in this result, implementation of the assumed automated detection and alerting system causes the minimum separation to reduce from 1.6 NM to **1.4 NM** under the assumptions considered, offering some benefit.

Effect of Fully Automated Mitigation

A completely automated mitigation system is posited to offer a large reduction in response time by decoupling the mitigation process from human performance. To evaluate the potential effect of an automated mitigation system on the required separation between AAM routes, new hypothetical time distributions are assumed for the various mitigation functions based on supposed automation improvements:

- Detection time assumed as a Gaussian with a 1-second average and a 0.5-second standard deviation. Improvement supposed from the use of high-update-surveillance (e.g., ADS-B) and automated detection with no requirement for human perception.

- Decision-making time assumed as a constant 0.5-second delay. Improvement supposed from automated planning of mitigation instructions.

- Communication time assumed as a constant 0.5-second delay. Improvement supposed from use of Datalink message for communication of mitigation instruction to aircraft.

- Maneuver initiation time assumed as a constant 0.5-second delay. Improvement supposed from automated aircraft response following receipt of Datalink instruction.

The resulting time distributions associated with each mitigation function as well as the resulting estimate for the total response time are shown in Figures 6-43 and 6-44 below.

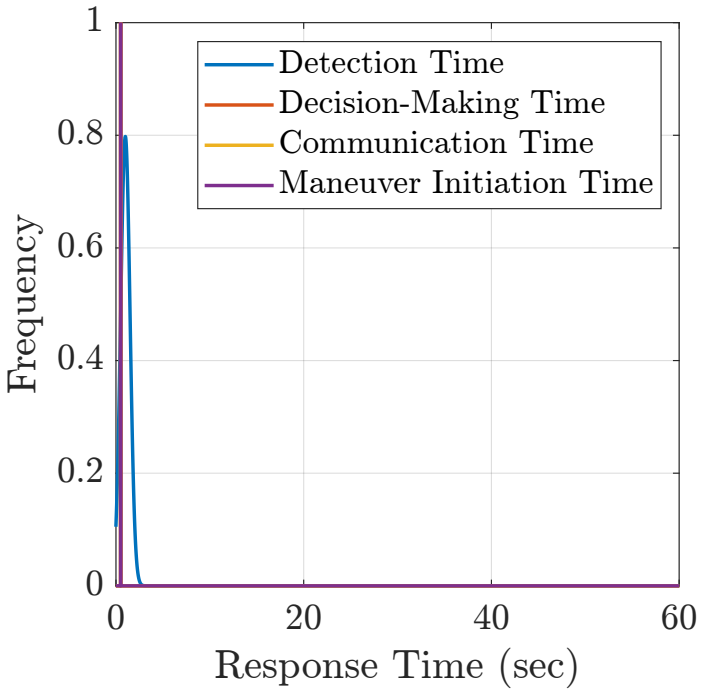

Figure 6-43: Estimates of individual response time components for a hypothetical automated mitigation system.

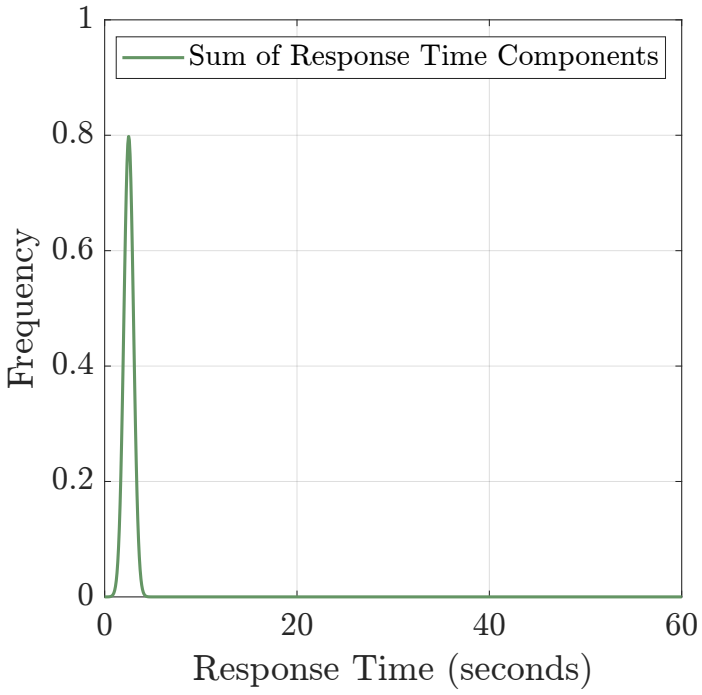

Figure 6-44: New estimate of response time distribution for a hypothetical automated mitigation system.

Using this new hypothetical response time distribution, the collision risk as a

function of the separation can be recalculated, with the result of this step shown in Figure 6-45.

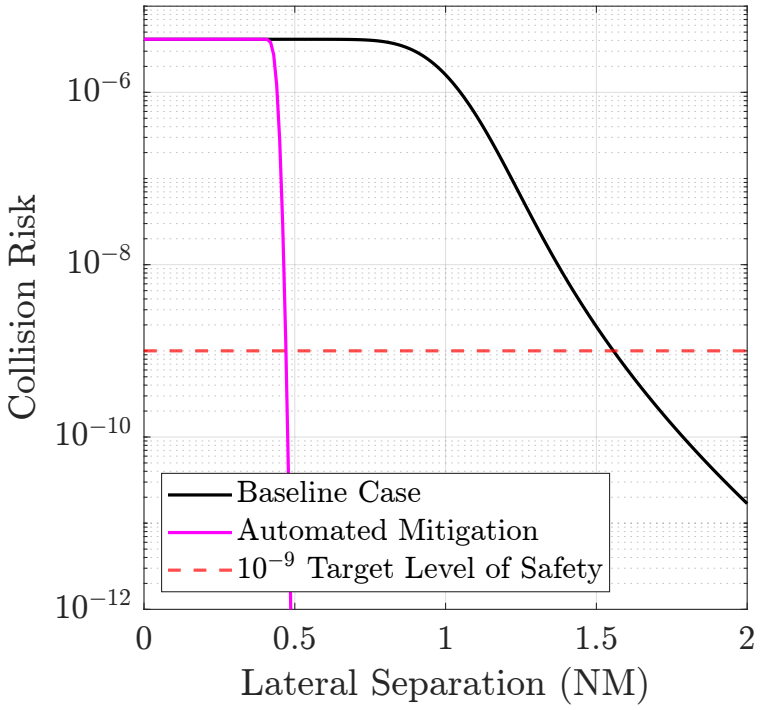

Figure 6-45: Effect of implementing an assumed automated mitigation system.

As can be observed in this result, the implementation of the assumed automated mitigation system provides a significant reduction in the required separation between AAM routes, from 1.6 NM in the baseline case to **0.5 NM** under the assumptions considered.

Next, this automated mitigation system is retained while additional improvements are considered.

Effect of Higher Navigation Reliability

By improving aircraft navigation reliability, the frequency of non-normal events, quantified by $P(NN)$, can be reduced. This may be achieved by requiring the use of autopilot systems, implementing higher-integrity navigation systems, and disallowing manual programming of Flight Management Systems (FMS), for instance.

While retaining the previously considered fully automated mitigation system, the

value of $P(NN)$ is reduced from 10^{-5} to 10^{-7} and finally to 10^{-9} to evaluate the effect of this improvement on the required separation. The result of this analysis is shown in Figure 6-46.

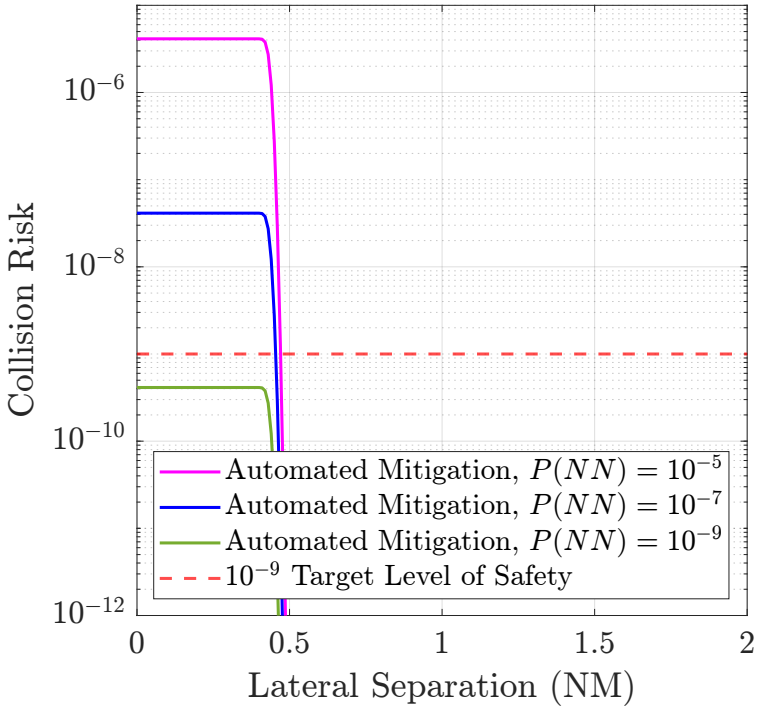

Figure 6-46: Effect of higher navigation reliability, which is posited to reduce the probability of non-normal events.

As can be observed in this result, initial reduction of $P(NN)$ from 10^{-5} to 10^{-7} does not meaningfully reduce the minimum separation due to the mitigation being extremely consistent already. Further reduction of $P(NN)$ to 10^{-9} allows the non-normal risk to meet the 10^{-9} target level of safety without any mitigations. In such a scenario, and at small separation distances (< 0.5 NM), the normal collision risk may become significant again.

Effect of Advanced Conformance Monitoring and Navigation Performance

The final system improvement considered is the implementation of advanced conformance monitoring and navigation performance. In this case, an advanced conformance monitor is assumed that can detect a non-conformance condition before any cross-track error develops. In the geometric model used to represent the mitigation

scenario, this improvement is represented by $D = 0$. In addition, aircraft will be assumed to navigate without any cross-track error during normal operations, which can be represented in the same geometric model by $C = 0$. These improvements are illustrated in Figure 6-47.

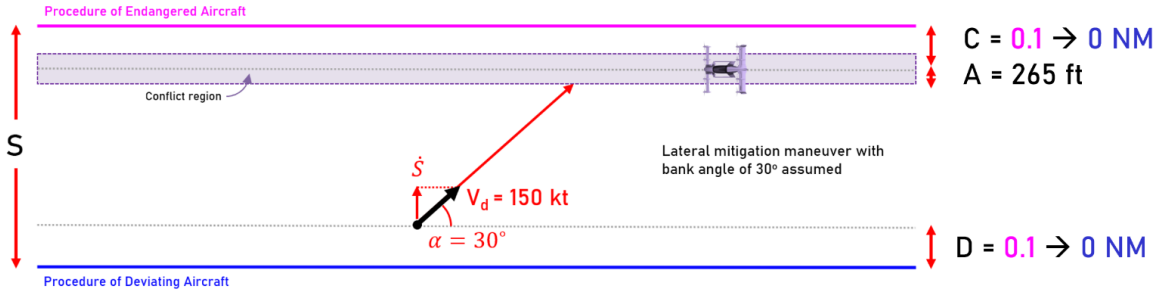

Figure 6-47: Representation of effects of advanced conformance monitoring and navigation performance on scenario geometry.

The effects of these changes on the minimum required separation are shown in Figure 6-48.

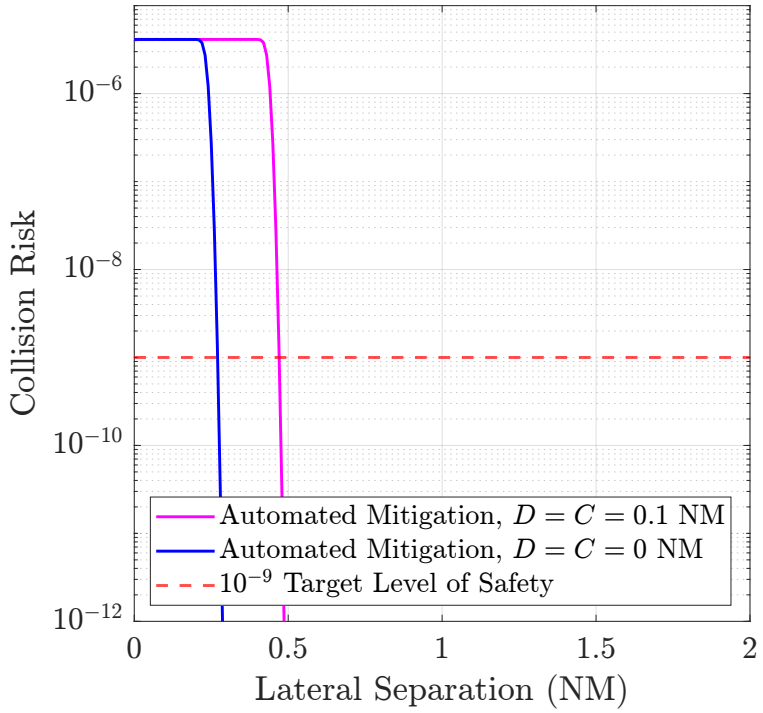

Figure 6-48: Effect of advanced conformance monitoring and navigation performance.

Based on this result, it can be observed that the implementation of advanced conformance monitoring and navigation performance reduces the minimum separation

from 0.5 NM to **0.3 NM** under the assumptions considered. While this represents a significant reduction from the original 1.6 NM required separation found in the baseline case, the normal collision risk may no longer be negligible at such a small separation value and would therefore need to be considered based on the actual navigation performance achieved by AAM vehicles.

6.3.3 Summary of AAM Example

This section evaluated the mitigated collision risk between two parallel, laterally separated AAM routes under the effect of mitigations using the methods introduced in Chapters 4 and 5, and explored how various system improvements may allow for future reductions in separation. Risk estimations were conducted based on representative estimates of mitigation response time distributions and an assumed worst-case deviation.

Based on mitigation by ATC, the minimum separation between two AAM routes was initially found to be 1.6 NM under an initial set of assumptions. Automation of the mitigation process was posited to provide a significant reduction in mitigation response time, and recalculation of the risk based on an assumed automated mitigation system resulted in a new minimum separation of 0.5 NM. The assumed automated mitigation system was presumed to rely on automated detection based on high-update-rate surveillance, automated decision-making, Datalink for communications, and automated execution of mitigation instructions by an onboard autopilot.

In order to reduce the separation further, improvements to conformance monitoring and navigation performance were found to allow for a limit separation of 0.3 NM at the limit where aircraft have no cross-track error at the time when they exceed the conformance and in normal operations. However, it was noted that the normal collision risk is expected to become significant at such small values of separation, and would need to be evaluated based on the actual navigation performance achieved by AAM vehicles.

Based on these exploratory findings, it is hypothesized that the development of new automated mitigation capabilities could be a key enabler of future high-density

AAM operations. While conformance monitoring, detection, and decision-making are currently performed on the ground in the case of ATC-based mitigation, opportunities may exist to develop these functions as airborne systems, e.g., AAM aircraft may be able to monitor each other's conformance. This may have the benefit of not requiring the development of new ATC/ATM capabilities.

Chapter 7

Conclusion

This thesis provided a study of factors limiting flexibility in the design and operation of instrument flight procedures, which were termed *flight procedure constraints*. Many constraints were found to originate from safety considerations, and constraints were found to sometimes interact in complex ways to limit flight procedure flexibility. It was hypothesized that opportunities to increase system performance and flexibility may exist through a better understanding of constraints and opportunities to reevaluate them based on technology improvements. Following a review of constraints, the required geometric separation between published procedures was identified as a major constraint and chosen as the subject of an in-depth study for identifying constraint reevaluation opportunities. Due to several system improvements related to communication (e.g., Datalink), navigation (e.g., RNAV and RNP) and surveillance (e.g., ADS-B) having occurred in the last few decades, this work sought to better understand how these and other technology improvements may affect the required separation between published procedures, which could lead to opportunities to increase flexibility.

The collision risk between aircraft on different procedures was identified as the main factor driving the minimum required separation between published flight procedures, which is required to meet a target level of safety of 10^{-9} collisions per operation based on safety policy established by the Federal Aviation Administration (FAA). Following a review of prior efforts to reevaluate the required separation between flight

procedures, it was posited that the consideration of collision mitigation capabilities represents a key mechanism for identifying how technology improvements may enable the reevaluation of separation. In many past safety assessments, it was argued that credit was not always taken for the availability of mitigations. To that end, a collision risk model was proposed for evaluating the mitigated collision risk between two geometrically separated flight procedures, which parsed the risk as normal and non-normal risk (Figure 7-1).

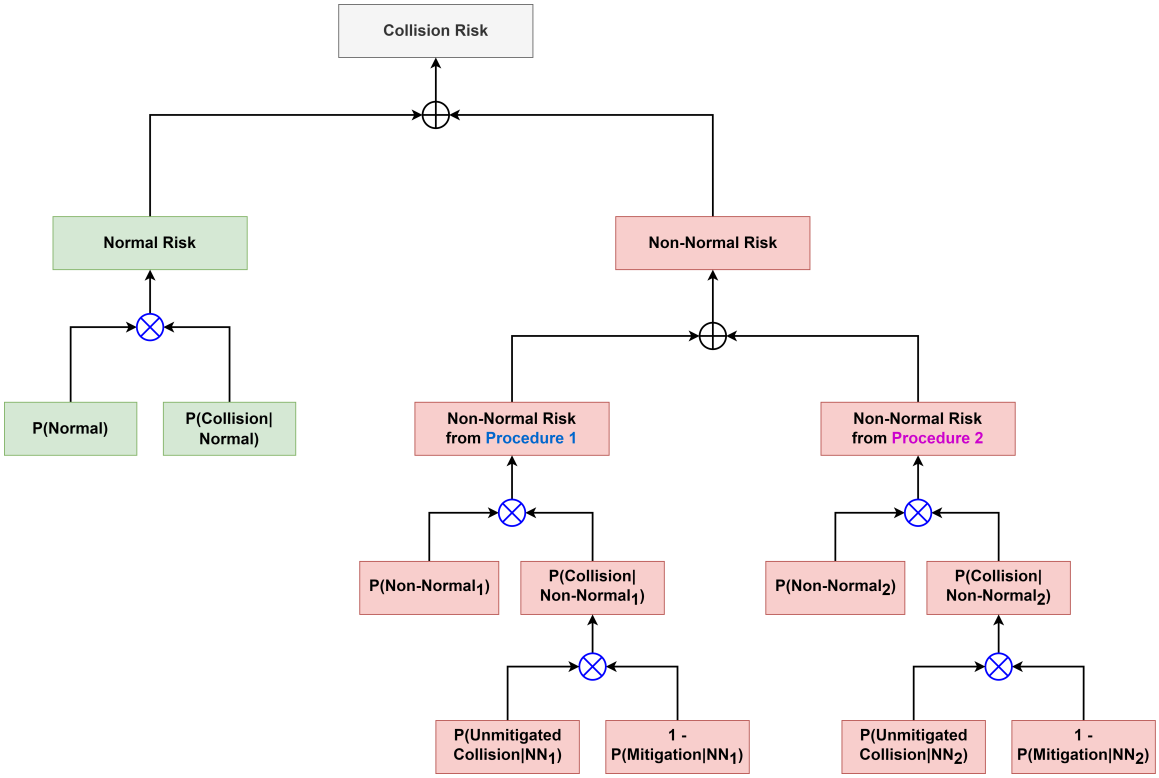

Figure 7-1: Parsing of the collision risk between geometrically separated flight procedures, which includes both normal and non-normal components.

The collision risk between aircraft in normal operations on PBN (i.e., RNAV and RNP) procedures was found to be negligible at lateral separation values greater than 0.5 NM due to the significant improvements in navigation performance experienced over the last several decades. As a result, the collision risk between aircraft on laterally separated flight procedures was found to be driven by non-normal risk. Evaluation of the non-normal risk considered the risk due to deviations from both procedures under the effect of mitigations, for which a geometry-based model was proposed. This model

was used to identify and discuss key parameters in mitigation and flight procedure design that can be used to control the probability of mitigation and the non-normal risk between flight procedures.

A mitigation's response time was found to be a key performance metric of the mitigation, and was defined as the time needed to detect a deviation, determine a mitigation plan, communicate a mitigation instruction, and initiate a mitigation maneuver. A review of these individual response time components was conducted for ATC-based deviation mitigation based on available historical data, with their distributions found to exhibit noticeable variance due to reliance on human performance. Based on this observation, a conceptual future mitigation system was discussed that could offer improvements in both average response times and response time variance through the use of modern CNS technologies and greater automation (Table 7.1).

Function	Current System	Potential Future System
Conformance Monitoring	Visual scan of aircraft position by controllers.	Automated conformance monitoring based on multiple aircraft states.
Detection	Radar-based surveillance (4.8-second updates).	High-update-rate surveillance (e.g., ADS-B).
Decision-Making	Planning by air traffic controllers.	Automated planning and maneuver calculation.
Communication	Mitigation instructions issued via voice (VHF).	Mitigation instructions issued via Datalink messages.
Maneuver Initiation	Maneuver executed manually by pilots.	Datalink instruction executed by autopilot.

Table 7.1: Comparison of mitigation functions currently used for deviation mitigation in the current system and those of a potential future mitigation system.

Related to aircraft operations and flight procedure design, the speed and the angle of a deviation were found to be key variables affecting the time available for mitigation and therefore the probability of a successful mitigation. Given the large effect of a deviation's angle on the time available for mitigation, it was hypothesized that the

monitoring of aircraft velocity and acceleration states (e.g., heading, bank angle) as part of conformance monitoring may enable the detection of deviations before they develop into large-angle trajectories, thus improving the probability of mitigation. The control of aircraft speeds through speed restrictions in flight procedures was also proposed as an additional mechanism for improving the probability of mitigation, since the reduction of aircraft speeds leads to an increase in the available time for mitigation.

Chapter 6 of this thesis presented three example studies in which the mitigated collision risk model introduced in earlier chapters was used to evaluate the mitigated collision risk between procedures in different scenarios. The examples considered included a generic case of two co-altitude jet aircraft procedures, a real case at Boston Logan Airport involving a departure and an approach procedure, and a hypothetical case of two Advanced Air Mobility (AAM) routes. For each of these cases, the proposed methodology was applied to explore how potential system improvements and changes could lead to opportunities to reduce separation and increase flexibility. Changes evaluated included improvements to mitigation functions (e.g., automated detection and alerting), improvements in navigation reliability (i.e., reduction of the probability of non-normal), changes to worst-case deviation assumptions, and changes to flight procedure geometry (e.g., adding vertical separation). In each example scenario analyzed, potential improvement paths for increasing flexibility were identified. In particular, the implementation of automated mitigation functions and the reduction of the assumed worst-case deviation angle were found to offer considerable reductions in the required separation between procedures under the assumptions considered. Based on these findings, it was posited that the future development of automated mitigation capabilities for general terminal operations coupled with a greater understanding of actual aircraft deviation behaviors could enable future flexibility improvements.

The analyses in Chapter 6 considered the use of a single mitigation capability. In current operations, TCAS is available as an additional mitigation, which can enable successful mitigations in scenarios in which ATC response time is insufficient. While

the effect of TCAS has historically not been credited in the evaluation of acceptable separation values as a policy choice, the potential future inclusion of conflict mitigation as part of collision risk assessments could provide an additional path by which a target level of safety can be demonstrated. This in turn could offer additional opportunities for increasing flexibility.

Finally, accurate estimation of non-normal risk was found to be presently limited by three main factors: the lack of data on the frequency with which deviations occur, a poor understanding of actual aircraft deviation behaviors and trajectories, and the lack of precise data on the performance of available mitigation capabilities such as ATC-based deviation mitigation. As a result, example calculations performed in this study relied on historical assumptions such as the assumption of a 30° lateral deviation angle, which was found to have a significant effect on the estimated risk. Similarly, the assumed rate of deviations, 10^{-5} per operation, represents data originally collected on ILS approaches, in which the approach may be hand-flown by pilots. As such, the deviation rate on PBN flight procedures may be lower when aircraft are flying on autopilot, and the requirement for an autopilot to be used may further reduce this rate. Finally, accurate estimation of the probability of mitigation was found to require information on the distribution of response times, which are currently available in small sample sizes. Based on these observations, it is therefore posited that the future collection of large-scale data on these three fronts — 1) the frequency of deviations, 2) aircraft deviation behaviors and trajectories, and 3) mitigation performance including response times — could offer substantial improvements in the ability to reevaluate the required separation between flight procedures and increase flexibility.

Bibliography

[1] Federal Aviation Administration. Aeronautical Information Manual (AIM), December 2021.

[2] Federal Aviation Administration. Order 8260.3E: United States Standard for Terminal Instrument Procedures (TERPS), September 2020.

[3] International Civil Aviation Organization. Doc 8168: Aircraft Operations, Volume II: Construction of Visual and Instrument Flight Procedures, 2014. Sixth edition.

[4] Federal Aviation Administration. Order 8260.3E: United States Standard for Performance Based Navigation (PBN) Instrument Procedure Design, August 2020.

[5] International Civil Aviation Organization. Doc 9905: Required Navigation Performance Authorization Required (RNP AR) Procedure Design Manual, September 2009. First edition.

[6] Federal Aviation Administration. Order 7110.65Z: Air Traffic Control, June 2021.

[7] Federal Aviation Administration. Order 7110.126B: Consolidated Wake Turbulence (CWT), November 2021.

[8] Federal Aviation Administration. Order A90 TRACON 7110.11L: Standard Operating Procedures, February 2018.

[9] Federal Aviation Administration. Introduction to TCAS II Version 7.1, February 2011.

[10] Federal Aviation Administration. Advisory Circular 25.1322, Alerting Systems, December 2010.

[11] Federal Aviation Administration. Safety Alert for Operators 22003, August 2022.

[12] Sheila R. Conway; Mary Beth Lapis; Jeffery D. Musiak; Michael L. Ulrey; Christian Hanses. Airborne Collision Avoidance Considerations for Simultaneous Parallel Approach Operations. 30th Congress of the International Council of the Aeronautical Sciences, Daejon, South Korea, September 2016.

[13] RTCA. DO-236: Minimum Aviation System Performance Standards: Required Navigation Performance for Area Navigation, September 2014.

[14] FAA Aeronautical Charting Forum (Instrument Procedures Group). Minutes of Meeting 14-01, April 2014. Accessible at `https://www.faa.gov/sites/faa.gov/files/about/office_org/headquarters_offices/avs/ACF-IPG_14-01_Minutes.pdf`.

[15] Luke Jensen. *Data-Driven Flight Procedure Simulation and Noise Analysis in a Large-Scale Air Transportation System.* PhD thesis, Massachusetts Institute of Technology, 2018.

[16] Flight Safety Foundation. Briefing Note 7.1 - Stabilized Approach. Technical report, November 2000.

[17] Federal Aviation Administration. Order JO 7100.41A - Performance Based Navigation Implementation Process, February 2014.

[18] Mark J. Rockman. A Review of the Current Radar Separation Minima and Some Thoughts on Reducing Them. Technical report, The MITRE Corporation, July 1994.

[19] S. D. Thompson. Terminal Area Separation Standards: Historical Development, Current Standards, and Processes for Change. Technical report, MIT Lincoln Laboratory, 1997.

[20] Air Traffic Organization. Safety Management System Manual. Technical report, Federal Aviation Administration, April 2019.

[21] Brian Marks. Air Traffic Control Separation Standards and Collision Risk. RAE Tech Note Math 91, Royal Aircraft Establishment, Farnborough, United Kingdom, 1963.

[22] Peter Reich. A Theory of Safe Separation Standards for Air Traffic Control. RAE Technical report 64041, 64042, 64043, Royal Aircraft Establishment, Farnborough, United Kingdom, 1964.

[23] Jacky Civil. The Longitudinal Reich Collision Risk Model. Information Paper SASP-WG/WHL/20-IP/10, International Civil Aviation Organization (ICAO), Montreal, Canada, 2012.

[24] Robert E. Machol. Thirty Years of Modeling Midair Collisions. *Interfaces*, 25(5):151–172, September 1995.

[25] Peter Reich. Analysis of Long-Range Air Traffic Systems: Separation Standards — I. *The Journal of Navigation*, 50(3):436–447, 1997.

[26] FAA Office of System Capacity and Requirements. Near Term Capacity Initiatives. Technical report, Federal Aviation Administration, Washington, D.C., 1992.

[27] A. L. Haines. Recommendations Concerning Reduction of Parallel Runway Spacing Under IFR Conditions. Technical Report MTR-6178, The MITRE Corporation, McLean, VA, 1972.

[28] Richard L. Fain. Blunder Assumptions in Past Simultaneous Parallel Approach Studies. Technical Report MP 94W0000090, The MITRE Corporation, McLean, VA, 1994.

[29] S. Vincent Massimini. Simultaneous Independent and Dependent Parallel Instrument Approaches: Assumptions, Analysis, and Rationale. Technical Report MP 06W0000127, The MITRE Corporation, McLean, VA, 2006.

[30] Flight Technologies and Procedures Division (AFS-400). Safety Study on Simultaneous Independent Approaches Using Established on Required Navigation Performance Approach Procedures with Track-to-Fix Design. Technical report, Federal Aviation Administration, June 2016.

[31] Logan M. Branscum, Cody T. Nichols. Quantification of Midair Collision Risk for Established on Required Navigation Performance Operations. 2017 IEEE/AIAA 36th Digital Avionics System Conference (DASC), St. Petersburg, FL, September 2017.

[32] Ralf H. Mayer; Matthew R. Pollock; Jonathan T. Schwalbe; Graham K. Glover; Remi L. Gottheil; Dennis J. Zondervan. Toward a performance-based nas: Airports for potential application of pbn-enabled departure separation standards. 2013 Integrated Communications, Navigation and Surveillance Conference (ICNS), Herndon, VA, April 2013.

[33] Flight Systems Laboratory (AFS-450). Safety Study Report on Separation Requirements for Simultaneous and Sequential Area Navigation (RNAV) Departures at Atlanta/Hartsfield International Airport (KATL). Technical report, Federal Aviation Administration, August 2011.

[34] Federal Aviation Administration. Equivalent Lateral Spacing Operations (ELSO), April 2015. Accessible at `https://www.faa.gov/newsroom/equivalent-lateral-spacing-operations-elso`.

[35] Flight Technologies and Procedures Division (AFS-400). Safety Study of Closely Spaced Parallel Operations Utilizing Paired Approach. Technical report, Federal Aviation Administration, April 2019.

[36] Flight Technologies and Procedures Division (AFS-400). Safety Study of Closely Spaced Parallel Operations with High Update Rate Surveillance. Technical report, Federal Aviation Administration, May 2018.

[37] Flight Technologies and Procedures Division (AFS-400). Altitude Sensitivity Study of Close Parallel Approaches - High Update Rate Surveillance Not Required. Technical report, Federal Aviation Administration, June 2017.

[38] Ashim Kumar Thapa, John Shortle, Lance Sherry. Air-to-Air Collision Risk Models (CRM) in the Terminal Airspace. 2023 Integrated Communications, Navigation and Surveillance Conference (ICNS), Williamsburg, VA, April 2023.

[39] Eric M. Shank, Katherine M. Hollister. Precision Runway Monitor. *The Lincoln Laboratory Journal*, 7(2), 1994.

[40] Flight Systems Laboratory (AFS-450). Controller Response Times from the August and December 2010 Human in the Loop Data Collection Efforts. Technical report, Federal Aviation Administration, August 2011.

[41] Flight Systems Laboratory (AFS-450). Pilot and Controller Response Times from the July, 2009 Human in the Loop Data Collection Effort. Technical report, Federal Aviation Administration, October 2010.

[42] R. R. LaFrey. Parallel Runway Monitor. *The Lincoln Laboratory Journal*, 2(3), 1989.

[43] V. Battiste, S. Holland-Bochow, N. H. Johnson. Airborne and Ground Information for Lateral Spacing During Closely Spaced Parallel Approach Operations. The 21st Digital Avionics Systems Conference, Irvine, CA, October 2002.

[44] James K. Kuchar Lee F. Winder. Evaluation of Collision Avoidance Maneuvers for Parallel Approach. *Journal of Guidance, Control, and Dynamics*, 22(6):801 – 807, November 1999.

[45] John E. Lebron. System Safety Study of Minimum TCAS II. Technical report, The MITRE Corporation, December 1983.

[46] Eurocontrol. Acas guide. Technical report, March 2022.

[47] ACASA/WP1.6/197D. Notes on the event tree for the ACAS collision risk ratio. Technical report, QinetiQ, September 2001.

[48] Allen C. Busch. Methodology for Establishing a Target Level of Safety. Technical note DOT/FAA/CT-TN85/36, Federal Aviation Administration, Atlantic City, NJ, 1985.

[49] International Air Transport Association (IATA). IATA Safety Report: Interactive Safety Report, 2022. Accessible at `https://www.iata.org/en/publications/safety-report/interactive-safety-report/`.

[50] The Boeing Company. Statistical Summary of Commercial Jet Airplane Accidents - Worldwide Operations - 1959-2021, 2022. Accessible at `https://www.boeing.com/resources/boeingdotcom/company/about_bca/pdf/statsum.pdf`.

[51] M. Granger Morgan. *Risk Communication - A Mental Models Approach*. Cambridge University Press, 2001.

[52] B. Fischhoff; P. Slovic; S. Lichtenstein; B. Combs. How Safe is Safe Enough? A Psychometric Study of Attitudes Towards Technological Risks and Benefits. *Policy Sciences*, 8:127–152, 1978.

[53] Robert E. Machol. How Much Safety? *Interfaces*, 16(6):50–57, November 1986.

[54] G. Tversky; D. Kahneman. The Framing of Decisions and the Psychology of Choice. *Science*, 211:453–458, 1981.

[55] R. L. Keeney. Equity and Public Risk. *Operations research*, 28(3), 1980.

[56] William D. Rowe. *An Anatomy of Risk*. John Wiley and Sons, Ney York, NY, 1977.

[57] Arnold Barnett. Letters to the editor. *Interfaces*, 17(2):109–110, 1987.

[58] Aleksandra Mozdzanowska. *System Transition: Dynamics of Change in in the US Air Transportation System*. PhD thesis, Massachusetts Institute of Technology, 2008.

[59] Roland Weibel. *Assuring Safety through Operational Approval: Challenges in Assessing and Approving the Safety of Systems-Level Changes in Air Transportation*. PhD thesis, Massachusetts Institute of Technology, 2010.

[60] Karen Marais; Annalisa Weigel. Encouraging and ensuring successful technology transition in civil aviation. *MIT Engineering Systems Division Working Paper Series*, 2006.

[61] Ralf H. Mayer, Dennis J. Zondervan. Concept and Benefits of a Unified Departure Operation Spacing Standard. 2012 IEEE/AIAA 31st Digital Avionics Systems Conference (DASC), Herndon, VA, October 2012.

[62] Tom G. Reynolds. *Investigating Conformance Monitoring Issues in Air Traffic Control Using Fault Detection Approaches*. PhD thesis, Massachusetts Institute of Technology, 2003.

[63] Lee F. Winder, James K. Kuchar. Generalized Philosophy of Alerting With Applications to Parallel Approach Collision Prevention. AIAA Guidance, Navigation, and Control Conference and Exhibit, Montreal, Canada, August 2001.

[64] Eric M. Shank, Katherine M. Hollister. A Statistical Risk Assessment Model for the Precision Runway Monitor System. *37th Annual Air Traffic Control Association Conference*, November 1992.

[65] International Civil Aviation Organization (ICAO). Manual on required communication performance (rcp). Technical Report Doc 9869, Montreal, Canada, 2006.

[66] Kim M. Cardosi. Time Required for Transmission of Time-Critical Air Traffic Control Messages in an En Route Environment. *The International Journal of Aviation Psychology*, 3(4):303–313, October 1993.

[67] Airbus. Safe Handling of TCAS Alerts, 2021. Accessible at `https://mms-safetyfirst.s3.eu-west-3.amazonaws.com/pdf/safety+first/safe-handling-of-tcas-alerts.pdf`.

[68] Federal Aviation Administration. Precision Runway Monitor Demonstration Report. Technical Report DOT/FAA/RD-91/5, February 1991.

[69] James Yates Shahar Ladecky Donna Templeton David N. Lankford, Gerry McCartor. Comparative Study of Airborne Information for Lateral Spacing (AILS) System with Precision Runway Monitor (PRM) System. Technical report, Federal Aviation Administration, April 2000.

[70] R. John Hansman, Sandro Salgueiro, Jacqueline Huynh, Clement Li, Madeleine Jansson, Ara Mahseredjian, Kevin Zimmer. Block 2 Procedure Recommendations for Boston Logan Airport Community Noise Reduction. Technical report, International Center for Air Transportation, June 2021.

[71] National Aeronautics and Space Administration. UAM Vision Concept of Operations (ConOps) UAM Maturity Level (UML) 4, Version 1.0, December 2020.

[72] Federal Aviation Administration. Urban Air Mobility Concept of Operations, Version 2.0, April 2023.

Appendix A

Derivation of Non-Normal Risk per Flight Hour in Two-Procedure Scenario

This appendix describes the calculation of the non-normal risk between two flight procedures or air traffic routes using a *collision per flight hour* risk metric, which the FAA Air Traffic Organization's Safety Management System recommends for analysis of enroute scenarios [20].

The non-normal risk between two flight procedures is the risk of collision due to deviations from either procedure. When viewed from an airspace perspective (i.e., on a *per airspace flight hour* basis), this risk can be stated as:

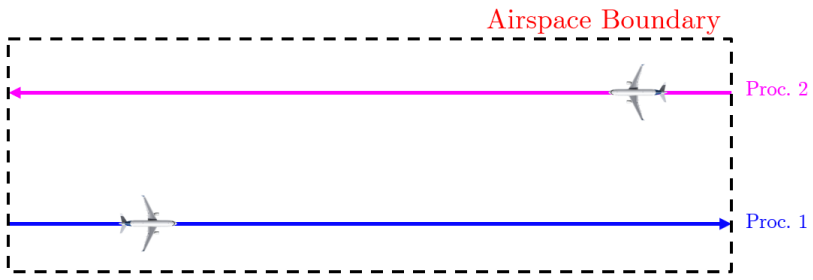

Figure A-1: Illustration of the scenario being analyzed, which considers the non-normal risk between two procedures on a *per airspace flight hour* basis.

$$\begin{aligned} Non\text{-}Normal\ Risk =& (Risk\ due\ to\ Deviations\ from\ Procedure\ 1) \\ &+ (Risk\ due\ to\ Deviations\ from\ Procedure\ 2) \end{aligned} \tag{A.1}$$

The non-normal risk due to deviations from a given procedure is:

$$\begin{aligned} &(Risk\ due\ to\ Deviations\ from\ Procedure\ i) = \\ &F_i \times P(Non\text{-}Normal_i) \times P(Collision \mid Non\text{-}Normal_i) \end{aligned} \tag{A.2}$$

Where F_i is the ratio of flight hours flown on *Procedure 'i'* for each cumulative flight hour in the entire airspace, and $P(Non\text{-}Normal_i)$ represents the probability of a deviation occurring per flight hour flown on *Procedure 'i'*.

To determine F_i, let $\mathbf{M_1}$ be the expected number of aircraft on procedure 1 at any given time, and let $\mathbf{M_2}$ be the expected number of aircraft on procedure 2 at any given time. These parameters are calculated as follows:

$$M_1 = \frac{Length\ of\ Segment_1}{In\text{-}Trail\ Spacing_1} \tag{A.3}$$

$$M_2 = \frac{Length\ of\ Segment_2}{In\text{-}Trail\ Spacing_2} \tag{A.4}$$

The expected number of aircraft present in the airspace considered at any given time, $\mathbf{M_{tot}}$, is therefore:

$$M_{tot} = M_1 + M_2 \tag{A.5}$$

During one cumulative flight hour flown in the entire airspace, the real time elapsed

T, in hours, is:

$$T = \frac{1}{M_{tot}} \tag{A.6}$$

In other words, if 10 aircraft are present in the airspace ($M_{tot} = 10$), they collectively fly 1 flight hour in 1/10th of a real hour.

During the period **T**, the expected number of flight hours $\mathbf{F_1}$ flown in procedure 1 is:

$$F_1 = T \times M_1 = \frac{M_1}{M_{tot}} \tag{A.7}$$

Similarly, the expected number of flight hours $\mathbf{M_2}$ flown in procedure 2 is:

$$F_2 = T \times M_2 = \frac{M_2}{M_{tot}} \tag{A.8}$$

By substituting Equations A.7, A.8 and A.2 into Equation A.1, the total non-normal risk of the airspace, measured in terms of the expected number of collisions per cumulative airspace flight hour, can be calculated as:

$$\begin{aligned} Non\text{-}Normal\ Risk = &\left(\frac{M_1}{Mtot}\right) \times P(Non\text{-}Normal_1) \times P(Collision \mid Non\text{-}Normal_1) \\ &+ \left(\frac{M_2}{M_{tot}}\right) \times P(Non\text{-}Normal_2) \times P(Collision \mid Non\text{-}Normal_2) \end{aligned} \tag{A.9}$$

In the symmetric case in which $(Length\ of\ Segment)_1 = (Length\ of\ Segment)_2$ and $(In\text{-}Trail\ Spacing)_1 = (In\text{-}Trail\ Spacing)_2$, this simplifies to:

$$\begin{aligned} \textit{Non-Normal Risk} = &\left(\frac{1}{2}\right) \times P(\textit{Non-Normal}_1) \times P(\textit{Collision} \mid \textit{Non-Normal}_1) \\ &+ \left(\frac{1}{2}\right) \times P(\textit{Non-Normal}_2) \times P(\textit{Collision} \mid \textit{Non-Normal}_2) \end{aligned} \tag{A.10}$$

Therefore, in the symmetric case, the total non-normal risk per cumulative flight hour within an airspace is the average of the non-normal risk introduced by each procedure.

Appendix B

Derivation of Non-Normal Risk Experienced by Single Operation in Two-Procedure Scenario

The non-normal risk between two flight procedures is the risk of collision due to deviations from either procedure. When viewed from an ownship perspective (i.e., on a *per operation* basis), this risk can be stated as:

$$\begin{aligned} Non\text{-}Normal\ Risk = &(Risk\ to\ Ownship\ due\ to\ Ownship\ Deviation) \\ &+(Risk\ to\ Ownship\ due\ to\ Other\ Deviations) \end{aligned} \tag{B.1}$$

The non-normal risk to the ownship due to an ownship deviation is:

$$\begin{aligned} &(Risk\ to\ Ownship\ due\ to\ Ownship\ Deviation) = \\ &P(Non\text{-}Normal_{Ownship}) \times P(Collision \mid Non\text{-}Normal_{Ownship}) \end{aligned} \tag{B.2}$$

Where $P(Non\text{-}Normal_{Ownship})$ represents the probability of the ownship deviating from its procedure, which is the same as the probability of a non-normal event for one aircraft operation (historically estimated at 10^{-5}). $P(Collision \mid$

$Non\text{-}Normal_{Ownship}$) represents the probability that an ownship deviation results in a collision.

Next, the risk imposed on the ownship by deviations from the other flight procedure must be considered. Here, this other procedure will be referred to as the *opposing* procedure. Similar application of Equation B.2 to the opposing flight procedure yields the non-normal risk experienced by a single aircraft on the opposing procedure due to its own deviation, which is not the same as the non-normal risk experienced by the ownship due to deviations from the opposing procedure. To determine the latter, the risk resulting from the application of Equation B.2 to the opposing procedure must be scaled appropriately.

Let $\mathbf{R}$ be the non-normal risk that a single operation in the opposing procedure poses to all aircraft in the ownship's procedure, calculated from Equation B.2. If this risk is assumed to be distributed uniformly across all aircraft sharing the ownship's procedure, then the non-normal risk posed by a **single** opposing operation to the ownship is $\mathbf{R}/\mathbf{M_1}$, where $\mathbf{M_1}$ is the expected number of aircraft sharing the ownship's procedure at any given time.

$$M_1 = \frac{(Length\ of\ Segment)_{Ownship}}{(In\text{-}Trail\ Spacing)_{Ownship}} \tag{B.3}$$

Next, let $\mathbf{T}$ be the time that it takes for the ownship to transit its flight procedure (i.e., the duration of one operation).

$$T = \frac{(Length\ of\ Segment)_{Ownship}}{(Groundspeed)_{Ownship}} \tag{B.4}$$

Because there may be multiple aircraft transiting the opposing procedure during this time, the probability of a deviation occurring in the opposing procedure that can affect the ownship must be scaled according to the number of operations completed in the opposing procedure during this period.

In other words, the expected number of deviations from the opposing procedure during the time **T** must be proportional to the total distance (**d**) flown by all aircraft in the opposing procedure during the same period. Let $\mathbf{M_2}$ be the expected number of aircraft in the opposing procedure at any given time.

$$M_2 = \frac{(Length\ of\ Segment)_{Opposing}}{(In\text{-}Trail\ Spacing)_{Opposing}} \tag{B.5}$$

It follows that **d** can be computed as:

$$d = M_2 \times (Groundspeed)_{Opposing} \times T \tag{B.6}$$

Now, let **K** be the number of completed operations of the opposing procedure segment during the time **T**, expressed as the total distance flown by all opposing aircraft divided by the length of the opposing segment (which corresponds to the length of one operation).

$$K = \frac{d}{(Length\ of\ Segment)_{Opposing}} \tag{B.7}$$

It follows that the non-normal risk posed by all aircraft in the opposing procedure to the ownship is equal to $\frac{\mathbf{K}}{\mathbf{M_1}} \times \mathbf{R}$.

$$\begin{aligned}&(Risk\ to\ Ownship\ due\ to\ Other\ Deviations) = \\ &\frac{K}{M_1} \times P(Non\text{-}Normal_{Opposing}) \times P(Collision \mid Non\text{-}Normal_{Opposing})\end{aligned} \tag{B.8}$$

Here, the parameter K can be interpreted as a scaling parameter for the expected number of deviations from the opposing procedure per ownship operation, $P(Non\text{-}Normal_{Opposing})$, while M_1 scales the equation used to compute the prob-

ability of collision due to a deviation from the opposing procedure, $P(Collision \mid Non\text{-}Normal_{Opposing})$, so that only collisions with the ownship are counted towards the resulting probability.

Substituting Equations B.3, B.4, B.5, B.6 and B.7 into Equation B.8 yields the final form of this equation:

$$\boxed{\begin{aligned}&(Risk\ to\ Ownship\ due\ to\ Other\ Deviations) = \\ &\left(\frac{(In\text{-}Trail\ Spacing)_{Ownship}}{(Groundspeed)_{Ownship}}\right) \times \left(\frac{(Groundspeed)_{Opposing}}{(In\text{-}Trail\ Spacing)_{Opposing}}\right) \times \\ &P(Non\text{-}Normal_{Opposing}) \times P(Collision \mid Non\text{-}Normal_{Opposing})\end{aligned}} \tag{B.9}$$

This result indicates that the risk posed to the ownship by deviations from the opposing procedure can be calculated from the risk posed by a single opposing aircraft scaled by the throughput of each procedure (i.e., in-trail separation and groundspeed).

For the symmetric case in which $(Groundspeed)_{Ownship} = (Groundspeed)_{Opposing}$ and $(In\text{-}Trail\ Spacing)_{Ownship} = (In\text{-}Trail\ Spacing)_{Opposing}$, the risk experienced by the ownship due to deviations from the opposing procedures simplifies to:

$$\begin{aligned}&(Risk\ to\ Ownship\ due\ to\ Other\ Deviations) = \\ &P(Non\text{-}Normal)_{Opposing} \times P(Collision \mid Non\text{-}Normal)_{Opposing}\end{aligned} \tag{B.10}$$

Which is the same as the non-normal risk posed by a single opposing operation to all aircraft in the ownship's procedure, due to symmetry.

In the symmetric scenario, the total non-normal risk experienced by the ownship, which is the total non-normal risk per operation of the ownship's procedure, is therefore simply:

$$
\begin{aligned}
&Non\text{-}Normal\ Risk = \\
&P(Non\text{-}Normal)_{Ownship} \times P(Collision \mid Non\text{-}Normal)_{Ownship} \\
&+ P(Non\text{-}Normal)_{Opposing} \times P(Collision \mid Non\text{-}Normal)_{Opposing}
\end{aligned}
\tag{B.11}
$$

Appendix C

PDF of Lateral and Vertical Separation in Normal Operations

The PDF of the difference between two independent random variables X and Y can be computed as an integral that closely resembles a conventional convolution (the PDF of the sum of two independent random variables is in fact a convolution). This result is derived as follows. Let f_X be the PDF of X, and f_Y be the PDF of Y. Then the cumulative density function $F_{X-Y}(a) = P(X - Y \leq a)$ can be computed as:

$$\begin{aligned} P(X - Y \leq a) &= \int_{-\infty}^{\infty} \int_{-\infty}^{a+y} f_X(x) f_Y(y) dx dy \\ &= \int_{-\infty}^{\infty} F_X(a + y) f_Y(y) dy \end{aligned} \tag{C.1}$$

The two sides of the equation can be differentiated wirth respect to a to yield the following:

$$f_{X-Y}(a) = \int_{-\infty}^{\infty} f_X(a + y) f_Y(y) dy \tag{C.2}$$

This is the PDF of $X - Y$. For comparison, the PDF of $X + Y$ is the *convolution* of f_X and f_Y, computed as $\int_{-\infty}^{\infty} f_X(a - y) f_Y(y) dy$.

Appendix D

Derivation of Probability of Exposure to Deviation

The probability of exposure as defined in this thesis, $P(Exposure \mid Trajectory\,Overlap, NN)$, is the probability that an intruder aircraft crossing another flight procedure will collide with a passing endangered aircraft. The two procedures are assumed to be operated independently. The scenario considered is illustrated in Figure D-1. The mathematical expression for this probability will be derived here based on the case of a linear deviation trajectory, though the final result will be shown to apply to any deviation trajectory.

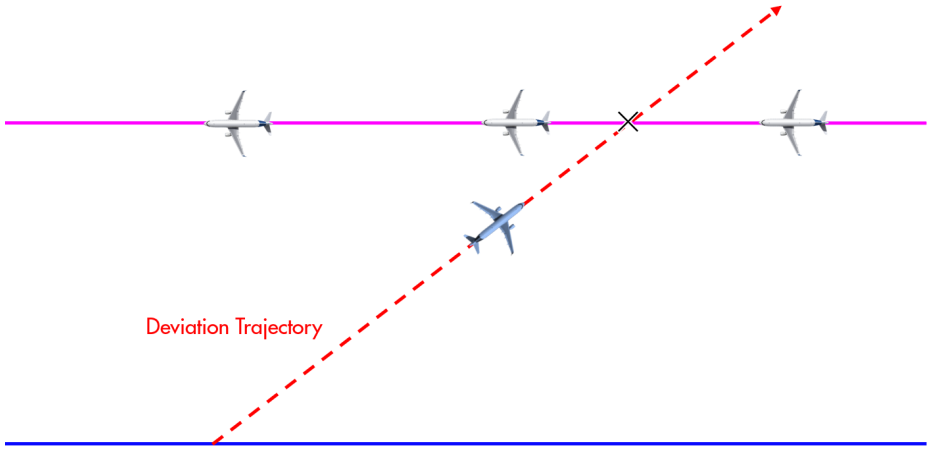

Figure D-1: The probability of exposure is the probability that an intruder aircraft crossing another flight procedure will collide with a passing endangered aircraft.

The following geometric transformations are made to the problem (Figure D-2). First, the intruder aircraft is treated as a point mass while endangered aircraft are treated as rectangular polygons of width $2A$ and length $2B$. The dimensions of this polygon are based on the joint geometry of two airplanes, and a collision condition is defined as a point mass intruder penetrating the collision box of an endangered aircraft. A conservative two-dimensional collision condition is used. Next, a Cartesian coordinate system is defined with its *x-axis* aligned with the endangered procedure and its *y-axis* oriented perpendicular to it. Then, the reference frame is manipulated such that endangered aircraft are moving along the *x-axis* at $V_{x,rel}$ (the closing speed between the intruder and endangered aircraft along the *x-axis*) and the intruder aircraft is moving along the *y-axis* at $V_{y,rel}$ (the perpendicular speed of the intruder aircraft towards the endangered procedure).

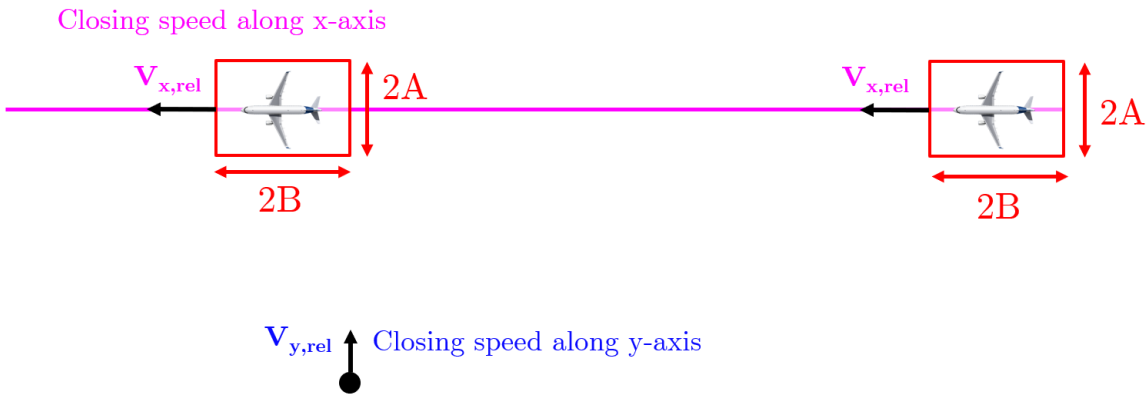

Figure D-2: The coordinate system's *x-axis* is aligned with the endangered procedure (magenta track), and relative speeds are used to represent the speeds of the intruder and endagered aircraft. The intruder is treated as a point mass and endangered aircraft as rectangular collision boxes.

While crossing the endangered procedure at random, an intruder aircraft may either cross at a *safe* location (i.e., one that does not result in a collision) or at an *unsafe* location (i.e., one that results in a collision). The probability of exposure can be stated geometrically as the length of the unsafe crossing region between two endangered aircraft divided by the total in-trail distance between two endangered

aircraft, as illustrated in Figure D-3.

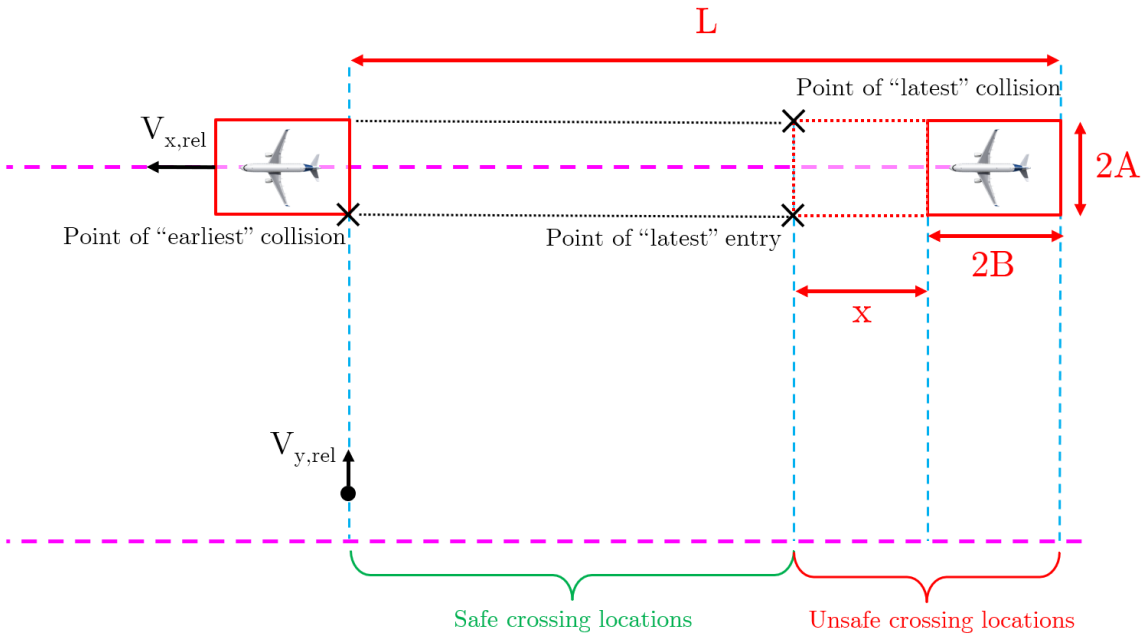

Figure D-3: The probability of exposure can be stated as the length of the unsafe crossing region between two endangered aircraft divided by the in-trail distance between two endangered aircraft.

$$P(Exposure \mid Trajectory\ Overlap, NN) = \frac{x + 2B}{L} \tag{D.1}$$

As illustrated in Figure D-3, the length of the unsafe region includes the length of a collision box ($2B$) as well as an additional length (x) that, if entered, leads to a collision before the intruder aircraft has finished crossing the endangered procedure. The length x can be computed by observing that the time spent in trajectory overlap by the intruder aircraft is the same time that it takes an endangered aircraft to travel the distance x, by definition (Equation D.2).

$$Time\ Spent\ in\ Overlap = Time\ for\ Endangered\ Aircraft\ to\ Travel\ Distance\ x$$
$$\frac{2A}{V_{y,rel}} = \frac{x}{V_{x,rel}} \Rightarrow x = \frac{2AV_{x,rel}}{V_{y,rel}} \tag{D.2}$$

Substituting Equation D.2 into Equation D.1 yields:

$$P(Exposure \mid Trajectory\ Overlap, NN) = \left(\frac{2A}{V_{y,rel}}\right) \times \left(\frac{V_{x,rel}}{L}\right) + \left(\frac{2B}{L}\right) \tag{D.3}$$

When the time spent in a trajectory overlap condition is sufficiently long, multiple aircraft on the endangered procedure may pass the intruder aircraft's position, which results in Equation D.3 producing a value greater than 1. Because of this, the probability of exposure should be limited to a maximum value of 1 since a collision with the first passing aircraft is assumed to be guaranteed.

$$P(Exposure \mid Trajectory\ Overlap, NN) = \min\left(\left(\frac{2A}{V_{y,rel}}\right) \times \left(\frac{V_{x,rel}}{L}\right) + \left(\frac{2B}{L}\right), 1\right) \tag{D.4}$$

This expression can be more generally written based on the average values of the relative speeds, $\bar{V}_{x,rel}$ and $\bar{V}_{y,rel}$, which do not require a linear deviation trajectory assumption.

$$\boxed{P(Exposure \mid Trajectory\ Overlap, NN) = \min\left(\left(\frac{2A}{\bar{V}_{y,rel}}\right) \times \left(\frac{\bar{V}_{x,rel}}{L}\right) + \left(\frac{2B}{L}\right), 1\right)} \tag{D.5}$$

These terms can be understood intuitively as follows:

- $\frac{2A}{\bar{V}_{y,rel}}$: The time that it takes the intruder aircraft to cross the conflict region around the endangered procedure.
- $\frac{\bar{V}_{x,rel}}{L}$: The relative throughput or frequency of endangered aircraft passes experienced by the intruder aircraft during the overlap condition.
- $\frac{2B}{L}$: The fraction of the endangered procedure's length that is populated by aircraft, analogous to traffic density.

Based on these definitions, $P(Exposure \mid Trajectory\ Overlap, NN)$ can be generally understood as:

$$\boxed{\begin{aligned} &P(Exposure \mid Trajectory\ Overlap, NN) = \\ &(Time\ Spent\ in\ Trajectory\ Overlap) \times (Relative\ Throughput\ During\ Overlap) \\ &+ (Occupancy\ Ratio\ of\ Endangered\ Procedure) \end{aligned}} \tag{D.6}$$

Appendix E

Comparison of Maneuver Time Margin Associated with Lateral and Vertical Maneuvers

Previous discussion of the maneuver time margin associated with a mitigation maneuver has assumed a lateral maneuver as a conservative example. In this appendix, the maneuver time margin associated with a vertical maneuver is compared to that of a lateral maneuver.

In Chapter 4, the maneuver time margin associated with a lateral maneuver was estimated as:

$$(Maneuver\ Time\ Margin)_{Lateral} = \frac{V_d \cdot tan(\alpha/2)}{g \cdot tan(\phi_{target})} + \frac{\phi_{target}}{\dot{\phi}} \tag{E.1}$$

Where V_d is the groundspeed of the maneuvering aircraft, α is the relative lateral angle at which the aircraft approaches the endangered procedure, g is the gravitational acceleration, ϕ_{target} is the target bank angle during the maneuver, and $\dot{\phi}$ is the roll rate during the maneuver.

By assuming a deviation angle of $\alpha = 30°$, a target bank angle of $\phi_{target} = 30°$ and a roll rate of $\dot{\phi} = 10$ deg/sec, the maneuver time margin associated with a lateral

maneuver can be plotted as a function of aircraft groundspeed as follows.

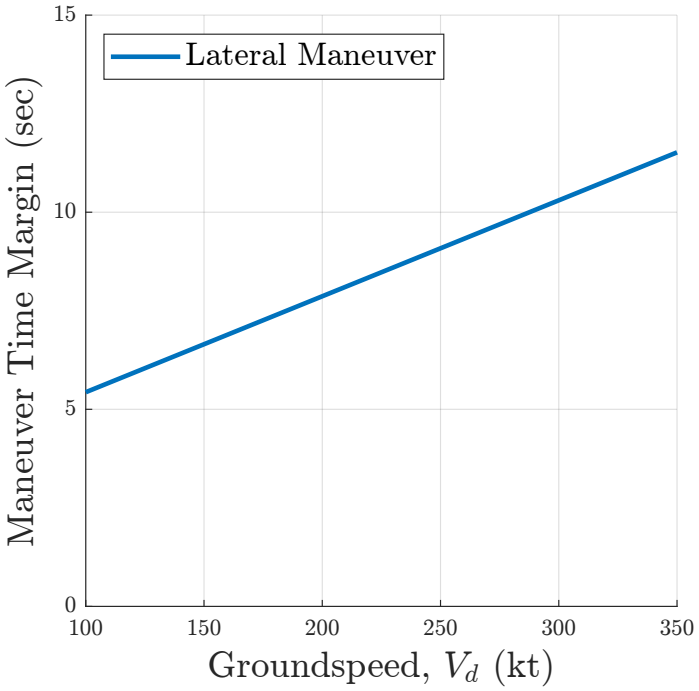

Figure E-1: Maneuver time margin associated with a lateral maneuver as a function of aircraft groundspeed.

The maneuver time margin associated with a vertical maneuver can be similarly derived. As an example, this appendix will consider a vertical maneuver with performance equivalent to a minimum TCAS maneuver, which requires a target vertical speed of $V/S_{target} = 1500$ ft/min and a load factor of $n = 1.25$ during a pull-up maneuver [9]. Aircraft will be assumed to be initially flying at the same altitude, and a collision is assumed to be prevented when the maneuvering aircraft passes above the endangered aircraft by more than $H = 80$ ft (the half-height of a standard collision box [36]).

The target flight path angle γ_{target} needed to achieve a target climb rate of V/S_{target} is calculated as:

$$\gamma_{target} = sin^{-1}\left(\frac{V/S_{target}}{V_d}\right) \tag{E.2}$$

The rate of change of the flight path angle $\dot{\gamma}$ during the initial pull-up maneuver is calculated as follows:

$$\dot{\gamma} = \frac{g}{V_d}(n-1) \tag{E.3}$$

Where g is the gravitational acceleration and n is the load factor during the pull-up maneuver.

By making the conservative assumption that the maneuvering aircraft's trajectory does not change until the target flight path angle γ_{target} is reached, the maneuver time margin is the time needed to climb an altitude of H and estimated as follows:

$$(Maneuver\ Time\ Margin)_{Vertical} = \frac{H}{V/S_{target}} + \frac{\gamma_{target}}{\dot{\gamma}} \tag{E.4}$$

Substituting Equations E.2 and E.3 into Equation E.4 yields:

$$(Maneuver\ Time\ Margin)_{Vertical} = \frac{H}{V/S_{target}} + \frac{sin^{-1}(\frac{V/S_{target}}{V_d})}{\frac{g}{V_d} \cdot (n-1)} \tag{E.5}$$

Assigning $H = 80$ ft, $V/S_{target} = 1500$ ft/min, and $n = 1.25$, the maneuver time margin of a vertical maneuver can be calculated as a function of aircraft groundspeed and plotted (Figure E-2).

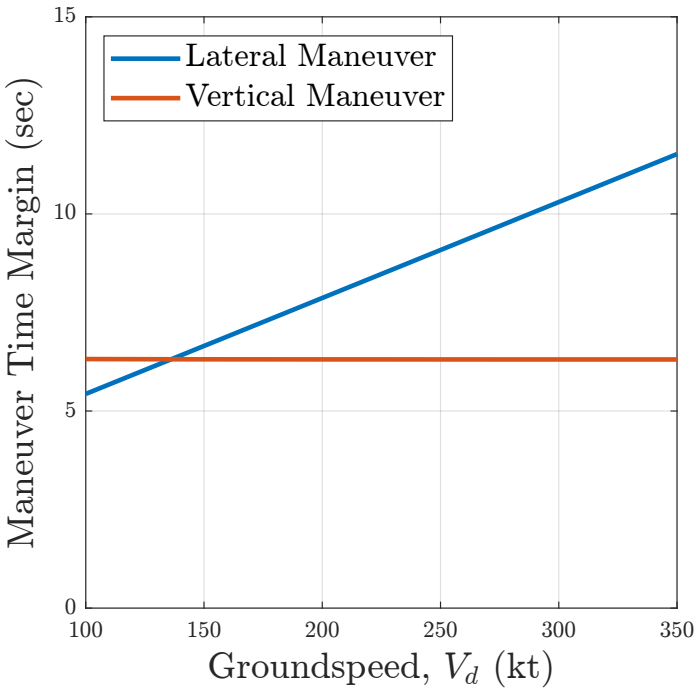

Figure E-2: Maneuver time margin associated with lateral and vertical maneuvers as a function of aircraft groundspeed.

As can be observed in this result, the maneuver time margin of a vertical maneuver is insensitive to groundspeed under the assumptions considered, although higher pitch angles are required at lower speeds. At speeds below 135 kt, a lateral maneuver is found to produce a lower maneuver time margin, while at higher speeds a vertical maneuver offers benefits. At a groundspeed value of 350 kt, the assumed vertical maneuver reduces the maneuver time margin by 6 seconds compared to the previously assumed lateral maneuver.

Appendix F

Effects of Multiple Available Mitigations on Overall Probability of Mitigation

The probability of mitigation by a single mitigation capability is computed as:

$$P(Mitigation) = \\ P(Mitigation\ Available) \times P(Timely\ Response) \times P(Correct\ Response) \tag{F.1}$$

When additional mitigations are available at the same time, the resulting mitigation probability is a function of both the individual performance of each capability as well as the mitigation concept of operations (CONOPS). In this context, a mitigation CONOPS refers to how system operators act in the availability of multiple mitigations.

The mitigation CONOPS in the current system consists of prioritizing instructions from TCAS over those provided by an air traffic controller. In this scenario, TCAS instructions are followed whenever they are timely, while ATC instructions supplement the overall mitigation performance. This CONOPS is appropriate when one mitigation is believed to have a higher probability of issuing a correct instruction

than the other (i.e., $P(Correct\ Response)_{TCAS} > P(Correct\ Response)_{ATC}$).

For brevity of writing, the terms in Equation F.1 are simplified as follows:

- A_n: $P(Mitigation\ Available)$ for Mitigation n
- $\neg A_n$: $1 - P(Mitigation\ Available)$ for Mitigation n
- T_n: $P(Timely\ Response)$ for Mitigation n
- $\neg T_n$: $1 - P(Timely\ Response)$ for Mitigation n
- C_n: $P(Correct\ Response)$ for Mitigation n
- $\neg C_n$: $1 - P(Correct\ Response)$ for Mitigation n

For the CONOPS in which one mitigation (mitigation 1) takes precedence over a second mitigation (mitigation 2) (e.g., TCAS case), the overall probability of mitigation is computed as follows:

$$P(Mitigation) = A_1T_1C_1 + A_2T_2C_2(\neg A_1 + A_1\neg T_1) \tag{F.2}$$

A different CONOPS may simply require aircraft to follow the earliest mitigation instruction received. This CONOPS may be adequate when mitigations have a similar probability of providing a correct response, and the objective is to achieve a lower response time. The overall probability of mitigation in this scenario, assuming two mitigations, is:

$$\begin{aligned} P(Mitigation) =& A_1T_1C_1(\neg A_2 + A_2\neg T_2) + A_2T_2C_2(\neg A_1 + A_1\neg T_1) \\ &+ A_1T_1A_2T_2(P(t_1 < t_2)C_1 + P(t_1 > t_2)C_2) \end{aligned} \tag{F.3}$$

In the case in which the two mitigations have an identical response time distribution (i.e., $P(t_1 > t_2) = P(t_1 < t_2)$), this simplifies to:

$$P(Mitigation) = A_1T_1C_1(\neg A_2 + A_2\neg T_2) + A_2T_2C_2(\neg A_1 + A_1\neg T_1) + \frac{A_1T_1A_2T_2(C_1 + C_2)}{2} \tag{F.4}$$

The highest theoretical performance of two combined mitigations is achieved when a correct response is always prioritized. Because this would require an aircraft to be able to discern between a correct and an incorrect maneuver instruction and thus prioritize a correct one, this CONOPS represents a theoretical limit for the overall mitigation performance. The probability of mitigation in this theoretical scenario is:

$$P(Mitigation) = A_1T_1C_1 + A_2T_2C_2 - (A_1T_1C_1)(A_2T_2C_2) \tag{F.5}$$

Which can similarly be written as:

$$P(Mitigation) = P(Mitigation)_1 + P(Mitigation)_2 - P(Mitigation)_1 \times P(Mitigation)_2 \tag{F.6}$$

In this theoretical scenario, the resulting mitigation performance follows the relationship shown in Figure F-1.

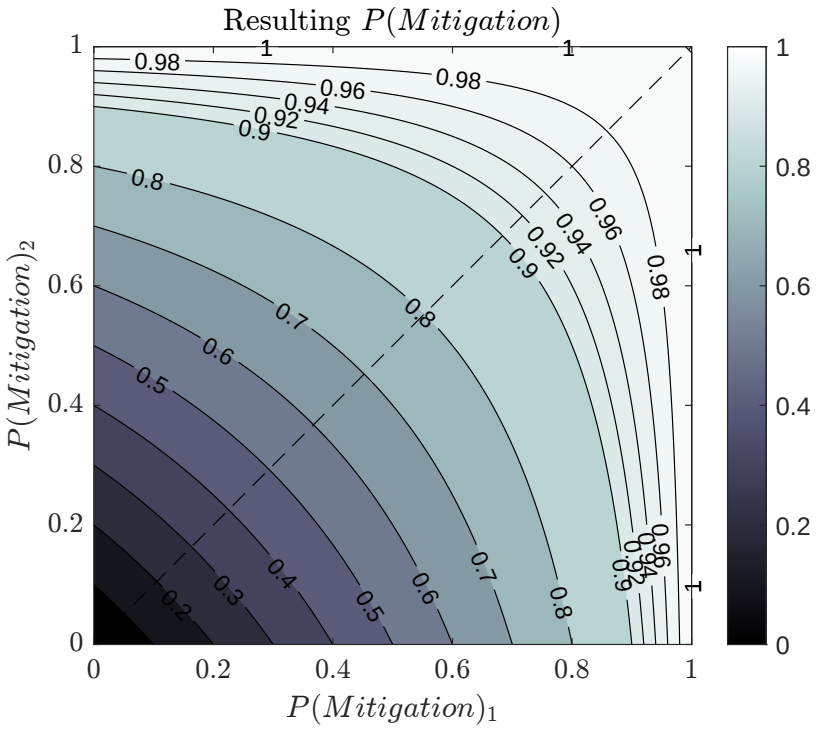

Figure F-1: Plot of the overall probability of mitigation as a function of the performance of two individual mitigation capabilities in a theoretical best-case scenario.

From this theoretical result, it can be observed that the combination of multiple mitigations can be an effective mechanism for achieving high probabilities of mitigation at the system level. However, in the event that the mitigations are not fully independent, such as in the case where they share communication or surveillance capabilities, evaluation of the overall probability of mitigation must consider how the multiple mitigations available are correlated.

Appendix G

BOS Example Study: Detailed Results of Evaluation of Probability of Trajectory Overlap

Probability of Trajectory Overlap due to Deviations from Approach

Number of descending approach deviations simulated	9,056
Number of descending approach deviations resulting in overlap	69
Fraction of descending approach deviations resulting in overlap	7.62×10^{-3}
Number of level approach deviations simulated	10,944
Number of level approach deviations resulting in overlap	110
Fraction of level approach deviations resulting in overlap	1.01×10^{-2}
Probability of overlap given a deviation from the approach	$\mathbf{8.84 \times 10^{-3}}$

Table G.1: Results of the evaluation of the probability of trajectory overlap for unmitigated deviations from the approach procedure in the Boston example discussed in Chapter 6.

Altitudes at which collisions occur in the Monte Carlo simulation of deviations from the approach procedure are shown in Figure G-1.

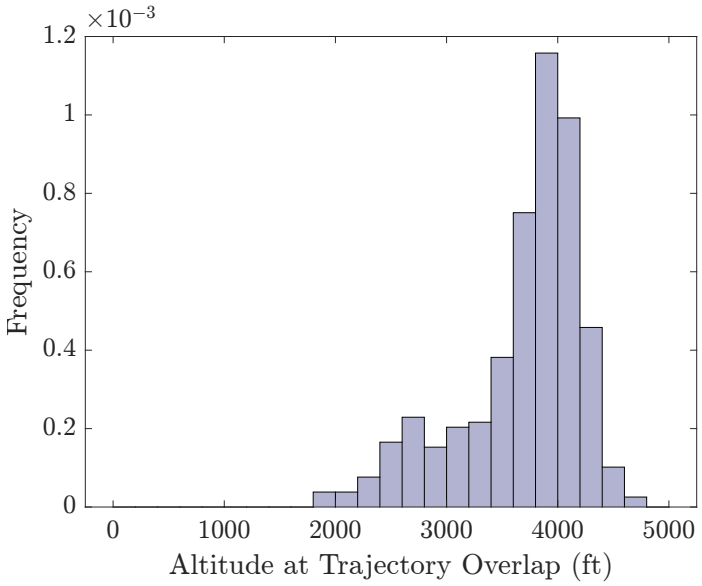

Figure G-1: Distributions of altitudes at which collisions occur following a deviation from the approach procedure, as evaluated in the Monte Carlo simulation according to deviation assumptions described in Chapter 6

Probability of Trajectory Overlap due to Deviations from Departure

Number of climbing departure deviations simulated	10,036
Number of climbing departure deviations resulting in overlap	0
Fraction of climbing departure deviations resulting in overlap	0
Number of level departure deviations simulated	9,866
Number of level departure deviations resulting in overlap	45
Fraction of level departure deviations resulting in overlap	4.56×10^{-3}
Probability of overlap given a deviation from the departure	$\mathbf{2.28 \times 10^{-3}}$

Table G.2: Results of the evaluation of the probability of trajectory overlap for unmitigated deviations from the departure procedure in the Boston example discussed in Chapter 6.

Altitudes at which collisions occur in the Monte Carlo simulation of deviations from the departure procedure are shown in Figure G-2.

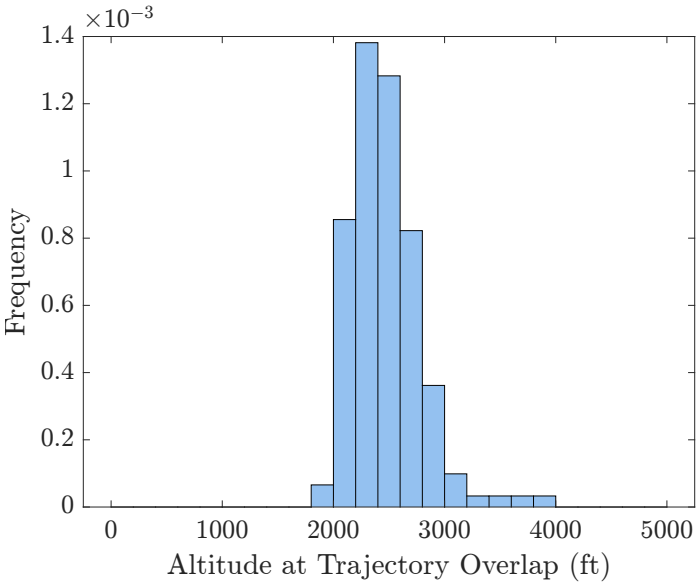

Figure G-2: Distributions of altitudes at which collisions occur following a deviation from the departure procedure, as evaluated in the Monte Carlo simulation according to deviation assumptions described in Chapter 6

Appendix H

BOS Example Study: Closer Separation of Procedures Causes Lower Probability of Trajectory Overlap due to Unmitigated Deviations

When the lateral separation between the two flight procedures considered in the BOS example in Chapter 6 is reduced, the probability of a trajectory overlap due to an unmitigated deviation is likewise reduced. This seemingly counterintuitive fact is explained by the relative geometry of the procedures, as explained below.

When the departure procedure is moved further north, a deviation from the approach crosses the departure path earlier and farther from the airport, which causes the departing aircraft to be at a higher altitude at the crossing location. This in turn causes the vertical separation between the two conflicting aircraft to increase. This scenario is illustrated in Figure H-1 below.

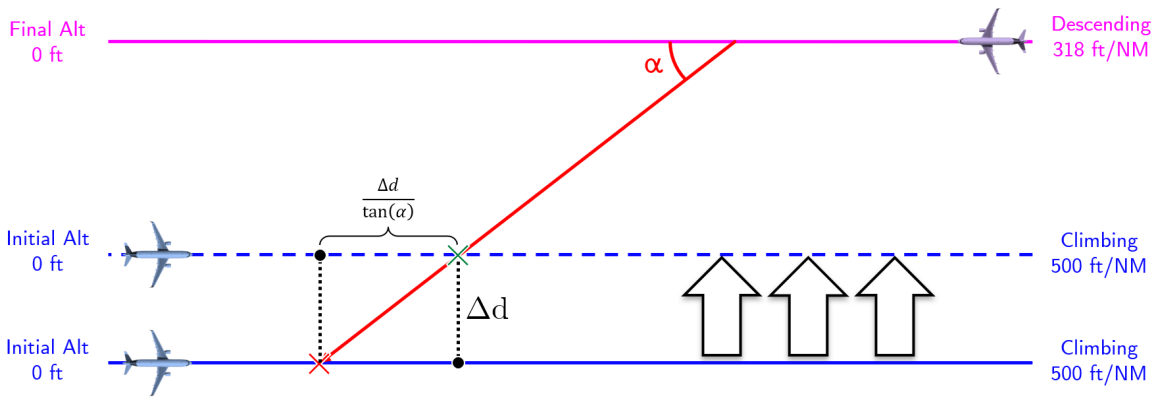

Figure H-1: When the procedures are brought closer, a deviation from the approach crosses the departure at a location farther from the airport, leading to an increase in vertical separation during deviations.

Similarly, when the procedures are brought closer, a deviation from the departure procedure crosses the approach at a location closer to the airport, where the aircraft on the approach procedure is lower. Therefore, the vertical separation separation between the two conflicting aircraft is also increased (Figure H-2).

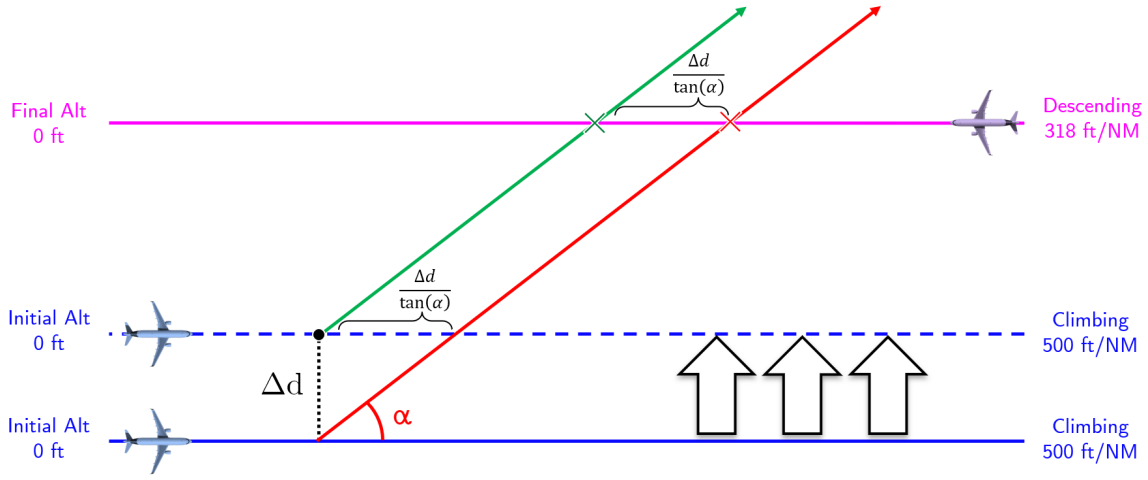

Figure H-2: When the procedures are brought closer, a deviation from the departure crosses the departure at a location closer to the airport, leading to an increase in vertical separation during deviations.